Modeling Pressure Drop and Heat Transfer in Plate Heat Exchanger Channels

by

© Mahmoud Hamoda

A Thesis submitted to the School of Graduate Studies in partial fulfillment

of the requirements for the degree of

Doctor of Philosophy

Department of Mechanical Engineering

Faculty of Engineering and Applied Science

Memorial University of Newfoundland

February 2022

St. John’s, Newfoundland and Labrador, Canada

Abstract

In compact heat exchangers, surface enhancements have been used for augmenting heat transfer due to the growing urgency for energy conservation and reduced environmental impact. Plates with corrugated walls are utilized in plate heat exchangers (PHEs) as they increase the effective heat transfer area, disrupt and reattach the boundary layer, and promote swirl flow resulting in a compact heat exchanger with high heat transfer performance. As a result, their applications have grown considerably to include a wide range of industries and processes, such as food, pharmaceutical, power generation, cooling engine oil, and dairy product processing. Due to heat exchanger size constraints, a compact heat exchanger's flow passages are often short in the automobile industry, especially for cooling engine oil and transmission oil. Hence, the heat exchanger is likely working with developing flow characteristics that have higher heat transfer and pressure drop compared to developed flow.

A review of the open literature reveals a gap in the knowledge regarding the influence of the channel length on the thermal-hydraulic performance of PHE, which needs additional research. Also, no general models or correlations have been developed for predicting heat transfer and pressure drop in the entrance region of PHEs. Therefore, this thesis aims to experimentally investigate the effect of the channel length on the thermal-hydraulic performance of PHEs and to develop models for use in predicting pressure drop and heat transfer of PHEs, including the entrance region.

An experimental facility is constructed to perform a series of single-phase flow tests

on pressure drop and heat transfer of chevron PHE with two different channel lengths, 20.3 cm and 10.1 cm, and three different chevron angles, 30°, 45°, and 60°. Mineral oil and water are used as the working fluids to cover laminar and turbulent flow regions. The results show that plates with a higher chevron angle experience higher pressure drop and heat transfer, which is consistent with the literature. Furthermore, the results of the effect of channel length on the Nusselt number of a PHE are very interesting as they demonstrate a significant impact of channel length on heat transfer performance of PHEs. The Nusselt number for short channels is considerably higher than for longer channels, indicating that thermal entrance effects are present. In addition, the Fanning friction factor results show that it is independent of the channel length at very low Reynolds numbers, while it is greatly impacted by the length of the channel at higher Reynolds numbers. The significance of these findings is that PHE channel length is an important factor that needs to be considered; however, it is often neglected due to assuming fully developed flow. This is important when designing a PHE and/or developing general models or correlations to predict the thermal and hydraulic performance of the PHE to cover a wide range of the Reynolds numbers. It is especially significant for applications where the length of the heat exchanger's flow passage is constrained.

Finally, models for predicting the Fanning friction factor and Colburn factor are developed, which are a function of the plate length, corrugation depth, chevron angle, and Reynolds number. Agreement between the proposed models and the present experimental data is within $\pm 20\%$. These models are also validated against numerical and experimental data from the literature and show good agreement within $\pm 20\%$ in most cases within the

range of applicability. Thus, the proposed models may be used for preliminary designs of a chevron PHE.

Acknowledgments

I would like to express my deep gratitude to my thesis supervisors, Dr. Kevin Pope and Prof. Dr. Yuri S. Muzychka, for their guidance, support, and patience throughout this work. This dissertation would not have been possible without their direction and constant assistance.

Thanks to everybody at the Heat Transfer Lab, Technical service, and workshop for their help while building up my experimental setup.

Finally, I would like to thank my family, especially my wife for her continuous encouragement, support, and sacrifice.

Table of Contents

List f Tables

List of Figures

Nomenclature

A	=	area, m^2
$\mathcal{A}$	=	composite solution coefficients
A_{eff}	=	effective heat transfer area, m^2
A_{proj}	=	projected heat transfer area, m^2
A_i	=	constants, $i = 1 \ldots 8$
$\mathcal{B}$		composite solution coefficient
B	=	constant
B_i	=	constants, $i = 1 \ldots 2$
b	=	corrugation depth, m
C	=	constant
C_i	=	constants, $i = 1 \ldots 15$
C_c	=	cold capacity rate, W/K
C_h		hot capacity rate, W/K
C_p	=	heat capacity, $J/kg.K$
c	=	empirical constant
D	=	diameter, m
D_e	=	equivalent diameter $= 2b$, m
D_h	=	hydraulic diameter $\equiv 4A/P$, m
D_p	=	port diameter, m
d	=	constant

e	=	error
f	=	Fanning friction factor,$\equiv \left(\frac{\Delta p\, D}{4L}\right)/\left(\frac{1}{2}\,\rho\overline{u}^2\right)$
f_D	=	Darcy friction factor, $\equiv 4f$
G	=	mass velocity, $kg/m^2.s$
G_p		mass velocity in the port, $kg/m^2.s$
g	=	constant
g	=	gravitational acceleration, m/s^2
h	=	heat transfer coefficient, $W/m^2.K$
j	=	Colburn factor $\equiv Nu/RePr^{1/3}$
k	=	thermal conductivity, $W/m.K$
K_0	=	shape factor
$K, K(\infty)$	=	incremental pressure drop factor
L	=	length, m
L_{eff}	=	effective flow length, m
L_{p-p}	=	projected length between the centre of ports, m
$\mathcal{L}$	=	characteristic length scale, m
$\mathcal{M}$	=	constant
m	=	constant
m_i	=	constant, $i = 1\ldots3$
$\dot{m}$	=	mass flow rate, kg/s
n	=	composite model combination parameter, Ch. 3,5,6

N	=	number of data points
N_p	=	number of pores
N_{cp}	=	number of channels per pass
$Nu_{\mathcal{L}}$	=	Nusselt number, $\equiv h\mathcal{L}/k$
P	=	perimeter, m
P_i	=	constants, $i = 1 \ldots 5$
Pr	=	Prandtl number, $\equiv \mu c_p/k$
Q	=	heat transfer, W
R	=	fluid thermal resistance, K/W
$Re_{\mathcal{L}}$	=	Reynolds number, $\equiv \rho\bar{u}\mathcal{L}/\mu$
T	=	temperature, K
	=	tortuousness coefficient, Ch. 3
t	=	wall thickness, m
U	=	overall heat transfer coefficient, $W/m^2 \cdot K$
$\dot{V}$	=	volumetric flow rate, m^3/s
$\bar{u}$	=	average velocity, m/s
w	=	plate width inside the gasket, m
$x_{\mathcal{L}}^*$	=	dimensionless axial distance for thermally developing flows, $\equiv x/\mathcal{L}\, Re_{\mathcal{L}} Pr$
$x_{\mathcal{L}}^+$	=	dimensionless axial distance for hydrodynamically developing flows, $\equiv x/\mathcal{L}\, Re_{\mathcal{L}}$

X	=	corrugation parameter, $\equiv \pi b/\lambda$
y	=	dependent parameter
z	=	independent parameter
Z	=	constant

Subscripts

0	=	corresponding to very small value
∞	=	corresponding to very large value
ave	=	average value
app	=	apparent
c	=	cold water
$cell$	=	whole cell
cp	=	constant property
ch	=	channel
D_e	=	based on equivalent diameter
D_h	=	based on hydraulic diameter
dev	=	developing flow
e	=	equivalent
eff	=	effective
f	=	fouling
fd	=	fully developed flow
furr	=	furrow

H	=	based upon isoflux condition
h	=	hot process fluid
hor	=	horizontal
hy	=	hydrodynamic
i	=	inlet fluid condition
l		laminar
LBL	=	laminar boundary layer
$long$	=	longitudinal
LowRe	=	Low Reynolds number
$\mathcal{L}$	=	characteristic length scale
m	=	mean value
o	=	outlet fluid condition
proj		projected
pp	=	pertaining to flat parallel-plate channel
$p-p$	=	distance between center of inlet and outlet ports
RMS	=	root mean square
T	=	based upon isothermal condition
t	=	turbulent
th	=	thermal
v	=	vertical
w	=	wall

Superscripts

a_i	=	constants, $i = 1 \ldots 6$
i	=	exponent in asymptotic solution for $z \to 0$
j	=	exponent in asymptotic solution for $z \to \infty$
m_i	=	constant, $i = 1 \ldots 4$
n_1	=	constant
p	=	constant
$\overline{(.)}$	=	average value of $\overline{(.)}$
$*$	=	dimensionless quantity
$+$	=	dimensionless quantity

Greek Symbols

β	=	corrugation inclination angle relative to flow direction, degree
θ	=	corrugation angle measured from the horizontal axis, degree
λ	=	corrugation pitch, m
τ	=	tortuosity coefficient
δ	=	hydrodynamic boundary layer thickness, m
γ	=	corrugation aspect ratio, $\equiv \gamma = 2b/\lambda$
φ	=	dimensionless parameter
ϕ	=	surface enlargement factor
μ	=	dynamic viscosity, $kg/m \cdot s$
Δ	=	thermal boundary layer thickness, m

ψ	=	empirical constant
ρ	=	density, $kg\ /\ m^3$
τ	=	wall shear stress, N/m^2
Δp	=	pressure drop, Pa
ΔT_{LMTD}	=	log-mean temperature difference, K

Acronyms

CFD	=	computational fluid dynamics
DAQ	=	data acquisition
LBL	=	laminar boundary layer
OGF	=	oval gear flowmeter
RMS	=	root mean square
UHF	=	uniform heat flux
UWT	=	uniform wall temperature
VFD	=	variable frequency drive

Chapter 1

Motivation and Scope

1.1 Introduction

Surface enhancements can be used for augmenting heat transfer in compact heat exchangers to ensure optimum utilization of available energy. Plates with corrugated walls are used in plate heat exchangers (PHEs) for heat transfer enhancement, usually at the expense of increased fluid friction. PHEs offer high heat transfer coefficients compared to the traditional shell and tube heat exchangers, as well as lower temperature gradients, and higher turbulence (which mitigates fouling) due to the complex flow inside the channels (Shah and Sekuli 2003). The plate corrugations increase heat transfer through several mechanisms, such as promoting swirl or helical flow, increased effective heat transfer area, disruption and reattachment of the boundary layer, and small hydraulic diameter flow passages (Wang et al. 2007). Consequently, the resulting heat exchanger is compact in size, with a very large surface area in a small volume, with high heat transfer performance. Although PHEs are firstly introduced for the dairy industry, in 1890, due to suitability in hygienic applications and ease of disassembling for cleaning, they are now widely used in many industrial applications, such as food processing, power generation, pulp and paper production, refinery and petrochemical systems, and refrigeration, among others (Wang et al. (2007) and Shah and Sekuli (2003)).

In the automotive industry, engine oil and transmission oil need to be cooled to prevent degradation and extend the life of moving parts. PHE is also used for cooling

engine oil (Sarraf et al. 2015). Lozano et al. (2008) conducted experimental and numerical studies on PHE prototype for the automobile industry for cooling engine oil; however, no heat transfer or pressure drop results were reported. They only documented information on flow distribution inside the heat exchanger. In the automotive industry, to fit a heat exchanger near the engine, the heat exchanger's flow passages have to be short because of heat exchanger size constraints. Thus, a heat exchanger is likely operating with developing flow characteristics due to the reduced length of the flow passage. Developing flow has high heat transfer rate and pressure drop compared to developed flow.

In the literature, no general correlations and/or models are reported for predicting pressure drop and heat transfer in the entrance region of PHEs. Furthermore, plate geometry characteristics are not always reported in detail, making the comparisons somewhat difficult. There is a need to develop models for predicting fluid friction and heat transfer in the entrance region of PHEs, which is the primary goal of this dissertation. Developing these models requires more precise data on the effect of geometric plate parameters, particularly, chevron angle, which is the most important parameter that affects the flow patterns inside PHE channels (Bond (1981), Gaiser and Kottke (1998) and Zhang et al. (2006)), and plate length on the thermal-hydraulic performance of PHEs. Thus, an experimental study is conducted to acquire the required data to validate the developed models. These models may be used as an initial tool for predicting the thermal-hydraulic performance of a PHE when it is expected to operate within the entrance region.

1.2 Research Objectives

The purpose of this thesis is to develop models for predicting the friction factor and heat transfer coefficient, for single-phase flow, in plate heat exchanger cores, including the entrance region. This study investigates the effects of different chevron angles and two channel lengths on the thermal-hydraulic performance of chevron plate heat exchanger and incorporate their effect in the developed models. Thus, the main objectives of this thesis are:

1. Conduct a comprehensive experimental study to collect data on single-phase flow using two types of working fluid: water and mineral oil. This covers both flow regimes, laminar and turbulent.
2. Investigate the effect of changing corrugation inclination angles, chevron angle, and plate lengths on the friction factor and Nusselt number in the entrance region of a plate heat exchanger.
3. Development of new general models for predicting pressure drop and heat transfer in PHEs including the entrance region by incorporating chevron angle, corrugation depth and channel length into the models.

1.3 Thesis Structure

The remainder of the thesis is organized in the following way. Chapter 2 presents a summary of plate heat exchangers, focusing on gasket chevron plate heat exchangers. It also presents the chevron plate geometrical characteristics that influence a heat exchanger's thermal-hydraulic performance. Chapter 3 reviews the state-of-the-art in terms of developed models for predicting heat transfer and pressure drop for single-phase flow in

plate heat exchangers. Furthermore, it discusses the asymptotic analysis technique, Churchill and Usagi (1972) method, which is used to develop Fanning friction factor , f, and Colburn factor, j, models for PHE. Chapter 4 describes the experimental setup, instrumentation, and a detailed test procedure. It also presents methodology to calculate pressure drop and heat transfer, as well as the experimental uncertainty. Next, the experimental results for the Fanning friction factor and Nusselt number, Nu, are presented. The results are compared with other studies from the literature when applicable. In Chapter 5, the procedure for developing the pressure drop model is discussed. Moreover, the developed model is validated using the obtained experimental data and data from the literature. The method for developing the heat transfer model is addressed in Chapter 6. Furthermore, a comparison between the experimental results and data from the literature with the proposed model is presented for validation. In chapter 7, conclusions and recommendations for future work are presented.

Chapter 2

Plate Heat Exchangers

2.1 Introduction

Plate heat exchangers (PHE) are widely used for numerous industrial applications, such as food, pharmaceutical, heating, ventilating, air conditioning (HVAC), and manufacturing, among others, because of their high performance, compactness, and design flexibility (Ayub, 2003a), (Shah and Sekulić (2003) Wang, et al. (2007)). Generally, in all types of PHEs, the basic geometry is built from thin, pressed metal plates stacked together to form several narrow channels. Each channel consists of two corrugated plates with corrugation angle measured relative to the main flow direction and operating in the reverse directions on adjacent plates (Dović and Švaić, 2007). Based on the leak tightness required, PHEs can be categorized as gasketed, welded, or brazed. The gasketed type with chevron corrugated plates, which is the most common type in use today, is utilized in this study. Consequently, it will be the only type discussed in the following section.

2.2 Gasketed Plate Heat Exchangers

The gasketed or plate-and-frame plate heat exchanger consists of a series of thin rectangular corrugated metal plates, made from metal or alloy such as stainless steel, aluminum, or titanium. Plates are sealed via an elastomer gasket around the edges and carried on a frame as shown Fig. 2.1 (Kakac et al. (2012), Shah and Sekulić (2003) Gut et al. (2004)). Typical materials for the gasket are fluorinated rubber, nitrile–butadiene

rubber, chloroprene rubber, ethylene–propylene, and butyl rubber (Reppich, 1999). The gasket is used to prevent intermixing of the two fluids and fluid

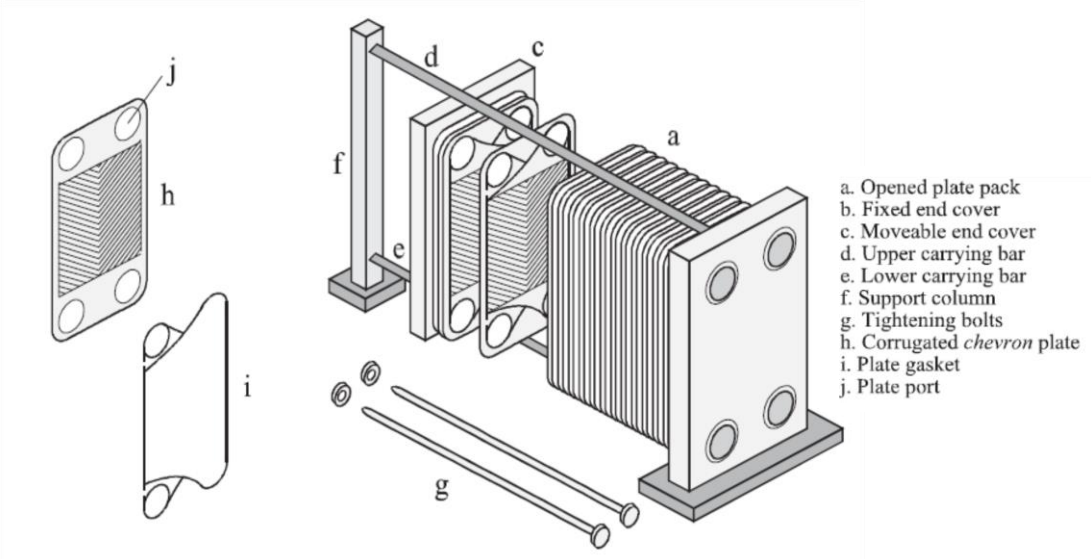

Fig. 2.1Gasketed plate heat exchanger structure (Gut et al. 2004)

leaking to the outside. These plates are stacked together to form multiple flow channels so that the two fluids can flow through alternate channels (Fig 2.2). Each corrugated or embossed plate has four parts for fluid entry and exit, serving as inlet and outlet ports.

More than sixty corrugation patterns have been developed to provide heat transfer enhancement; some of them are shown in Fig. 2.3. A plate with a corrugated sinusoidal shape surface is denoted by chevron type, Fig. 2.3-c, is used in most modern plate heat exchangers (Kakac et al. 2012).

Depending on the heat transfer duty, available pressure drop and other conditions such as minimum and maximum velocities, different possible flow arrangement can be obtained,

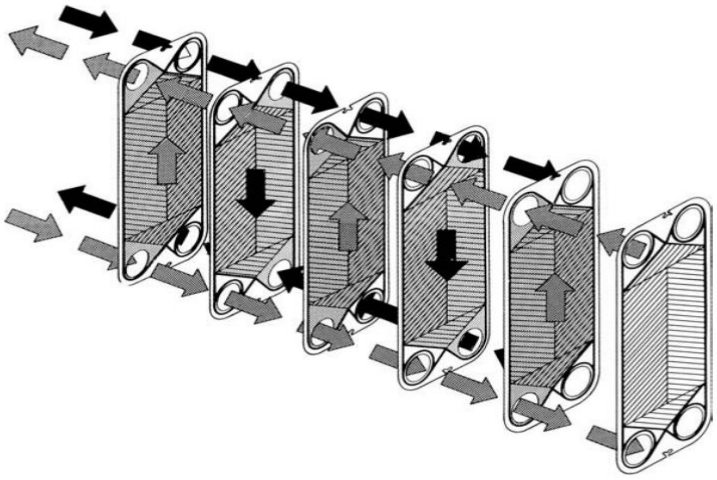

Fig. 2.2 Flow paths diagram in a gasketed plate heat exchanger (Kakac et al. 2012)

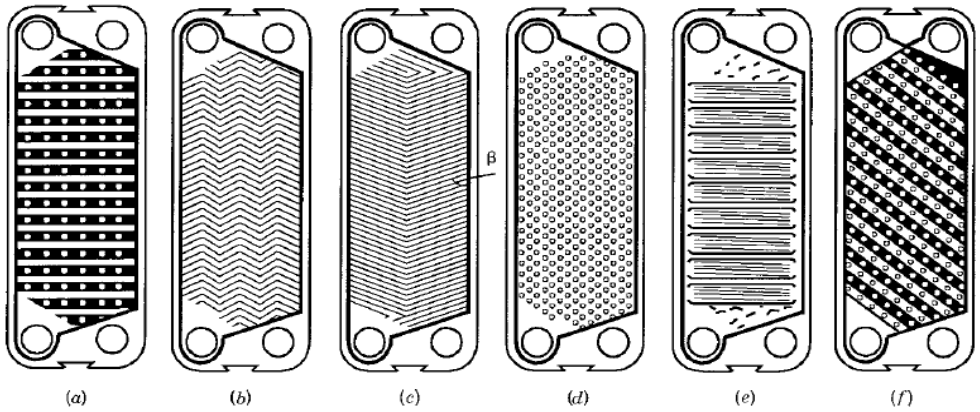

Fig. 2.3 Plates with different corrugation patterns: (a) washboard, (b) zig-zag, (c) chevron/herringbone, (d) protrusions and depressions (e) washboard with secondary corrugations (f) oblique washboard (Shah and Sekulić 2003).

e.x., U-arrangement, Z-arrangement, and multipass arrangements (Shah and Sekulić 2003).

PHEs offer several attractive features compared with traditional shell and tube heat exchangers, including (1) plate surface corrugations increase effective heat transfer area

and enhance heat transfer by promoting swirl or helical secondary flows, which mitigates fouling, disruption, and reattachment of boundary layers. This results in a heat exchanger that is compact in size with high performance. (2) PHE has a flexible thermal sizing, and the ease of assembly and disassembly provides PHE the ability to deal with the heat load requirement by adding or removing plates, which also allows accessibility for maintenance. (3) Heat losses to the surroundings are negligible because all the plate edges are only exposed to the atmosphere. (4) In a single PHE, different surface corrugation patterns can be used for balancing heat transfer load and available pressure drop to provide better optimization of operating conditions. (5) PHEs can work in very precise temperatures within approximately 1°C. However, the main disadvantage is that they are restricted to low operational pressures under 25 bars and temperatures under 250 °C due to the gasket materials and construction details (Wang et al. (2007), Kakac et al. (2012)).

The thermal hydraulic performance of PHEs is strongly affected by the geometrical characteristics of the plate surface features (Wang et al. 2007), which are discussed in the following section.

2.2.1 Chevron plate geometrical characteristics

The geometrical characteristics of the chevron plate are mainly characterized by the corrugation inclination angle, β, the corrugation amplitude, b, and the corrugation aspect ratio, γ, as presented in Fig 2.4, (Wang et al. 2007) which can be defined in the following way.

1. Chevron angle (corrugation inclination angle), β, is the angle between the corrugation and the vertical axis (main flow direction). In industry, it varies between $25° \leq \beta \leq 65°$ (Kakac et al. 2012).

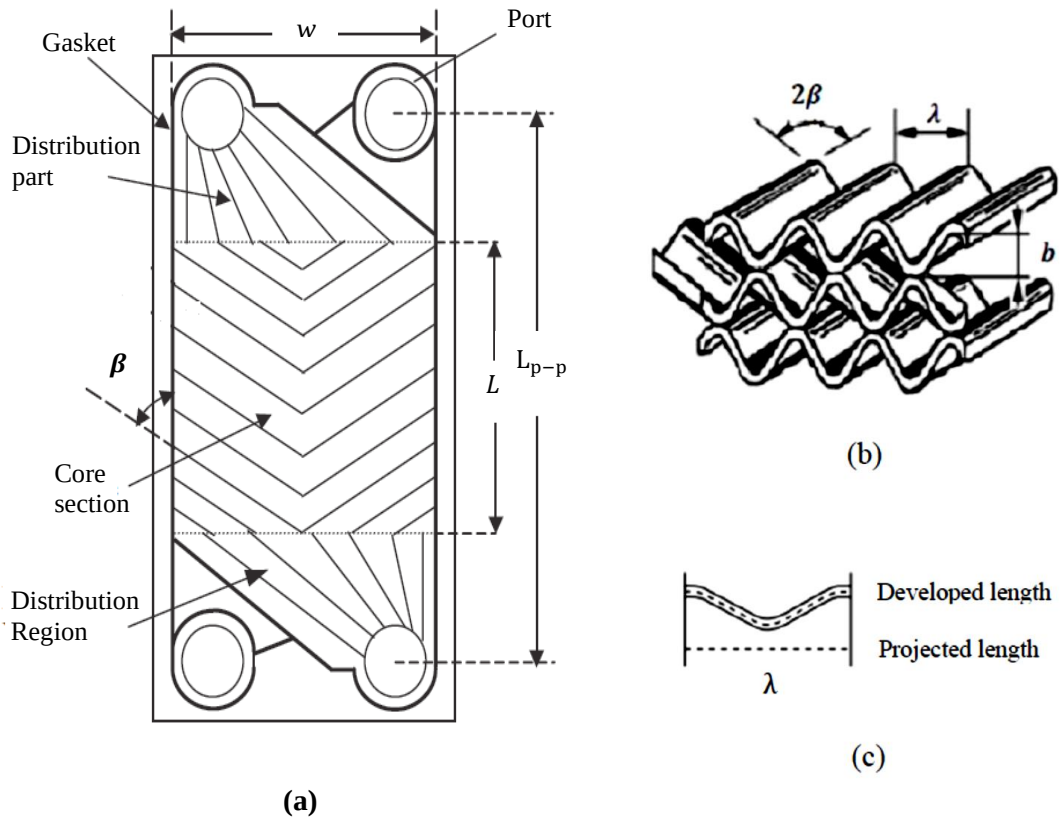

Fig. 2.4 Chevron plate parameters, (b) inter-plate flow channel
(c) developed and projected lengths ((after Wang et al. (2007) and Kakac et al. (2012))

Plates with high β, called hard plates, exhibit high heat transfer and pressure drop while others with low β, soft plates, experience low heat transfer and pressure drop. A common practice in industry is to build units with channels from different chevron angles, mixed configurations, as shown in Fig 2.5, to optimize the surface area at minimum pumping

power (Ayub 2003). In the mixed plate arrangments, the effective chevron angle is usually approximated by (Heavner et al. 1993)

$$\beta_{ave} = \left(\frac{\beta_1 + \beta_2}{2}\right) \tag{2.1}$$

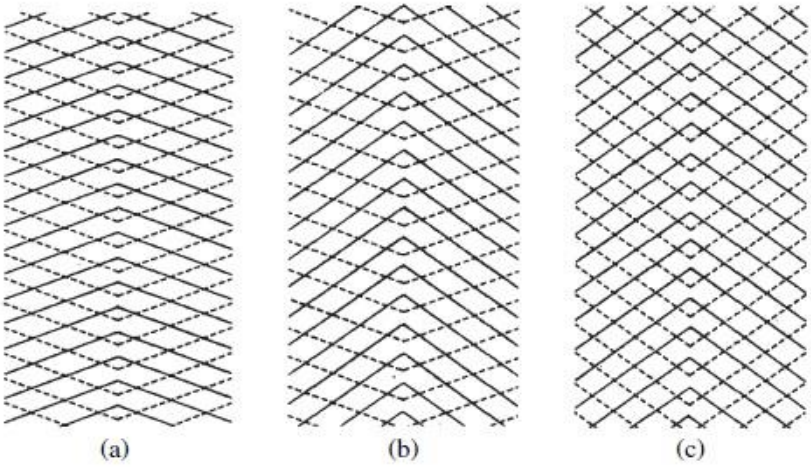

Fig. 2.5 Three different channel arrangements: (a) High Channel, (b) M Channel, (c) L Channel (Wang et al. 2007).

2. Surface enlargement factor, ϕ, is defined as the ratio between the effective area and the projected area.

3. Corrugation aspect ratio, γ, is defined as

$$\gamma = 2b/\lambda \tag{2.2}$$

where: b is the corrugation depth, and λ is a wavelength or the distance between two consecutive corrugation peaks.

The channel flow area can be calculated by

$$A_{ch} = b\, w \tag{2.3}$$

where b is the corrugation depth and w is the channel width inside the gasket.

Calculating heat transfer and pressure drop for a chevron PHE channel needs a characteristic length scale, which is a hydraulic diameter, D_h, or effective diameter, D_e. Hydraulic diameter D_h is defined as

$$D_h = \frac{4 \times minimum\ free\ flow\ area}{wetted\ perimeter} = \frac{4 \times b \times w}{2(b + w\phi)} \approx \frac{2b}{\phi} \tag{2.4}$$

with the approximation that $b \ll w$.

The equivalent diameter is

$$D_e = \frac{4\,wb}{2(w + b)} \approx 2b \tag{2.5}$$

Both definitions, D_e and D_h, are used for determining Reynolds number, friction factor, and Nusselt number. Moreover, there are also four definitions for channel flow length, see Fig. 2.4, which are

- L_{p-p} is the projected length between the center of inlet and outlet port (this will include effects of the distribution zones; their design differs from one manufacturer to another).
- L is the length of the corrugated core.
- L_{eff} is the effective flow length, which is the ratio between the developed (actual) heat transfer area and the width of the plate inside the gasket.

$$L_{\text{eff}} = \frac{A_{\text{eff}}}{w} \tag{2.6}$$

- $L_{p-p} - D_p$ is the length between L_{p-p} and L (it still includes the effects of the distribution zones).

In this study, the following definitions, as suggested in Shah and Sekulić (2003), are used:

equivalent diameter, D_e, length of the corrugated core, L and the projected area, A_{proj}. From the definitions of D_e and D_h, the relationship between them is $D_e = \phi D_h$.

2.3 Flow Pattern

Despite the long history of PHEs, only a few authors have conducted visualization studies with the aim of understanding the flow structure inside a PHE channel. The authors include Focke and Knibbe (1986), Gaiser and Kottke (1998), Hessami (2003), Dović et al. (2002) and Dović and Švaić (2007). These investigations were for single-phase flow and generally revealed the presence of two main flow patterns occurring simultaneously (Dović and Švaić (2007) and Sarraf et al. (2015)):

1- When $\beta < 45°$*:* the fluid flows mainly along the furrows on each wall and changes its direction only when it reaches the plate edge at which it is reflected to return along the furrows on the opposite wall (furrow flow pattern), sometimes called crossing flow, see Fig 2.6. (a).

2- When $\beta > 60°$: the fluid flows along the furrow, but reflection occurs at plate contact points instead of at the plate edge (zig-zag or helical flow pattern) sometimes referred to as longitudinal wavy flow, Fig. 2.6. (b). These experimental observations are also confirmed numerically by Zhang et al. (2006) and recently confirmed by Sarraf et al. (2015).

A schematic of the longitudinal component and the furrow component, which are dominant for flow in a channel with $\beta > 60°$ and $\beta < 45°$, respectively, within a basic cell of the corrugated channel, Fig. 2.7 (Dović and Švaić, 2007). For the case when $\beta = 90°$, Focke,

et al. (1985) and Focke and Knibbe (1986) reported that the two plates create a wavy channel and flow separation occurs at low Reynolds numbers, $Re \sim 20$, and the main flow becomes turbulent for $Re > 260$.

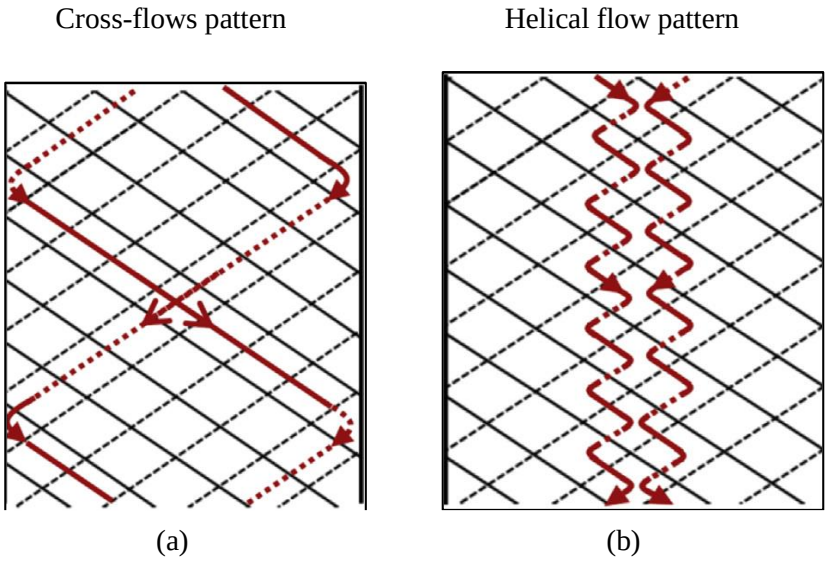

Fig. 2.6 Flow patterns in PHE channel (Sarraf et al. 2015)

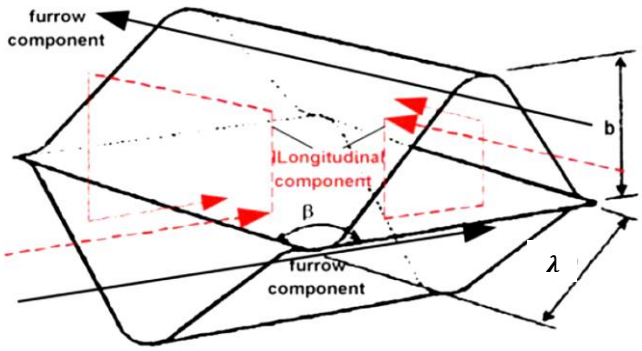

Fig. 2.7 Two flow components occur in a basic cell (Dović and Švaić 2007)

From the experimental study of Hessami (2003), it was found that the flow structure in chevron PHE channels is always erratic, random, and fully mixed with cross-streamline movements, even at low Reynolds numbers. Dović and Švaić (2007) noted that chevron

PHE channels produce a complex 3D flow pattern. Hessami (2003) also pointed out that using a laminar flow expression in chevron PHEs appears inappropriate since the flows may not strictly satisfy the definition of laminar flow, even at low Reynolds numbers. Thus, it was suggested that it is more appropriate to call these flows low Re mixed flow and high Re mixed flow rather than laminar and turbulent flow, respectively. Furthermore, Dović and Švaić (2007) reported that transition from laminar to turbulent flow may occur as early as $Re = 10$ and fully turbulent flow is obtained at $Re \cong (300 - 700)$, which mainly depends on the chevron angle.

2.4 Parameters Affecting Performance of Chevron Plate Heat Exchangers

Thermal-hydraulic performance of the PHE is affected by varying plate surface parameters such as corrugation angle, aspect ratio, and surface area enlargement factor (Wang et al. 2007).

2.4.1 Chevron Angle

The effect of chevron angle on heat transfer and / or pressure drop in PHEs has been studied by several authors, such as Okada et al. (1972), Bond (1981), Focke et al. (1985), Heavner et al. (1993), Stasiek et al. (1998), Muley et al. (1999), Muley and Manglik (1999), Hessami (2003), Dović and Švaić (2007), Khan et al. (2010), and Sarraf et al. (2015), Mohebbi and Veysi (2019), Alzahran et al. (2019), among many others. All these studies generally lead to the same conclusions: bothNu and f increase with increased chevron angle up to a certain angle, as illustrated in Fig. 2.8 and 2.9. This was attributed by Muley and Manglik (1999) to the increased intensity of swirl flows generated by larger chevron angles. Moreover,

Hessami (2003) found that plates with $\beta = 60°$ showed an early transition from laminar to turbulent flow compared to other plates with $\beta = 45°$.

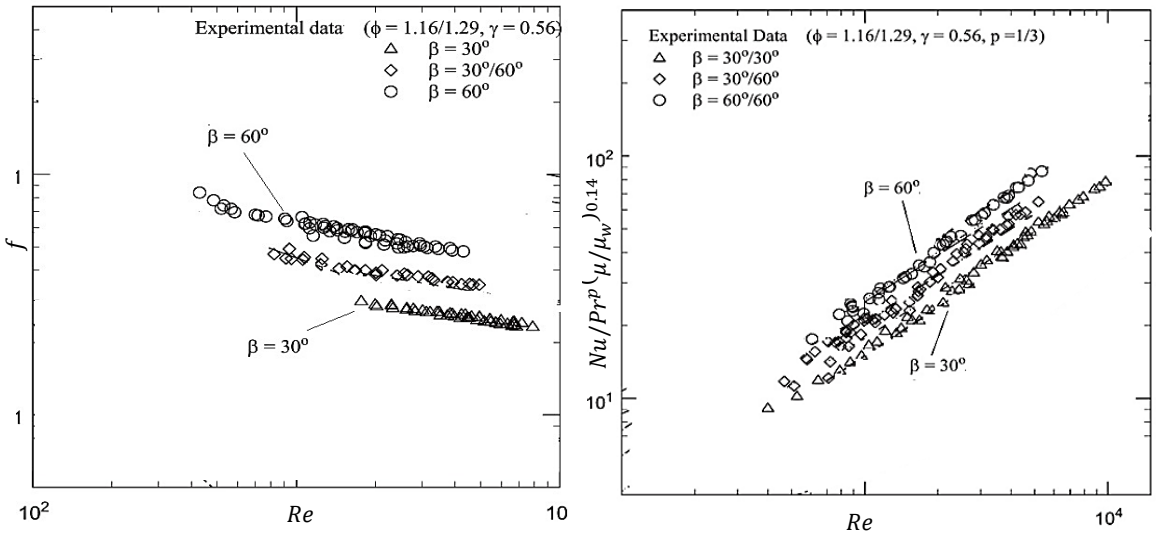

Fig. 2.8 Variation of f and Nu with chevron angle for turbulent flow (after Muley and Manglik 1999).

2.4.2 Aspect ratio

In the literature, different definitions have been used for the aspect ratio of PHEs. Some authors referred to the aspect ratio of the plate, as in the work of Lee et al. (2000), which was the ratio between the plate length and plate width. Other researchers, such as Gaiser and Kottke (1998), used the ratio between the corrugation wavelength and corrugation depth. Wang et al. (2007) defined it as referenced in this thesis, which is twice the corrugation depth to the corrugation wavelength. According to the experimental results of Gaiser and Kottke (1998) and Okada et al. (1972) for turbulent flow conditions and Dović et al. (2002) for laminar flow, as well as the numerical work of Lee and Lee (2014), both Nu and f increase as the ratio of the corrugation depth to the corrugation pitch increases

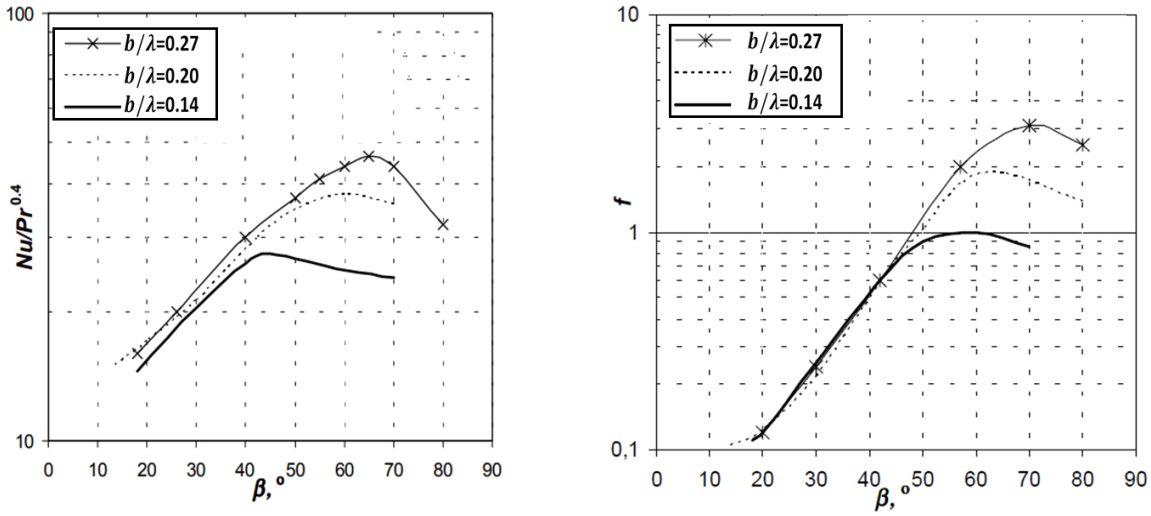

Fig. 2.9 Influence of (b/λ) and β on *Nu* and *f* of chevron channels at $Re = 2000$ (after Dović and Švaić 2007)

for plates with $\beta > 45°$. Gaiser and Kottke (1998) noted that for plates with $\beta < 45°$ the b/λ ratio does not have a significant effect on the thermal-hydraulic performance of PHE, as shown in Fig. 2.9. This result is anticipated, as a decrease of b/λ causes a reduction of the corrugation height, hence, the flow inside the channel will approach that in a flat plate channel.

2.4.3 Surface Enlargement Factor

Muley and Manglik (1999) found that the Nusselt number and isothermal friction factor increase by increasing the surface area enlargement factor, Fig. 2.10. By increasing the surface enlargement factor, ϕ, deeper corrugations are obtained, which leads to an increase in the effective surface area and promotes more turbulence, which yields an increase in heat transfer and pressure drop. Martin (1996) found an expression from a three-point integration formula approximate ϕ,

$$\phi(X) \approx \frac{1}{6}\left(1+\sqrt{1+X^2}+4\sqrt{1+X^2/2}\right) \tag{2.7}$$

where $X = \pi b/\lambda$.

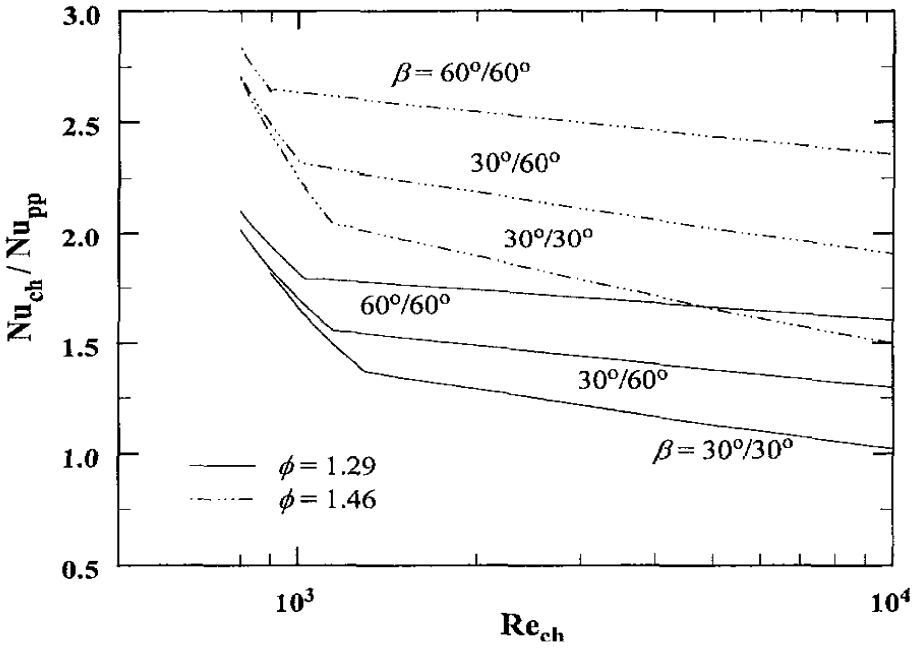

Fig. 2.10 Effect of β and ϕ on heat transfer enhancement in a PHE (Muley and Manglik 1999)

2.5 Conclusions

This chapter reviewed plate heat exchangers with a focus on the chevron type and presented the geometrical characteristics of the chevron plate. Flow patterns inside PHE channels were also addressed. The main chevron plate surface parameters that influence the thermal-hydraulic performance of the PHE were discussed, which are namely, chevron angle, aspect ratio, and surface area enlargement factor.

Chapter 3

Literature Review

3.1 Introduction

This chapter provides a review of the present state of the art in predictive models / correlations for predicting the heat transfer coefficient and friction factor, in single phase flow, through plate heat exchangers. The survey includes general heat transfer and pressure drop models and /or correlations based on experimental and numerical studies.

3.2 Fluid Flow and Heat Transfer Models for Chevron Plate Heat Exchangers

A review of the available literature has shown that only a few authors attempted to develop a general model to predict the friction factor and /or heat transfer coefficient for single-phase flow in chevron plate heat exchangers. The papers include Wanniarachchi et al. (1995), Martin (1996), Charre et al. (2002), Abu-Khader (2007), Dović et al. (2009), Arsenyeva et al. (2011) and Arsenyeva et al. (2014).

Wanniarachchi et al. (1995) proposed general correlations to predict Nu and *f* in single-phase chevron plate heat exchangers. For laminar and turbulent regions, they used curves presented by Bond (1981) and experimental data documented by Heavner et al. (1993) to develop their correlations. The correlations were combined in a third–order asymptotic form to cover all flow regions, including the transition regime:

$$f_{D_h} = \left[f_l^3 + f_t^3\right]^{1/3} \tag{3.1}$$

where

$$f_l = \frac{1774}{Re_{D_h}\theta^{1.026}} \tag{3.2}$$

$$f_t = \frac{46.6}{Re_{D_h}^{(0.00423\theta - 0.0000223\theta^2)}\theta^{1.08}} \tag{3.3}$$

$$Nu_{D_h} = [Nu_l^3 + Nu_t^3]^{1/3} \cdot Pr^{\frac{1}{3}}\left(\frac{\mu_m}{\mu_w}\right)^{0.17} \tag{3.4}$$

and

$$Nu_l = \frac{3.65}{Re_{D_h}^{0.339}\theta^{0.455}} \tag{3.5}$$

$$Nu_t = \frac{12.6}{\theta^{1.142}} Re_{D_h}^{(0.646 - 0.00111\theta)} \tag{3.6}$$

These correlations are valid for $1 \leq Re_{D_h} \leq 10{,}000$, $22.5° \leq \theta \leq 62°$, $\theta = 90 - \beta$. However, they recommended that if $\theta < 28°$, then $\theta = 28°$ should be used to reduce the over prediction of Nu.

Martin (1996) developed semi-theoretical correlations to predict the Nusselt number and friction factor for chevron plate heat exchangers based on the analogy between heat transfer and pressure drop. The results of the experimental work of Heavner et al. (1993) and the flow pattern observations of Focke et al. (1985) and Gaiser and Kottke (1989) were employed to develop the models. These observations demonstrated that two flow patterns exist simultaneously: furrow flow and longitudinal flow. The developed model for the friction factor was based on the superposition of the aforementioned flow components over the range of $15° \leq \beta \leq 85°$. For the heat transfer coefficient, the author extended the Lévêque theory into the turbulent region to develop a Nu correlation. The heat transfer

coefficient and the friction factor were given as a function of ($f\ Re^2$ and β) and (β, Re), respectively. Most constants in the correlations were determined from the experimental work of Heavner et al. (1993) and Focke et al. (1985). The correlations were based on D_h for the Darcy friction factor and the following for the Nusselt number

$$\frac{1}{\sqrt{f_D}} = \frac{\cos\beta}{\sqrt{0.18\tan\beta + 0.36\sin\beta + f_0/\cos\beta}} + \frac{1-\cos\beta}{\sqrt{3.8\cdot f_{1,0}}} \tag{3.7}$$

$$Nu_{D_h} = 0.122\left[f_D . {Re_{D_h}}^2 \sin(2\beta)\right]^{0.374} \cdot \ \ Pr^{1/3} \cdot (\mu/\mu_w)^{1/6} \tag{3.8}$$

where

$$f_{1,0} = \begin{cases} \dfrac{597}{Re_{D_h}} + 3.85 & Re_{D_h} < 2000 \\ \dfrac{39}{{Re_{D_h}}^{0.289}} & Re_{D_h} \geq 2000 \end{cases} \tag{3.9}$$

$$f_0 = \begin{cases} \dfrac{64}{Re_{D_h}} & Re_{D_h} < 2000 \\ \left(1.8\ log_{10}Re_{D_h} - 1.5\right)^{-2} & Re_{D_h} \geq 2000 \end{cases} \tag{3.10}$$

The variables f_0 and $f_{1,0}$ represent the friction factors for the two limiting cases: $\beta = 0°$ for a straight channel and $\beta = 90°$ for a flow across a wavy channel between two parallel plates. The range of the Reynolds number was not given in the original work, however, it appears to be from 400 to 10,000 since determining many of the equations' constants depended on the work of Heavner et al. (1993).

Charre et al. (2002) proposed a general model to predict Nu and *f* for single phase flow for PHEs based on the theory of porous media. The authors determined two new equations to calculate the number of pores and hydraulic diameter (pore diameter) to be used in the model. The developed equations for predicting Nu and *f* were

$$\frac{f}{2} = C_1(T_v, T_{hor})\, Re_{pore}^{c_1(T_v, T_{hor})} \tag{3.11}$$

$$Nu = A_1(T_v, T_{hor})\, Re_{pore}^{a_1(T_v, T_{hor})}\, Pr^{\frac{1}{3}} \left(\frac{\mu}{\mu_m}\right)^{p_1} \tag{3.12}$$

where

$$D_{h\,pore} = \frac{2b\lambda}{\sqrt{4b^2 + \lambda^2}} \tag{3.13}$$

where T_v , T_{hor} and Re_{pore} are the vertical and horizontal tortuousness coefficients, and Reynolds number of the pore, respectively. The constants A_1, a_1, C_1, c_1 and $p_1$need to be determined experimentally. This model can be used in the core region of the plate and the distribution zone. It predicted the Nusselt number within $\pm$ 30 % and the friction factor within $\pm$ 15 %. However, they did not compare their own model results and experimental data with other results reported in the literature.

Abu-Khader (2007) proposed two semi-theoretical correlations for pure and mixed plate angles to calculate the *Nu* of plate heat exchangers. The developed equations were based on the Modified Generalized Lévêque Equation and data from Kumar (1984). It has been observed that the Generalized Lévêque Equation and Modified Generalized Lévêque Equation provide acceptable results for $\theta = 30°, \text{and } 50°$ and fail to provide acceptable results for $\theta = 45°,\ 60° \text{ and } 65°$. The new developed equations for soft plates, $\theta > 50°$, and hard plates, $\theta \leq 50°$, showed good agreement when compared with some correlations from the literature. These correlations are divided into two categories for pure and mixed angle plates.

$$\text{Pure plates} \begin{cases} \text{Hard}, Nu_{D_h} = 0.124\ Pr^{1/3} \left(\frac{\mu}{\mu_w}\right)^{1/6} \left(f_{D_{D_h}} Re_{D_h}^2 \sin(2\theta)\right)^{0.378} \\ \text{Soft},\ Nu_{D_h} = 0.071\ Pr^{1/3} \left(\frac{\mu}{\mu_w}\right)^{1/6} \left(f_{D_{D_h}} Re_{D_h}^2 \sin(2\theta)\right)^{0.397} \end{cases} \tag{3.14}$$

$$\text{Mixed plates} \begin{cases} \text{Hard}, Nu_{D_h} = 0.122\ Pr^{1/3} \left(\frac{\mu}{\mu_w}\right)^{1/6} \left(f_{D_{D_h}} Re_{D_h}^2 \sin(2\theta)\right)^{0.374} \\ \text{Soft}, Nu_{D_h} = 0.099\ Pr^{1/3} \left(\frac{\mu}{\mu_w}\right)^{1/6} \left(f_{D_{D_h}} Re_{D_h}^2 \sin(2\theta)\right)^{0.385} \end{cases} \tag{3.15}$$

Dović et al. (2009) conducted theoretical and experimental study with the aim of developing a general model to predict the heat transfer and pressure drop in PHEs' channels of arbitrary geometry $(\beta, b/\lambda)$. The authors also conducted visualization tests on two different chevron plates with $\beta = 28\,°,\ \beta = 65°$ and $b/\lambda = 0.26$ to investigate the flow characteristics in the channels of PHEs. The tested fluids were water and glycol / water mixture as two different viscous fluids. Based on the visualization tests and link between heat transfer and pressure drop, they developed a semi-theoretical model, similar to that of Martin (1996). A large disagreement of $\pm\,(10-50)\%$ was found between the newly developed model and experimental data with respect to the friction factor. However, the Nu correlation has reasonable agreement, on average within $\pm$ 14% of their experimental results and within $\pm$ 35% when compared to the works of Bond (1981), Heavner et al. (1993), Muley and Manglik (1999) and Thonon et al. (1995). The proposed equations, based on D_h, for the whole channel are

$$Nu_{D_h} = C_2\left(C_3 + Re_{D_h,\text{sine}}\, B\right)^{0.375} Re_{D_h,\text{sine}}^{0.375}\ Pr^{\frac{1}{3}} \left(\frac{\mu}{\mu_w}\right)^{0.14} \frac{D_h}{D_{h,\text{sine}}} \tag{3.16}$$

$$f_{D_h} = \begin{cases} \dfrac{f_{\text{sine}}}{2\cos^3\beta}\ \dfrac{D_h}{D_{h,\text{sine}}} & \beta \le 60° \\ \dfrac{f_{\text{sine}}}{\cos^2\beta}\ \dfrac{D_h}{D_{h,\text{sine}}} & \beta > 60° \end{cases} \tag{3.17}$$

where

$$f_{\text{sine}} = f_{app} = \frac{C_2}{Re_{D_h,\text{sine}}} + B_1\,,\; C_2 = 0.25804\left(\frac{D_{h,\text{sine}}}{L_{cell}}\right)^{0.375} \tag{3.18}$$

$$C_3 = f_{\text{fd}}\, Re_{D_h,\text{sine}}\,,\; B_1 = \frac{K(\infty)\, D_{h,\text{sine}}}{4L_{cell}} \tag{3.19}$$

$$Re_{D_h,\text{sine}} = Re_{D_h}\frac{1}{\cos\beta}\,\frac{D_{h,\text{sine}}}{D_h} \tag{3.20}$$

$$D_{h,\text{sine}} = \lambda(0.1429x^3 - 0.6235x^2 + 1.087x - 0.0014) \tag{3.21}$$

$$L_{cell} = \begin{cases} L_{\text{furr}} = \dfrac{\lambda}{\sin(2\beta)} & \beta \le 60° \\ L_{long} = \dfrac{\lambda}{\sin\beta} & \beta > 60° \end{cases} \tag{3.22}$$

$$f_{fully}\, Re_{\text{sine}} = 2.662x^4 - 10.586x^3 + 11.262x^2 - \; 0.1036x + 9.6 \tag{3.23}$$

$$K_e(\infty) = -5.888x^4 + 9.4613x^3 - 4.248x^2 - 0.1333x + 2.648 \tag{3.24}$$

$$K_d(\infty) = -1.7237x^4 + 2.7669x^3 - 1.2651x^2 - 0.0097x + 1.512 \tag{3.25}$$

$$K(\infty) = 2[K_e(\infty) - K_d(\infty)],\; x = b/\lambda \tag{3.26}$$

where $K(\infty)$ is the incremental pressure drop, $K_d(\infty)$ is the momentum flux correction factor, and $K_e(\infty)$ is the kinetic energy correction factor. The authors used $K(\infty)$ for the fully developed region in a sine duct from (Shah, 1975), for the entrance region because there was no K(∞) equation for the entrance region of a sine duct available in the literature. These correlations are valid for $Re_{D_h} = 2 - 10{,}000, \beta = 15° - 67°$ and $\text{b}/\lambda = (0.26 - 0.4)$. It should be noted that constants in the developed expressions have been adjusted to fit the experimental data.

Arsenyeva et al. (2011) proposed another general correlation to predict the friction

factor for PHEs' channels in the corrugated region as a function of the chevron angle, β, aspect ratio, γ, and Reynolds number. The suggested equation was developed based on experimental data of Focke et al. (1985) and Tovazhnyansky et al. (1980) for channels with sinusoidal, $\gamma = 1$, and triangular corrugation, with rounded edges, $\gamma = 5/9$, respectively. The equation form was quoted from Churchill (1977) for straight tubes and covered all flow regions. Their correlation for the Fanning friction factor was

$$f_{D_e} = 2\left[\left(\frac{12 + P_2}{Re_{D_e}}\right)^{12} + \frac{1}{(A_2 + B_2)^{3/2}}\right]^{1/12} \tag{3.27}$$

$$A_2 = \left[P_4\, ln\left(P_5\left(\left(\frac{7 \times P_3}{Re_{D_e}}\right)^{0.9} + 0.27 \times 10^{-5}\right)^{-1}\right)\right]^{16},\ B_2\left(\frac{37530 \times P_1}{Re_{D_e}}\right)^{16} \tag{3.28}$$

where, P_1, P_2, P_3, P_4 and P_5 are parameters defined by channel corrugation shape.

$$P_1 = exp(-0.15705 \cdot \beta), P_2 = \frac{\pi \cdot \beta \cdot \gamma^2}{3},\ P_3 = exp\left(-\pi \cdot \frac{\beta}{180} \cdot \frac{1}{\gamma^2}\right) \tag{3.29}$$

$$P_4 = \left[0.061 + \left(0.69 + \tan\left(\beta \frac{\pi}{180}\right)\right)^{-2.63}\right](1 + (1 - \gamma)\ 0.9\beta^{0.01}),$$
$$P_5 = 1 + \frac{\beta}{10} \tag{3.30}$$

This correlation predicted the data of Focke et al. (1985) and Tovazhnyansky et al. (1980), with an average mean-square error deviation of less than 10% and differed by less than 20% for $\beta = 65°$ and from 20% to 50% for $\beta = 28°$, when compared to experimental data from Dović et al. (2009). Regarding channels with a triangular form of corrugation, the agreement was within 20% for $\beta = 14°$ to 72° and up to 35% for $\beta = 10°$ relative to

the experimental data from Savostin and Tikhonov (1970). The preceding correlation is valid for $5 < \mathrm{Re}_{D_e} < 25{,}000, 14° \leq \beta \leq 72°$, and $0.52 \leq \gamma \leq 1.02$.

Kapustenko et al. (2011) used a modified Reynolds analogy of heat and momentum transfer to propose a new equation to predict the film heat transfer coefficients in PHE channels based on a data of hydraulic resistance of the main corrugated region. They assumed that the relation between friction shear stress on the channel wall and heat transfer in plate and tube heat exchangers are equal. This correlation is applicable for both sinusoidal and triangular plates with rounded edges and presented as follows:

$$Nu = 0.065\, Re^{6/7} \left(\psi \frac{f}{\phi}\right)^{3/7} Pr^{0.4} \left(\frac{\mu}{\mu_w}\right)^{0.14} \tag{3.31}$$

where

$$A_3 = 380/[\tan(\beta)]^{1.75}, \psi = \begin{cases} (Re/A_3)^{-0.15\sin\beta} & Re > A_3 \\ 1 & Re \leq A_3 \end{cases} \tag{3.32}$$

The variable f can be calculated from Eq. (3.27). This equation is valid for $100 < Re < 25{,}000, 14° \leq \beta \leq 65°, 0.5 \leq \gamma \leq 1.5,\ 1.14 < \phi < 1.5$.

Arsenyeva et al. (2014) proposed a new equation to predict the film heat transfer coefficients for turbulent flows inside PHE channels based on the Lyon Equation, which takes the form

$$Nu_{D_e} = \frac{0.131 \cdot R_S \cdot Pr}{ln\left(\frac{R_S}{760}\right) - \frac{14450}{R_S^2} + \frac{340}{R_S} + B_z + 2.52Pr \cdot \varphi(Pr)} \tag{3.33}$$

where

$$B_z = 1.85\left[Z^3 \ln\left(\frac{1+5Pr}{1+0.36Pr}\right) + \frac{131.24}{R_S}(1 - Z + Z^2)\right] \tag{3.34}$$

$$R_S = Re_{D_e} \cdot \sqrt{4f \cdot \psi/\phi}\,, Z = 1 - \frac{(Pr-1)\sqrt{32}}{0.2PrR_S} \tag{3.35}$$

$$\varphi(Pr) \approx 0.167Pr^{-0.04} \cdot \arctan\left(6.8\sqrt[3]{0.00065Pr}\right) \tag{3.36}$$

Here, f and ψ are given by Eqns. (3.27) and (3.32) respectively, some empirical constants were determined from the PHE experiment with water as a working fluid. Equation (3.33) gives reasonable results in the range of $0.7 \leq Pr \leq 7$.

3.3 Correlations

Numerous correlations have been suggested for predicting heat transfer and pressure drop for single phase flow in PHEs with symmetric or mixed-plate arrangements. Each study is limited to a particular PHE geometry, fluid, and operating condition. Most of the correlations have a similar form to the Dittus-Boelter equation, which was originally developed for turbulent heat transfer in a smooth tube, while others added the viscosity ratio term as a correction factor. Thus, for single phase flow, empirical expressions are usually used to represent *Nu* and *f* in PHEs (Palm and Claesson (2005) and Wang et al. (2007)):

$$Nu = B\ Re^c\ Pr^d \tag{3.37}$$

$$f = C\ Re^g \tag{3.38}$$

where B, C, c, g and d are constants depending on the heat exchanger geometry. Some investigators expressed the constants B, C, c and g as a function of the chevron angle and surface area enlargement factor or the aspect ratio to consider their effects on the thermal hydraulic performance of PHEs. A comprehensive list of devised correlations for

predicting the heat transfer and pressure drop in PHEs for single phase flow was reported by Talik et al. (1995) and almost a decade later by Ayub (2003).

3.3.1 Experimental Studies

The experimental study conducted by Focke et al. (1985), based on mass transfer and pressure drop data, aimed to investigate the effect of the corrugation inclination angle, β, on the thermal-hydraulic performance of PHEs. The tested plates had inclination angles of $\beta = 0°, 30°, 45°, 60°, 72°, 80°$ and $90°$, an enlargement factor of $\phi = 1.464$ and a corrugation depth of 2.5 mm. The working fluid was water and the range of Reynolds number, based on the equivalent diameter (twice average plate spacing), was $20 < \mathrm{Re}_{D_e} < 56{,}000$. It was observed that at a constant Reynolds number, increasing β from 0° to 80° causes an increase in pressure drop by more than 2.5 orders of magnitude, while the heat transfer increases by a factor of 4 to 10. Moreover, at higher angles, especially $\beta = 90°$, flow separation occurred, resulting in a notable decrease in pressure drop and heat transfer, which was almost the same magnitude as $\beta = 60°$. At an angle $\beta = 80°$, parallel zig-zag flow patterns occurred, the pressure drop and heat transfer were only slightly higher than $\beta = 72°$. They also mentioned that increasing β from 30° to 60° tended to generate more secondary flows, which enhances heat transfer, however, this also increases the pressure drop. The heat transfer data were obtained using the mass transfer analogy and the Colburn factor, j, correlations were proposed based on the projected area. They proposed sets of correlation for f and j depending on Re and β.

Gaiser and Kottke (1998) experimentally investigated the effects of wavelength and

inclination angle in the turbulent regime, at fixed $Re = 2000$, on the homogeneity of the local heat transfer coefficient in corrugated plate heat exchangers. Heat transfer was enhanced by increasing the inclination angle up to 80°, due to an increase of the longitudinal flow components' effect, while at low inclination angles, the furrow flow component dominates, resulting in a low heat transfer coefficient. For the wavelength effects, it was concluded that plates with low inclination angles, especially with short wavelengths, lead to an inhomogeneous distribution in local heat transfer, as well as in plates with high inclination angles and long wavelengths. However, plates with high inclination angles and short wavelengths (deeper corrugations) showed high heat transfer coefficients, which was attributed to the ratio between the longitudinal flow and furrow flow components being approximately equal at high inclination angles. The authors determined that as Reynolds number increases, at a fixed wavelength, $\lambda/\mathrm{b} = 5.5$ and $\beta = 45°$, the intensity of the interaction between the furrow flow component and the longitudinal flow component rises, leading to more uniform distribution of local heat and mass transfer coefficients.

Muley and Manglik (1999) conducted experimental studies on three (PHE) units of different chevron angles, $\beta = 30°/30°,\ 30°/60°$, and $60°/60°$ and the same enlargement factor, $\phi = 1.29$. Water was used as the working fluid, $2 < Pr < 6$, and the flow rate varied from $600 \leq Re_{D_e} \leq 10000$, in the turbulent regime. The authors found that by increasing β, Nu increased two to five times more than in a flat plate channel. However, this was accompanied by a high pressure drop as f increased 13 to 44 times higher compared to flat plate channels. Also, increasing ϕ causes an increase in Nu. To extend

the applicability of their correlations, the results were correlated with other data to cover a wide range of ϕ values. It should be noted that for Nu calculations, the experimental data have been reduced based upon the total effective heat transfer area. The final correlations for Nu and f, including β and ϕ effects, were proposed in the following forms:

$$\begin{aligned} Nu_{D_e} = {} & [0.2668 - 0.006967\beta + 7.244 \times 10^{-5}\,\beta^2] \\ & \times [20.78 - 50.94\phi + 41.16\phi^2 - 10.51\phi^3] \\ & \times Re_{D_e}^{\left[0.728+0.0543\times\sin\left[\left(\pi\frac{\beta}{45}\right)+3.7\right]\right]} \times Pr^{1/3}\left(\frac{\mu}{\mu_w}\right)^{0.14} \end{aligned} \tag{3.39}$$

$$\begin{aligned} f_{D_e} = {} & [2.917 - 0.1277\,\beta + 2.016 \times 10^{-3}\,\beta^2] \\ & \times [5.474 - 19.02\phi + 18.93\phi^2 - 5.341\phi^3] \\ & \times Re_{D_e}^{-\left[0.2+0.0577\times\sin\left[\left(\pi\frac{\beta}{45}\right)+2.1\right]\right]} \end{aligned} \tag{3.40}$$

These correlations are generally valid for $30° \le \beta \le 60°$, $1 \le \phi \le 1.5$ and $Re_{D_e} \ge 10^3$. The Nu and *f* correlations were in good agreement with experimental data, within $\pm 10\%$ and $\pm 5\%$, respectively.

Muley et al. (1999) performed experiments on a single-pass plate heat exchanger and presented their *Nu* and f results for the cooling of hot vegetable oil ($2 < Re_{D_e} < 400$, $0.118 < \frac{\mu}{\mu_w} < 0.393, 130 < Pr < 290$) in a single-phase flow. The plates had three different corrugation angles of $\beta = 30°/30°$, $30°/60°$, and $60°/60°$, an enlargement factor of $\phi = 1.29$ and a corrugation aspect ratio of $\gamma = 0.56$. They studied the influence of the chevron angle, and corrugation aspect ratio γ on Nu and f and found that increasing β tended to generate more secondary flows or increase the intensity of swirl, which

enhances heat transfer. The Nusselt number was three times higher than for an equivalent flat plate at the same Re. However, this also increases f up to 6.6 times that of an equivalent flat plate. Although there was no swirl mixing observed in the low Re regime $(Re_{D_e} < 25)$, f was higher than in a flat-plate channel. This was due to the increased surface area or effective length. For $Re_{D_e} > 25$, the influence of the onset of swirl flows on f was clearly seen by the deviation of f from the log-linear behavior of $f - Re$ as Re increased. They found that the Nusselt number, as well as the friction factor increased as β and/or γ increased. Their proposed equations for predicting Nu and f, based on the effective flow length, in a single-phase laminar flow were:

$$f_{D_e} = \left[\left(\frac{30.2}{Re_{D_e}}\right)^5 + \left(\frac{6.28}{{Re_{D_e}}^{0.5}}\right)^5\right]^{\frac{1}{5}} \cdot \left(\frac{\beta}{30}\right)^{0.83} \tag{3.41}$$

which is valid for $30° \leq \beta \leq 60°$, $\gamma = 0.56$, $2 \leq Re_{D_e} \leq 300$, and

$$Nu_{D_e} = 1.6774(D_e/L)^{\frac{1}{3}}\left(\frac{\beta}{30^\circ}\right)^{0.38} {Re_{D_e}}^{0.5} Pr^{1/3}\left(\frac{\mu}{\mu_w}\right)^{0.14} \tag{3.42}$$

which is valid for $30° \leq \beta \leq 60°$,$\gamma = 0.56$, $30 \leq Re_{D_e} \leq 400$.

The effect of corrugation height and depth on Nu and f in a corrugated channel has been studied experimentally by Islamoglu and Parmaksizoglu (2003) for two channel heights, 5mm and 10mm and a slope angle of $20°$, with air as a working fluid. They found that both the fully developed friction factor and Nusselt number increase by increasing the channel height over the range of $1200 < Re_{Dh} < 4000$. Similar channel configurations were also studied in the past by O'Brien and Sparrow (1982).

Khan et al. (2010) conducted an experiment to study the effect of corrugation angle on the thermal performance of a commercial chevron plate heat exchanger in a single-phase flow (water-to-water). They examined three different chevron plate arrangements" two symmetric,$30°/30°$,$60°/60°$ and one mixed, $30°/60°$. The mixed configuration, $30°/60°$, is usually approximated by $45°$. All plates were tested under turbulent flow conditions in a range of $500 < Re_{D_h} < 2500$ and $3.5 < Pr < 6.5$. They found that the Nusselt number increases with an increasing Reynolds number and chevron angle. Based on the experimental results, they derived a Nu correlation as a function of chevron angle, Prandtl number, Reynolds number and viscosity variation, which was

$$Nu_{D_h} = \left(0.0161\frac{\beta}{\beta_{max}} + 0.1298\right) Re_{D_h}^{\left(0.198\frac{\beta}{\beta_{max}}+0.6398\right)} Pr^{0.35} \left(\frac{\mu}{\mu_w}\right)^{0.14} \qquad (3.43)$$

The mean deviations of the proposed correlation were $\pm 2\%$, $\pm 1.8\%$ and $\pm 4\%$ for $30°/30°$, $60°/60°$ and $30°/60°$ plate configurations, respectively.

3.3.2 Numerical Studies

Considerable research work on the flow in corrugated plate heat exchangers using numerical simulations and CFD has been reported by Ciofalo et al. (1996), Ding and Manglik (1996), Fischer and Martin (1997), Mehrabian and Poulter (2000), Ciofalo et al. (2000), Kanaris et al. (2005), Metwally and Manglik (2004), Pelletier et al. (2005), Zhang et al. (2006), Kanaris et al. (2006), Fernandes et al. (2007), Tsai et al. (2009) Gherasim et al. (2011), Zhang and Che (2011), Ikegami et al. (2015), Sarraf et al. (2015), and Wang et al. (2017) among many others. Some of them will be discussed.

Hydrodynamic and thermal fully developed laminar flows in double-sine shaped

straight ducts, $\beta = 0°$, with a constant property have been studied analytically by Ding and Manglik (1996). Solutions for the velocity and temperature fields were obtained by applying the Galerkin integral method. Both heat transfer boundary conditions, constant heat flux and constant wall temperature were considered. An increase in the friction factor was observed with the increase in the duct aspect ratio from 0.125 to 8 while the Nusselt number rises for almost all values of the aspect ratio for $\gamma < 2$ and then started to decrease for $\gamma > 2$.

Fischer and Martin (1997) employed Poiseuille's law, $fRe = \mathrm{K}$, and performed a numerical study using the finite element method to calculate the constant , K values for ducts confined by two corrugated walls for a wide range of b/λ. Two cases were considered, including when the corrugation of the two walls was in phase and phase shifted by π. The values of K as a function of the aspect ratio has been tabulated for different types of sine ducts.

Ciofalo et al. (1996) performed a numerical study to simulate the fluid flow and heat transfer in corrugated channels using different approaches. Laminar flow assumptions, standard $\mathrm{k}-\varepsilon$ turbulence model with wall functions, a low Reynolds number $\mathrm{k}-\varepsilon$ model, direct numerical simulations and large-eddy simulations (LES) were tested under the conditions $2 \leq \lambda/b \leq 4,\ 30° < 2\beta < 150°, 1000 < Re < 10{,}000$. The results were compared with experimental data from the literature to find the best model to predict heat transfer and friction factors in channels. At high Reynolds numbers, the standard $\mathrm{k}-\varepsilon$ model with wall functions gave acceptable results, whereas it was not applicable in the

range of Re ~ 2000 and lower. For Re < 3000 and at moderate angles, simple laminar flow assumptions provided acceptable results.

Zhang et al. (2006) employed the RNG $k-\varepsilon$ model to simulate the flow fields between plates in plate heat exchangers with the aim of examining the effect of the inclination angle on the flow patterns. The simulation results showed that the flow pattern is affected by the corrugation angle. When $\beta < 45°$, the flow pattern follows the furrows, L-shaped, while when $\beta = 80°$, the flow pattern changes to zig-zag flow, Z-shaped. These observations are very similar to those noted in the experimental work of Focke and Knibbe (1986) which was later also confirmed experimentally by Dović and Švaić (2007).

Fernandes et al. (2007) conducted numerical study using the finite-element computational fluid dynamics software POLYFLOW on double sine-chevron plate heat exchanger channels in fully developed laminar flow regime to predict the tortuosity coefficient, τ, and the shape factor, K_0, based on an analogy to porous media. Seven consecutive unitary cells were used with a range of $5° < \beta < 61°$, $0.38 < \gamma < 0.76$ and $1 \leq \phi \leq 1.5$. The authors employed the power law relation to determine the Fanning friction factor in the laminar flow regime:

$$f = A_4 \, Re_{D_h}^{-1} \tag{3.44}$$

$$A_4 = K_0 \, \tau^2 \tag{3.45}$$

where K_0 is the shape factor and τ is the tortuosity coefficient. The product $K_0 \, \tau^2$, in the granular beds area, is known as Kozeny's coefficient. The authors suggested the following expressions to determine the tortuosity coefficient, τ, and the shape factor K_0:

$$\tau = 1 + 0.5\sqrt{\left(\frac{1}{\sin(90-\beta)}\right)^{(2b/\lambda\cos(90-\beta))} - 1} \tag{3.46}$$

$$K_0 = 16\left(\frac{90}{(90-\beta)}\right)^{0.6554-0.0929(2b/\lambda\cos(90-\beta))} \tag{3.47}$$

It was observed that the tortuosity coefficient and the A_4 coefficient increase with an increase of the corrugation angle and the aspect ratio, while the shape factor is almost independent of the aspect ratio but increases with the increase of the corrugation angle.

Zhang and Che (2011) investigated the effect of corrugation profile on the thermal-hydraulic performance of cross corrugated plates numerically, using CFD. The working fluid was air and a low Reynolds number $k-\varepsilon$ model was employed, and six types of corrugation profiles were studied, which included sinusoidal, isosceles triangular, trapezoidal, rectangular, and elliptical corrugations. They found that both flow and heat transfer become fully developed in the fifth cell, for $2\beta = 60°, \mathrm{Re} = 2000$. The trapezoidal channel gave the highest Nu and f and then was followed by the rectangular, triangle, sine and ellipse channel, respectively. This was attributed to the effect of the corrugation profile. It was generally noted that an increase in chevron angle, leads to higher heat transfer and pressure drops in all geometries but with different levels.

In addition to the previous studies, thirty selected experimental and numerical studies correlations for heat transfer coefficient and/or friction factor were summarized in Table 3.1. It can be summarized that no models or correlations were found in the open literature to predict the heat transfer and friction factor in the entrance region of chevron plate heat exchanger.

Table 3.1 Summary of experimental and numerical correlations for PHE from selected articles*

Investigator	Parameters $\boldsymbol{\beta, b, \lambda, \gamma, \phi}$	Correlation	Comments
Troupe et al. (1960)	*Not given*	$Nu = \left(0.383 - 0.505^{\frac{L}{b}}\right) Re^{0.65} Pr^{0.4}$	$D_e = 2b$, *water* $Re > Re_{cr}, 10 \leq Re_{cr} \leq 400$
Emerson (1967,c)	$\beta = 45°, b = 2.94mm,$ $\phi = 1.2$	$Nu = 0.755 Re^{0.46} Pr^{1/3} (\mu/\mu_w)^{0.14}$ $f = 10.225\ Re^{-0.74}$ $Nu = 0.520 Re^{0.61} Pr^{1/3} (\mu/\mu_w)^{0.14}$ $f = 2.625\ Re^{-0.33}$	$D_e = 2b, A_{\text{proj}}$, *Oil- water, industrial* $10 < Re < 25$ $10 < Re < 40$ $40 < Re < 5{,}000$
Savostin and Tikhonov (1970)	$0° \leq \beta \leq 33°,$ $b = 1.17, 1.19, 1.20,$ $1.22, 1.87, 3.15, 1.85, 1.78$ mm	$f = 6.25(1 + 0.95\xi^{1.72})\phi^{1.84}\ Re^{-0.84}$ $Nu = 1.26(0.62 + 0.38\cos(2.35\xi))\phi^{1-a_2} Re^{a_2} Pr^{1/3}$ $a_2 = 0.22(1 + 1.1\xi^{1.5})$ $f = 0.925(0.62 + 0.38\cos(2.6\xi))\phi^{1+a_3}\ Re^{-a_3}$ $Nu = 0.072\phi^{0.33}\ Re^{0.67} \exp^{(0.5\psi+\xi^2)} Pr^{1/3}$ $a_3 = 0.53(0.58 + 0.42\cos(1.87\xi))$	$\xi = 2\beta$ radians $200 \leq Re/\phi \leq 600$ $600 \leq Re/\phi \leq 4{,}000$
Okada et al. (1972)	$\beta = 30°, 45°, 60°, 75°,$ $b = 4, \lambda = 4, 10, 15$ $\phi = 1.29, 1.41$	$Nu = 0.14\phi^{0.34} Re^{0.66} Pr^{0.4}$ $Nu = 0.22\phi^{0.36} Re^{0.64} Pr^{0.4}$ $Nu = 0.34\phi^{0.36} Re^{0.64} Pr^{0.4}$ $Nu = 0.29\phi^{0.35} Re^{0.65} Pr^{0.4}$ $Nu = 0.32\phi^{0.37} Re^{0.63} Pr^{0.4}$ $Nu = 0.42\phi^{0.38} Re^{0.62} Pr^{0.4}$	water $400 \leq Re/\phi \leq 15{,}000$

Investigator	Parameters $\boldsymbol{\beta, b, \lambda, \gamma, \phi}$	Correlation	Comments
Edwards et al. (1974)	$b = 2.03, \phi = 1.18$ $\beta = 60°$	$Nu = C_4\phi^{0.666}(Re\ Pr)^{1/3}$ $\quad C_4$ =? $Nu = C_5\phi^{0.30}Re^{0.7}Pr^{1/3}$ $\quad C_5$ =? $f = \frac{34}{Re/\phi} + 0.8$	$Re < 10$ $Re > 200$ $0.04 < Re/\phi < 1{,}000$ water, glucose sol, lubricating oil
Tovazhnyansky et al. (1980)	$\beta = 30°, 45°, 60°$	$f = 0.085 \exp(1.52 \tan\beta)/Re^{(0.25-0.06\tan\beta)}$ $Nu = 0.085 \exp(0.64 \tan\beta)\, Re^{0.73}Re^{0.43}\, (Pr/Pr_w)^{0.25}$	$2{,}000 < Re < 25{,}000$
Chisholm, and Wanniarachchi (1992)	$30° \le \beta \le 80°$	$f = 0.8\phi^{1.25}\, Re^{-0.25}(\beta/30)^{3.6}$ $Nu = 0.72\phi^{0.41}\, Re^{0.59}(\beta/30)^{0.66}Pr^{0.4}$	water $1{,}000 < Re/\phi < 4{,}000$
Heavner et al. (1993)	$\beta = 23°/23°$ $\beta = 23°/45°$ $\beta = 45°/45°$ $\beta = 23°/90°$ $\beta = 45°/90°$	$\begin{cases} f = 0.571\phi^{1.1841}\, Re^{-0.1814} \\ Nu = 0.089\phi^{0.282}\, Re^{0.718}Pr^{1/3}(\mu_m/\mu_w)^{0.17} \end{cases}$ $\begin{cases} f = 649\phi^{1.1555}\, Re^{-0.1555} \\ Nu = 0.118\phi^{0.28}\, Re^{0.720}Pr^{1/3}(\mu_m/\mu_w)^{0.17} \end{cases}$ $\begin{cases} f = 0.81\phi^{1.1405}\, Re^{-0.1405} \\ Nu = 0.195\phi^{0.308}\, Re^{0.692}Pr^{1/3}(\mu_m/\mu_w)^{0.17} \end{cases}$ $\begin{cases} f = 1.645\phi^{1.1353}\, Re^{-0.1353} \\ Nu = 0.308\phi^{0.333}\, Re^{0.667}Pr^{1/3}(\mu_m/\mu_w)^{0.17} \end{cases}$ $\begin{cases} f = 1.715\phi^{1.0838}\, Re^{-0.0838} \\ Nu = 0.278\phi^{0.317}\, Re^{0.683}Pr^{1/3}(\mu_m/\mu_w)^{0.17} \end{cases}$	water, industrial plates $400 < \mathrm{Re}/\phi < 10{,}000$

Investigator	Parameters $\boldsymbol{\beta, b, \lambda, \gamma, \phi}$	Correlation	Comments
Talik et al. (1995)	$\beta = 60°, b = 2.84mm,$ $\phi = 1.22$	$f = 12.065\, Re^{-0.74}$ $Nu = 0.20 Re^{0.75} Pr^{0.4}$	Propylene-glycol/ water mixture, industrial plates $10 < \text{Re} < 80$ $80 < \text{Re} < 720$
Lee et al. (2000)	$\beta = 63°, \phi = 1.29$	$f = \begin{cases} 7.824 Re^{-0.1} & AR \geq 2.4 \\ 11 Re^{-0.1} & AR = 2 \end{cases}$ $Nu = C_6 Re_{D_e}^{m_1} \times Pr^{1/3} \left(\frac{\mu}{\mu_w}\right)^{0.14} + C_7$ where: $C_6 = 0.76[0.2668 - 0.006967\beta + 7.244 \times 10^{-5}\, \beta^2] \times [20.78 - 50.94\phi + 41.16\phi^2 - 10.51\phi^3]$ $m_1 = \left[0.728 + 0.0543 \times \sin[(\pi\beta/45) + 3.7]\right]$ $C_7 = 14.002 - (19.73/AR)$	water $AR = L_{p-p}/w$ $(4 < Pr < 7),$ $600 < Re < 3{,}200$
Kanaris et al. (2006)	$\beta = 60°, b = 2.4mm,$ $\phi = 1.29$	$f = 9.38\, Re^{-0.135}$ $Nu = 0.51 Re_{D_e}^{0.58} Pr^{1/3}$	water, $600 < Re < 1{,}800$ $1{,}200 < Re < 2{,}500$

Investigator	Parameters $\beta, b, \lambda, \gamma, \phi$	Correlation	Comments
Durmuş et al. (2009)	$\beta = 90°$	$Nu = C_8 Re_{D_e}^{m_2} Pr^{1/3}$ $Parallel\ flow \begin{cases} Hot\ side & C_8 = 0.05774, m_2 = 0.8091 \\ Cold\ side & C_8 = 0.04319, m_2 = 0.8368 \end{cases}$ $Counter\ flow \begin{cases} Hot\ side & C_8 = 0.0488, m_2 = 0.8640 \\ Cold\ side & C_8 = 0.0443, m_2 = 0.8709 \end{cases}$	Corrugated plates water $(3 < Pr < 7)$ $50 < Re < 1{,}000$
Akturk et al. (2011)	$\beta = 30°, \phi = 1.304$	$f = 4291\phi^{2.278}\, Re^{-1.278} + 0.3343$ $\mathrm{Nu} = 0.32592\phi^{0.3875}\, Re^{0.61258} Pr^{1/3} (\mu/\mu_w)^{0.14}$	water, industrial plates $450 < Re/\phi < 5{,}250$
Gulenoglu et al. (2014)	$\beta = 60°, b = 2.64, 2.76,$ $\phi = 1.17, 1{,}288$	$f = 259.9\phi^{1.9227}\, Re^{-0.9227} + 1.246$ $\mathrm{Nu} = 0.32867\phi^{0.32}\, Re^{0.68} Pr^{1/3} (\mu/\mu_w)^{0.14}$ $f = 1371\phi^{2.146}\, Re^{-1.146} + 1.139$ $\mathrm{Nu} = 0.3277\phi^{0.325}\, Re^{0.675} Pr^{1/3} (\mu/\mu_w)^{0.14}$ $f = 0.003743\phi^{0.4019}\, Re^{0.5981} + 0.9132$ $Nu = 0.17422\phi^{0.30}\, Re^{0.70} Pr^{1/3} (\mu/\mu_w)^{0.14}$	water, industrial plates, $300 < Re/\phi < 5{,}000$
Yildiz and Ersöz (2015)	$\beta = 45°, \phi = 1.273$	$Nu = C_9 \phi^{1-m_3} Re^{m_3} Pr^{0.333} (\mu_b/\mu_w)^{0.17}$ $C_9 = 0.718,\ m_3 = 0.349$ $C_9 = 0.4,\ m_3 = 0.598$ $C_9 = 0.3,\ m_3 = 0.663$	water $Re/\phi < 10$ $10 < Re/\phi < 100$ $Re/\phi > 100$
Lee and Lee (2015)	$\beta = 60°$ $\lambda/b = 2.8$	$f = 3.7235 Re^{-0.2118}$ $Nu = 0.1312\, Re^{0.78} Pr^{1/3}$	water, industrial plates $Re < 5000$

Investigator	Parameters $\boldsymbol{\beta, b, \lambda, \gamma, \phi}$	Correlation	Comments
Kumar and Singh (2017)	$\beta = 30°, b = 2.5\ mm,$ $\lambda = 11mm$	$f = 2.573\phi^{1.1513}Re^{-0.1513}$	water, industrial plates $800 < Re/\phi < 5{,}900$
Kim and Park (2017)	$\beta = 65°, b = 2, 1.3, 1.02\ mm, \lambda = 7.3, 7.2mm,$ $\phi = 1.166, 1.221$	$f = \phi^4(0.6796\phi(\phi^{1.0551}\ Re^{-0.0551}) + 0.2$ $Nu = 0.1452\phi^{2.079}(\phi^{0.1564}\ Re^{0.8436})Pr^{1/3}$	water, industrial plates $450 < Re/\phi < 1{,}400$
Khan et al. (2017)	$\beta = 60°/60°, 30°/60°, 30°/30°, \lambda = 13.25mm, \phi = 1.117,$ $b = 2.2, 2.9, 3.6\ mm$	$f = 34.43\ \phi^{-1.5}Re^{-0.5}$ for $\beta = 60°/60°,$ $f = 2.07\ \phi^{-1.27}Re^{-0.27}$ for $\beta = 30°/60°$ $f = 1.76\ \phi^{-1.26}Re^{-0.26}$ for $\beta = 30°/30°$	water $50 < Re/\phi < 2{,}500$
Junqi et al. (2018)	$\beta = 30°, 30°/60°, 60°, b = 2.35\ mm,$ $, \lambda = 8mm, \phi = 1.16$	$f = 0.0395\ Re^{-0.189}\ Pr^{0.031}(\sin\beta)^{-1.642}\ (\cos\beta)^{5.076}$ $Nu = 0.964\ Re^{0.671}\ Pr^{0.32}\left(\frac{\beta}{180}\right)^{1.022}$	water, glycol $400 < Re < 7{,}000$ $Pr = 2 - 12$ $200 < Re < 7{,}000$
Mohebbi and Veysi (2019)	$\beta = 60°, b = 2.3mm,$ $\phi = 1.17, \lambda = 8.3mm$	$f = 32{,}533\ \phi^{-2.91}Re^{-1.91}$ $f = 33.967\ \phi^{-1.484}Re^{-0.484}$ $Nu = 0.025\ \phi^{-0.246}Re^{1.246}\ Pr^{1/3}\ (\mu_m/\mu_w)^{0.14}$	$Re < 125$ $Re \geq 125$ $50 < Re < 350$ $4 < Pr < 7$

Investigator	Parameters $\boldsymbol{\beta, b, \lambda, \gamma, \phi}$	Correlation	Comments
Asif et al. (2017)	$\beta = 30°, b = 2.2mm$, $\lambda = 6.25mm$ $\beta = 60°, b = 3.6\ mm, \lambda = 13.25mm$	$Nu = 0.093\ Re^{0.7106}\ Pr^{0.333}\ (\mu/\mu_w)^{0.14}$ $Nu = 0.112\ Re^{0.714}\ Pr^{0.333}\ (\mu/\mu_w)^{0.14}$	CFD study water $500 < Re < 2500$
Gullapalli and Sundén (2014)	$b = 2\ mm$ $\beta = 67°, \lambda = 7$ $\beta = 32°, \lambda = 7$ $\beta = 66.5°, \lambda = 7.7$	$\begin{cases} f = 6.91Re^{-0.198} \\ j = 0.2983Re^{0.6588}(\mu/\mu_w)^{0.14} \end{cases}$ $\begin{cases} f = 3.23Re^{-0.463} \\ j = 0.6963\ Re^{0.4561}(\mu/\mu_w)^{0.14} \end{cases}$ $\begin{cases} f = 4.484Re^{-0.192} \\ j = 0.3045\ Re^{0.6449}(\mu/\mu_w)^{0.14} \end{cases}$	CFD study water $600 < Re < 3{,}000$
Sarraf et al. (2015)	$\beta = 55°\ b = 2.2mm$	$f = 88.35Re^{-1}$ $f = 4.4Re^{-0.7}$ $f = 2.55Re^{-0.125}$	CFD study, water $Re \leq 20$ $20 < Re \leq 200$ $Re > 200$
Alzahran et al. (2019)	$\beta = 60°$	$f = 2.15Re^{-0.1342}$ $Nu = 0.238\ Re^{0.6417}\ Pr^{0.333}(\mu/\mu_w)^{0.14}$	CFD study, water $500 < Re < 3{,}000$
Saha and Khan (2020)	$\beta = 30°, 45°, 60°, 72°, 80°$	$Nu = C_{10}\ \times Re^{m_4} \times Re^{\left(\frac{\phi}{\beta}\right)} \times Re^{\left(\frac{\gamma}{\beta}\right)}\ Pr^{1/3}\ \left(\frac{\mu}{\mu_w}\right)^{0.14}$	CFD study, C_{10} and m_4 values are tabulated for each β. $900 \leq Re \leq 6{,}000 \quad Pr = 6.991$ $900 \leq Re \leq 10{,}000$ ($0.744 \leq Pr \leq 65.04$) for $\beta = 72°, 80°$

* All correlations are based on equivalent diameter D_e

3.4 Asymptotic Analysis

In many complex physical systems, a phenomenon varies smoothly between two known limiting asymptotic solutions. The smooth transition between two asymptotic solutions means no discontinuous transition behavior or sudden changes in slop within the transition region (Yovanovich, 2003). These asymptotes can be found in many applications, such as natural and forced internal and external convection, fluid flow, mass transfer, and steady and transient internal and external conduction (Yovanovich, 2003).

The asymptotic analysis technique, which was first introduced by Churchill and Usagi (1972), is used to develop f and j models in this thesis. The dependent parameter is y, and the independent parameter is z. The parameter y has two asymptotes. The first asymptote is y_0 which corresponds to a very small value of the independent parameter:

$$y_0 = c_0 z^i \quad \text{as} \quad z \to 0 \tag{3.48}$$

The second asymptote y_∞ corresponds to the very large value of the independent parameter z:

$$y_\infty = c_\infty z^j \quad as \quad z \to \infty \text{ or } z \to 1 \tag{3.49}$$

The asymptotes y_0 and y_∞ are obtained from analytical solutions, and they consist of a constant which has a positive real value. The first constant c_0 is for the case as $z \to 0$ and the second constant c_∞ is for the case as $z \to \infty$ or $z \to 1$. In Eq. (3.48) and (3.49), the exponents i and j for example can take the values $0, 1, 1/2$, and $1/3$ (Churchill and Usagi, 1972) and (Yovanovich, 2003).

For friction factor and Colburn factor in chevron plate heat exchangers, a smooth transition between two asymptotes y_0 and y_∞ is exist. Both the asymptotes y_0 and y_∞ are decreasing with increasing y and the solution of y is concave upwards. The procedure for combining the two asymptotes is discussed in the next section.

3.4.1 Superposition of Asymptotic Solutions

There are two different ways to combine the asymptotes y_0 and y_∞ depending on the trends between y_0 and y_∞ with respect to y ((Churchill and Usagi, 1972) and (Yovanovich, 2003)).

1- For the case $y_0 > y_\infty$ as $z \to 0$, the asymptotes y_0 and y_∞ can be combined as in the following form:

$$y = [y_0^n + y_\infty^n]^{1/n} \tag{3.50}$$

The solution is concave upwards. Since f and j in PHEs exhibit this trend, Eq. (3.50) is used to combine the asymptotic solutions for small and large values of z

2- For the case $y_0 < y_\infty$ as $z \to 0$, the solution is concave downwards, and the asymptotes y_0 and y_∞ can be combined in the following form:

$$\frac{1}{y} = \left[\left(\frac{1}{y_0}\right)^n + \left(\frac{1}{y_\infty}\right)^n\right]^{1/n} \tag{3.51}$$

The parameter n is referred to as the fitting or "blending" parameter. The results for small and large values of the independent parameter z remain unchanged with changing the parameter n and its effect on Eq. (3.50) is only important in the transition region, as shown

in Fig. 3.1. The higher the value of the fitting parameter, n, the greater close of the model to catch the asymptotic solutions near the intersection point of the two limiting solutions, e.x when $n = n_2$ in Fig. 3.1 (Yovanovich (2003) and Teertstra et al. (2006))

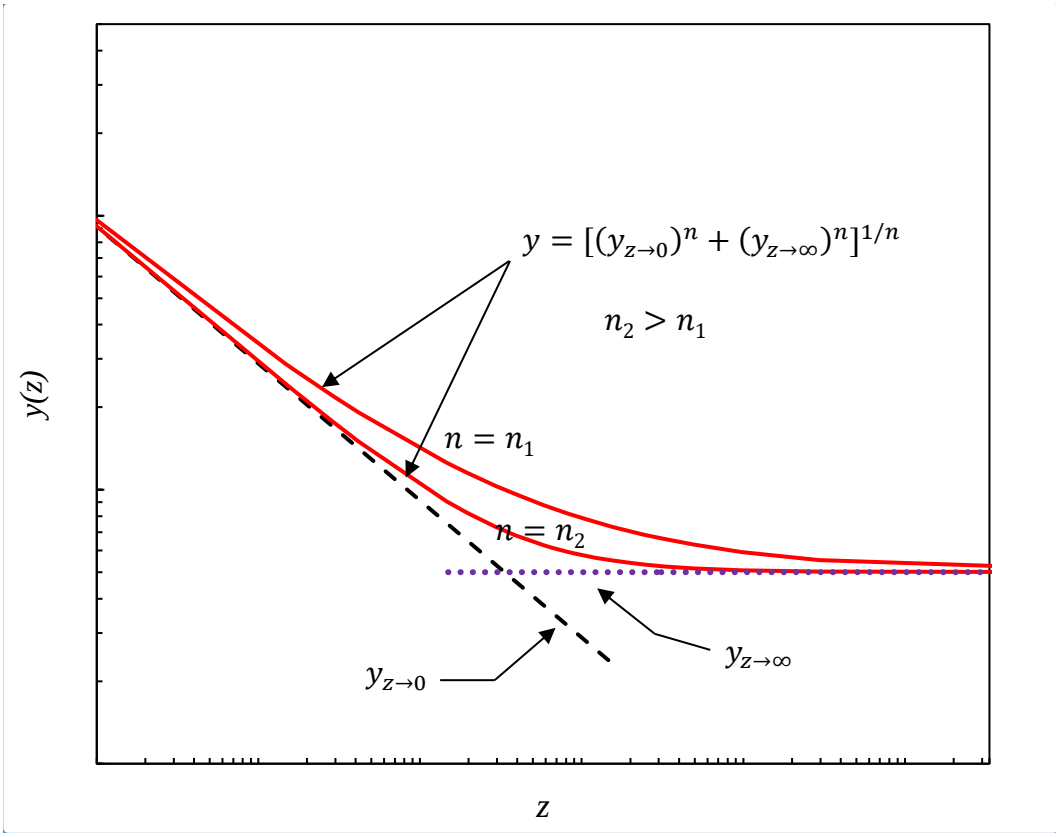

Fig. 3.1 Asymptotes and compact model

The value of the blending parameter is calculated by choosing n value, which provides the minimum root mean square (RMS) error, e_{RMS}, between the developed model predictions and the experimental data. The fractional error (e), is defined as:

$$e = \left|\frac{\text{Predicted} - \text{Available}}{\text{Available}}\right| \tag{3.52}$$

And root mean square error for groups of data,e_{RMS}, can be calculated from

$$e_{RMS} = \left[\frac{1}{N}\sum_{k=1}^{N} e_k^2\right]^{1/2} \tag{3.53}$$

The approximate solution y is often written in a form which is based on one of the two asymptotes y_0 and y_∞. So, Eq. (3.50) can be rearranged in the two more convenient forms (Churchill and Usagi (1972) and Yovanovich (2003)):

$$y = y_0\left[1 + \left(\frac{y_\infty}{y_0}\right)^n\right]^{1/n} \tag{3.54}$$

$$y = y_\infty\left[1 + \left(\frac{y_0}{y_\infty}\right)^n\right]^{1/n} \tag{3.55}$$

This technique has been found to be remarkably successful in developing models for many applications, such as forced internal and external convection, natural convection, and steady and transient conduction (Churchill and Usagi (1972) and Yovanovich (2003)). Teertstra et al. (1997) employed this method to develop a model for predicting the pressure drop for fully developed flow through a parallel plate channel with an array of periodic cuboid blocks on one wall. Muzychka (1999) also applied this technique to develop analytical models for predicting the fluid friction and heat transfer for plain non-circular duct of constant cross-section, the rectangular offset strip fin, and the turbulator strip for low Reynolds number flow conditions. Moreover, it has been applied to flow through porous media by Awad and Butt (2009) and two-phase flow in mini-channels and microchannels by Awad and Muzychka (2010).

3.5 Conclusions

This chapter reviewed the present state of the art in terms of general models and correlations available in the open literature, for predicting the single-phase friction factor and the heat transfer coefficients in plate heat exchangers. According to the literature, in general, the Nusselt number was correlated with the Reynolds number, Prandtl number, and the viscosity ratio, but the friction factor was expressed as a function of the Reynolds number. Some investigators also attempted to incorporate the effects of the plate surface characteristics on the heat exchanger's thermal-hydraulic performance by introducing variables such as chevron angle, surface enlargement factor, and / or aspect ratio into their models or correlations. Finally, the Churchill and Usagi (1972) asymptotic correlation technique was discussed.

Chapter 4

Experimental Procedure and Results Discussions

4.1 Introduction

This chapter provides an overview of the experimental test apparatus, procedure, and results. A new apparatus was built in Heat Transfer Laboratory to examine six sets of corrugated channels, with three different chevron angles and two channel lengths. The experimental facility components, data reduction techniques, experimental uncertainties, and test results are presented in the following sections.

4.2 Test Apparatus

A schematic of the experimental facility is illustrated in Fig. 4.1, along with the main components and instrumentation. This setup consists of a test section, PVC connection pipes, fittings, valves, two isothermal baths, three flow meters, power supply, pressure transducer, T- type thermocouples, one storage tank, pump with a variable frequency drive (VFD), and data acquisition system connected to a computer (PC).

4.2.1 Test Fixture

The test apparatus is constructed from aluminum with a configuration based on a single pass shell and tube heat exchanger and operated in a counterflow arrangement. This heat exchanger was used for the first time by Muzychka et al. (1999). All the test section cores have a chevron pattern with approximately sinusoidal shape corrugations. Six sets of corrugated channels with the same width and three chevron angles $30°, 45°, 60°$ were

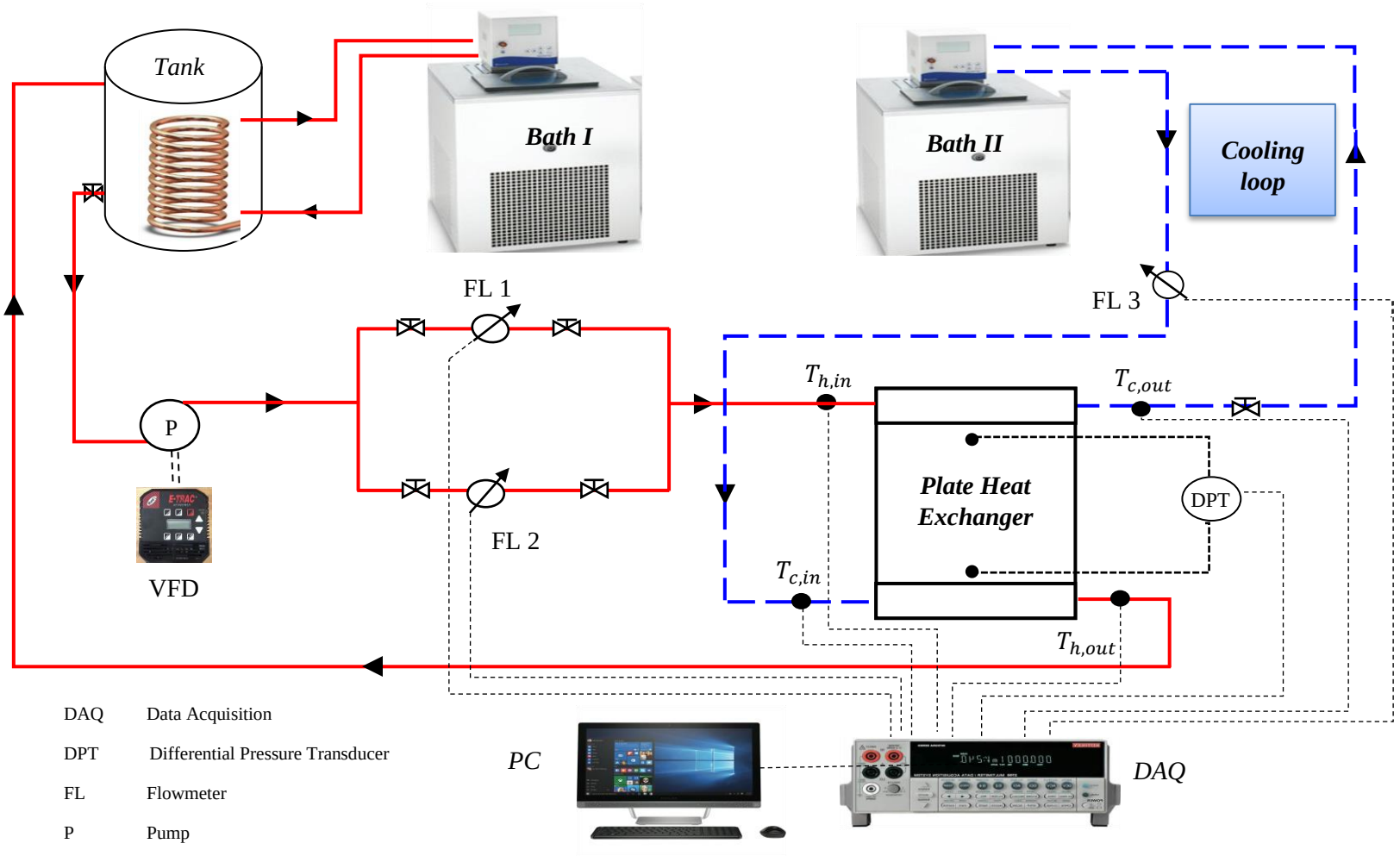

DAQ	Data Acquisition
DPT	Differential Pressure Transducer
FL	Flowmeter
P	Pump
VFD	Variable Frequency Drive
- - -	Data Acquisition Connections

Fig. 4.1 Schematic of the experimental setup

examined. These sets were divided into two groups based on the channel length: long channel and short channel. The geometric details of the test sections are summarized in Table 4.1.

Table 4.1 Dimensional specifications of the tested plates

Parameter	Value
β (°)	$30, 45, 60$
$b\ (mm)$	1.14
$\lambda\ (mm)$	4.52
ϕ	1.13
$L\ (mm)$	203 / 101
$w\ (mm)$	139.7
$D_e\ (mm)$	2.28

Four manifolds were used for the working fluid's and coolant's inlets and outlets. A rubber gasket with 1.8 mm diameter was used in O-ring grooves, which were originally machined inside the cover plate around the formed channel to prevent leakage from the test section. To measure the pressure drop directly on the corrugated region, two 1/8 National Pipe Taper NPT fittings were installed on the top plate. The photograph of the complete heat exchanger assembled is shown in Fig. 4.2. More details about the dimensions of the test sections, manifolds, and the jacket sides are provided in Appendix B.

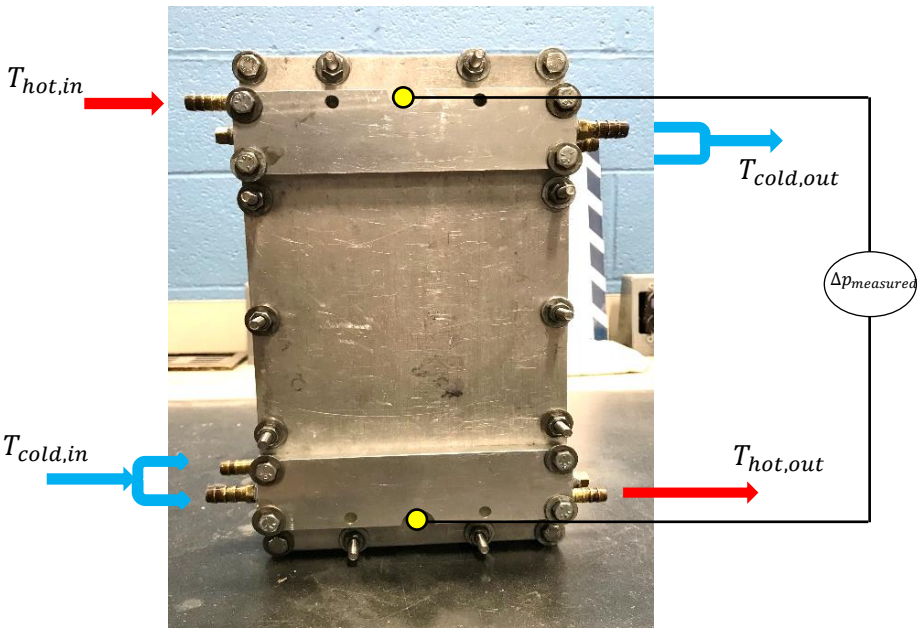

Fig. 4.2 Photograph of a fully assembled PHE used in the experiment.

4.2.2 Flow Measurements

The volumetric flow rates for the hot and cold fluids were measured using three flow meters with signal conditioners. The cooling water flow rates were measured by a turbine flow meter from Omega, FTB 101, with a flow range from 0.35 to 3.5 gallons per minute. For the hot loop, process fluid flow rate measurements were obtained using a turbine flow meter from Omega, FTB-101, 0.35 to 3.5 gpm, and an oval gear flowmeter, OGF, model OM006H513-222RS, 0.0083 to 0.45 gpm. A Tee-Type filter from Swagelok was installed before the flowmeter to protect the flow meter from foreign particles, which may be suspended in the fluid. All flow meters were calibrated by the manufactures. Each calibration result was fit using a linear regression analysis, except for OGF which has an option to provide the reading directly in gpm. The resulting equations were entered into

the data acquisition system to show the flow rate readings in gpm.

4.2.3 Pressure Measurements

The pressure drop on the core (corrugated) region of the heat exchanger was measured using a differential pressure transducer from Omega, model DPGM409-350HDWU, 0 to 5 psi with a corresponding voltage output of 0 to 5 Vdc. The sensor calibration was done by the manufacturer. All the measurements were conducted when the heat exchanger was in a horizontal position.

4.2.4 Temperature Measurements

T-type thermocouples from Omega were used for temperature measurements. Four thermocouples were employed to measure the inlet and outlet temperatures of the hot and cold fluids to the heat exchanger. The thermocouple's readings were checked to be accurate within $\pm 0.1℃$ using a constant temperature bath and an ice / water mixture.

4.2.5 Thermal Baths

The test facility uses two constant temperature baths to control the temperature of the hot and cold fluids. A Fisher brand 6200 R35 constant temperature bath, which has a cooling capacity of up to 800 W and temperature stability $\pm 0.05℃$, was used to maintain the inlet coolant temperature fairly constant. The bath provides volumetric flow rates up to 5.5 gpm and can hold up to 2.27 gallon. The other Fisherbrand 5150 R35 constant temperature bath, connected with a copper coil immersed in the working fluid reservoir, was utilized to keep the working fluid inlet temperature fairly constant. It has a 1000 W heating capacity,

temperature stability ± 0.1℃, and can hold up to 2.27 gallon. Each thermal bath can be used for either open or closed-loop circulation.

Test Fluids

Tap water and white mineral oil, FG WO 15 from Petro-Canada, were used as the working fluids while the coolant was water. The reasons for choosing these two fluids was that they have two different orders of magnitude of viscosity, which allowed different flow regimes to be investigated. The mineral oil properties have been provided by the manufacturer for a temperature range from 0 ℃ to 100 ℃ and have been correlated as a function of the temperature. These correlations are listed below.

$$\rho = 868.27 - 0.6109T \quad (kg/m^3) \tag{4.1}$$

$$\mu = 0.0000571723 \text{ Exp}\left(\frac{815.114}{110.884 + \text{T}}\right) \quad (kg/m.s) \tag{4.2}$$

$$k = 0.1365 - 0.00007\text{T} \quad (W/m.K) \tag{4.3}$$

$$C_p = 1.8292 + 0.0036T \quad (kJ/kg.K) \tag{4.4}$$

The maximum deviations of the predicted properties from these correlations are within $\pm 0.5\%$. The equations for water properties are taken from the Handbook of Dixon (2007), which are listed below, and their accuracy is reported to be within $\pm 0.5\%$ (Dixon 2007). The temperatures are specified in Degree Celsius, and all properties of fluids were evaluated at the average of the measured inlet and outlet temperatures.

$$\rho = 1001.3 - 0.155T - 2.658 \times 10^{-3}T^2 \quad (kg/m^3) \tag{4.5}$$

$$0 \leq T \leq 200\ ℃$$

$$log_{10}(\mu) = -2.75 - 0.0141T + 91.9 \times 10^{-6}T^2 - 311 \times 10^{-9}T^3 (N.s/m^2) \tag{4.6}$$

$$3 \leq T \leq 100\ ℃$$

$$k = 0.5706 + 1.756 \times 10^{-3}T - 6.46 \times 10^{-6}T^2 \quad (W/m.K) \tag{4.7}$$

$$1 \leq T \leq 100\ ℃$$

$$C_p = 4209 - 1.31T + 0.014T^2 \quad (J/kg.K) \tag{4.8}$$

$$3 \leq T \leq 200\ ℃$$

4.2.6 Data acquisition system

A Keithley 7200 data acquisition system (DAQ) was used to record the raw data. The thermocouples, flow meters, and pressure transducer were connected to the DAQ that was connected to a PC.

4.2.7 Test Procedure

The first step was assembling the heat exchanger, including the test section, shell or jacket sections, and manifolds, and then the fluids were pumped through the cold and hot loops at very high flow rates to ensure there was no leakage before starting the experiments. Next, the fixture was placed inside an insulated cooling box to reduce heat losses. The heating of the working fluid and cooling the coolant were initiated by switching on the thermal baths until they reached the desired initial temperatures from where data would be obtained. The inlet temperatures for water and oil were 40 ℃ and 47 ℃, respectively, while the coolant inlet temperate was 27 ℃. Afterward, the process fluid was pumped from the tank through the system, using a 1.5 HP pump controlled by the VFD, while the coolant was circulated

by means of the thermal bath pump and controlled manually by a valve. Test fluid flow was set to a starting flow rate $8.2\ cm^3/s$, while the water flow rate in the cooling loop was set to $94.6\ cm^3/s$. Once the system reached steady-state conditions, data was recorded, and the test fluid flow rate was then increased incrementally by $3.2\ cm^3/s$ using the VFD. This procedure was repeated until the maximum flow rate attainable was reached. All required fluids properties, such as density, thermal conductivity, and viscosity were evaluated at the average bulk temperature for the corresponding side. All connection tubes were insulated to minimize heat loss to the surroundings. Experiments of pressure drop were conducted separately, with no heating or cooling of the test fluid during the runs. The collected data were saved in Excel files and then averaged to be used in the data reduction procedure, which is presented in the following section.

4.3 Data Reduction technique

The aim of this section is to discuss the methodology used to calculate the friction factors and Nusselt numbers from the measured parameters, namely, inlet and outlet temperatures, volumetric flow rates, and pressure drops.

The average velocity in the heat exchanger channel, $\bar{u}$, can be calculated by dividing the volumetric flow rate through the channel and the channel flow area:

$$\bar{u} = \frac{\dot{V}}{b\ w} \tag{4.9}$$

where $\dot{V}$ is the volumetric flow rate, w is the channel width inside the gasket, and b is the corrugation depth. The Reynolds number can be then determined using Eq. (4.10) based on mass velocity and equivalent diameter of the channel (Shah and Sekulić, 2003)

$$Re_{De} = \frac{G D_e}{\mu} \tag{4.10}$$

where G is the mass velocity through the core, which is defined as

$$G = \frac{\dot{m}}{N_{\mathrm{cp}}\, b\, w} \tag{4.11}$$

where N_{cp} is the number of channels per pass and $\dot{m}$ is the mass flow rate. In these experiments, only one channel has been used, hence, $N_{\mathrm{cp}} = 1$.

4.3.1 Pressure Drop Analysis

For plate heat exchangers, the total pressure drop consists of the pressure drop due to inlet and outlet ports and manifolds, the pressure drop within the heat exchanger core (corrugated passage), the pressure drop associated with elevation change for a vertical heat exchanger. The total pressure drop for one fluid side can be expressed as (Shah and Sekulić, 2003)

$$\Delta p = \frac{1.5\, G_p^2\, N_p}{2 g_c \rho_i} + \frac{4 f L\, G^2}{2 g_c D_e}\left(\frac{1}{\rho}\right)_m + \frac{G^2}{g_c}\left(\frac{1}{\rho_o} - \frac{1}{\rho_i}\right) \pm \frac{\rho_m \mathrm{g} L}{g_c} \tag{4.12}$$

where $G_p = \dot{m}/\left(\pi\, D_p^2/4\right)$ is the fluid mass velocity in the port, D_{port} is the port diameter, N_p is the number of passes on the given fluid side, L is the core length, and ρ_i and ρ_o are fluid densities calculated based on local bulk temperatures and mean pressures at the inlet and outlet, respectively. The pressure drop is measured directly on the core (corrugated) region of the heat exchanger when it is positioned horizontally. Thus, the first and last terms on the right-hand side of Eq. (4.12) are equal to zero. Furthermore, both the test fluids were liquids, and no heating or cooling was involved during the pressure

drop measurements. Hence, the fluid densities are assumed to be approximately equal to the mean density, since the temperature difference between the inlet and outlet is small. Therefore, the total pressure drop across the heat exchanger core can be expressed as

$$\Delta p_{core} = f \frac{4L\ G^2}{2D_e}\left(\frac{1}{\rho}\right)_m \tag{4.13}$$

Rearranging Eq. (4.13), the Fanning friction factor can be determined from the following equation

$$f = \frac{D_e}{4L}\left(\frac{\Delta p_{core}}{\frac{1}{2}\rho_m \overline{u}^{\,2}}\right) \tag{4.14}$$

All fluids properties were evaluated at the average inlet and outlet fluid temperatures.

4.3.2 Heat Transfer Analysis

The heat transfer rates from the hot and the cold fluids can be calculated by an energy balance for the hot and cold side, as follows

$$Q_h = C_h\left(T_{h,i} - T_{h,o}\right) \tag{4.15}$$

$$Q_c = C_c\left(T_{c,o} - T_{c,i}\right) \tag{4.16}$$

where subscripts *c* and *h* represent the cold and hot fluids, respectively, *i* and *o* refer to inlet and outlet, and C is the fluid heat capacity rate. The heat capacity rates for the cold and hot fluid streams are given by (Bergman et al. 2011)

$$C_c = \dot{m}_c C_{p,c} \tag{4.17}$$

$$C_h = \dot{m}_h C_{p,h} \tag{4.18}$$

where $\dot{m}$ is the mass flow rate and C_p is the specific heat of the fluid. Due to the uncertainty in the fluid properties on hot and cold fluids, the average heat transfer rate, $\bar{Q}$, was calculated by taking the arithmetic mean of Q_h and Q_c, as follows

$$\bar{Q} = \frac{C_h\left(T_{h,i} - T_{h,o}\right) + C_c\left(T_{c,o} - T_{c,i}\right)}{2} \tag{4.19}$$

The value of $\bar{Q}$ was then used as the total heat load of the heat exchanger, and the energy balance between the two fluids was maintained within ±7%. Hot and cold fluid properties were evaluated at the average fluid temperature,

$$T_m = \frac{(T_i + T_o)}{2} \tag{4.20}$$

The overall heat transfer coefficient was calculated using the log mean temperature difference (LMTD) method.

To determine the Nusselt number, the product of the overall heat transfer coefficient and total heat transfer area, UA is first calculated, as follows

$$UA = \frac{\bar{Q}}{\Delta T_{LMTD}} \tag{4.21}$$

where A is the total hot-side or cold-side heat transfer area and ΔT_{LMTD} is the log mean temperature difference for the counterflow arrangement, which can be calculated from the following equation (Bergman et al. 2011)

$$\Delta T_{LMTD} = \frac{\left(T_{h,i} - T_{c,o}\right) - (T_{h,o} - T_{c,i})}{ln\frac{\left(T_{h,i} - T_{c,o}\right)}{(T_{h,o} - T_{c,i})}} \tag{4.22}$$

The projected heat transfer area, A_{proj}, has been used to eliminate the effects of ϕ on heat transfer enhancement. Thus, the average heat transfer coefficient for the corrugated side can then be determined from the overall thermal resistance,

$$\frac{1}{UA_{\text{proj}}} = \frac{1}{h_h A_{\text{proj}}} + R_{\text{f},h} + \frac{t}{k_w A_{\text{proj}}} + R_{\text{f},c} + \frac{1}{h_c A_{\text{proj}}} \tag{4.23}$$

where h_h is the heat transfer coefficient of the hot fluid on the rib side, $R_{\text{f},h}$ is the fouling resistance on the hot fluid side, t is the plate thickness, k_w is the thermal conductivity of the plate, h_c is the heat transfer coefficient of the cold fluid, and $R_{\text{f},c}$ is the fouling resistance on the cold fluid side. Fouling resistance is assumed to be negligible because the tested plates were only used a few times in the past by Muzychka et al. (1999). Moreover, the heat exchanger was dismantled and cleaned each time before conducting the next experiment. Furthermore, there are no standard values available in the open literature for the fouling factors for PHEs, as in the traditional shell-and-tube heat exchangers, due to the wide range of corrugation patterns used (Wang et al. 2007). Hence, Eq. (4.23) simplifies to

$$\frac{1}{UA_{\text{proj}}} = \frac{1}{h_h A_{\text{proj}}} + \frac{t}{k_w A_{\text{proj}}} + \frac{1}{h_c A_{\text{proj}}} \tag{4.24}$$

The heat transfer coefficient on the rib side, h_h in Eq. (4.24) was obtained by the modified Wilson Plot technique, which is discussed in the next section. The Nusselt number can then be calculated as follows

$$Nu_{De} = \frac{h_h D_e}{k} \tag{4.25}$$

where k is the thermal conductivity of the fluid.

4.3.3 Modified Wilson Plot

The hot and cold fluid side resistances in Eq. (4.24) can be determined from measured experimental data by employing the Wilson plot method (Wilson, 1915), or its modifications such as (Briggs and Young 1969, Shah, 1990, and Khartabil and Christensen, 1992). Beginning with the original Wilson plot method to explain how this method works. Next, the technique described by Khartabil and Christensen (1992), which uses a nonlinear least square regression analysis to determine heat transfer coefficients, is discussed as it has been used here to calculate the heat transfer coefficient.

The heat transfer coefficient on the rib or hot side, h_h, determined based on the proposed Nusselt number correlation which takes the following form

$$Nu_{D_e} = C_{11} Re_{D_e}^{a_4} Pr^{1/3} \tag{4.26}$$

where C_{11} and a_4 are constants to be determined. The heat transfer coefficient of the hot fluid side, h_h, based on Eq. (4.26) can be expressed as

$$h_h = C_{11} Re_{D_e}^{a_4} Pr^{1/3} \left(\frac{k}{D_e}\right) \tag{4.27}$$

From Eq.(4.24), if the cold fluid flow is kept at a high mass flow rate, h_c is maintained approximately constant to ensure the validity of this method, while the testing fluid flow rate is varied systematically, then the change in the overall thermal resistance is mainly due to the variation in h_h. Consequently, the remaining thermal resistances can be taken as constant. Therefore, Eq. (4.24) can be rewritten as

$$\frac{1}{UA_{\text{proj}}} = \frac{1}{h_h A_{\text{proj}}} + C_{12} \tag{4.28}$$

where C_{12} is a constant given by

$$C_{12} = \frac{t}{k_w A_{\text{proj}}} + \frac{1}{h_c A_{\text{proj}}} \tag{4.29}$$

Substituting h_h, from Eq. (4.27) into Eq. (4.28), we obtain

$$\frac{1}{UA_{\text{proj}}} = \frac{1}{C_{11} Re_{D_e}^{a_4} Pr^{1/3} (A_{\text{proj}} k/D_e)} + C_{12} \tag{4.30}$$

The value of UA_{proj} in this equation is obtained from the experimental measurements using Eq. (4.21). The resulting equation, Eq. (4.30), is a nonlinear regression problem with three unknowns, a_4, C_{11} and C_{12}.

If the Reynolds number exponent a_4 in Eq. (4.30) is known a prior, the problem reduces to a linear regression problem which can be easily solved using original Wilson plot method as follows:

Equation (4.30) can be re-written in the following form

$$\frac{1}{UA_{proj}} = \frac{1}{C_{13} Re_{D_e}^{a_4}} + C_{12} \tag{4.31}$$

where C_{13} is a constant given by

$$C_{13} = C_{11} Pr^{1/3} (A_{proj} k/D_e) \tag{4.32}$$

Equation (4.31) has the from $y = mx + b$ where $y = 1/UA_{\text{proj}}$, $m = 1/C_{13}$, $x = Re_{D_e}^{-a_4}$, and $b = C_{12}$. Figure 4.3 shows $1/UA_{\text{proj}}$ vs. $Re_{D_e}^{-a_4}$ on a linear scale. The slop $1/C_{13}$ and

the intercept C_{12} can then be determined from this plot. Once C_{13} is found, the constant C_{11} can then be calculated from Eq. (4.32). Consequently, the heat transfer coefficient, h_h in Eq. (4.27) is known (Shah and Sekulić, 2003).

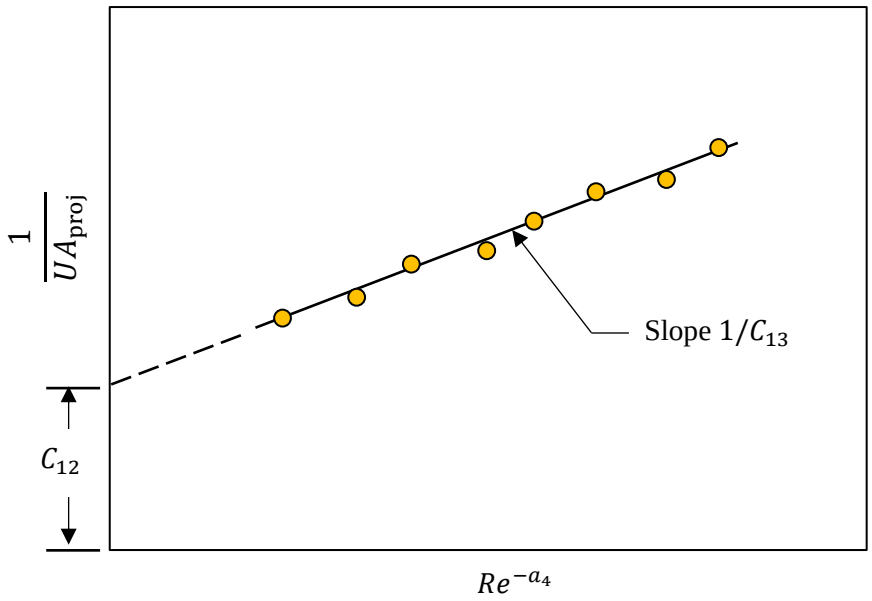

Figure 4.3 Original Wilson plot

On the other hand, in many practical situations, the Reynolds number exponent a_4 in Eq. (4.30) is not known as in the chevron PHE. The resulting equation is a nonlinear regression problem with three unknowns, a_4, C_{11} and C_{12}. Therefore, the modified Wilson plot technique using Khartabil and Christensen (1992) method has been used here. Applying the method of least squares to Eq. (4.30) requires minimizing the sum of squares of deviations between measured and fitted dependent variables, S

$$S = \sum_{i=1}^{N} \left[\left(\frac{1}{UA_{\text{proj}}} \right)_i - \frac{1}{C_{11} Re_{D_e,i}^{a_4} \left[Pr^{1/3} (A_{\text{proj}} k / D_e) \right]_i} - C_{12} \right]^2 \qquad (4.33)$$

The procedure of minimizing S in Eq. (4.33) with respect to the unknowns a_4, C_{11} and C_{12}

is discussed in detail in Khartabil and Christensen (1992), and the final equations to determine these unknowns are presented as follow

$$C_{11} = \left[\frac{N \sum_{i=1}^{N} \frac{\left(1/UA_{\text{proj}}\right)_i}{Re_{D_e,i}^{a_4} W_i} - \sum_{i=1}^{N} \frac{1}{Re_{D_e,i}^{a_4} W_i} \sum_{i=1}^{N} \left(\frac{1}{UA_{\text{proj}}}\right)_i}{N \sum_{i=1}^{N} \frac{1}{Re_{D_e,i}^{2a_4} W_i^2} - \left(\sum_{i=1}^{N} \frac{1}{Re_{D_e,i}^{a_4} W_i}\right)^2} \right]^{-1} \tag{4.34}$$

$$C_{12} = \left[\frac{\sum_{i=1}^{N} \frac{1}{Re_{D_e,i}^{2a_4} W_i^2} \sum_{i=1}^{N} \left(\frac{1}{UA_{\text{proj}}}\right)_i - \sum_{i=1}^{N} \frac{\left(1/UA_{\text{proj}}\right)_i}{Re_{D_e,i}^{a_4} W_i} \sum_{i=1}^{N} \frac{1}{Re_{D_e,i}^{a_4} W_i}}{N \sum_{i=1}^{N} \frac{1}{Re_{D_e,i}^{2a_4} W_i^2} - \left(\sum_{i=1}^{N} \frac{1}{Re_{D_e,i}^{a_4} W_i}\right)^2} \right] \tag{4.35}$$

and

$$\sum_{i=1}^{N} \frac{\left(1/UA_{\text{proj}}\right)_i \ln(Re_{D_e,i})}{Re_{D_e,i}^{a_4} W_i} = \frac{1}{C_{11}} \sum_{i=1}^{N} \frac{\ln(Re_{D_e,i})}{Re_{D_e,i}^{2a_4} W_i^2} + C_{12} \sum_{i=1}^{N} \frac{\ln(Re_{D_e,i})}{Re_{D_e,i}^{a_4} W_i} \tag{4.36}$$

where $W = Pr^{1/3}(A_{\text{proj}} k/D_e)$. The exponent a_4 can then be obtained by solving Eq. (4.36) numerically. Thus, a Mathematica code was written to solve for a_4.

4.4 Temperature-Dependent Fluid Properties

The property ratio method is the most often employed technique to account for fluid property variations in a heat exchanger. In this method, the relationship between Nu and f for the variable fluid property and the constant property value for the liquids is presented as follows (Rohsenow et al. 1998)

$$\frac{Nu}{Nu_{cp}} = \left(\frac{\mu_w}{\mu_m}\right)^{n_1} \tag{4.37}$$

$$\frac{f}{f_{cp}} = \left(\frac{\mu_w}{\mu_m}\right)^m \tag{4.38}$$

where the subscript cp represents the constant property variable. For laminar flow, values of the constants n_1 and m for heating are $n_1 = -0.14, m = 0.58$ and for cooling are $n_1 = -0.14, m = 0.54$ (Rohsenow et al. 1998). All properties in Eq. (4.37) and (4.38) are evaluated at the average mean temperature, except for μ_w which is evaluated at the wall temperature, T_w. When there is no fouling on either fluid side, T_w can be determined by the following equation (Shah and Sekuli, 2003)

$$T_w = \frac{(T_h/R_h) + (T_c/R_c)}{(1/R_h) + (1/R_c)} \tag{4.39}$$

where R_h and R_c refer to the hot and cold side film resistances, respectively. To find R_c, the heat transfer coefficient on the cold side needs to be determined. Therefore, the modified Wilson plot technique, discussed in the previous section, was employed to calculate h_c. Two correlations were obtained for the long and short channels,

For long channel $$h_c = 0.227 Re^{0.57} Pr^{1/3} \left(\frac{k}{D_h}\right) \tag{4.40}$$

For short channel $$h_c = 0.46 Re^{0.54} Pr^{1/3} \left(\frac{k}{D_h}\right) \tag{4.41}$$

All data obtained in the present experiment involved small temperature differences, therefore, the $(\mu_w/\mu_b)^{-0.14}$ ratio is found to vary within 4.5 percent for oil and within 1 percent for water.

4.5 Experimental Uncertainty

The uncertainty analysis was conducted by employing Kline and McClintock's (1953) method. The experimental uncertainty in Re, f, Nu, Pr and j depends on the uncertainty in the experimental measurement of temperature, flow rate, pressure, and uncertainty in the thermo-physical properties of working fluids. A summary of the analysis results are reported in Table 4.2, and details of the uncertainty analysis are provided in Appendix A. The small temperature difference measured for the lower inlet temperature tests was the main reason for the upper limit of uncertainty in Nu and j. Furthermore, when reducing the data, the average value of the total heat transfer $\bar{Q}$ was employed rather than the more accurate process fluid side, Q_h, measurements. If Q_h was used to reduce the data, the uncertainties in Nu and j were found to be $8.6/5.55$ percent and $8.85/5.94$ percent, respectively.

Table 4.2 Uncertainty in f, Re, Nu, j and Pr

Parameter	**Uncertainty**
f	$4.54/3.65$ %
Re	$2.5/2.09$ %
Nu	$13.9/7.39$ %
j	$14.08/7.70$ %
Pr	0.87 %

4.6 Experimental Results and Discussion

The experimental apparatus was benchmarked by obtaining the friction factor in a pipe and Nusselt number in a parallel plate smooth channel for which accurate theoretical and /or numerical equations are known. Performing this test ensured accuracy of the pressure transducer, flow meters, thermocouples, and data acquisition system. Water and oil were used in the benchmark experiment. Thus, pressure drop and heat transfer benchmarking tests were performed for each fluid to ensure that the thermophysical property correlations also provide a good prediction to the fluid properties.

Pressure Drop Benchmark Test

The pressure drop tests using water and oil were conducted on 1.81 m straight copper pipe with 7.6 mm diameter over a wide range of flow rates. For oil, the experimental results are compared with the Fanning friction factor for laminar flow in a pipe (Shah and London, 1978). The results are shown in Fig. 4.4 and agreed within $\pm 10\%$ of the laminar flow theory.

$$f = \frac{16}{Re_{D_h}} \tag{4.42}$$

As for water, the results, see Fig. 4.5, are in the turbulent flow region, so they are compared with the theoretical model of Swamee and Jain's (Swamee and Jain 1976)

$$f = \frac{1}{16\left[log\left(\frac{\varepsilon}{3.7D} + \frac{5.74}{Re_{D_h}^{0.9}}\right)\right]^2} \tag{4.43}$$

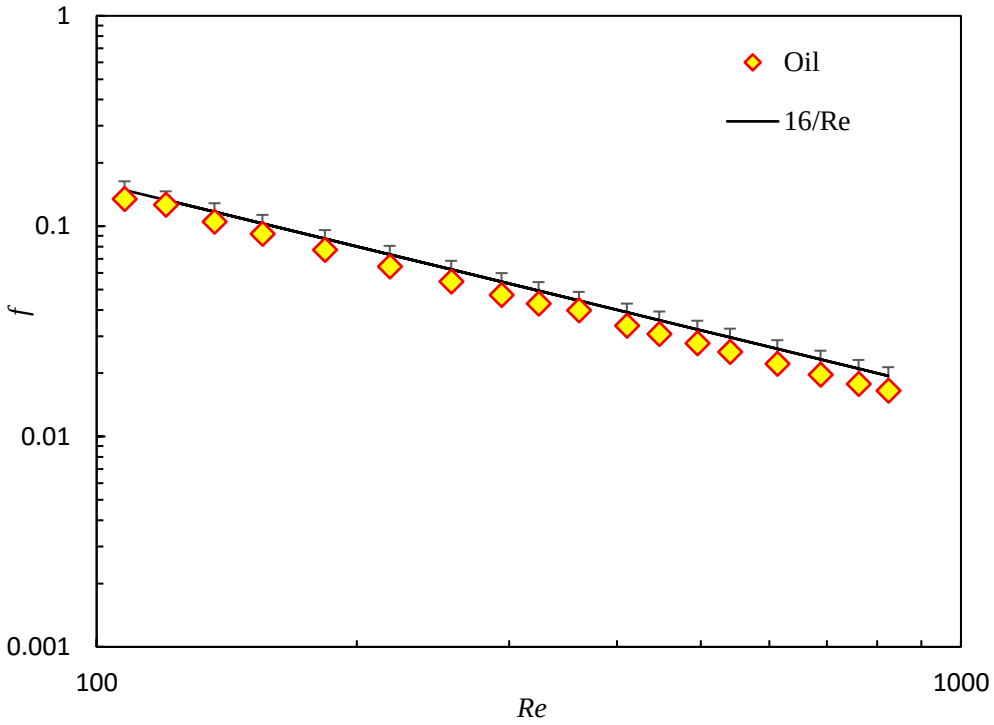

Fig. 4.4 Pressure drop benchmarking test using oil with ±10% error bars

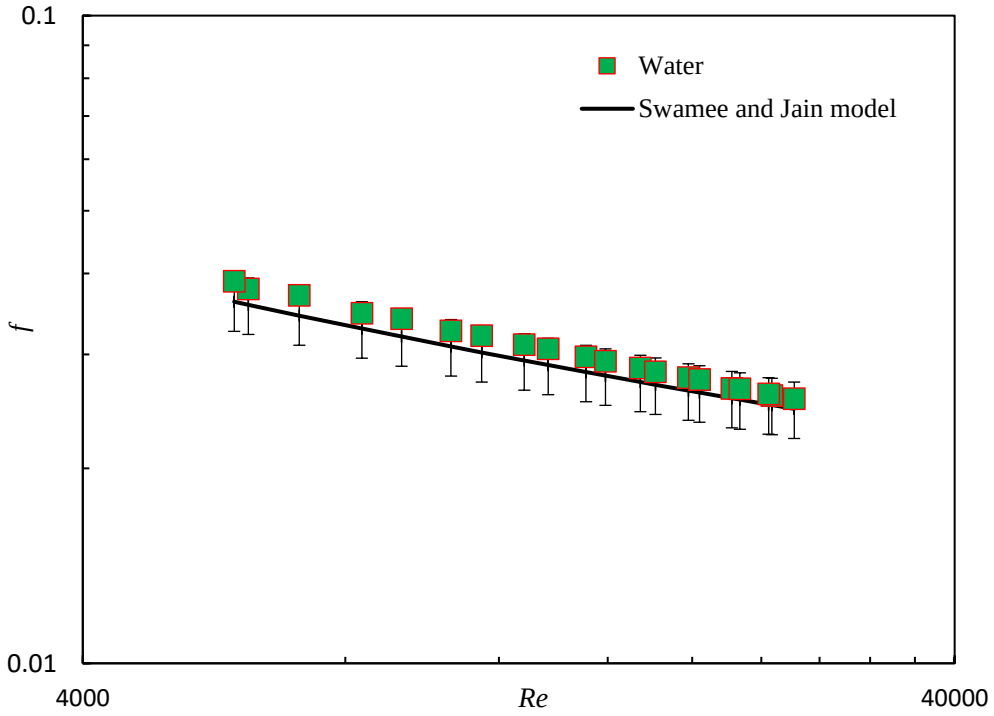

Fig. 4.5 Pressure drop benchmarking test using water with ±10% error bars

where D and ε are the pipe diameter and the surface roughness, respectively. The ε value $0.0015\ mm$ is obtained from Çengel and Cimbala (2010) for new commercial copper pipes. The results are agreed within $\pm 10\%$ of the theoretical model.

Heat Transfer Benchmark Test

The parallel plate smooth channel is constructed from aluminum with a configuration based on a single pass shell and tube heat exchanger and operated in a counterflow arrangement. Two aluminum plate cores were machined and then tightened together to form a smooth channel which was built for heat transfer benchmark testing. A rubber gasket with 1.8 mm diameter was used in O-ring grooves machined inside the cover plate around the formed channel to prevent leakage from the channel. The smooth channel's dimensions details are provided in Appendix B, and the plate spacing is 2.8 mm. The inlet temperatures for water and oil were 40 ℃ and 47 ℃, respectively, while the coolant inlet temperate was 27 ℃. The flow inside the channel was not in the fully developed flow region because the channel length was not long enough. Thus, the results were compared with Nusselt number of a parallel plate channel for a combined entry problem using Stephan (1959) equation

$$Nu_{m,T} = 7.55 + \frac{0.024\left(\frac{L}{D_h Re_{D_h} Pr}\right)^{-1.14}}{1 + 0.0358\left(\frac{L}{D_h Re_{D_h} Pr}\right)^{-0.64} Pr^{0.17}} \tag{4.44}$$

where

$$x^*_{D_h} = \frac{L/D_h}{Re_{D_h} Pr} \tag{4.45}$$

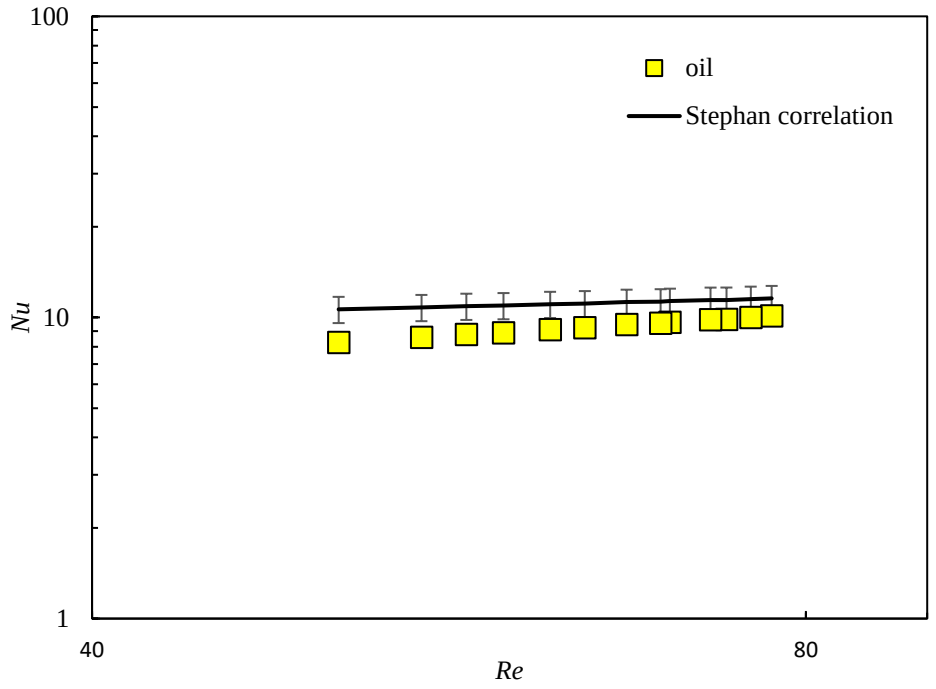

Fig. 4.6 Heat transfer benchmarking test using oil with ±10% error bars

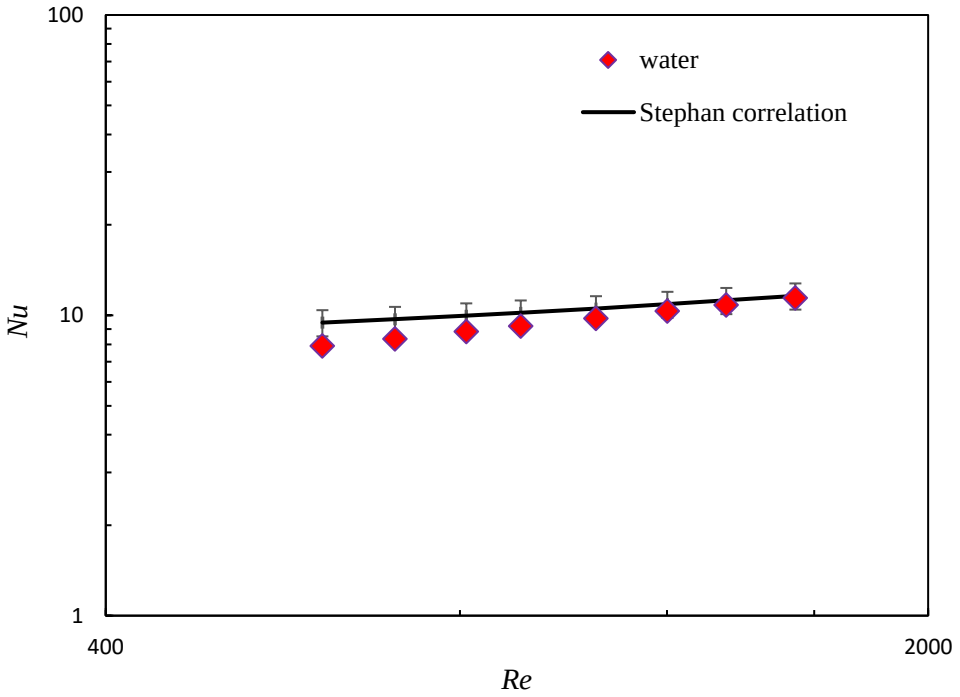

Fig. 4.7 Heat transfer benchmarking test using water with ±10% error bars

This correlation is valid for $0.1 \leq \mathrm{Pr} \leq 1000$ (Shah and London 1978). The experimental results for oil and water are illustrated in Fig 4.6 and 4.7, respectively, and most of the data agreed within ±10 percent to the Stephan equation.

4.6.1 Pressure Drop Results

Experimental results for the Fanning friction factor for all examined plates using oil and water are presented in this section. The friction factor results for fully developed and developing flow for an equivalent smooth channel are included in all plots as a reference.For fully developed laminar flow in a smooth channel, the Fanning friction factor is given by (Shah and London 1978)

$$f = \frac{24}{Re_{D_h}} \tag{4.46}$$

For developing flow, Muzychka (1999) developed a general model to predict the apparent Fanning friction factor, f_{app}, for parallel plate channel which has the following form

$$f_{app} = \frac{1}{Re_{D_h}}\left[\left(\frac{3.44}{\sqrt{x_{D_h}^+}}\right)^2 + 24^2\right]^{1/2} \tag{4.47}$$

where

$$x_{D_h}^+ = \frac{x/D_h}{Re_{D_h}} \tag{4.48}$$

This model is valid over the entire duct length.

In the chevron PHE channel, the equivalent diameter is selected as the characteristic length, while the friction factor for the smooth channel is based on the hydraulic diameter. Thus, using the smooth parallel plates channel as a reference point needs to scale appropriately Re_{D_h} and $x_{D_h}^+$ in Eqs. (4.46), (4.47), and (4.48). From Fig. 4.8, the equivalent diameter in PHEs is defined as twice the corrugation depth (Wang et al. 2007), hence, $D_e = 2b$.

The hydraulic diameter for a channel between parallel plates is defined as twice the space between the two plates. If we assume no ribs on the surface of the plates, the space between

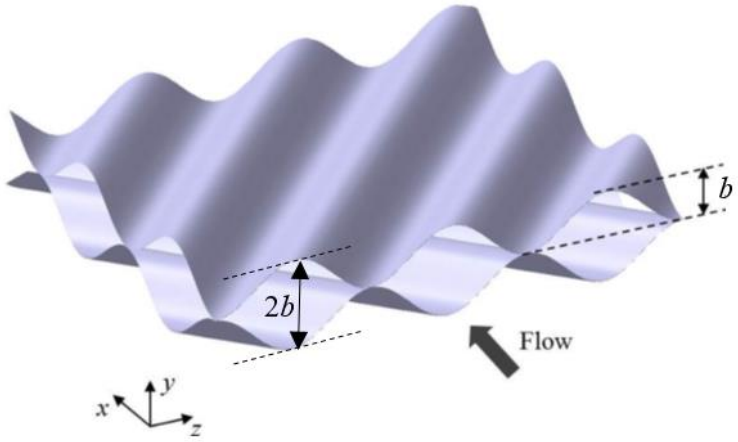

Fig. 4.8 Schematic of inter-plate flow channel for chevron PHE (Lee and Lee 2014)

the two plates becomes $2b$ and yields $D_h = 2 \times 2b$. Thus, the relationship between D_e and D_h can be written as

$$D_e = D_h/2 \tag{4.49}$$

Therefore, Eq. (4.46) and Eq. (4.47) will be re-scaled based on D_e for consistency.

$$f = 12/Re_{D_e} \tag{4.50}$$

$$f_{app} = \frac{1}{Re_{D_e}}\left[\left(\frac{3.44}{\sqrt{x_{D_e}^+}}\right)^2 + (12)^2\right]^{1/2} \tag{4.51}$$

where

$$x_{D_e}^+ = \frac{x/D_e}{Re_{D_e}} \tag{4.52}$$

The rib channel results are now plotted in Figs. 4.9-4.14 against the friction factor for an equivalent smooth channel, Eqs. (4.50) and (4.51). Graphs are divided into two groups: (1) in Figs 4.9 to 4.11, data is plotted at a fixed chevron angle while the channel length varies

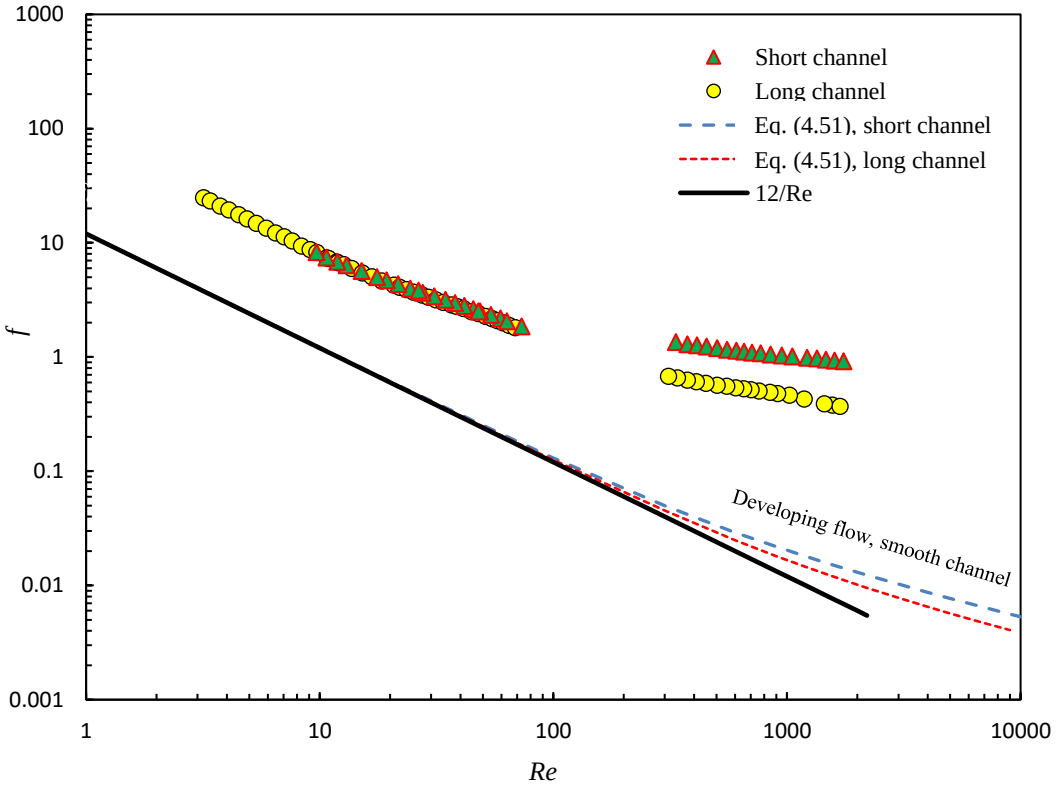

Fig. 4.9 Friction factor for long and short channels, $\beta = 60°$

to show the effect of channel length on f (2) the influence of changing the chevron angle on f at a fixed channel length is presented in Fig 4.13 and 4.14. All chevron plate results are significantly higher than those for an equivalent smooth channel.

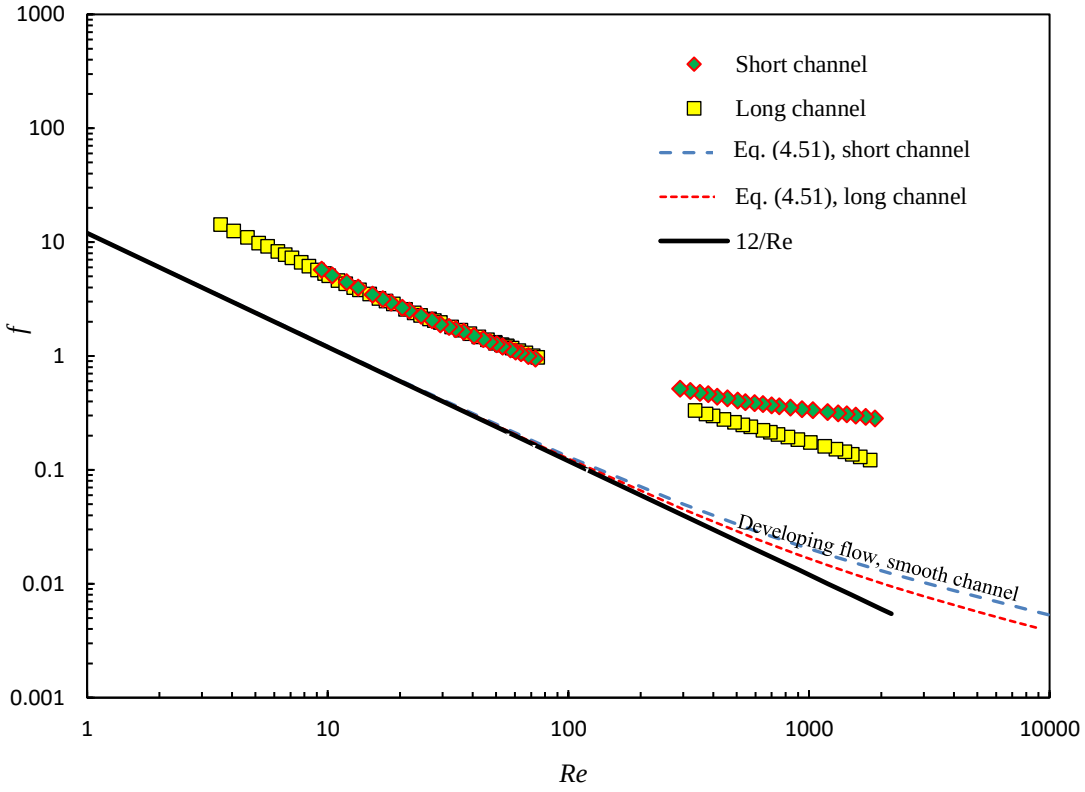

Fig. 4.10 Friction factor for long and short channels, $\beta = 45°$

Furthermore, it is apparent from Figs 4.9 - 4.11 that the short channel results are higher than those of the long channels at higher Reynolds numbers. This implies the presence of the entry effects. At low Reynolds numbers, the results for long and short channels are reasonably similar, implying that fully developed flow conditions. As a result, the entry effects can be neglected. This becomes more apparent when all the data is plotted as $f.Re_{D_e}$ vs Re_{D_e}, Fig. 4.12.

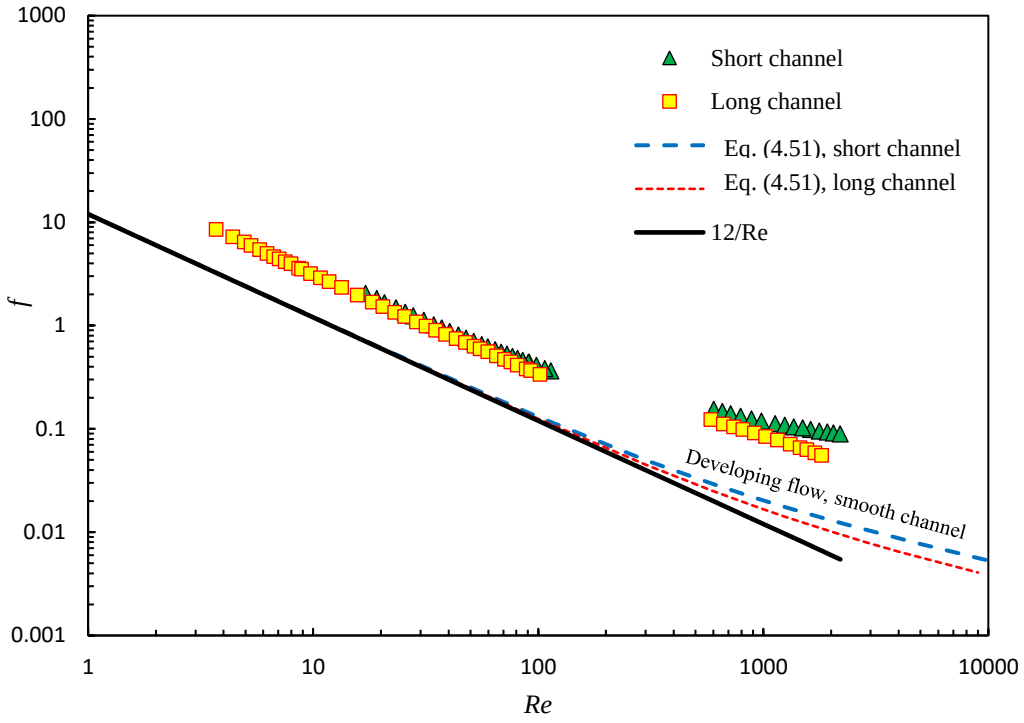

Fig. 4.11 Friction factor for long and short channels, β=30°

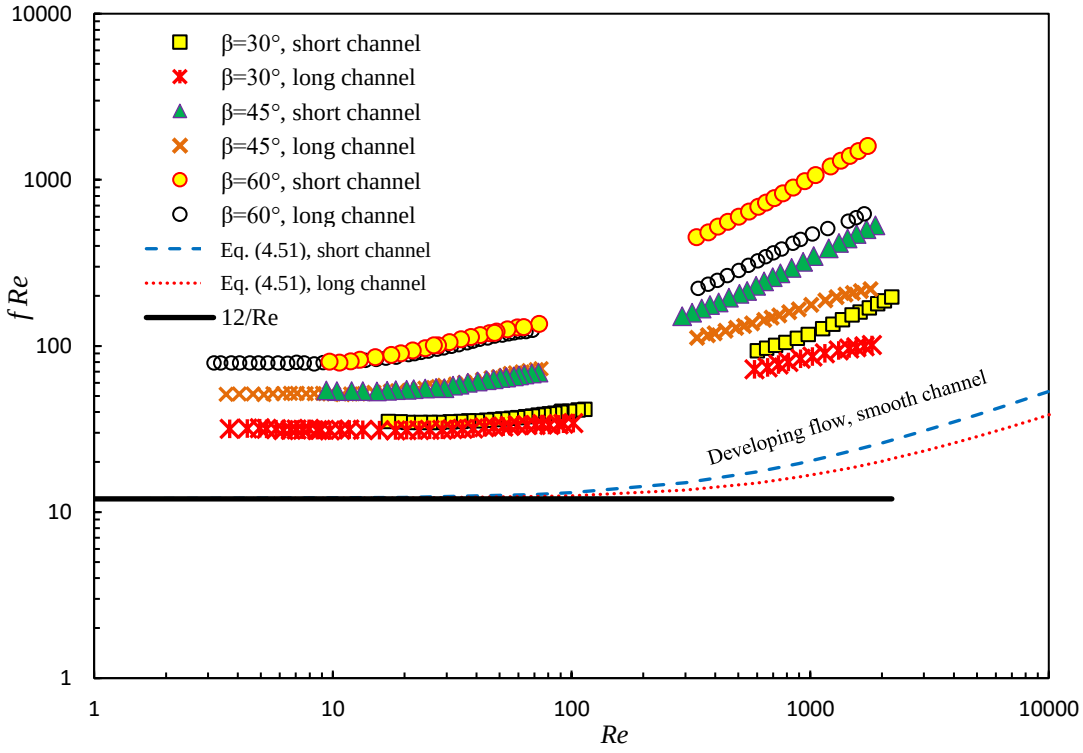

Fig. 4.12 $f.Re_{D_e}$ factors for all chevron channels

The effect of chevron angle on f at two different lengths for a wide range of Reynolds numbers is shown in Fig 4.13 and 4.14. For all tested plates, regardless of the channel length, the results indicate that the chevron angle has a strong effect on f, which increases by increasing the chevron angle. This is consistent with the literature (Saha and Khan (2020), (Khan et al. (2017), Focke et al. (1985)), and Wang et al. (2007)).

When $Re_{D_e} < 20$, there appears to be no swirl generation effect in this region, as all the chevron data exhibit the smooth channel fully developed flow behavior. The dependency of the convoluted flow path length on β is the reason why f increases with increasing β in this region (Wang et al. 2007).

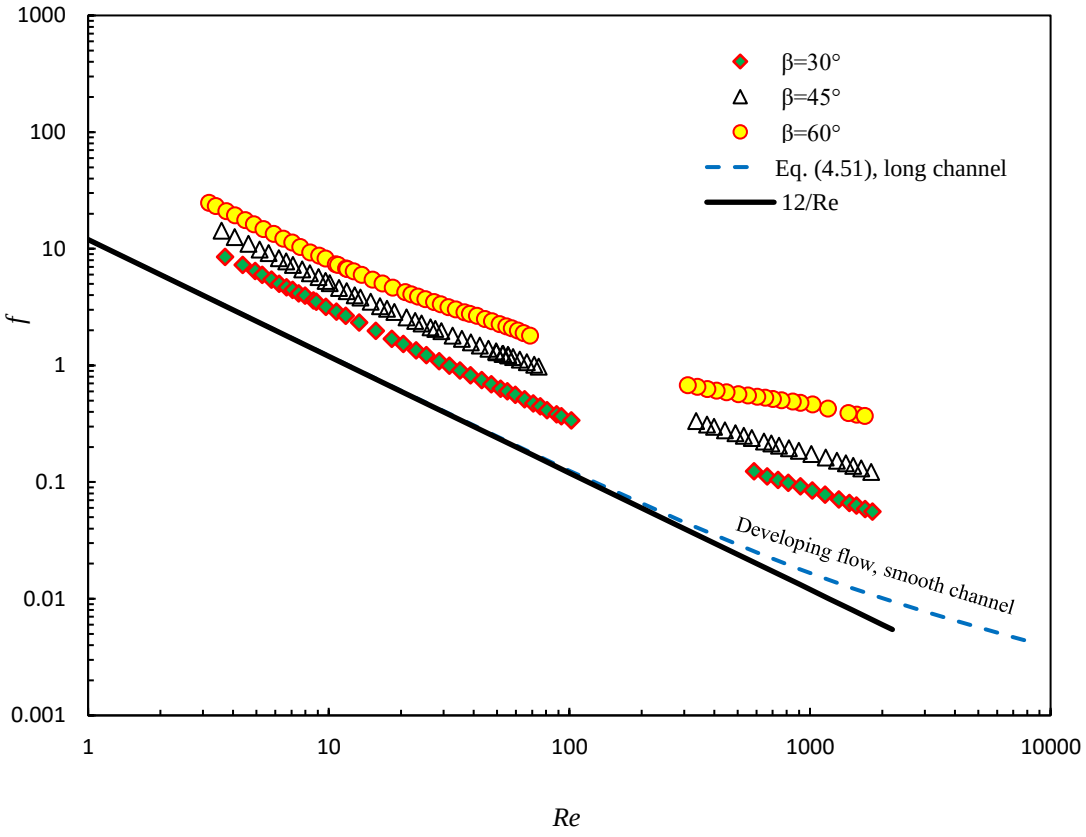

Fig. 4.13 Friction factor for all long channels

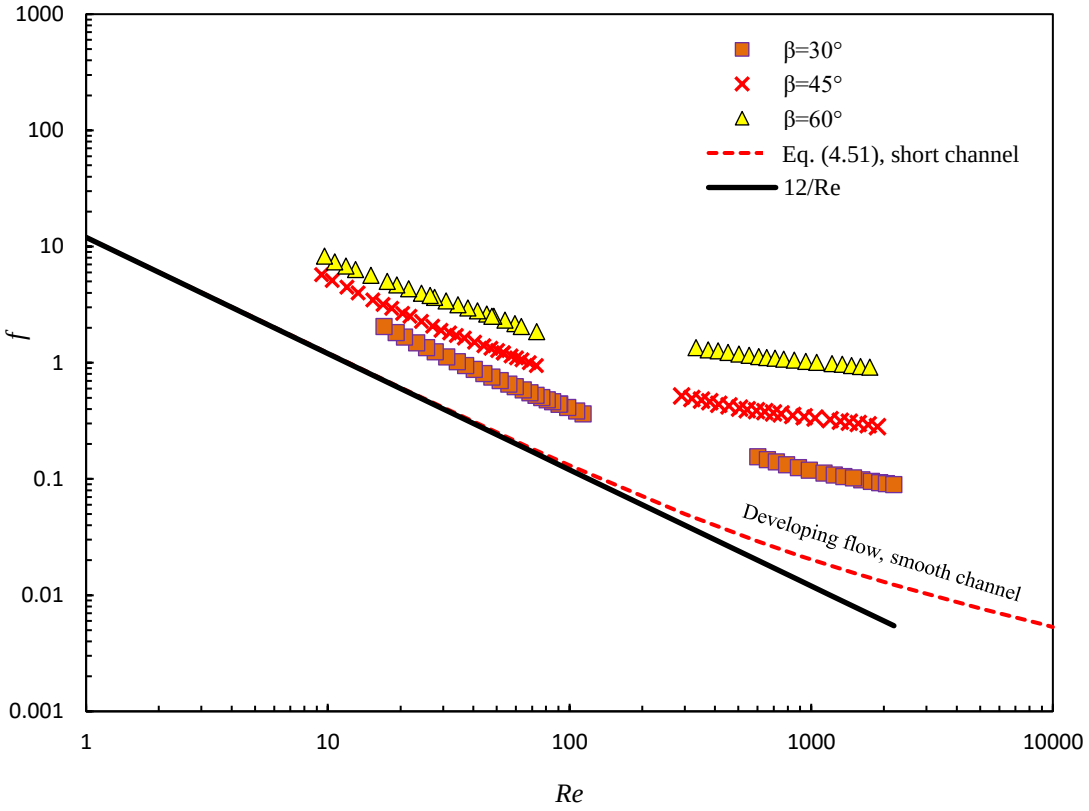

Fig. 4.14 Friction factor for all short channels

The experimental data can be compared with a selection of reported results from the literature for the same chevron angles, $\beta = 30°, 45°$, and $60°$, which are shown in Figs. 4.15 - 4.17. As seen in Fig 4.15, for $\beta = 30°$, there is a good agreement between the present data and those of Junqi et al. (2018), Bond (1981), and Thonon et al. (1995). However, the results of Khan et al. (2017), Shaji and Das (2013) are considerably higher. In the case of $\beta = 45°$, the results of the present experiment compare well with the data of Junqi et al. (2018), Khan et al. (2017), Bond (1981), and Thonon et al. (1995), as shown in Fig 4.16 Shaji and Das's (2013) data, however, are much higher. For $\beta = 60°$, Figure 4.17 shows that there is a fair agreement between the current data and those of Shaji and Das (2013),

Alzahran et al. (2019), and Junqi et al.(2018). The results of Thonon et al. (1995), however, are higher, and Bond (1981) for $Re < 20$ are lower.

Disagreements between the present and reported data are difficult to explain. This inconsistency may be attributed to a variety of factors such as corrugation profile (e.g., trapezoidal or sinusoidal), corrugation depth, corrugation wavelength, and plate sizes that are not identical in all studies. As seen in the current results, another reason that leads to a disagreement is the entrance effect or channel length. Another factor to consider is the pressure drop associated with manifolds and distribution zones, which differ in design between the manufacturers.

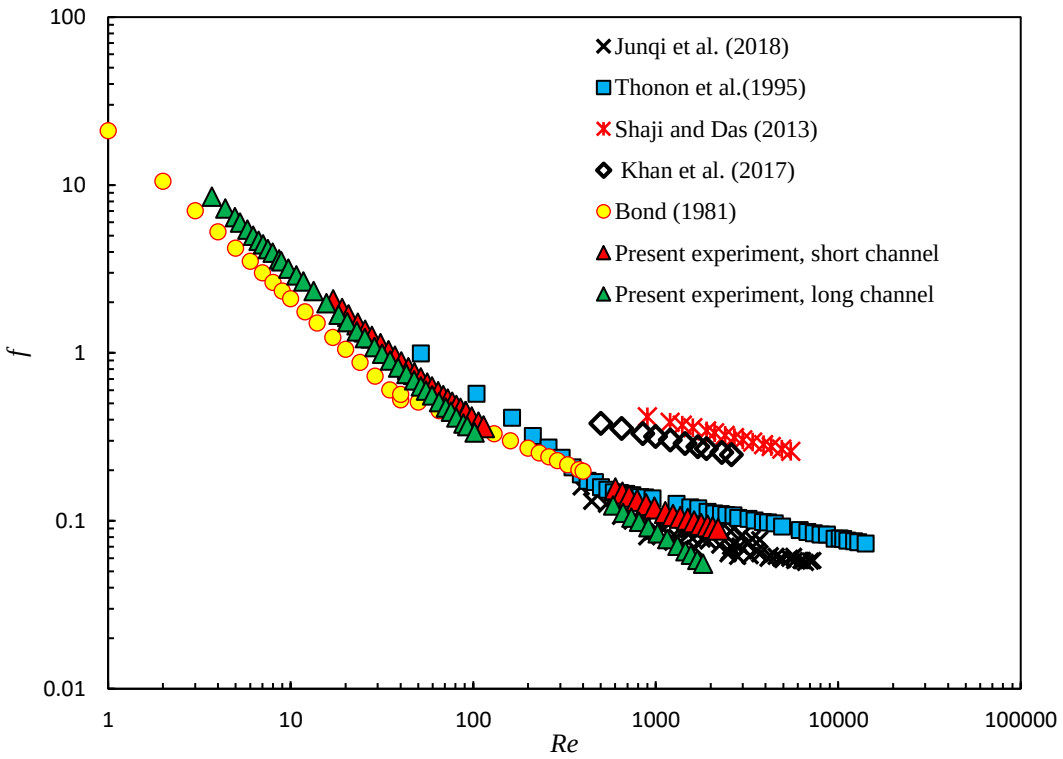

Fig. 4.15 Comparison of Friction factor results with literature for $\beta = 30°$

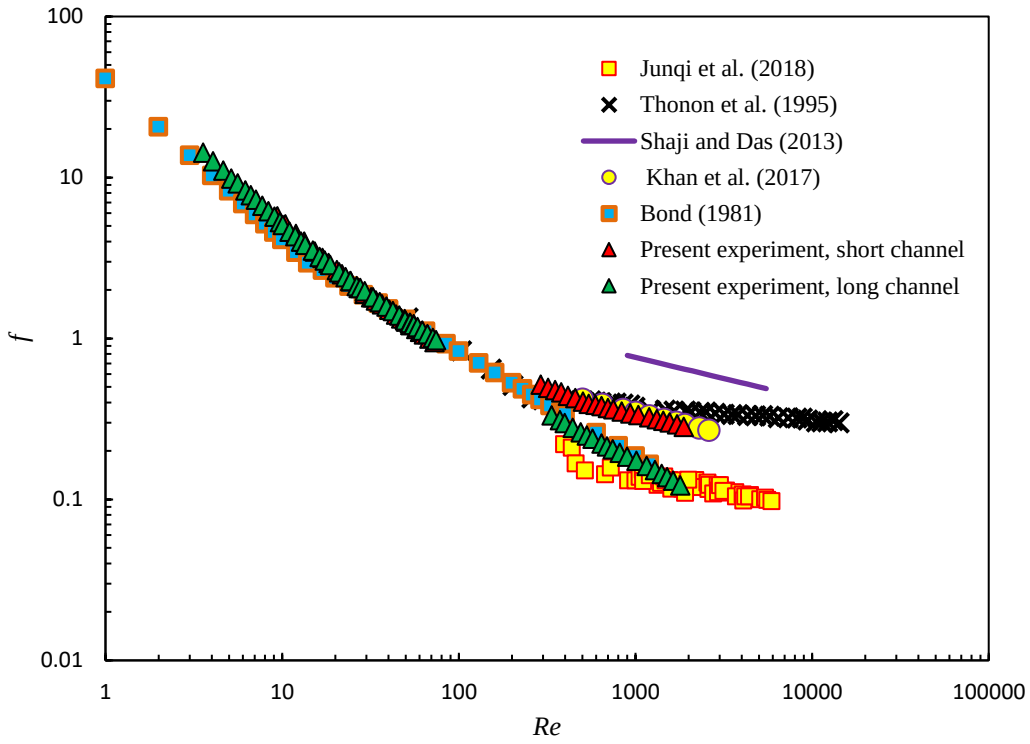

Fig. 4.16 Comparison of Friction factor results with literature for $\beta = 45°$

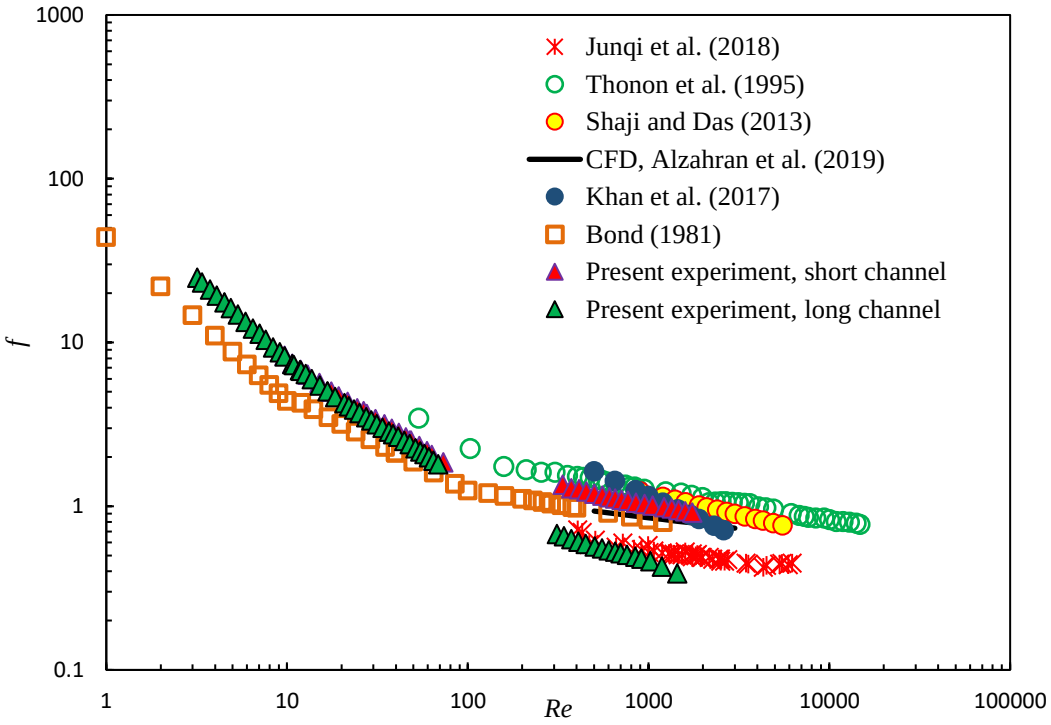

Fig. 4.17 Comparison of Friction factor results with literature for $\beta = 60°$

4.6.2 Heat Transfer Results

Nusselt number data for the chevron plates are presented in this section. All results are compared with Nu for an equivalent parallel plate channel using the Stephan correlation, Eq. (4.44), which has been re-scaled based on Eq. (4.49), as follows

$$\left(Nu_{D_e}\right)_{m,T} = 3.78 + 0.5\left[\frac{0.024\left(x^*_{D_e}\right)^{-1.14}}{1 + 0.0358\,Pr^{0.17}\left(x^*_{D_e}\right)^{-0.64}}\right] \tag{4.53}$$

where

$$x^*_{D_e} = \frac{L/D_e}{Re_{D_e}Pr} \tag{4.54}$$

The results are separated into two groups of plots based on how they are presented: (1) Figures 4.18 to 4.20 show the data at a fixed β while the channel length changes to investigate its effect on Nu. These plots show that the Nusselt number for the short plates is considerably higher than those of the longer channels, which indicates the presence of thermal entry effects. (2) the influence of varying β on Nu at a fixed channel length is presented in Figs 4.21 and 4.22. Heat transfer augmentation is clearly observed, which appears to increase by increasing the chevron angle and Reynolds numbers as compared to the smooth channel. This may be attributed to the increase of the induced secondary flow or swirl flow with the rise of β (Wang et al. 2007).

The current data can be compared to several previously published results for the same chevron angles. In Fig. 4.23, Nu data for $\beta = 60°$ is in fair agreement with all the reported data, except those of Thonon et al. (1995) for $Re > 100$ and Vlasogiannis et al. (2002) for

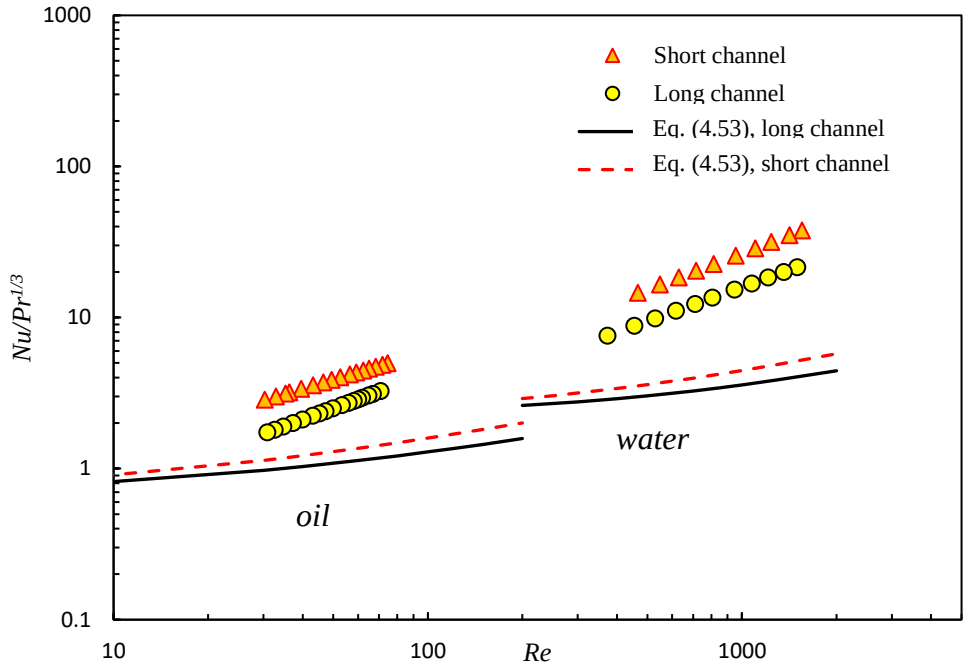

Fig. 4.18 Nusselt Number for long and short channels for β=60°

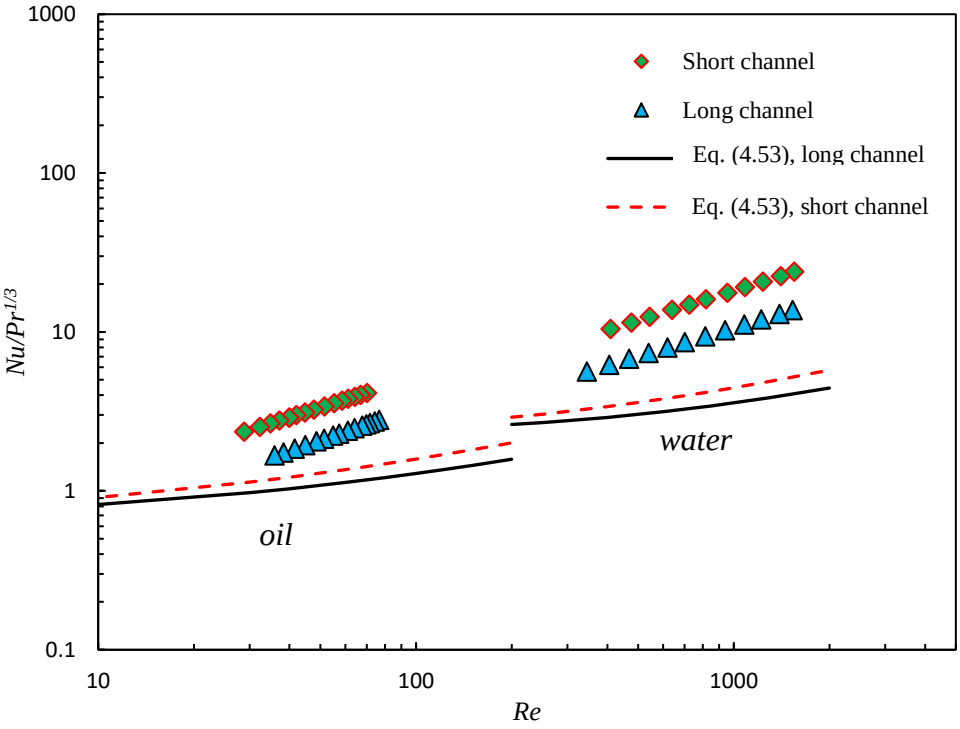

Fig. 4.19 Nusselt Number for long and short channels for β=45°

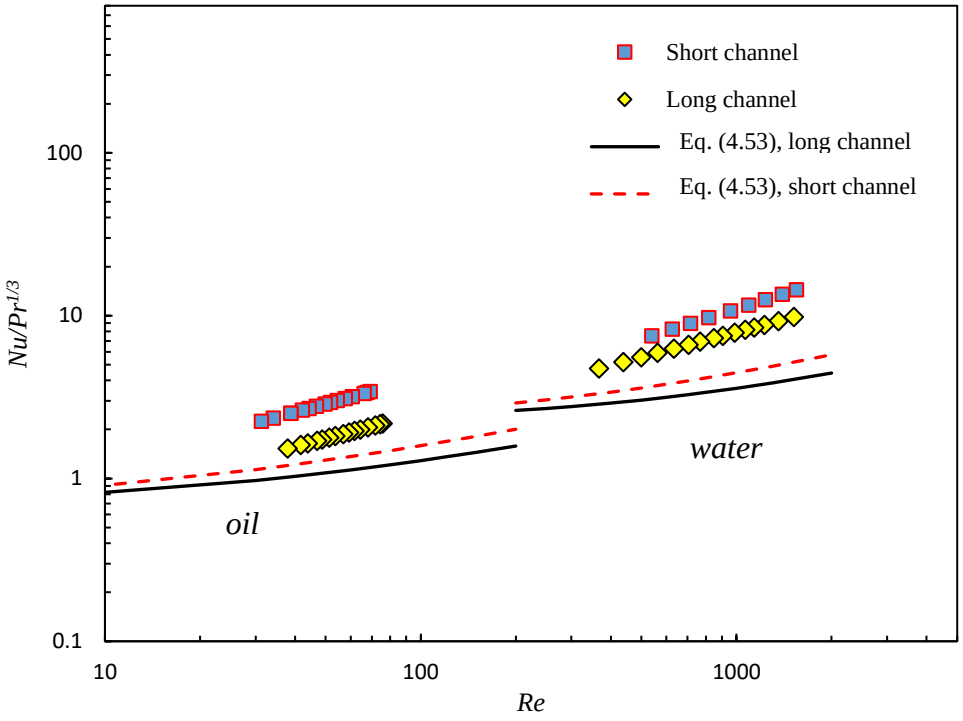

Fig. 4.20 Nusselt Number for long and short channels for β=30°

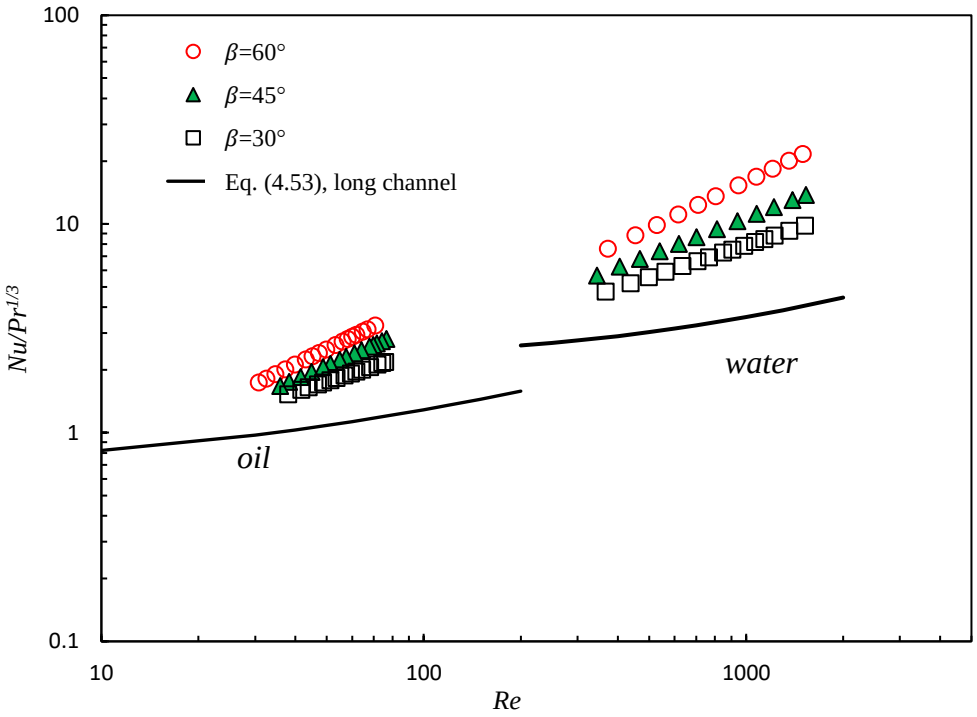

Fig.4.21 Nusselt Number for all long channels

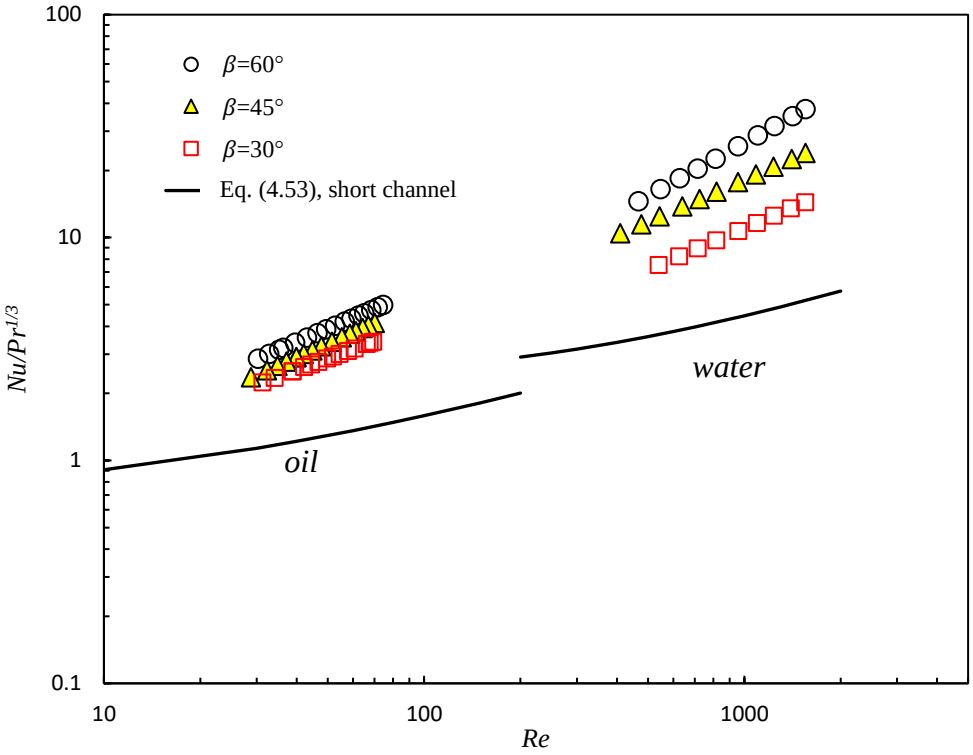

Fig. 4.22 Nusselt Number for all short channels

$Re < 300$. It can be observed from Figs. 4.24 and 4.25 that there is a good agreement between the present data for short plates and the work of Shaji and Das (2013), Muley et al. (1999), and Muley and Manglik (1999) for $\beta = 30°$ and 45°, whereas the results of Junqi et al. (2018) and Thonon et al. (1995) are much higher.

The discrepancy between results from different authors, including the present results, as shown in Figs 4.23 - 4.25, can be attributable to a variety of factors including the differences of plate surface geometries such as corrugation profile (e.g., trapezoidal, or sinusoidal), b, λ, ϕ and also number and size of plates, port size, and orientation, and flow distribution channels are not identical in all studies. Another possible reason, which should not be ignored, is the entrance effect as found in the current result.

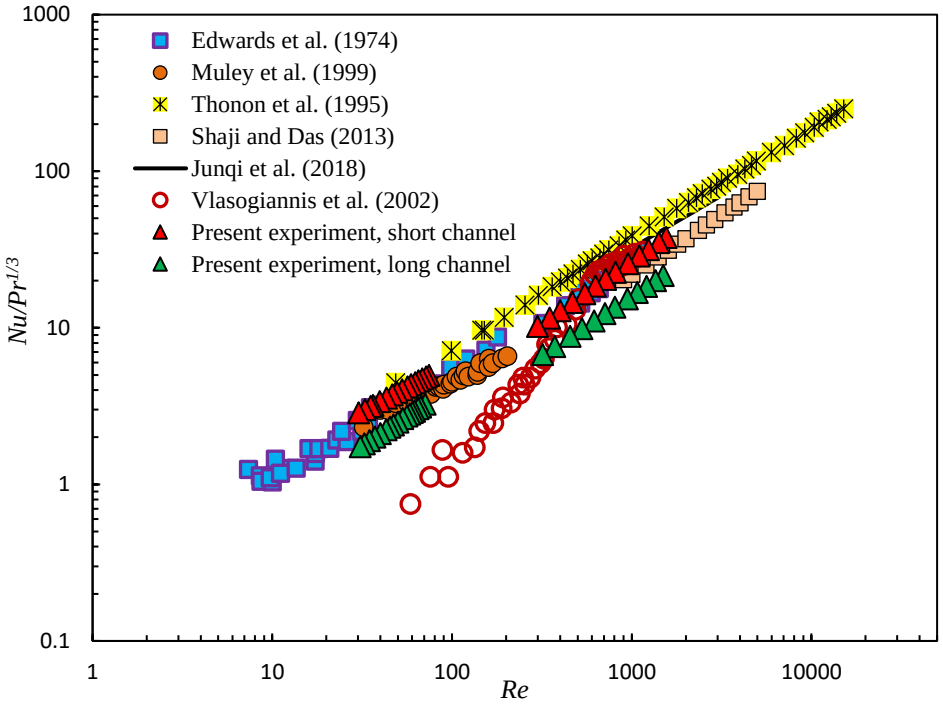

Fig. 4.23 Comparison of Nusselt number results with literature for $\beta = 60°$

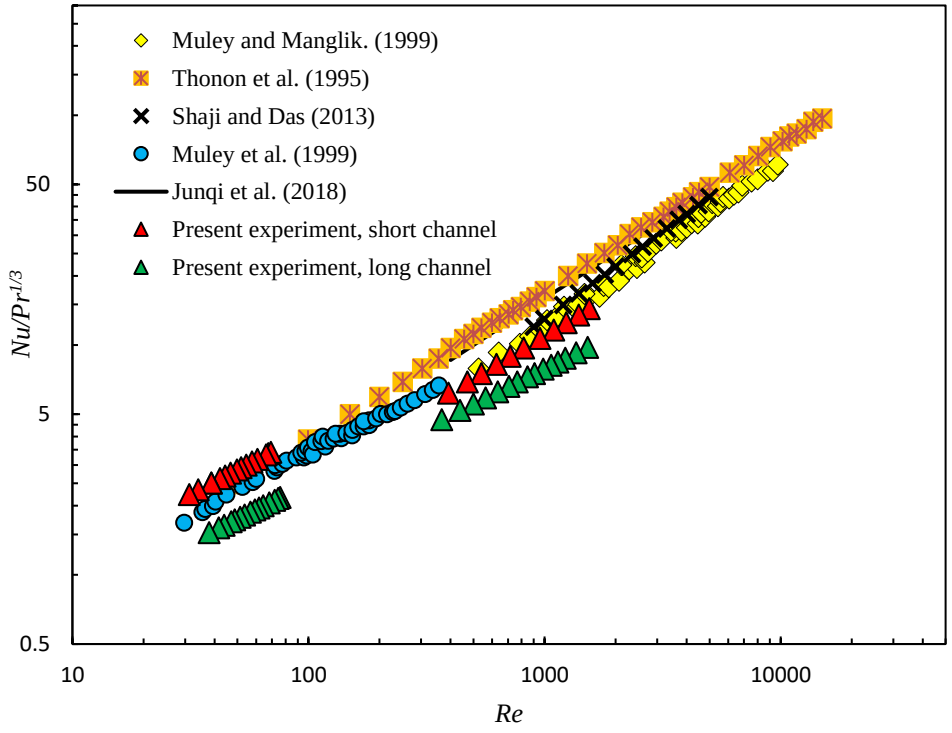

Fig. 4.24 Comparison of Nusselt number results with literature for $\beta = 30°$

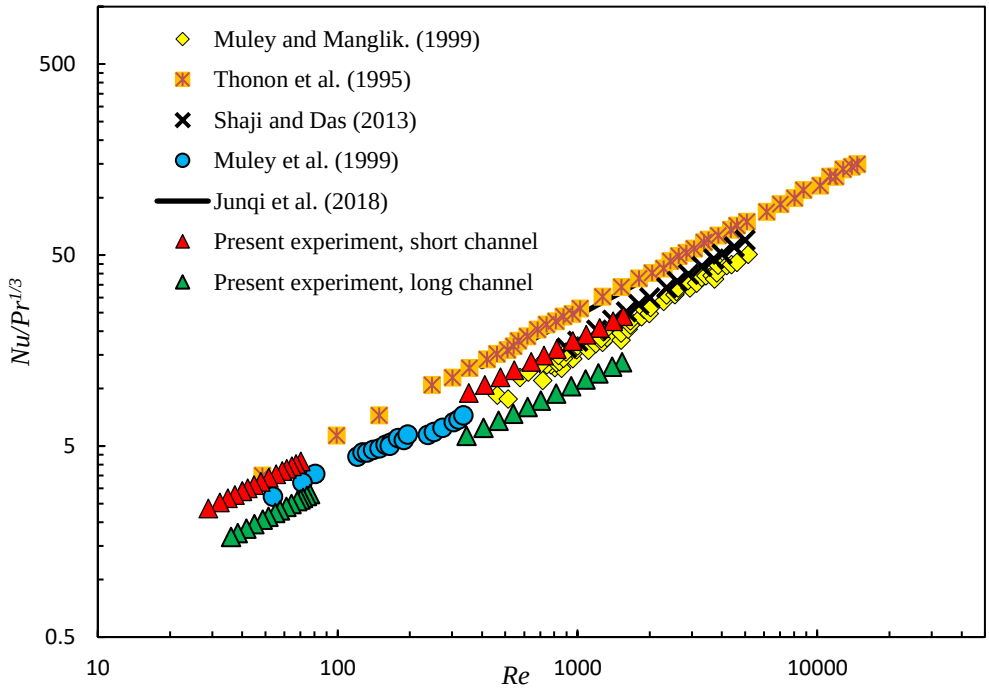

Fig. 4.25 Comparison of Nusselt number results with literature for $\beta = 45°$

4.7 Conclusions

The details of the experimental procedure and results for six chevron plates with three different angles, $\beta = 30°, 45°$ and $60°$, and two lengths were presented in this chapter. The data reduction technique was described in detail. The benchmarking test results for pressure drop and heat transfer in a pipe and smooth channel were also presented. The agreement between the results and the theoretical values was within $\pm 10\%$. A comparison between the long and short chevron plate results showed that both the friction factor (except for very low Reynolds numbers) and Nusselt number were significantly affected by the entrance effect. Moreover, the experimental results demonstrated that the chevron angle has a significant effect on the heat transfer and pressure drop which increase by increasing the chevron angle. The current results were then compared to data from the literature, and fair

agreement was observed in many cases, however, some discrepancies were noted. The experimental uncertainty in the Reynolds number, Fanning friction factor, and Colburn factor was found to be $\pm 2.09 - 2.5\%$ and $\pm 3.65 - 4.54\%$, and $\pm 7.70 - 14.08\%$, respectively.

Chapter 5

Development of Pressure Drop Model for Chevron PHEs

5.1 Introduction

This chapter is divided into three sections. First, a review of the friction factor equations for fully developed and developing laminar flow for a smooth channel is presented, which are used in the development of the proposed model. Next, model development for the chevron PHE channel is discussed. Finally, comparisons of the proposed model with new experimental data, as well as data from the literature are presented to validate the developed model.

5.2 Friction Factor for a Parallel plate channel

Initially, expressions that have been used to calculate the friction factor for developing and fully developed laminar flow in a parallel plate channel are presented as a reference point. The reason for choosing the laminar flow region is that all the experimental data obtained are considered to be within the laminar flow regime in a smooth channel.

In the hydrodynamic entrance region, the velocity profile changes from the initial profile at the entrance to invariant form downstream. The flow in this region is hydrodynamically developing flow due to the viscous fluid behavior. The apparent friction factor, f_{app}, is higher than the friction factor for the fully developed region because it takes into account both the skin friction and the change in momentum rate in the entrance region (Shah and London, 1978). Shah and London (1978) defined $f_{app}\ Re$ as follows

$$f_{app}Re = f_{\text{fd}}\, Re + \frac{K(x)}{4x^+} \tag{5.1}$$

where

$$x^+ = \frac{x}{D_h\, Re} \tag{5.2}$$

f_{fd} represents the friction factor for fully developed flow, x^+ is the dimensionless axial distance and $K(x)$ is the incremental pressure drop number. The value of $K(x)$ increases from 0, at $x = 0$, to a constant value, $K(\infty)$, in the fully developed region. The $f_{app}Re$ for a parallel plate channel is given by Shah and London (1978)

$$f_{app}Re_{D_h} = \frac{3.44}{\sqrt{x^+}} \qquad x^+ < 0.001 \tag{5.3}$$

$$f_{app}Re_{D_h} = f_{\text{fd}} + \frac{K(\infty)}{4x^+} \qquad x^+ > 0.01 \tag{5.4}$$

where $K(\infty)$ is the incremental pressure drop for the fully developed flow, which is found to be 0.674.

For the fully developed flow region, the velocity profile is fully developed and the pressure gradient in the flow direction becomes constant. Therefore, the friction factor becomes independent of position. The Fanning friction factor is defined as

$$f = \frac{\bar{\tau}_w}{\frac{1}{2}\rho\bar{u}^2} \tag{5.5}$$

where $\bar{\tau}_w$ is the average wall shear stress, ρ is the density of the fluid and $\bar{u}$ is the average velocity in the duct. Equation (5.5) can be expressed in terms of the Reynolds number as follows

$$fRe_{D_h} = \frac{\bar{\tau}_w D_h}{\frac{1}{2}\mu \bar{u}} \tag{5.6}$$

Since the wall shear stress does not change axially beyond the hydrodynamic entry length, $f\ Re$ is found to approach a constant value for very large values of x^+, which is given by

$$fRe_{D_h} = \mathcal{M} \tag{5.7}$$

where $\mathcal{M}$ is a constant dependent on the geometry of the duct's cross section and equals 24 for fully developed laminar flow in parallel plate channel (Shah and London 1978).

Shah (1978) proposed a general correlation to predict $f_{app}Re$, which covers all vales of x^+, as follow

$$f_{app}Re_{D_h} = \frac{3.44}{\sqrt{x^+}} + \frac{24 + (0.674/4x^+) - \left(3.44/\sqrt{x^+}\right)}{1 + 0.000029\ (x^+)^{-2}} \tag{5.8}$$

Muzychka (1999) developed a general model simpler than that of Shah (1978) using Churchill and Usagi (1972) asymptote correlation method. This was achieved by combining the developing flow asymptote in Eq. (5.3), and fully developed flow asymptote in Eq. (5.7). The developed model, refer to Eq. (4.47), is valid over the entire duct length and predicts $f_{app}Re$ of Shah (1978) within $\pm 2.4\%$. This model is used to generate Fig. 5.1 for different L/D_h ratios. The purpose of this graph is to show the entrance effect on the friction factor for arbitrary values of L/D_h ratios over a wide range of Reynolds numbers. It can be clearly seen that at higher Reynolds numbers the results for short channel, for instance $L/D_h = 10$, are significantly higher than those of the long channels, for example $L/D_h = 200$. This indicates that hydrodynamic entrance effects are present and

of considerable magnitude. On the other hand, at low Reynolds number, $Re \leq 20$, the L/D_h ratio has no influence on the friction factor which implies fully developed flow conditions exist.

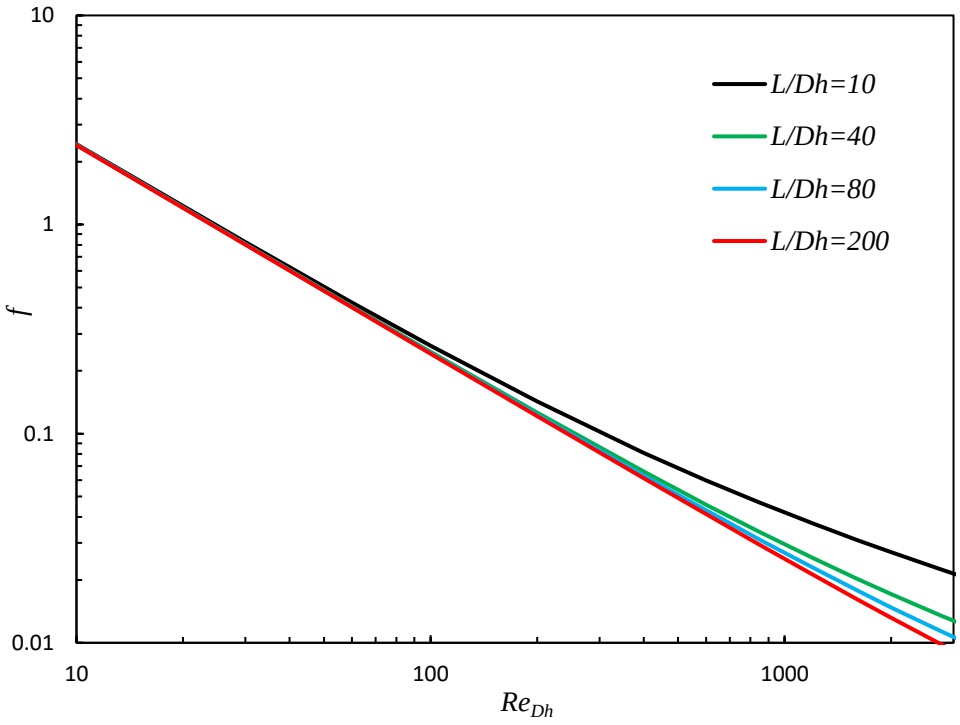

Fig. 5.1 Apparent friction factor of a smooth channel for different L/D_h ratios

It should be emphasized that in all the above equations, the $x^+$and Re_{D_h} definitions are based on the hydraulic diameter, twice the space between two parallel plates.

5.3 Friction Factor Model development

In this section, the details of the model development for the chevron channel geometry are discussed. The equivalent diameter is chosen as the characteristic length in the chevron PHE channel and the friction factor for the smooth channel is based on the hydraulic

diameter. Thus, using the smooth parallel plates channel as a reference point needs to scale appropriately Re and x^+in Eqs. (5.3) and (5.7). Therefore, $f_{app}Re$ in Eq. (5.3) and fRe in Eq. (5.7) will be re-scaled based on $D_e = D_h/2$, refer to Eq. (4.49), for consistency.

$$f_{app}Re_{D_e} = \frac{3.44}{\sqrt{x^+_{D_e}}} \tag{5.9}$$

$$fRe_{D_e} = 12 \tag{5.10}$$

The plots in Figs 5.1 and 5.2 show the behaviour of Eqs. (5.9) and (5.10) in comparison with the friction factors of chevron plates for two selected cases: (1) when the chevron angle is fixed, $\beta = 30°$, which has the lowest pressure drop, while the channel length is changing; (2) the channel length is fixed, and the chevron angle is changing $\beta = 30°, 45°$ and $60°$. The reason for choosing long channels in this case is because they have lower friction factors compared to the short channels.

Examining the plots, Figs. 5.2 and 5.3 reveal some important characteristics of the experimental data and the two limiting asymptotes of the smooth channel. First, the friction factor for the developing and fully developed flow of the smooth channel act as lower limits. Secondly, the plot in Fig. 5.2 demonstrates that for fixed chevron angle, the friction factor at low Reynolds number, $Re < 20$, for long and short lengths are approximately the same, which means fRe is independent on the channel length, see Fig. 5.4. At a higher Reynolds number, the short channel has a higher friction factor than the long one, which indicates that f is dependent on the channel length as everything is kept constant, including the rib angle and geometry. The only thing that is changing is the nominal channel length. Finally, Fig (5.3) shows that for fixed channel length, the chevron angle has a significant

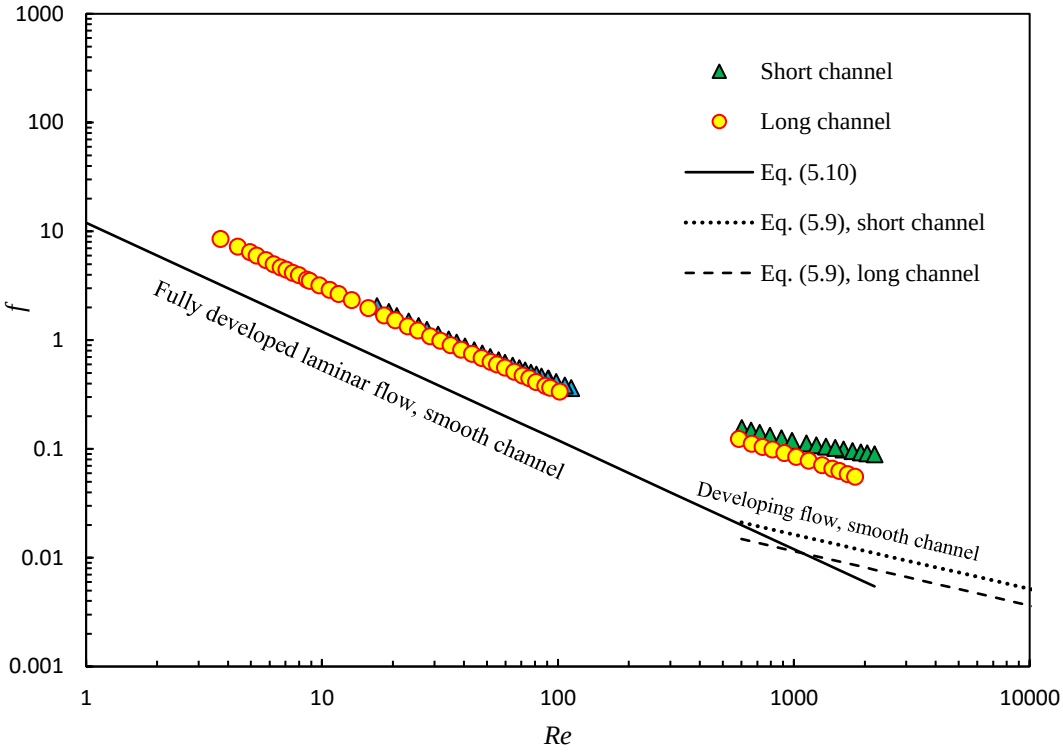

Fig. 5.2 Friction factor for long and short channels for $\beta = 30°$

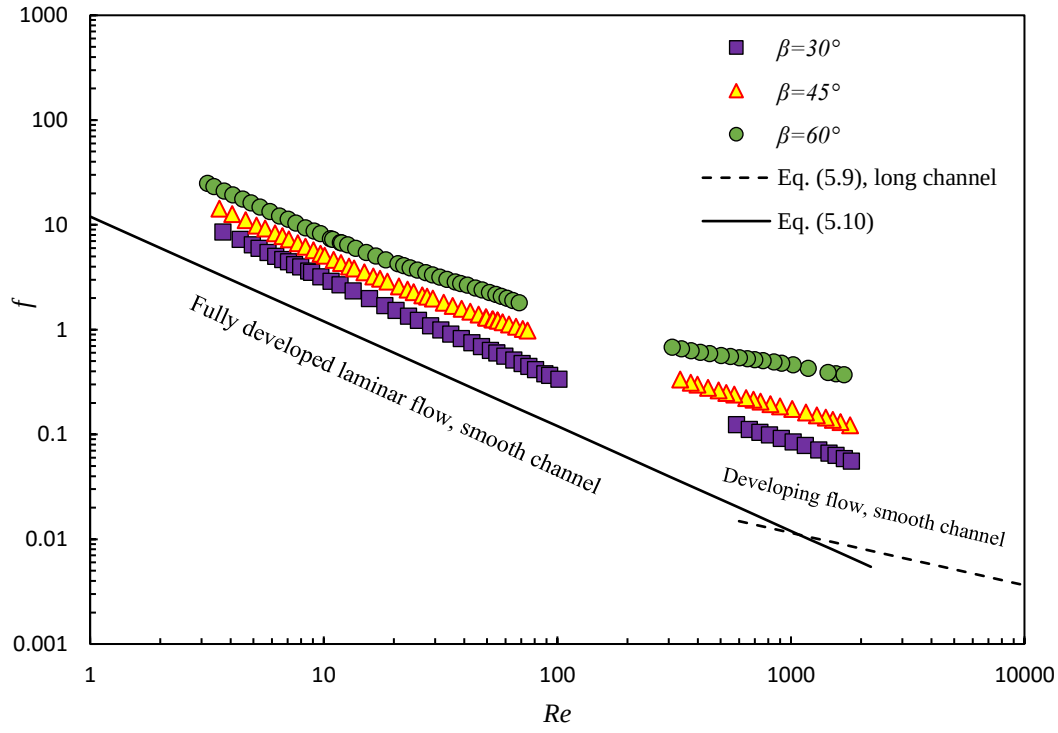

Fig. 5.3 Friction factor for all long channels

effect on f in both regimes, at low and high Reynolds numbers.

Based on these observations, the $f_{app}Re$ product model for the chevron channel is proposed to take the form

$$f_{app}Re_{D_e} = \left[\left(fRe_{D_e}\right)_{\text{fd}}^{n} + \left(f_{app}Re_{D_e}\right)_{\text{dev}}^{n}\right]^{1/n} \tag{5.11}$$

where $\left(fRe_{D_e}\right)_{\text{fd}}$ and $\left(f_{app}Re_{D_e}\right)_{\text{dev}}$ are the asymptotic solutions for fully developed flow and developing flow, respectively. The fitting parameter, n, is used to control the model behavior in the transition region and its value will be selected as the value which minimizes the root mean square error between the model prediction and the available data.

Fully Developed Flow Asymptote

Figure 5.4 shows that for $x^+ \geq 3$, $f\,Re$ for chevron plates is parallel to that in a smooth channel, regardless of the channel length and is found to approach a constant value for each β. Thus, only the rib angle has an influence on the friction factor in this regime.

$$(f\,Re)_{60^\circ} = C_{14} \tag{5.12}$$

$$(f\,Re)_{45^\circ} = C_{15} \tag{5.13}$$

$$(f\,Re)_{30^\circ} = C_{16} \tag{5.14}$$

where, $C_{14} > C_{15} > C_{16}$. Therefore, the fully developed flow term of the smooth channel in Eq. (5.10) has been modified by a coefficient, $\mathcal{A}$, to take into account the effect of β on the friction factor.

$$\left(fRe_{D_e}\right)_{\text{fd}} = \mathcal{A} \tag{5.15}$$

where

$$\mathcal{A} = g_1(\beta) \tag{5.16}$$

Based on the experimental data, the coefficient $\mathcal{A}$ is correlated by

$$\mathcal{A} = \frac{24}{\cos(\beta)^{1.73}} \tag{5.17}$$

Substituting Eq. (5.17) into Eq. (5.15), the fully developed asymptote for the chevron channel becomes:

$$\left(fRe_{D_e}\right)_{\text{fd}} = \frac{24}{\cos(\beta)^{1.73}} \tag{5.18}$$

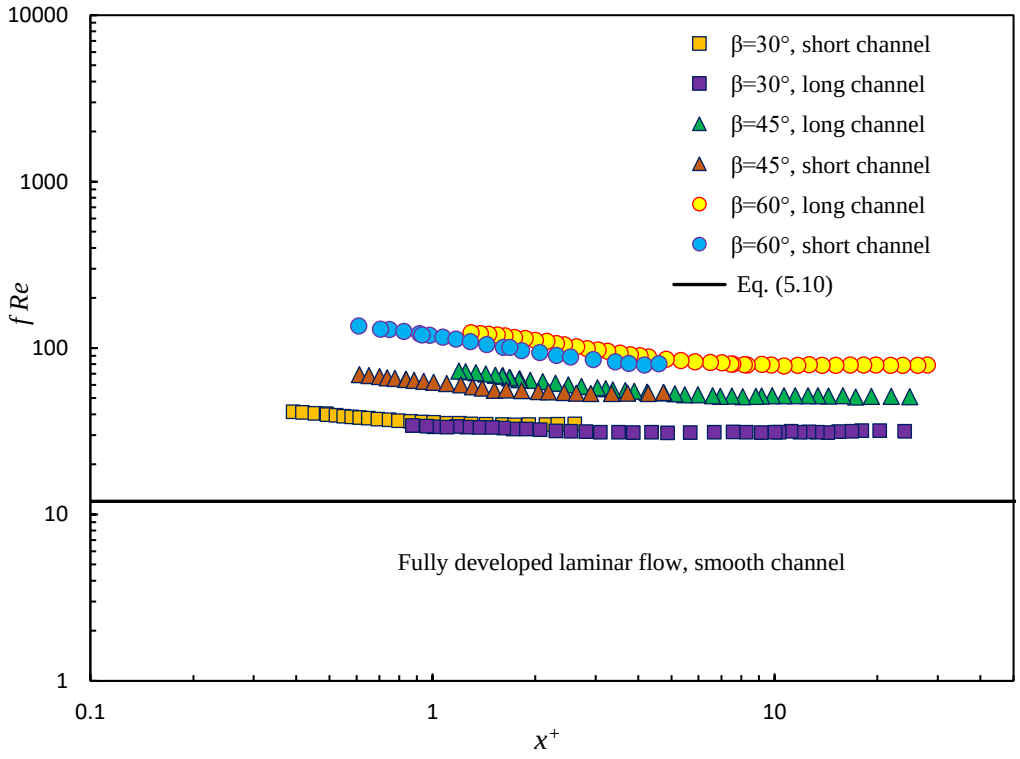

Fig. 5.4 fRe factor for all chevron plates at low Reynolds number

Developing Flow Asymptote

For a high Reynolds number flow region, Fig (5.2), it can be seen that the friction factor is not independent of length as in fully developed flow. Moreover, it is found that the Re

exponent is also not constant as in the smooth channel. Thus, the developing flow term for the smooth channel in Eq. (5.9) has been modified by a coefficient $\mathcal{B}$ as follows

$$\left(f_{app}Re_{D_e}\right)_{\text{dev}} = \mathcal{B} \tag{5.19}$$

where

$$\mathcal{B} = g_2(\sqrt{L/D_e}, Re, \beta) \tag{5.20}$$

Based on the experimental results, the coefficient $\mathcal{B}$ can be calculated using an expression of the form

$$\mathcal{B} = \frac{\mathcal{H}}{\sqrt{L/D_e}}\, Re^{\mathcal{K}\beta^{0.675}} \tag{5.21}$$

where

$$\mathcal{H} = 32,\ \mathcal{K} = 0.0439 \quad \text{for the long channel, } \sqrt{L/D_e} = 9.43$$

$$\mathcal{H} = 16,\ \mathcal{K} = 0.0551 \quad \text{for the short channel, } \sqrt{L/D_e} = 6.67$$

Composite Model

The asymptotes developed for fully developed flow and developing flow in the previous sections are combined using Churchill and Usagi (1972) composite solution technique. Hence, substituting the fully developed and developing flow asymptotes defined in Eqs. (5.15) and (5.19) into Eq. (5.11), the $f_{app}Re_{D_e}$ model for the chevron channel becomes

$$f_{app}Re_{D_e} = [(\mathcal{A})^n_{\text{fd}} + (\mathcal{B})^n_{\text{dev}}]^{1/n} \tag{5.22}$$

The blending parameter is found to be $n = 2$, for long and short channels. Substituting Eq. (5.18) and Eq. (5.21) into Eq. (5.22) and rearranging, produces the following expression

$$f_{app} = \frac{1}{Re_{D_e}}\left[\left(\frac{24}{\cos(\beta)^{1.73}}\right)^2_{\text{fd}} + \left(\frac{\mathcal{H}}{\sqrt{L/D_e}}Re^{\mathcal{K}\beta^{0.675}}\right)^2_{\text{dev}}\right]^{1/2} \tag{5.23}$$

Since the developed model is a function of the channel length, we will have one model for the long channel and one model for the short channel. The f_{app} model for the long channel when $\mathcal{H} = 32$ and $\mathcal{K} = 0.0439$ in Eq. (5.23) is

$$f_{app} = \frac{12}{Re_{D_e}}\left[\left(\frac{2}{\cos(\beta)^{1.73}}\right)_{\text{fd}}^{2} + \left(\frac{2.66}{\sqrt{L/D_e}}Re^{0.0439\beta^{0.675}}\right)_{\text{dev}}^{2}\right]^{1/2} \tag{5.24}$$

This model is valid for $L/D_e = 89.12,\ \gamma = 0.504,\ 30° \le \beta \le 60°$ and $2 \le Re_{D_e} \le 2{,}300$. The f_{app} model for the short channel, when $\mathcal{H} = 15.99$ and $\mathcal{K} = 0.055$ in Eq. (5.23) is

$$f_{app} = \frac{12}{Re_{D_e}}\left[\left(\frac{2}{\cos(\beta)^{1.73}}\right)_{\text{fd}}^{2} + \left(\frac{1.33}{\sqrt{L/D_e}}Re^{0.0551\beta^{0.675}}\right)_{\text{dev}}^{2}\right]^{1/2} \tag{5.25}$$

This model is valid for $L/D_e = 44.56,\ \gamma = 0.504, 30° \le \beta \le 60°$ and $2 \le Re_{D_e} \le 2{,}300$.

In Eq. (5.21), the coefficient $\mathcal{H}$ is determined to vary between 16 to 32, while the coefficient $\mathcal{K}$ is found to vary from 0.0439 to 0.0551 for short and long channels. Thus, averaging these values yields $\mathcal{H} = 24$ and $\mathcal{K} = 0.0495$. Substituting the new values of $\mathcal{H}$ and $\mathcal{K}$ into Eq. (5.23) leads to one general model which predicts f_{app} for short and long channels within an average RME error $\pm 20\%$ or less.

$$f_{app} = \frac{24}{Re_{D_e}}\left[\left(\frac{1}{\cos(\beta)^{1.73}}\right)_{\text{fd}}^{2} + \left(\frac{1}{\sqrt{L/D_e}}Re^{0.0495\beta^{0.675}}\right)_{\text{dev}}^{2}\right]^{1/2} \tag{5.26}$$

This general model is valid for $44.56 \le L/D_e \le 89.12, \gamma = 0.504, 30° \le \beta \le 60°$ and $2 \le Re_{D_e} \le 2{,}300$.

To check if the general model can interpolate and extrapolate the friction factor for different L/D_e ratios and chevron angles below or above or in between the validation range, arbitrary values of L/D_e and β have been plotted in Figs 5.5 and 5.6, respectively, using the general model equation, Eq. (5.26). Figure 5.5 demonstrates that at fixed $\beta = 45°$, the proposed model could interpolate and extrapolate. For example, for $Re_{D_e} > 10$, when $L/D_e = 150$, the friction factor prediction line is between $L/D_e = 90$ and $L/D_e = 200$.

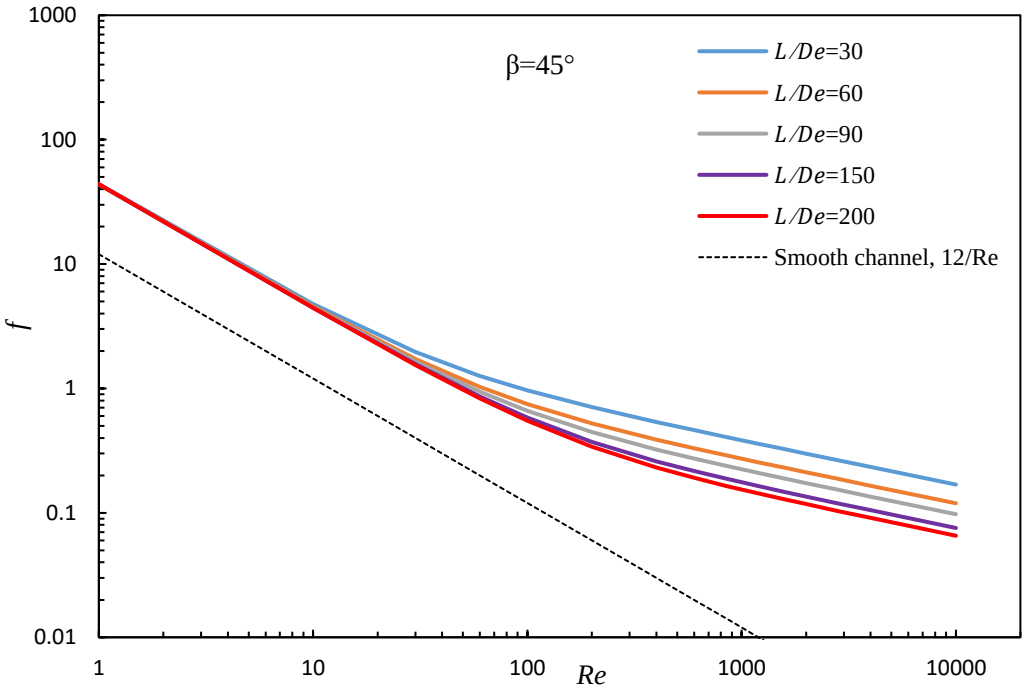

Fig. 5.5 General model prediction for $\beta = 45°$, and different L/D_e ratios

Figure (5.6) illustrates the general model prediction for constant $L/D_e = 55$ and five different chevron angles. To perform an interpolation $\beta = 50°$ is selected, and the model prediction line is between that for $\beta = 60°$ and that for $\beta = 30°$. For $\beta = 15°$, the prediction line is supposed to be below that for $\beta = 30°$, which is the same as illustrated in Fig (5.6). Generally, the friction factor in PHEs increases by increasing the chevron

angle and vice versa. This trend agrees with the literature (Heavner et al. (1993), Focke et al. (1985), Muley et al. (1999)). However, in industry, PHEs often have chevron angle between $30° \leq \beta \leq 65°$ (Wang et al. 2007).

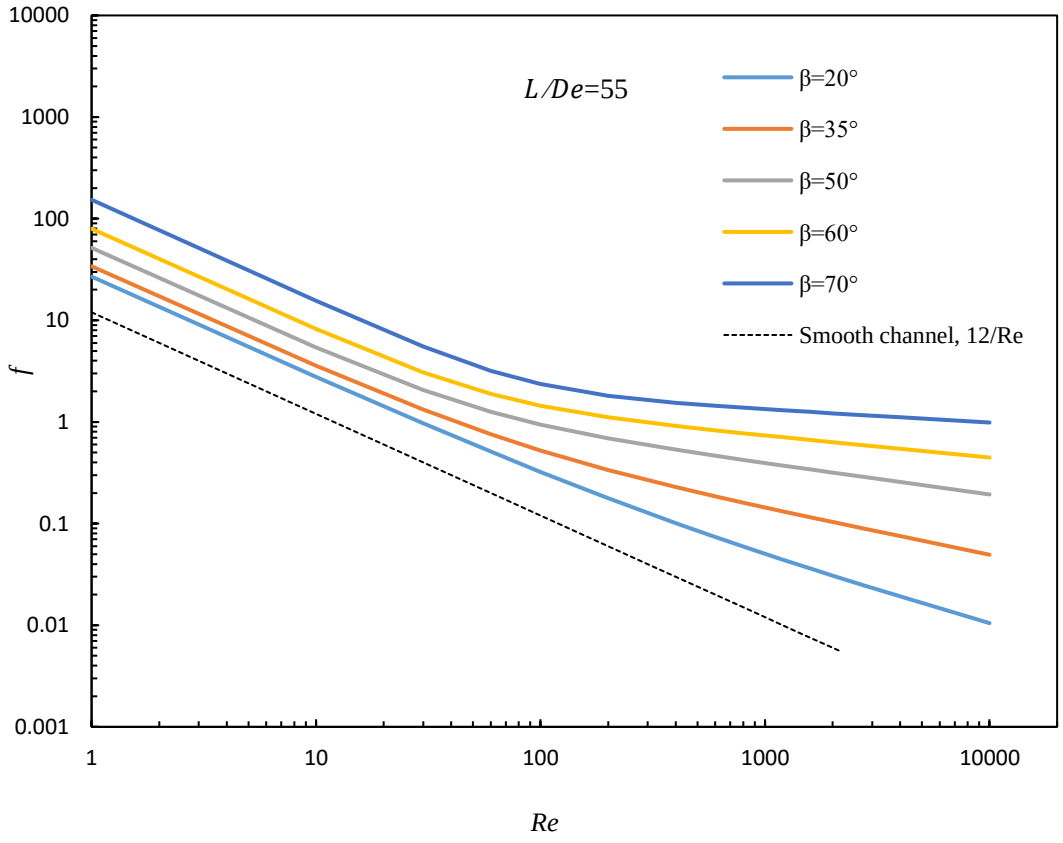

Fig. 5.6 General model prediction for $L/D_e = 55$, and different chevron angles

5.4 Comparison of Models with Data

In this section, the long and short channel models, Eq. (5.24) and Eq. (5.25), are compared with the obtained experimental data, which are depicted in Figs 5.7 and 5.8. Next, the general model, Eq. (5.26), is used to predict the experimental data for both long and short channels, which are shown in Figs. 5.9 – 5.13. Later, comparisons of the general model with data published in the literature for different chevron plate configurations, including

different angles, plate lengths, corrugation depths and wavelengths are presented.

A validation of the long channel model, Eq. (5.24), with the experimental data for all long plates is presented in Fig 5.7. The agreement between the model and data is quite good with an average RMS error $\pm 8.83\%, \pm 12.46\%$ and $\pm 9.21\%$ for chevron angles $60°, 45°$ and $30°$, respectively.

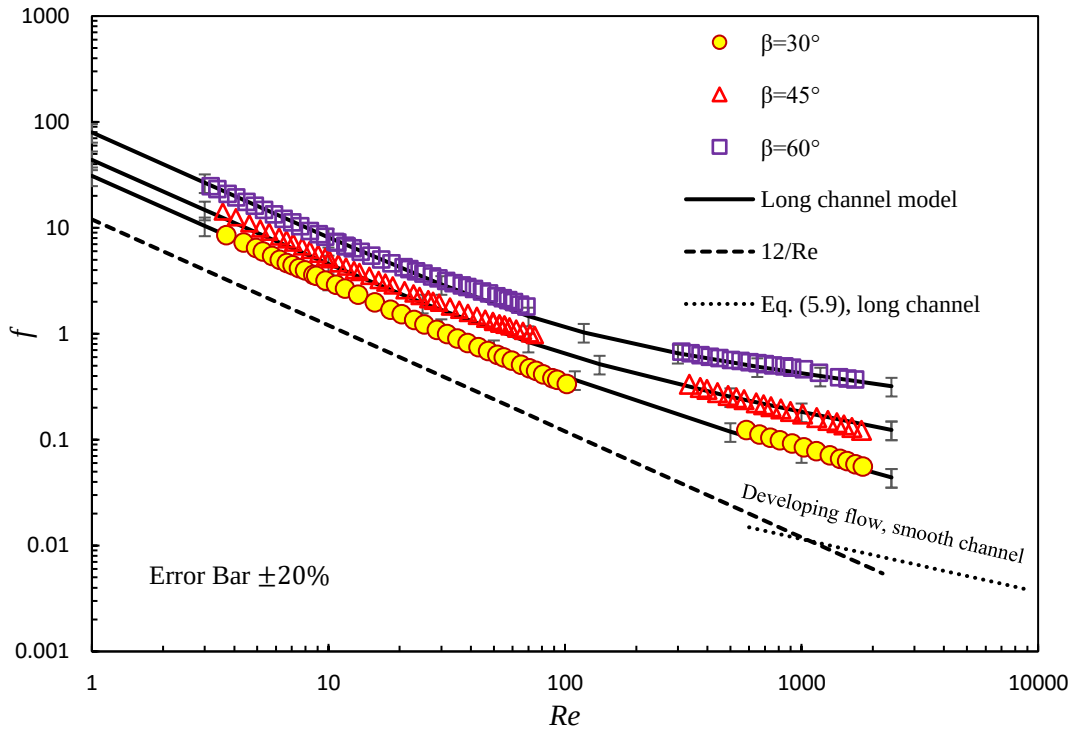

Fig. 5.7 Proposed long channel model prediction for all long channels

Figure 5.8 compares the short plates experimental results with the predictions of the short channel model, Eq. (5.25). The model and the data are in excellent agreement with an average RMS error $\pm 8\%, \pm 7.46\%$ and $\pm 7.32\%$ for chevron angles $60°, 45°$ and $30°$, respectively.

The general model predictions are compared with the experimental data for long and short channels in Figs. 5.9 – 5.13. Examinations of these plots show that the results follow

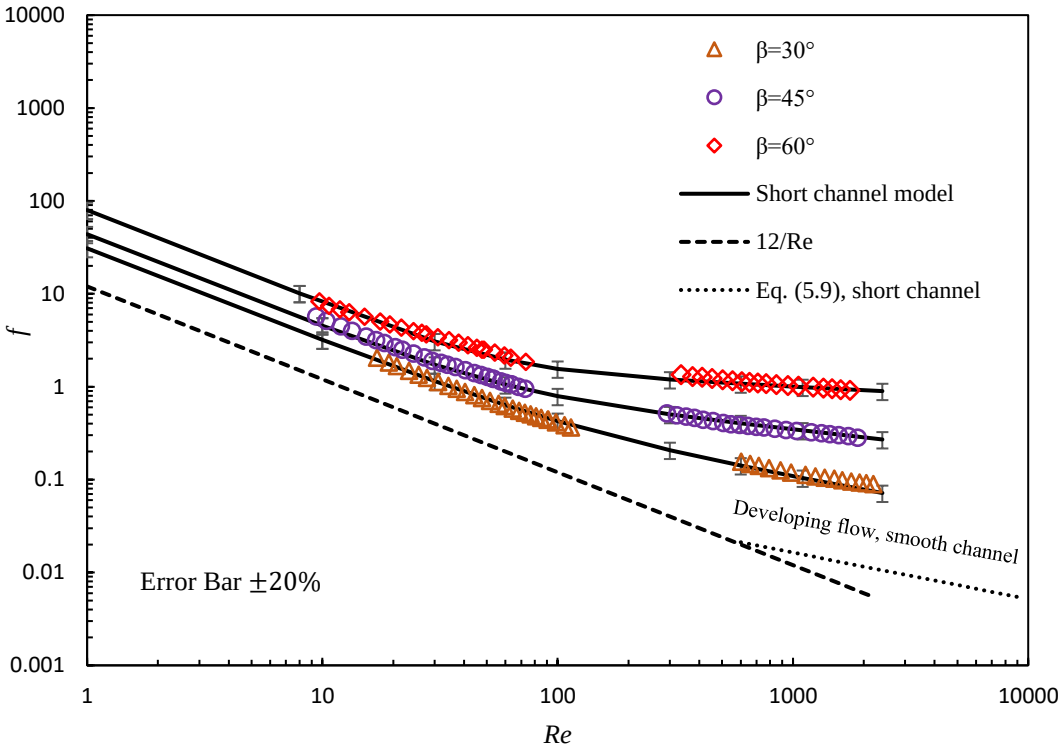

Fig. 5.8 Proposed short channel model prediction for all short channels

the trend of the proposed model, which is in fair agreement with the experimental results. All data is predicted within an average RMS error ±20% or less. Table 5.1 summarizes the average RMS error between the general model and the experimental data for all plates with different chevron angles.

Table 5.1 General model validation results

Chevron angle (β)	RMSE %	
	Long channel	Short channel
60°	±15.89	±14.64
45°	±19.43	±6.28
30°	±6.75	±10.04

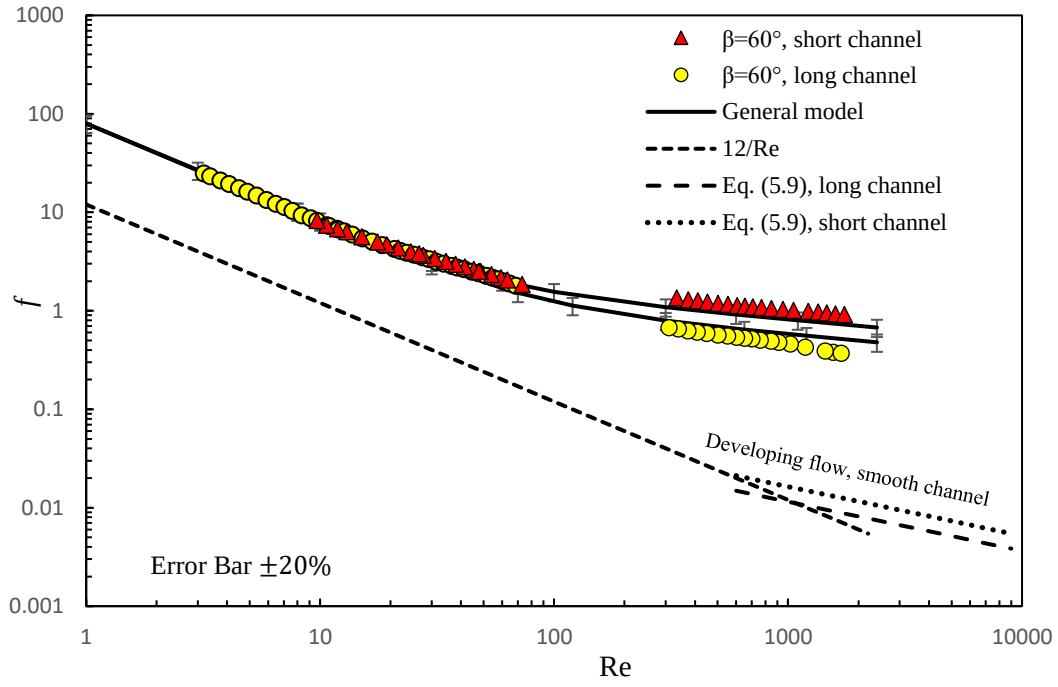

Fig. 5.9 Proposed general model prediction for long and short channel, β = 60°.

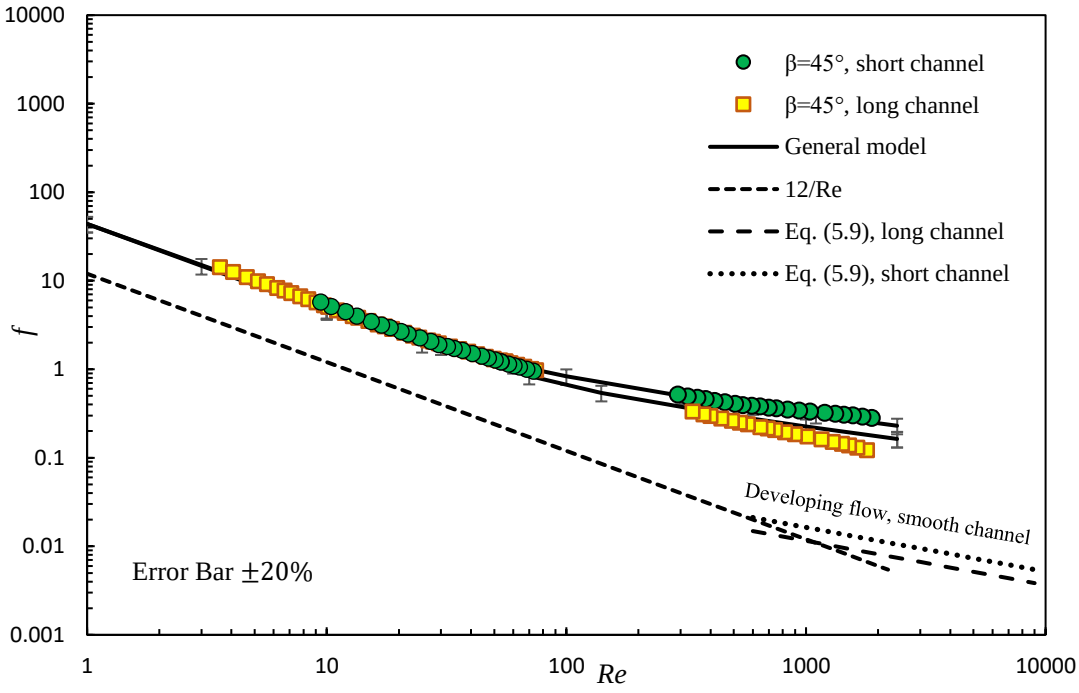

Fig. 5.10 Proposed general model prediction for long and short channel, β = 45°.

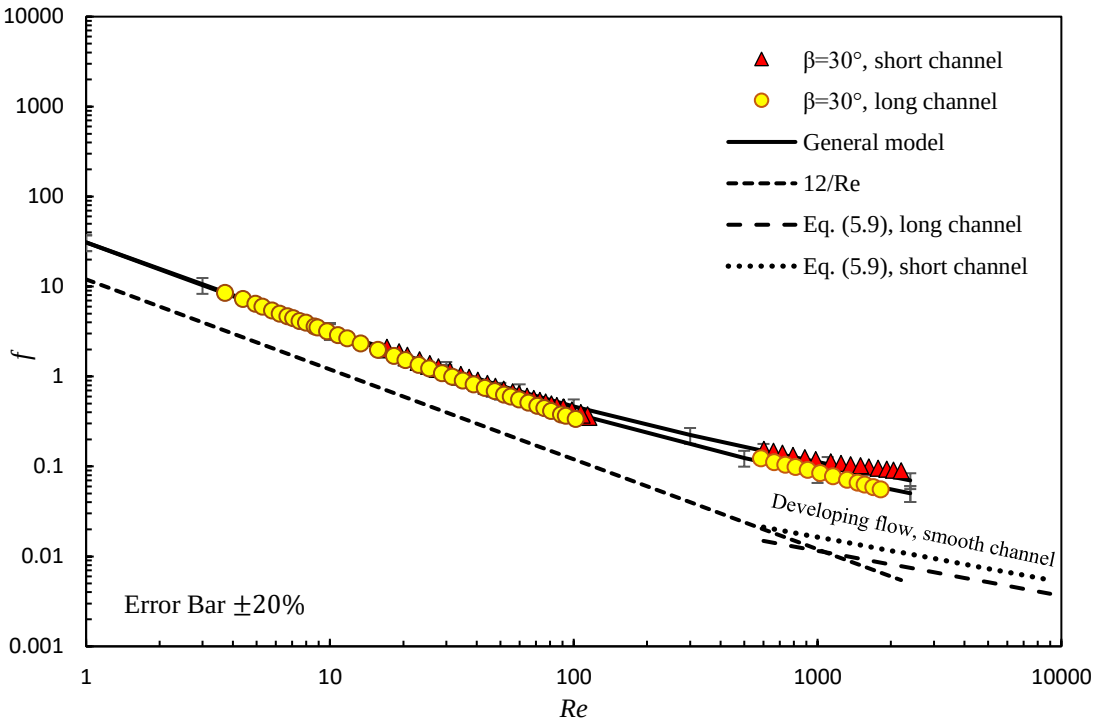

Fig. 5.11 Proposed general model prediction for long and short channel, β = 30°.

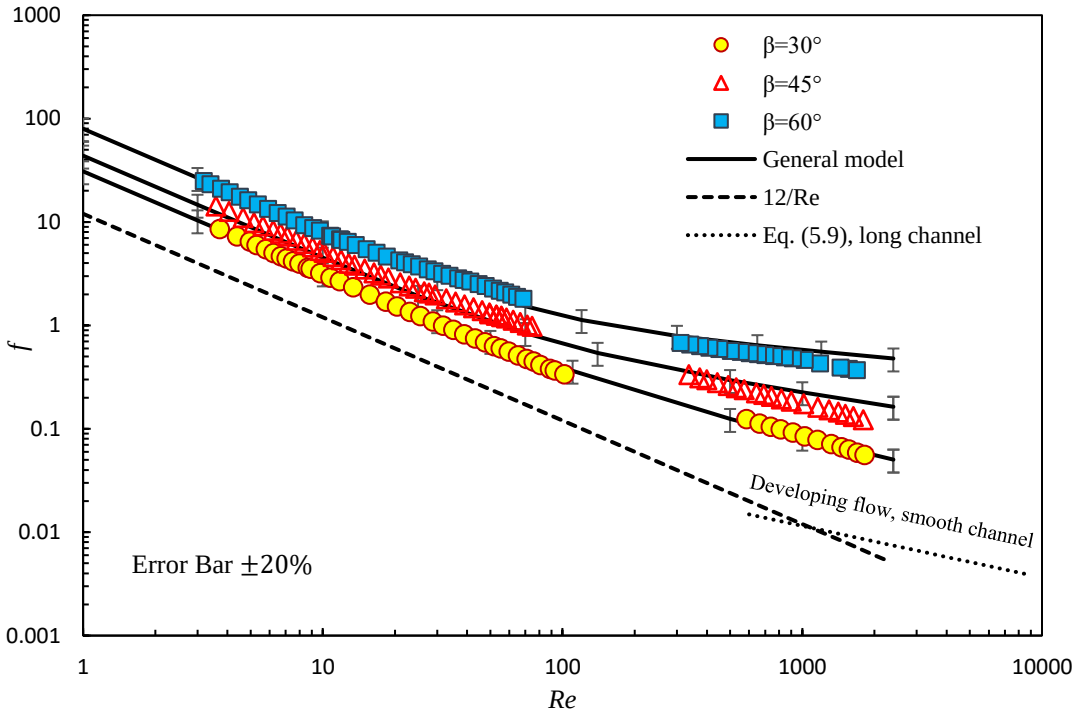

Fig. 5.12Proposed general model prediction for all long channels

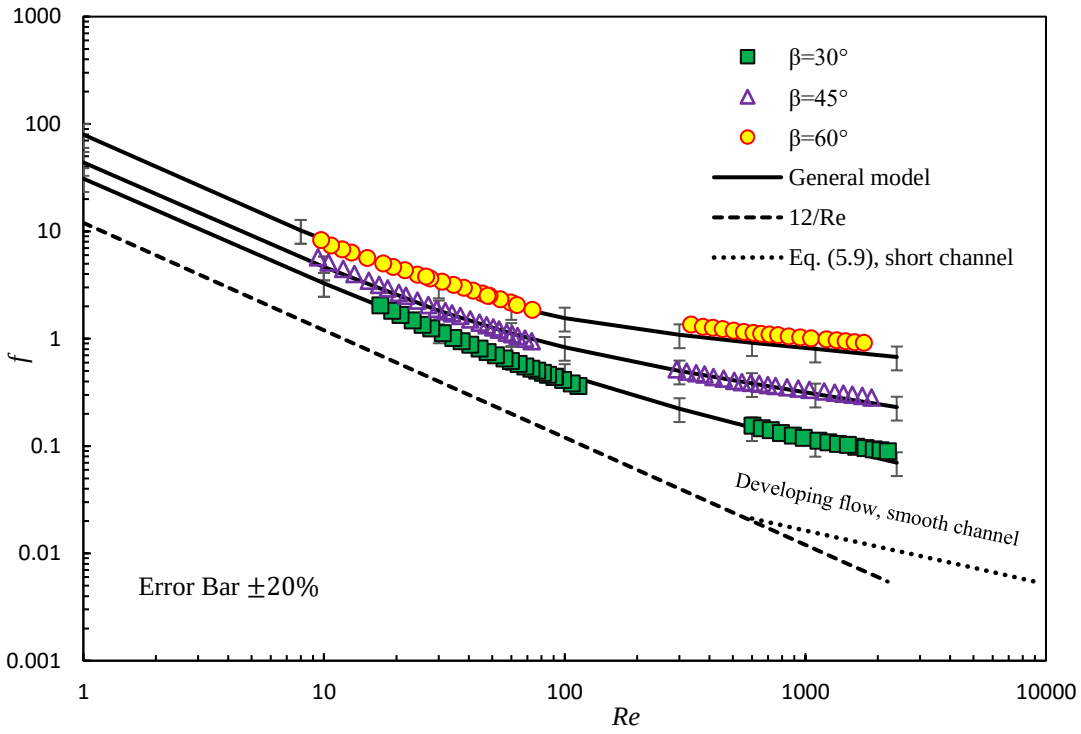

Fig. 5.13 Proposed general model prediction for all short channels

Before comparing the developed model predictions with the literature, some of the selected studies are plotted against each other. The purpose of the comparison is to show variation in the friction factor between these studies, even though they are all for chevron PHEs with the same $\beta = 60°$. From Figure 5.14, it can be observed that there are considerable discrepancies between these investigations. This inconsistency may be attributed to a variety of factors such as corrugation profile (e.g. trapezoidal or sinusoidal), corrugation depth, corrugation wavelength and plate size (non-identical in all studies). Another important reason for the difference can be attributed to the pressure drop associated with manifolds and distribution zones, which differ between the manufacturers. Bond (1981) reported that because of the diverse design of ports, which produces variation

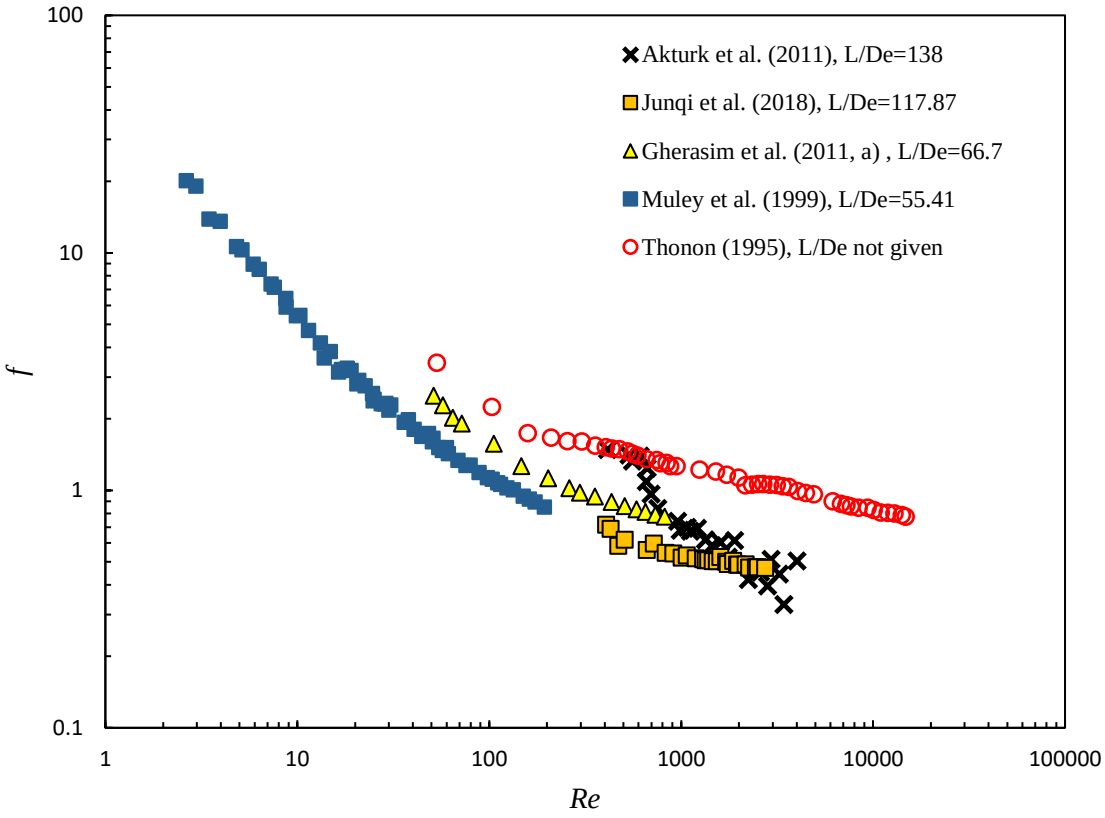

Fig. 5.14 Friction factor for PHEs from the literature for different L/D_e ratios and fixed $\beta = 60°$

in port manifold roughness, the overall pressure drop could be two to three times higher than the passage pressure drop. Later, Shah and Sekulić (2003) also mentioned that, in general, the pressure drop in the manifolds is lower than 10% of the overall pressure drop, however, it can be 30% or higher in certain designs. For example, in Fig. 5.14, at $Re \approx 825$, the results of Thonon (1995) are 2.34 times higher than that of Junqi et al. (2018) while Gherasim et al. (2011, a) results are 1.45 times higher than that of Junqi et al. (2018).

It is a challenging task to develop a general model that would consider the effects of all the parameters identified above in addition to the experimental error. Furthermore, only a

few authors provide all chevron plate configuration details, such as plate dimensions, $b, \beta, \gamma,$ and ϕ, which does not allow the use of the published results to validate and/or improve the developed model prediction.

In the literature, friction factor is usually correlated as a function of β and Re, which may not predict f for other studies unless they have identical plates. For example, a correlation developed based on the work of Junqi et al. (2018) as a function of β and Re can not predict the higher friction factors of Thonon (1995), as illustrated Fig. 5.14, as only one parameter is changing, which is the Reynolds number, $\beta = 60°$ in both cases. However, the proposed model is a function of another parameter, $\sqrt{L/D_e}$, in addition to β and Re. The $\sqrt{L/D_e}$ ratio has a key role in the model prediction. For example, at constant Reynolds number, i.e., $Re = 800$, the model can approximately predict the friction factor of Junqi et al. (2018) and Gherasim et al. (2011) by only changing L/D_e. With regard to the results of Akturk et al. (2011), their data behaviour look somehow questionable as they did not show a similar trend as the other plotted studies. Moreover, data of Thonon (1995) is also excluded as no geometric details are given. Therefore, these two studies will not be compared with the proposed model but reported here to show discrepancy in the literature.

Experimental and numerical data from selected studies in the literature have been gathered to validate the developed model. Figures 5.15 and 5.16 show a comparison of the general model prediction with the experimental data of Muley et al. (1999) for three different chevron angles. The general model shows good agreement with the experimental results for $\beta = 30°$ in the range of $Re < 40$, however, data points for $Re > 60$ are under-

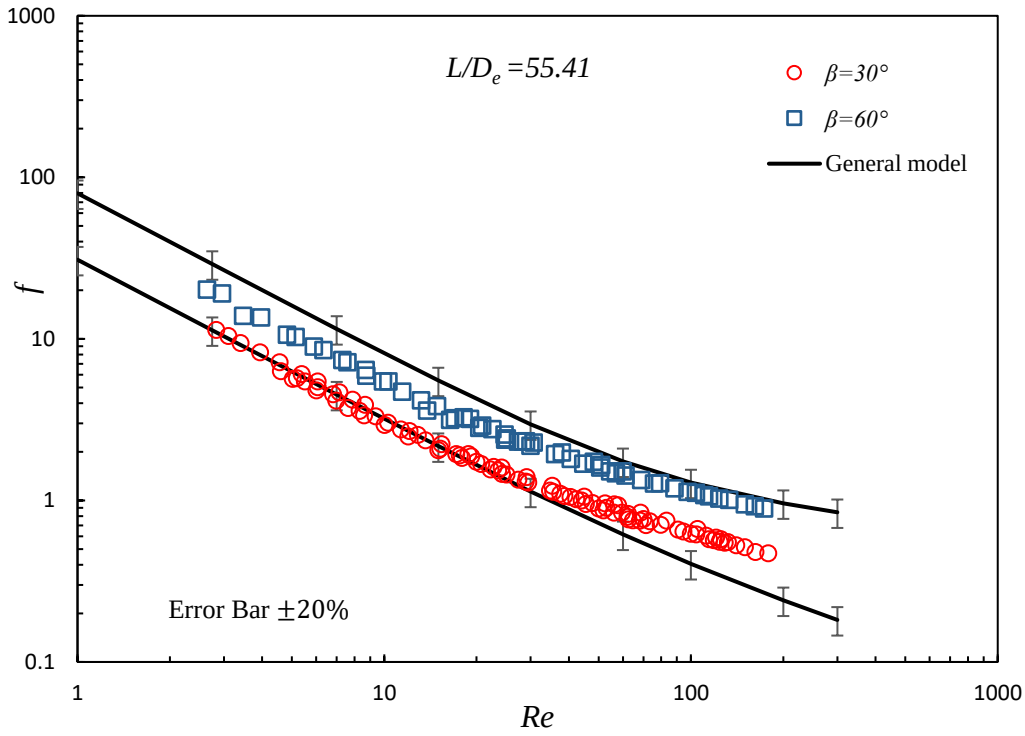

Fig. 5.15 Friction factor for chevron plates, $\beta = 30°$ and $60°$, data from Muley et al. (1999)

predicted which may be due to the effect of the distribution zones and/or roughness of the corrugated surface. The average RMS error is $\pm 22.35\%$. For $\beta = 60°$, the model predicted all the data with an average RMS error $\pm 37.7\%$; however, data in the range $25 \leq Re \leq 200$ are predicted within an average RMS error $\pm 22.12\%$. Furthermore, Fig 5.16 illustrates excellent agreement between the proposed model and all data for $\beta = 60°/30°$, with an average RMS error $\pm 10.45\%$. The working fluid was vegetable oil. It should be mentioned that for Re range $Re \leq 30$ the model predicted data for $\beta = 30°$ and 45° very well while data for $\beta = 60°$ are over-predicted. This may be due to an issue with the data of $\beta = 60°$.

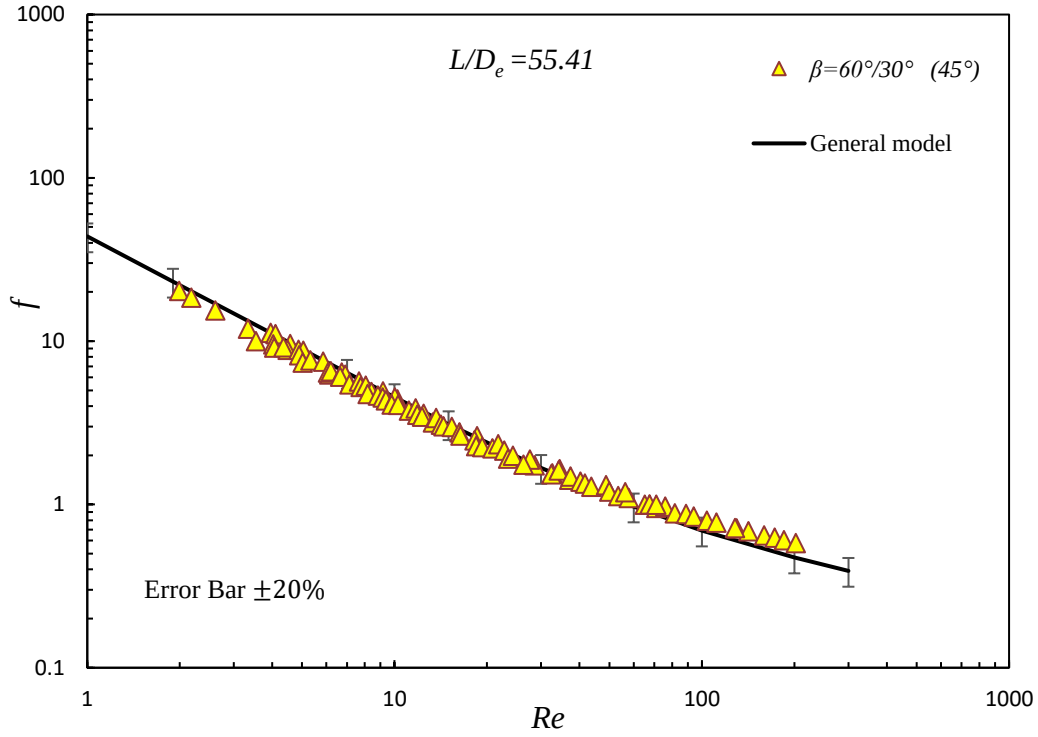

Fig. 5.16 Friction factor for chevron plates, $\beta = 60°/30°$, data from Muley et al. (1999)

Good agreement between the proposed model and the experimental data obtained by Junqiet al. (2018), as illustrated in Fig 5.17. For $\beta = 30°$ and up to $Re \approx 1500$, the prediction of the proposed model agree with the data to an average RMS error $\pm 19.76\%$, while data for $Re > 1500$ are under-predicted. There is a clear fluctuation in the data between $Re = 1000$ to 3000. For $\beta = 45°$, the model predicts all the data with average RMS error $\pm 29.77\%$ or $\pm 23.54\%$, if the four lower points between $459 < Re < 1000$ are not considered as they showed a discrepancy. This discrepancy may be due to experimental error. All the friction factor data are well predicted for $\beta = 60°$, with average RMS error $\pm 12.62\%$. The working fluids were water and glycol.

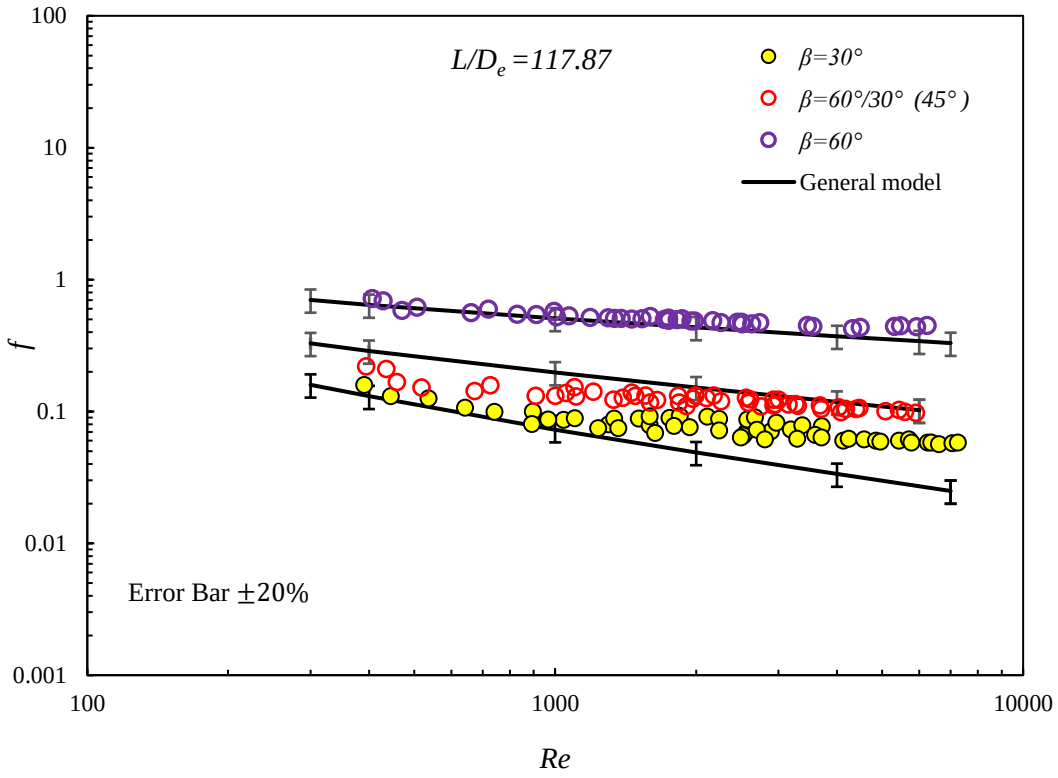

Fig. 5.17 Friction factor for chevron plates, data from Junqi et al. (2018)

Predictions of the proposed model along with the experimental data of Gherasim et al. (2011, a), are plotted in Fig 5.18. The model and the data are in good agreement with an average RMS error $\pm 12.06\%$. The working fluid was water and $\beta = 60°$.

Experimental work of Edwards et al. (1974) and the prediction of the general model are plotted in Fig 5.19 for chevron angle of $60°$. There is a good agreement between the proposed model and the data in the range of $0.05 < Re < 20$, with an average RMS error $\pm 12.27\%$. The data for $Re > 20$ are under-predicted. The tendency of the data $30 < Re < 1200$ to be higher than the model predictions may be due to manifold losses and/or experimental error, considering the data was collected approximately 50 years ago. It is also noted that the plate length was 45 cm while its width was only 5.3 cm (uncommon).

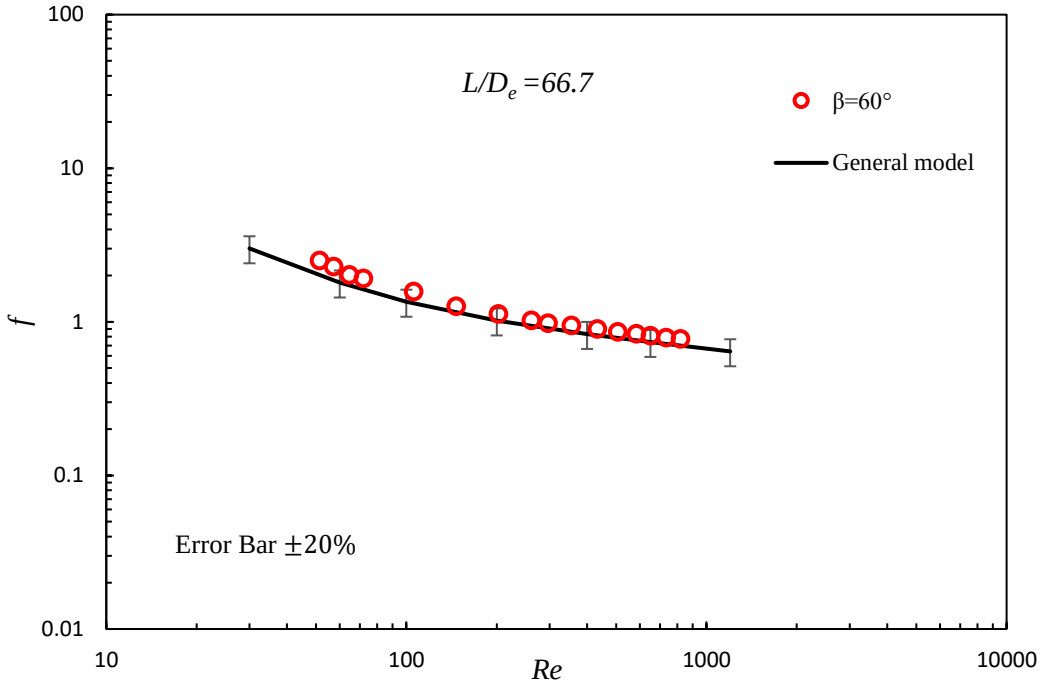

Fig. 5.18 Friction factor for chevron plates, data from Gherasim et al. (2011, a)

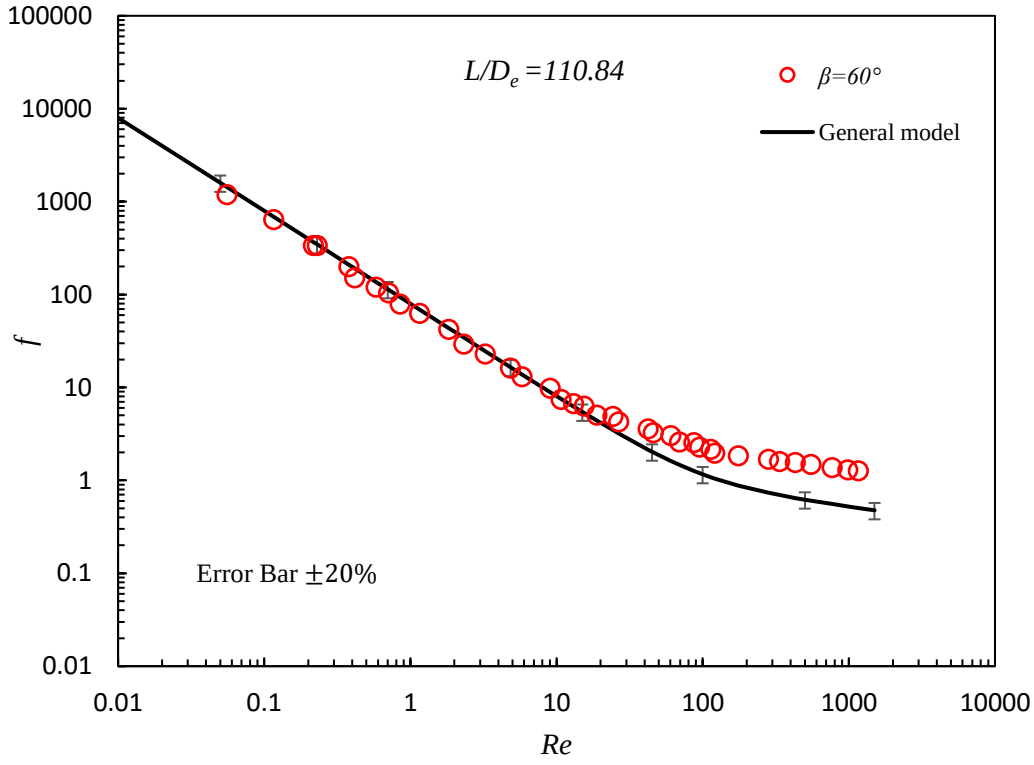

Fig. 5.19 Friction factor for chevron plates, data from Edwards et al. (1974)

Different test fluids were used, including water, glucose solutions, lubricating oil, and various non-Newtonian liquids such as polyacrylamide or acrylamide dissolved in water.

Figure 5.20 shows the numerical friction factors of Jain et al. (2007), which are predicted with an average RMS error $\pm 18.01\%$ by using the general model for $\beta = 60°$. The working fluid was water.

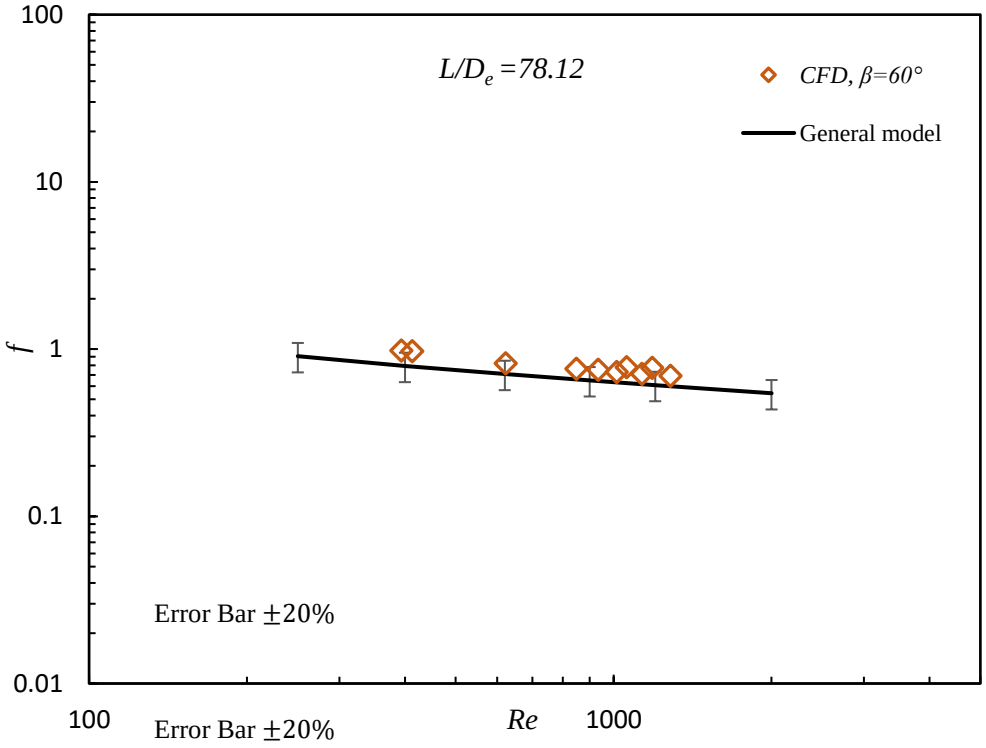

Fig. 5.20 Friction factor for chevron plates, data from Jain et al. (2007)

Good agreement between the general model and the numerical data of Gherasim et al. (2011b), which can be seen in Fig. 5.21. The numerical data are well predicted with an average RMS error $\pm 10.14\%$. The working fluid was water, and the chevron angle was 60°.

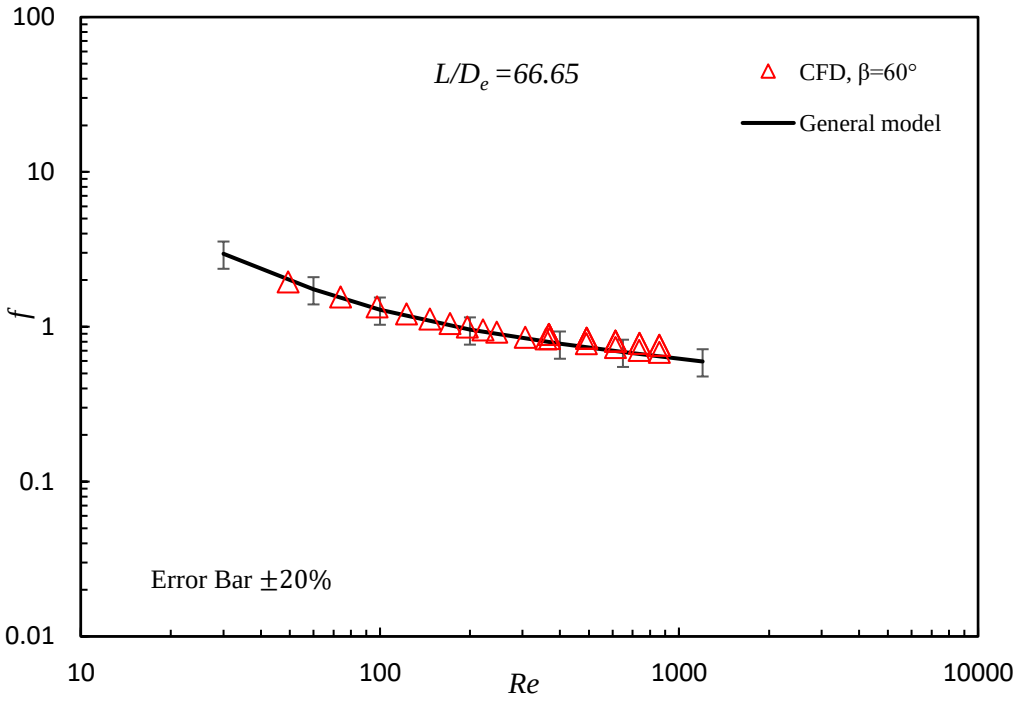

Fig. 5.21 Friction factor for chevron plates, data from Gherasim, et al. (2011, b)

5.5 Conclusions

A general model to predict the friction factor in the entrance region of chevron plate heat exchangers has been developed. The proposed model was developed using the asymptotic correlation method proposed by Churchill and Usagi (1972). This model covers the laminar, transition, and turbulent flow regions. Model predictions agreed well with the obtained experimental data within an average RMS error ±20% or less, for both long and short channels examined. Finally, the proposed model showed a very good agreemen with numerical, CFD, results from the literature and predicted the data within ±20 percent or better. Moreover, a good agreement was also observed between the model prdictions and expeirmntal data from the literature within ±20 percent in most cases within the range of applicability.

Chapter 6

Development of Heat Transfer Model for Chevron PHEs

6.1 Introduction

This chapter is divided into three sections. First, a review of the Nusselt number equations, for laminar flow in a smooth channel, for the hydrodynamically and thermally fully developed flow, the Graetz flow, and the hydrodynamically and thermally developing flow are presented. Next, Colburn factor model development for the chevron PHE channel is discussed. Finally, comparisons are made with new experimental data, as well as numerical and experimental data collected from the literature to validate the developed model.

6.2 Nusselt Number for a Parallel Plate Channel

Beginning with expressions that have been used to calculate the laminar Nusselt number in a parallel plate channel for three fundamental flows: hydrodynamically and thermally fully developed flow, thermal entry problem, and combined entry problem. A schematic of the thermal entry condition between two parallel plates is shown in Fig. 6.1. The boundary conditions considered are uniform wall temperature, UWT, T = constant, and uniform heat flux, UHF, q_w = constant, which will be referred to as T and H, respectively. All experimental data obtained are considered to be within the laminar flow regime in a smooth channel.

To determine if the flow is hydrodynamically and/or thermally fully developed or developing flow, the hydrodynamic entrance length, L_{hy}, and the thermal entrance length,

L_{th}, need to be calculated. Shah and London (1978) defined L_{hy} as the duct length required for the centreline velocity to achieve 99% of the fully developed value when the entring fluid velocity profile is uniform. The hydrodynamic entrance length can be determined from the following equation

$$L_{hy} \approx 0.05\, D_h\, Re_{D_h} \tag{6.1}$$

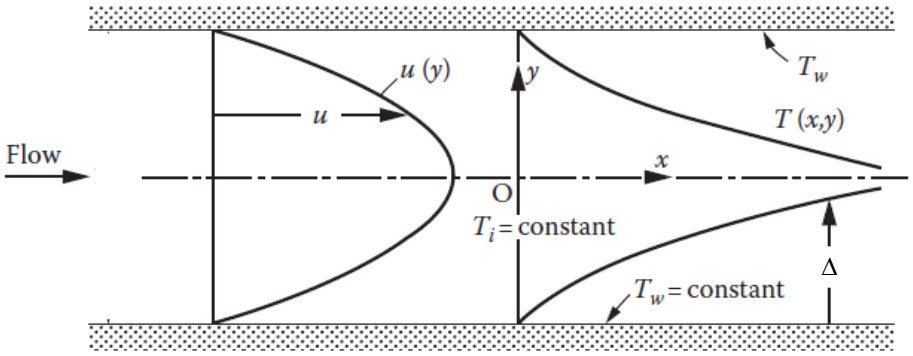

Fig. 6.1 Thermal entrance region between two parallel plates (Kakac et al. 2014)

The thermal entrance length is defined as the duct length required to achieve a value of the local Nusselt number, Nu_x, $1.05\, Nu_m$ for fully develped flow which is given by the following equation (Shah and London, 1978)

$$L_{th} \approx 0.05\, D_h\, Re_{D_h}\, Pr \tag{6.2}$$

The difference between equations 6.1 and 6.2 is the Prandtl number which represents the ratio of momentum diffusivity to thermal diffusivity. Thus, for fluids with $Pr > 1$ the hydrodynamic boundary layer, δ, develops quicker than the thermal boundary layer, Δ, $L_{hy} > L_{th}$, while the opposite is true for fluids with $Pr < 1$, (Bergman et al. 2011).

6.2.1 Fully developed flow

In this region, where $L \gg L_{hy}, L_{th}$, both the velocity and temperature profiles are fully developed and no longer change downstream. Hence, the Nusselt number is independent from the Reynolds number and Prandtl number and is found to approach a constant value for fully developed flow. This constant depends strongly on the duct shape and the boundary conditions imposed at the duct wall. The fluid flow is also called hydrodynamically and thermally fully developed flow. The Nusselt number values for a parallel plate channel for UWT and UHF boundary conditions are given by (Shah and London 1978):

$$\left(Nu_{D_h}\right)_{m,T} = 7.54 \tag{6.3}$$

$$\left(Nu_{D_h}\right)_{m,H} = 8.235 \tag{6.4}$$

6.2.2 Developing Flow

In the thermal entrance region of the duct, the dimensionless temperature profile varies from the initial profile at the point where the heating process is begun to fully developed downstream. Furthermore, the velocity profile in this region can be either developed or developing (Shah and London 1978). The effect of Prandtl number on L_{hy} and L_{th} for both $Pr \ll 1$ and $Pr \gg 1$ is illustrated in Fig. 6.2. Hence, two problems arise in the region near the channel entrance: (1) Graetz flow problem or thermal entrance problem: the velocity profile is fully developed, $L \gg L_{hy}$, while the temperature profile develops, $L \ll L_{th}$, (refer to Fig. 6.1), which is the case when $Pr \gg 1$. Analytical expressions to calculate the mean Nusselt number in the entrance region of a parallel plate channel for the UWT and UHF

boundary conditions are (Shah and London 1978)

$$\left(Nu_{D_h}\right)_{m,T} = \begin{cases} 1.849\left(x^*_{D_h}\right)^{-1/3} & x^*_{D_h} \le 0.0005 \\ 1.849\left(x^*_{D_h}\right)^{-1/3} + 0.6 & 0.0005 < x^*_{D_h} \le 0.006 \\ 7.541 + \dfrac{0.0235}{x^*_{D_h}} & x^*_{D_h} > 0.006 \end{cases} \tag{6.5}$$

$$\left(Nu_{D_h}\right)_{m,H} = \begin{cases} 2.236\,(x^*)^{-1/3} & x^*_{D_h} \le 0.001 \\ 2.236\,(x^*)^{-1/3} + 0.9 & 0.001 < x^*_{D_h} < 0.01 \\ 8.235 + \dfrac{0.0364}{x^*_{D_h}} & x^*_{D_h} > 0.01 \end{cases} \tag{6.6}$$

where $x^*_{D_h}$ is defined by Eq. (4.47).

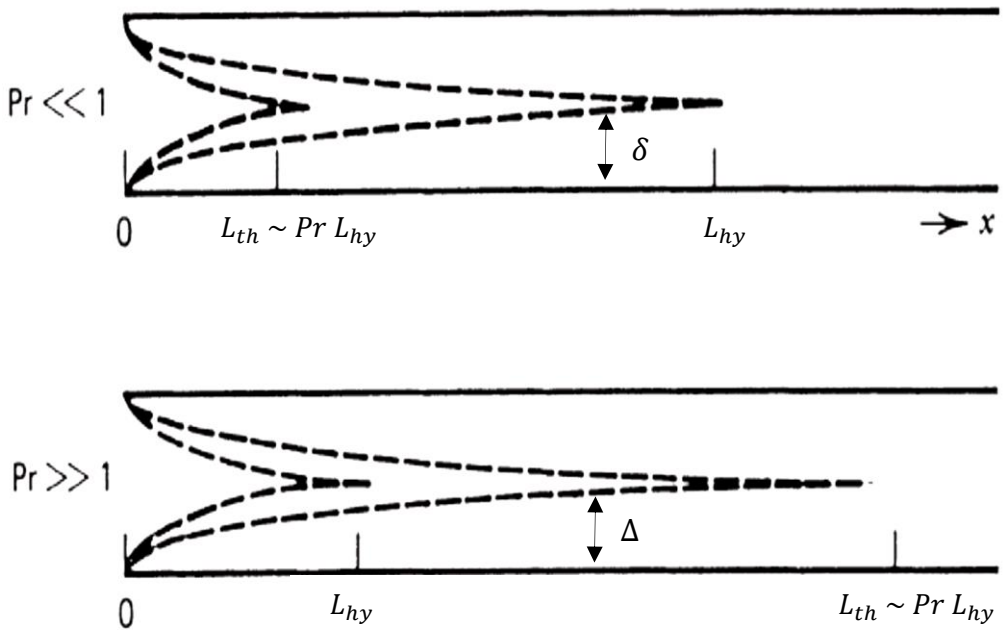

Fig. 6.2 Prandtl number effect on L_{hy} and L_{th} (Bejan and Kraus 2003)

(2) Combined entry problem or simultaneously developing flow: both the velocity and the temperature profiles develop simultaneously, $L \ll L_{hy}, L_{th}$, so the heat transfer results are strongly dependent on the Prandtl number. It is also called the laminar boundary layer,

LBL, flow. This is the case for fluid with a Prandtl number not significantly greater than 1, particularly when L_{hy} and L_{th} are comparable (Bejan and Kraus 2003). For a parallel plate channel with the UWT boundary condition, Stephan (1959) equation, Eq. (4.44), can be used to calculate the mean Nusselt number, which is valid for $0.1 \leq \mathrm{Pr} \leq 1000$

Before ending this section, Stephan (1959) equation, Eq. (4.44), has been used to examine the effect of varying the channel length at a fixed D_h, different L/D_h ratios, on the heat transfer of a smooth parallel plate channel for $Pr = 8$. Figures 6.3 and 6.4 show that at higher Reynolds numbers, j and Nu are significantly higher for the short channels compared to the long ones which indicates that thermal entrance effects are present. At low Reynolds numbers, however, j and Nu results are the same for all channels indicating that fully developed flow condition are exist.

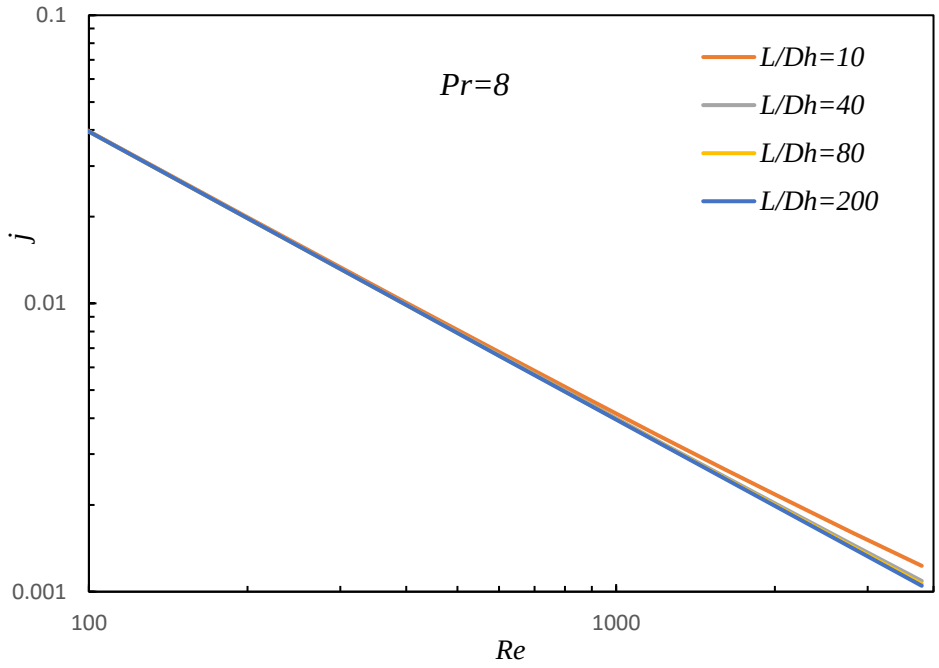

Fig. 6.3 Colburn factor of a parallel plate channel for a combined entry problem

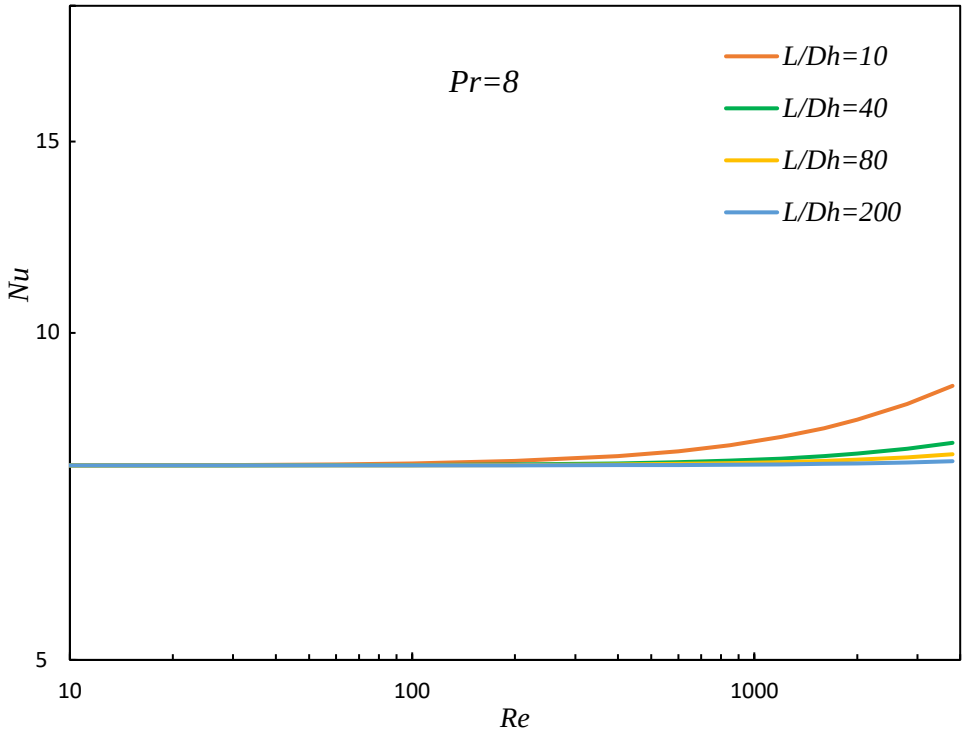

Fig. 6.4 Nusselt number of a parallel plate channel for a combined entry problem

6.3 Colburn Factor Model development

In this section, the details of the model development for the chevron channel geometry are discussed. Since two fluids, oil and water, with different Pr have been utilized in the experiment, Colburn j factor is used in the modeling as it makes the model more general or fluid type independent.

Nusselt number equations for the smooth parallel plates channel need scale appropriately based on Eq. (4.49) to be used as a reference point. So, $Nu_{D_e} = Nu_{D_h} \times D_e/D_h$. Stephan (1959) equation, Eq. (4.44) has already been rescaled in Chapter 4, refer to Eq. (4.53) while Eq. (6.7) will be re-scaled based on D_e for consistency.

$$\left(Nu_{D_e}\right)_{m,T} = \begin{cases} 0.924\left(x^*_{D_e}\right)^{-1/3} & x^*_{D_e} \le 0.0005 \\ 0.924\left(x^*_{D_e}\right)^{-1/3} + 0.3 & 0.0005 < x^*_{D_e} \le 0.006 \\ 3.78 + \dfrac{0.01175}{\left(x^*_{D_e}\right)} & x^*_{D_e} > 0.006 \end{cases} \tag{6.7}$$

where $x^*_{D_e}$ is given by Eq. (4.54).

Figures 6.5 and 6.6 show the behavior of Eqs. (4.53) and (6.7) in comparison with the Colburn j factors of chevron plates, at fixed β, while channel length is changing, and at fixed channel length, while β is varying, respectively.

Figure 6.3 illustrates that for fixed chevron angle, the heat transfer results are length

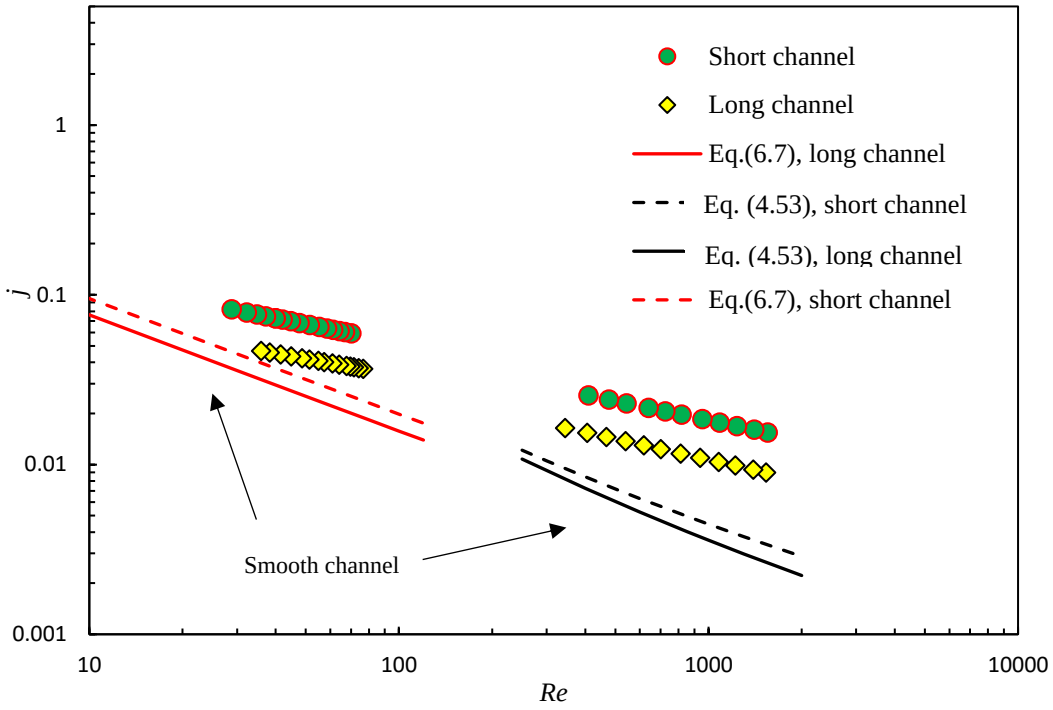

Fig. 6.5 Colburn factor for long and short channels for $\beta = 45°$

dependent for low and high Reynolds number regimes. Figure 6.6 shows that for fixed channel length, the chevron angle influences the Colburn j factor in both flow regimes. In

the present experiment, for $Re < 100$ regions, oil with large Pr is used as the working fluid, therefore, for a parallel plates channel, $L \gg L_{hy}, L_{th}$, it is reasonable to assume Graetz flow in this region. For $Re > 300$ regions, the working fluid is water, therefore, a

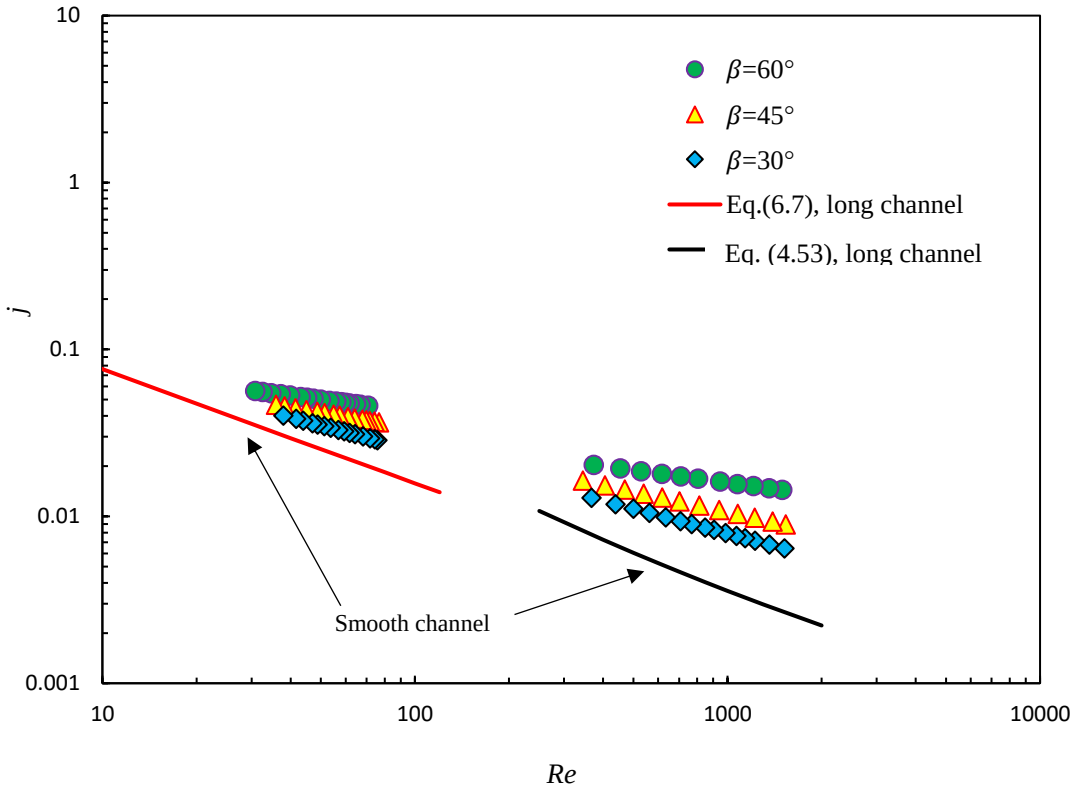

Fig. 6.6 Colburn factor for all long channels

combined entry problem or LBL flow is expected because Pr of water is not significantly greater than 1. Therefore, the Colburn j factor model for the chevron channel

at the UWT boundary condition is proposed to take the form

$$j = [(j)^n_{\text{LowRe}} + (j)^n_{\text{LBL}}]^{1/n} \tag{6.8}$$

where $(j)_{\text{LowRe}}$ and $(j)_{\text{LBL}}$ are the asymptotic solutions for low Reynolds number flow and laminar boundary layer flow, respectively. The fitting parameter, n, is used to control the

model behavior in the transition region and its value will be selected as the value which minimizes the root mean square error between the model prediction and the available data

.**Low Reynolds Number Asymptote**

From the low Re region, $Re < 100$, the working fluid is mineral oil which is a highly viscous fluid and $Pr \gg 1$. Thus, for non-circular duct and channel, the velocity profile develops much quicker than the temperature profile, and the flow may be considered as hydrodynamically fully developed and thermally developing since the thermal boundary layers are thinner and $L_{hy} \ll L_{th}$. In the thermal entrance region, the results are a weak function of the shape and geometry of the duct. For the Graetz flow problem and near the duct inlet, Muzychka and Yovanovich (2004) showed that the Nusselt number can be expressed in the following form

$$Nu_{\mathcal{L}} = \frac{A_5}{(L^*)^{1/3}} \tag{6.9}$$

where $L^* = L/\mathcal{L}Re_{\mathcal{L}}\,Pr$, A_5 is a constant and $\mathcal{L}$ is the characteristic length scale. For PHEs the D_e is chosen as a characteristic length scale. Then the following expression for Nusselt number is obtained

$$Nu_{D_e} = \frac{A_5}{\left(\frac{L/D_e}{Re_{D_e}Pr}\right)^{1/3}} \tag{6.10}$$

Alternatively, it can be written in terms of the Colburn j factor,

$$j_{D_e} = \frac{A_5}{\left(\frac{L}{D_e}\right)^{1/3}\left(Re_{D_e}\right)^{2/3}} \tag{6.11}$$

From the experimental results, the Colburn j factor is length-dependent and is also found that A_5 and the exponent of the Re are not constant. Thus, Eq. (6.11) is re-written by introducing coefficients A_6 and a_5 to represent the low Re number asymptote term for chevron PHE as follows

$$\left(j_{D_e}\right)_{\text{LowRe}} = \frac{A_6}{\left(\frac{L}{D_e}\right)^{1/3}\left(Re_{D_e}\right)^{a_5}} \tag{6.12}$$

The coefficients A_6 and a_5 have the following values based on the present experimental results

$$A_6 = 1,\ a_5 = 1.32\beta^{-0.289} \quad \text{for the long channel, } L/D_e = 89.12$$

$$A_6 = 1.3,\ a_5 = 1.488\beta^{-0.32} \quad \text{for the short channel, } L/D_e = 44.56$$

At the same L/D_e, the coefficient a_5 has a certain value for each angle. Hence, a_5 values have been correlated as a function of β.

Laminar Boundary Layer Asymptote

For the region, $Re > 100$, water is used as the working fluid. Therefore, for a duct, one may expect that the temperature and velocity profiles develop simultaneously because the Prandtl number of water is not much greater than 1. Thus, the boundary layer behavior for very small values of x^*, may be modeled by treating the duct wall as a flat plate (Muzychka and Yovanovich 2004). The Nusselt number for the laminar flow over a flat plate for a UWT boundary condition is given by (Bergman et al. 2011)

$$Nu_L = A_7 Re_L^{1/2}\, Pr^{1/3} \tag{6.13}$$

where the value of $A_7 = 0.664$ for the average Nu_L if the flow is laminar over the entire

surface (Bergman et al. 2011). For non-circular duct, Eq. (6.13) has to be converted to be based on the dimensionless duct length using $Re_L = Re_{D_e} L/D_e$ as follows

$$Nu_{D_e} = \frac{A_7}{\sqrt{L^*}\ Pr^{1/6}} \tag{6.14}$$

Alternatively, it can be presented in terms of the Colburn j factor

$$j_{D_e} = \frac{A_7}{\sqrt{L/D_e}\ Re_{D_e}^{1/2}} \tag{6.15}$$

Based on the present experimental results, it is found that the A_7 value and Re exponent are not constant, but they are a function of the chevron angle at fixed channel length. Thus, the $\left(j_{D_e}\right)_{LBL}$term for the flat plate in Eq. (6.15) is re-written by introducing coefficients A_8 and a_6 as follows

$$\left(j_{D_e}\right)_{\text{LBL}} = \frac{A_8}{\sqrt{L/D_e}\ \ Re^{a_6}} \tag{6.16}$$

Based on the experimental results, the coefficients A_8 and a_6 have the following values

$A_8 = 6.35/\beta\,,\ a_6 = 0.706 - 0.007\beta$ for the long channel, $\sqrt{L/D_e} = 9.43$

$A_8 = 9.02/\beta\,,\ a_6 = 0.721 - 0.0077\beta$ for the short channel, $\sqrt{L/D_e} = 6.67$

Composite Model

The asymptotes developed in the previous sections are combined using Churchill and Usagi (1972) composite solution technique. Hence, substituting Eqs. (6.12) and (6.16) into Eq. (6.8), the Colburn j factor model for the chevron channel becomes

$$j_{D_e} = \left[\left(\frac{A_5}{(L/D_e)^{1/3} Re_{D_e}{}^{a_5}}\right)_{\text{LowRe}}^{n} + \left(\frac{A_8}{\sqrt{L/D_e}\ \ Re^{a_6}}\right)_{\text{LBL}}^{n}\right]^{1/n} \tag{6.17}$$

The blending parameter is determined to be $n = 6$, for long and short channels.

Since the developed model is a function of the channel length, we will have one model for the long channel and one model for the short channel. The Colburn j factor model for the long channel is

$$j_{D_e} = \left[\left(\frac{0.224}{Re^{1.32\beta^{-0.289}}}\right)_{\text{LowRe}}^{6} + \left(\frac{6.35/\beta}{Re^{0.706-0.007\beta}}\right)_{\text{LBL}}^{6}\right]^{1/6} \tag{6.18}$$

This model is valid for $L/D_e = 89.12,\ \gamma = 0.504,\ 30° \le \beta \le 60°$ and $30 \le Re_{D_e} \le 1600$. The Colburn j factor model for the short channel is

$$j_{D_e} = \left[\left(\frac{0.367}{Re^{1.48\beta^{-0.32}}}\right)_{\text{LowRe}}^{6} + \left(\frac{9.02/\beta}{Re^{0.721-0.0077\beta}}\right)_{\text{LBL}}^{6}\right]^{1/6} \tag{6.19}$$

This model is valid for $L/D_e = 44.56,\ \gamma = 0.504, 30° \le \beta \le 60°$ and $30 \le Re_{D_e} \le 1600$.

Equations (6.18) and (6.19) have been unified after administering simplifications such as averaging the exponents of the Reynolds numbers in Eqns. (6.18) and (6.19) for each $(j)_{\text{LowRe}}$ and $(j)_{\text{LBL}}$ asymptotic solutions. This results in one general model that can predict j for short and long channels within an average RMS error $\pm 10\%$ or less.

$$j_{D_e} = \left[\left(\frac{5.25}{(L/D_e)^{0.7} Re^{1.42\beta^{-0.304}}}\right)_{\text{LowRe}}^{5} + \left(\frac{60/\beta}{(L/D_e)^{0.5} Re^{0.714-0.00735\beta}}\right)_{\text{LBL}}^{5}\right]^{1/5} \tag{6.20}$$

This general model is valid for $44.56 \le L/D_e \le 89.12, \gamma = 0.504, 30° \le \beta \le 60°$ and $30 \le Re_{D_e} \le 1600$.

The ability of the general model to interpolate and extrapolate has been checked and plotted in Figs 6.7 and 6.8 for different L/D_e ratios and β angles below, in between, and above the validation range. Figure 6.7, for example, illustrates that at fixed $L/D_e = 50$, the

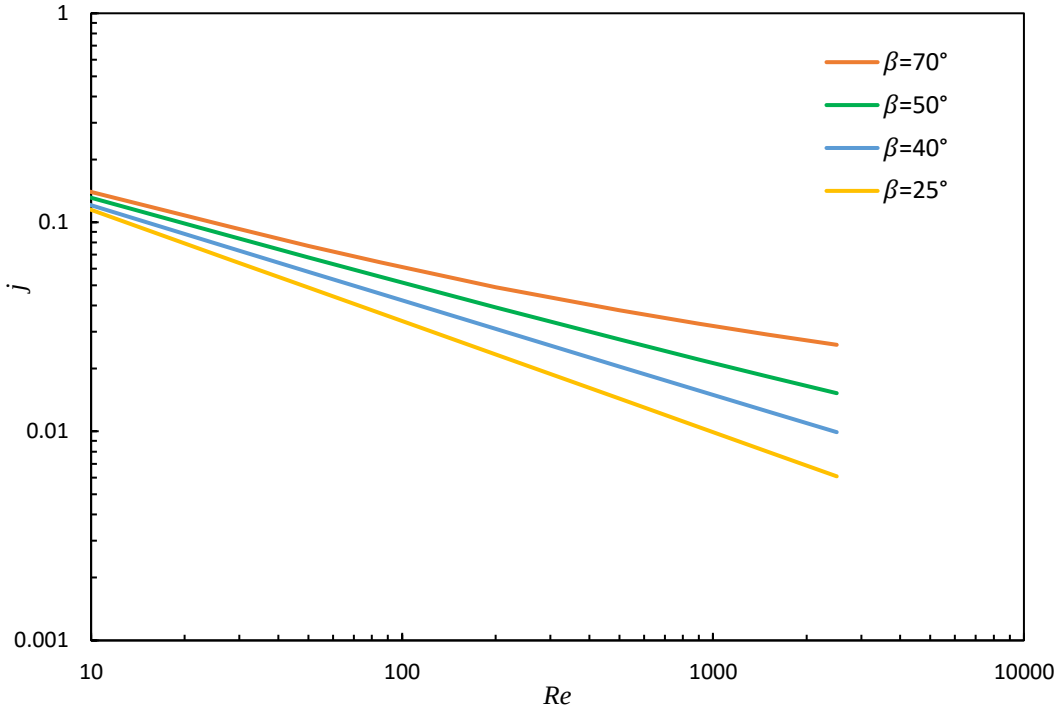

Fig. 6.7 General model prediction for $L/D_e = 50$, and different chevron angles

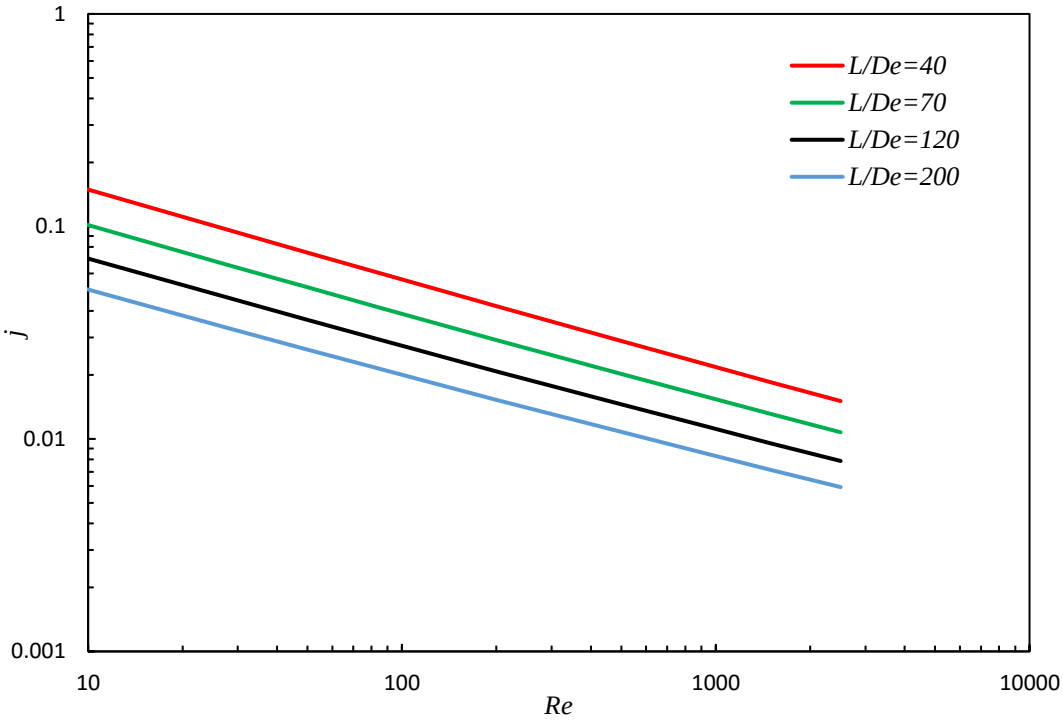

Fig. 6.8 General model prediction for $\beta = 50°$, and different L/D_e ratios

results for $\beta = 25°$ are lower than those of $\beta = 40°$ while data for $\beta = 70°$ are much higher, the Colburn j factor increase with β. This trend agrees with the literature (Focke et al. (1985), Heavner et al. (1993), Lee and Lee (2014)). PHEs often have chevron angles between $30° \leq \beta \leq 65°$ (Wang et al. 2007). With regard to the model prediction for fixed $\beta = 50°$ and different L/D_e ratios, Fig. 6.8 shows that for $L/D_e = 120$, the Colburn j factor prediction line is between $L/D_e = 70$ and $L/D_e = 200$, as expected.

6.4 Comparison of Models with Data

In this section, validation of the long and short channel models, Eq. (6.18) and Eq. (6.19), with the present experimental data for all long and short plates are shown in Figs 6.7 and 6.8. Next, the general model, Eq. (6.20), is also validated using the experimental data for both long and short channels, which are plotted in Figs. 6.11 – 6.115. Finally, the general model is also compared with data published in the literature for different chevron plate configurations such as b, λ, L and β.

A comparison of the long channel model, Eq. (6.18), with the experimental results of the long plates is shown in Fig. 6.9. The model and the data are in excellent agreement with an average RMS error $\pm 5.61\%, \pm 6.18\%$, and $\pm 1.3\%$ for chevron angles $60°, 45°,$ and $30°$, respectively.

Validation of the short channel model, Eq. (6.19), with the experimental data for all short plates is illustrated in Fig 6.10. The model and data are in good agreement with an average RMS error $\pm 3.5\%, \pm 2.19\%$, and $\pm 9.09\%$ for chevron angle $60°, 45°,$ and $30°$, respectively.

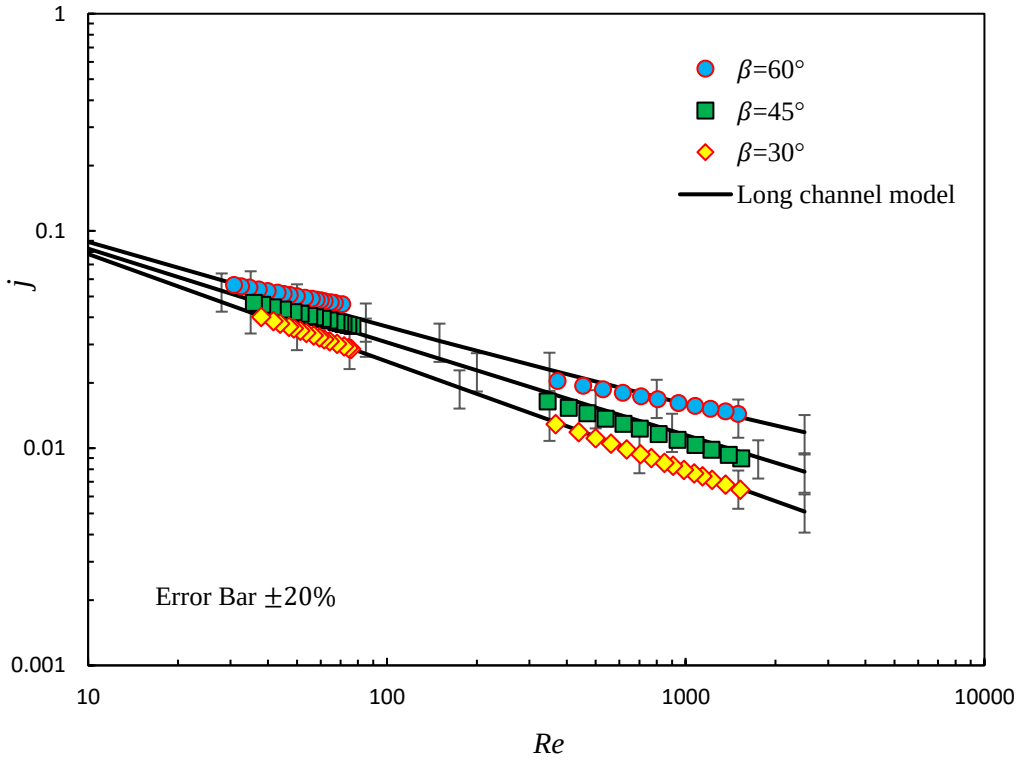

Fig. 6.9 Proposed long channel model prediction for all long channels

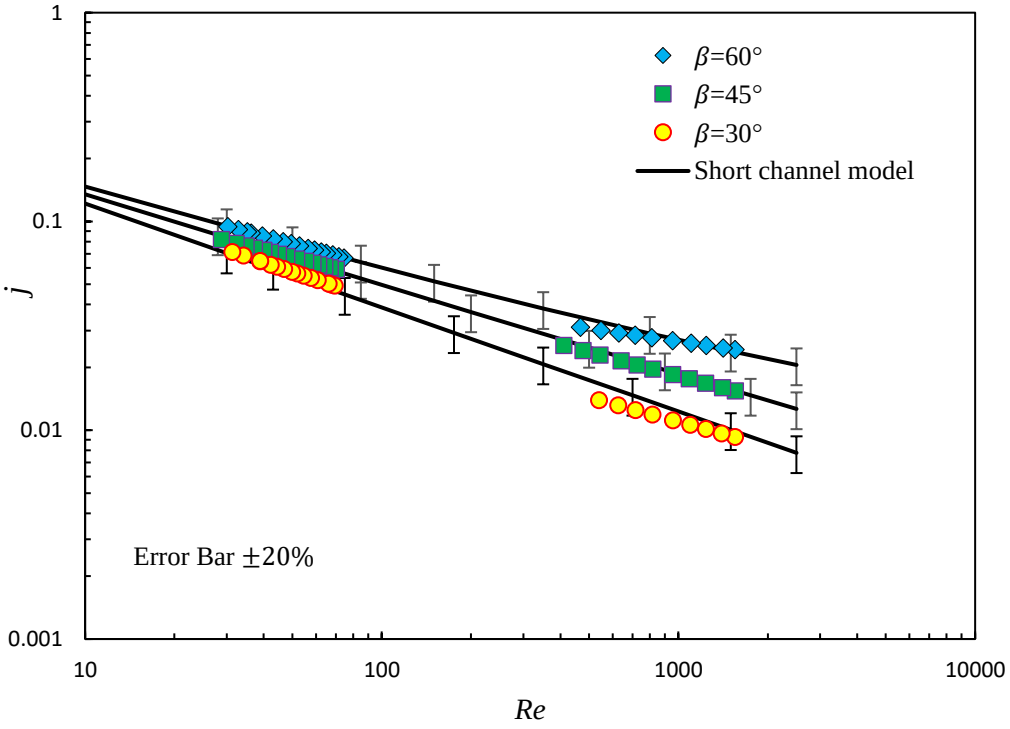

Fig. 6.10 Proposed short channel model prediction for all short channels

The comparison between the general model, Eq. (6.20), predictions and the experimental data for long and short channels is presented in Figs. 6.11 – 6.15. All data are well predicted within an average RMS error of $\pm 10\%$ or less. The average RMS error between the general model and the experimental data for all plates with different chevron angles is summarized in Table 6.1.

Table 6.1 General model validation results

Chevron angle (β)	RMSE %	
	Long channel	Short channel
60°	± 6.84	± 3.6
45°	± 7.27	± 3.42
30°	± 1.43	± 9.11

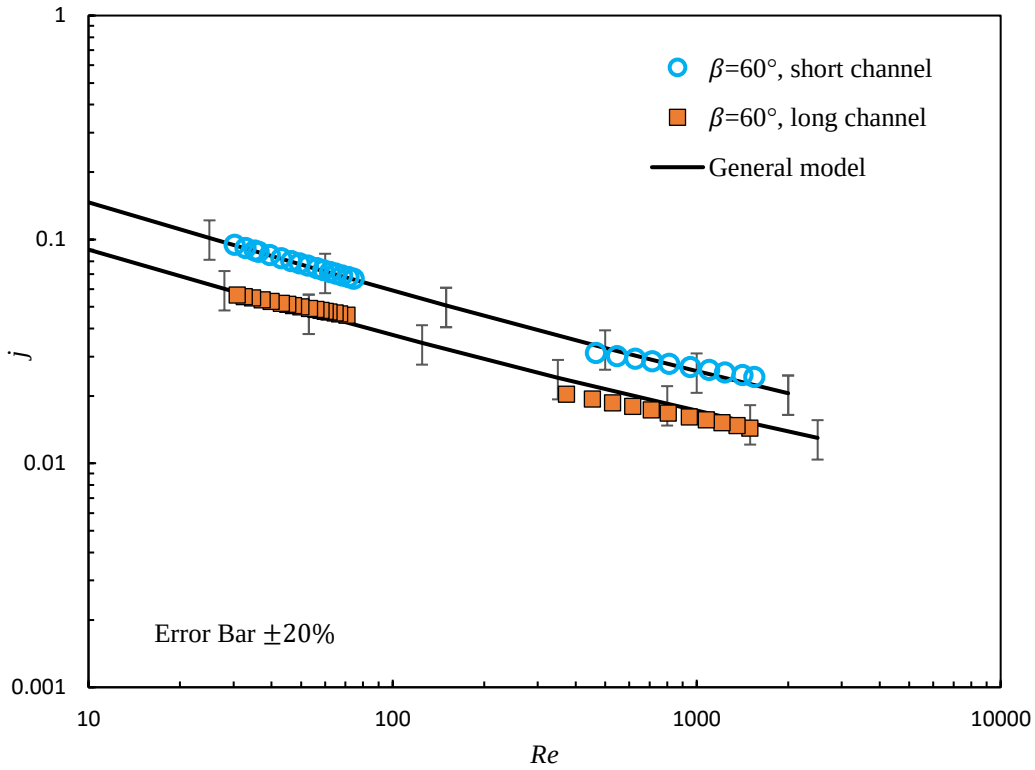

Fig. 6.11 Proposed general model prediction for long and short channel, $\beta = 60°$.

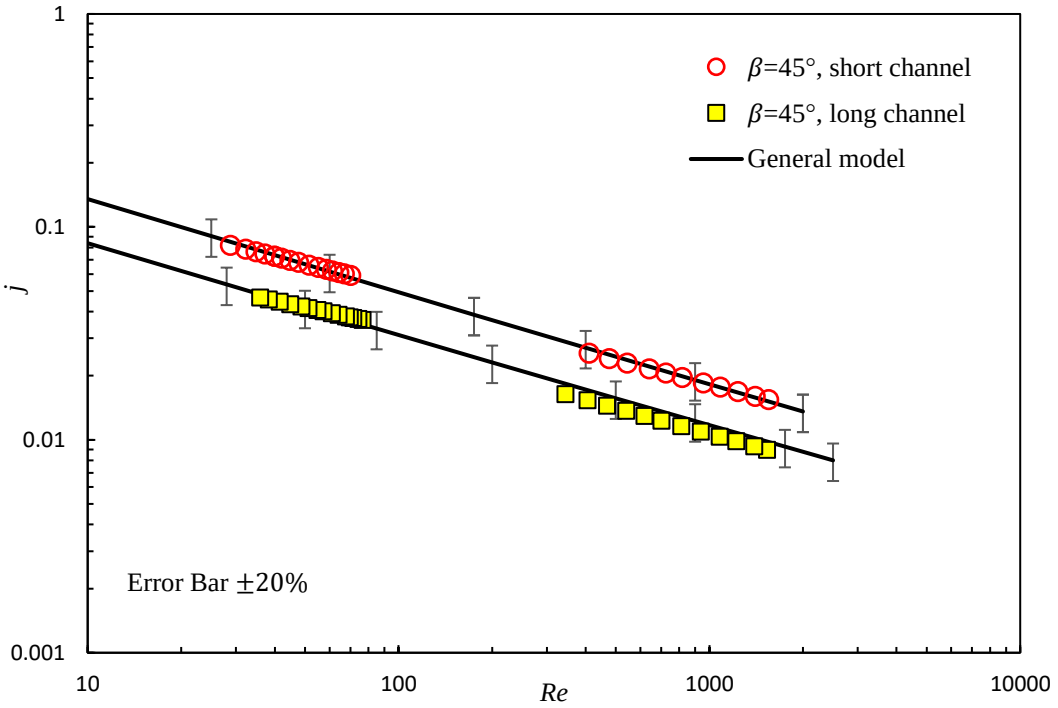

Fig. 6.12 Proposed general model prediction for long and short channel, $\beta = 45°$

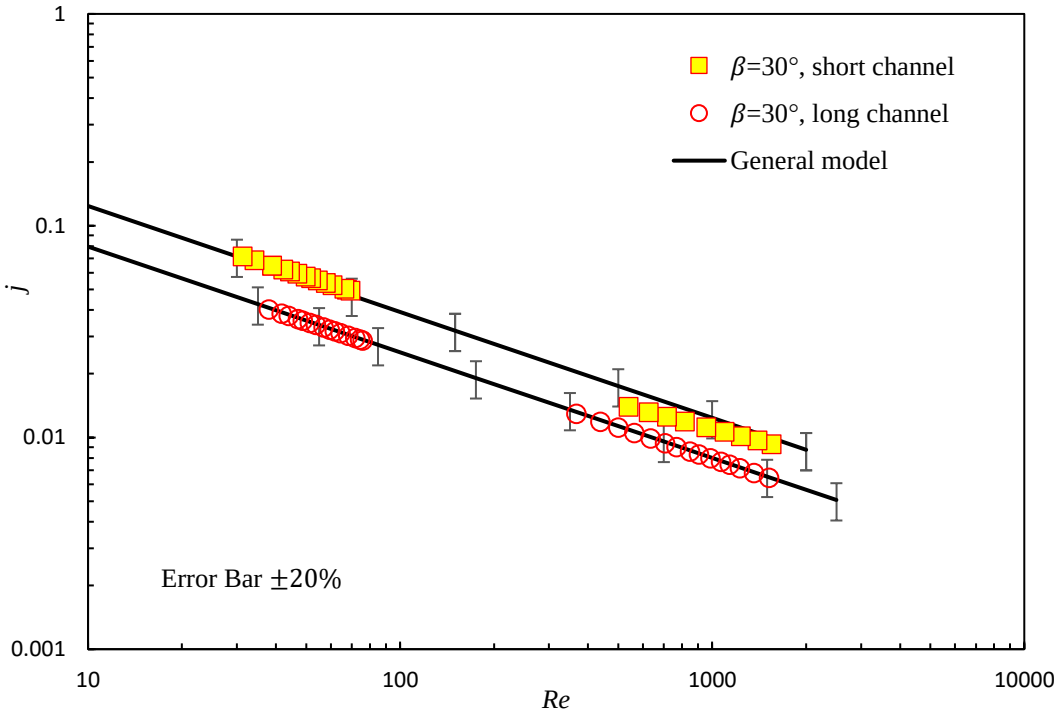

Fig. 6.13 Proposed general model prediction for long and short channel, $\beta = 30°$

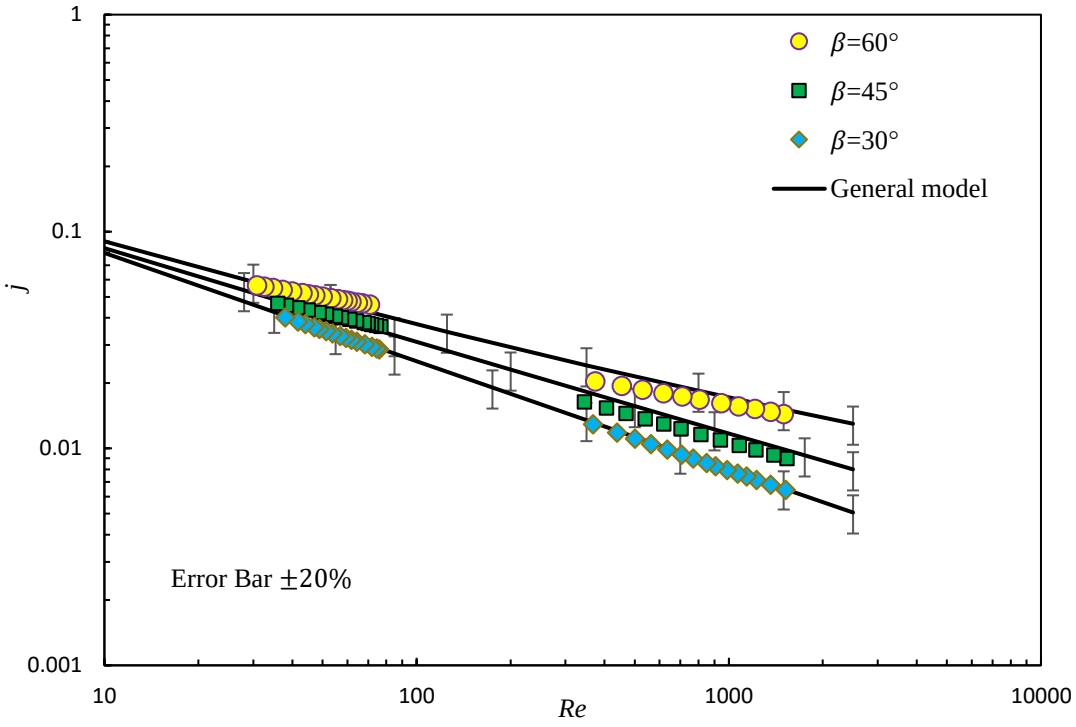

Fig. 6.14 Proposed general model prediction for all long channels

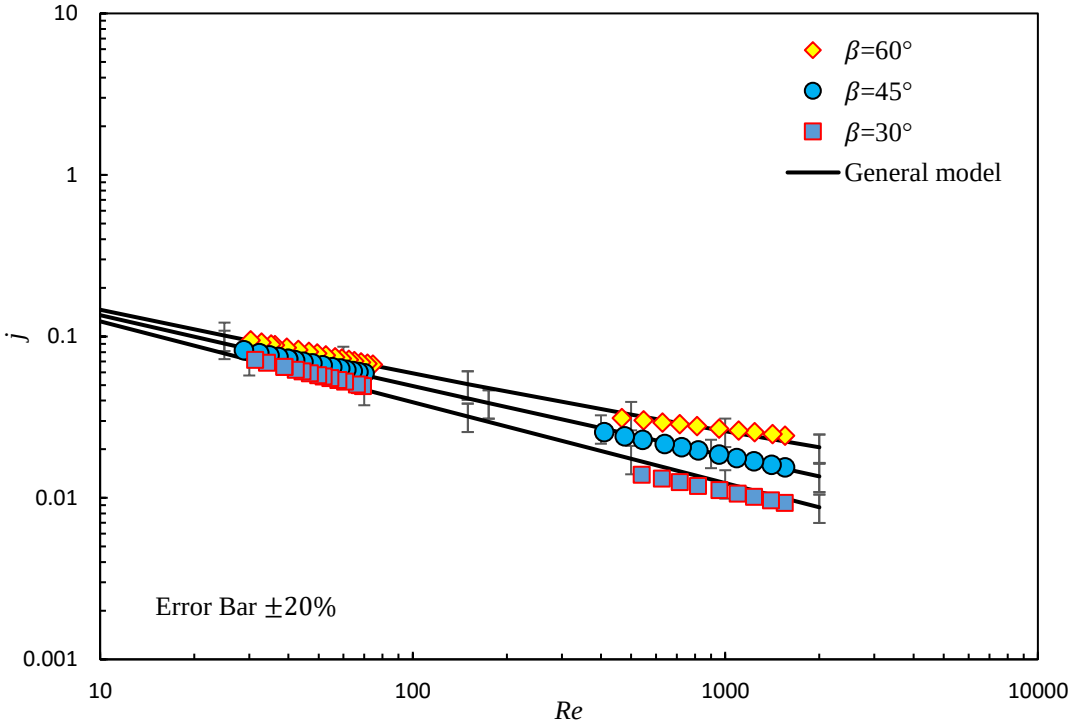

Fig. 6.15 Proposed general model prediction for all short channels

Similar to what has been done in the pressure drop chapter, studies from the literature have been plotted against each other to show variation in the heat transfer data for laminar and turbulent flows even though they are all for chevron PHEs with $\beta = 60°$. As seen in Fig 6.16, a large scatter between these studies can be observed. These discrepancies may be attributed to the following four main factors. (1) the geometry of the plates, including corrugation profile (e.g., trapezoidal or sinusoidal), b, λ, ϕ and number and size of plates are not identical in all studies. (2) the experimental procedures and methods used to reduce/analyze the data. For instance, the results of Focke et al. (1985) are based on mass transfer, while Muley and Manglik (1999) are based on modified Wilson plot technique. Moreover, two definitions of the heat transfer area have been used in the literature; effective area, A_{eff}, and projected area, A_{proj}. The ratio between A_{eff} and A_{proj} is the surface area enlargement factor, ϕ, where $\phi > 1$. Therefore, using different heat transfer areas when reducing the data may lead to different results even at the same β as $A_{\text{eff}} > A_{\text{proj}}$ by a factor equal to ϕ. Also, the ϕ value is not always reported. Thonon (2005) mentioned that care should be exercised when using published correlations as using wrong definitions of the reference heat transfer area and the reference diameter can affect the final results by up to $\pm 30\%$. (3) Another reason may be fouling, which introduces an additional resistance to the overall heat transfer resulting in a lower heat transfer rate (Wang et al. 2007). (4) Other sources of differences are also mentioned in Kakac et al. (2012), such as port orientation, flow distribution channels, plate width, and length.

As illustrated in Fig. 6.16, by using the results of Muley and Manglik (1999) as a

reference and at $Re \approx 1000$, the results of Focke et al. (1985), Edwards's et al. (1974), and Vlasogiannis's et al. (2002) are higher by 8.8, 2.12, and 1.6 times, respectively.

Difficulties that arose while obtaining data from the literature to validate the developed model are summarized as follows: (1) the plate geometric information required are not

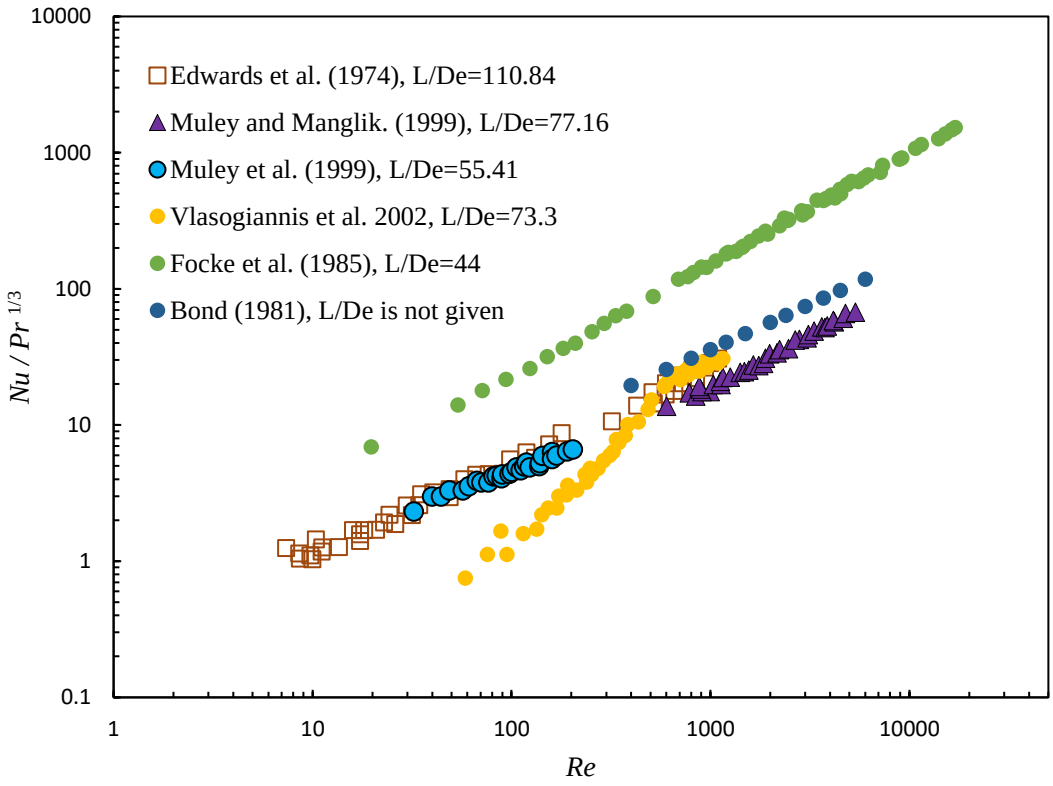

Fig. 6.16 Nusselt Number for PHEs from the literature for different L/D_e ratios and fixed $\beta = 60°$

given or partially provided whether for numerical or experimental studies such as in Lee and Lee (2014), Alzahran et al. (2019), Dović et al. (2009) Heavner et al. (1993) and Bond (1981). (2) Some investigators reported their heat transfer data as Nu versus Re, which requires the Prandtl number of the working fluid to be known to make a valid comparison

with another type of fluid results. While other authors presented the data as $Nu/Pr^{0.4}$ versus Re such as Okada et al. (1972) and Talik et al. (1995). The exponent on the Prandtl number is varying in the literature from 0.3 to 0.5. Once again, such data may not be used for a direct comparison and/or validation without error associated with estimating the Pr exponent to be $1/3$ as in the $Nu/Pr^{1/3}$ or the Colburn j factor. (3) In many studies such as in Gulenoglu et al. (2014) and Gherasim et al. (2011, a) the heat transfer area used in the data reduction has not been identified whether A_{eff} or A_{proj}.

Developing a general model that would take into account the effects of all the factors identified above in addition to the experimental errors becomes a challenging task. Once again, the lack of geometric details does not allow us to fully utilize the results published in the literature to validate and/or improve the developed model prediction. Thonon (2005) pointed out that for the last 35 years, about 15 studies have reported the geometric plate details. This may be due to proprietary rights.

In the literature, Nusselt Number is usually correlated using a power-law equation of Re and Pr as a function of β, such as in the work of Okada et al. (1972), Focke et al. (1985), and Junqi et al. (2018), while some investigators added the viscosity variation factor $(\mu/\mu_w)^{0.17}$ as in the work of Heavner et al. (1993), Bond (1981) and Yildiz and Ali Ersöz (2015). The exponent on the viscosity variation factor is presented as 0.14 in Emerson (1967) and Khan et al. (2010). Using such correlations may not predict the heat transfer results for other studies with different plate configurations as the only parameter changing is Re. Therefore, the proposed model is a function of another parameter, L/D_e,

in addition to Re, Pr and β. This parameter takes into account change in the plate length and corrugation depth. With regard to comparison the plotted studies with the developed model, the results of Focke et al. (1985) will be excluded as they have been reported to overestimate the heat transfer of PHE, such as in Talik et al. (1995), Muley and Manglik (1999) and Wang et al. (2007). For the results of Vlasogiannis et al. (2002), the data did not show similar trend behaviour to other similar studies, especially in the region $Re < 600$. Moreover, data of Bond (1981) is also excluded as no geometric details are given. Therefore, these studies will not be compared with the proposed model but reported here to show discrepancy in the literature.

The comparisons of the developed model predictions with studies from the literature for different plate surface characteristics such as; b, λ and L for chevron angles, $\beta = 30°, 45°, 60°, 65°$, and $70°$, are shown in Figs 6.15-6.26. The data of Kim and Park (2017), Muley et al. (1999), Roetzel et al. (1994), Muley and Manglik (1999), and Edwards et al. (1974) are based upon A_{eff} whereas the developed model, present experimental data, are based upon A_{proj}. Therefore, all of the mentioned studies data have been rescaled to be based on A_{proj} by dividing the results by ϕ, which varies from 1.13 to 1.29 for the selected studies.

Figure 6.17 illustrates the numerical, CFD, and experimental results of Kanaris et al. (2006) along with the developed model for PHE with $\beta = 60°$, using water as the working fluid. The general model predicted all the data with an average RMS error $\pm 29.2\%$. The plate corrugation shape was a rounded trapezoidal and not sinusoidal. Zhang and Che

(2011) reported that a channel with a trapezoidal corrugation profile has higher Nu and f than the sinusoidal channel, based on which the present model was developed.

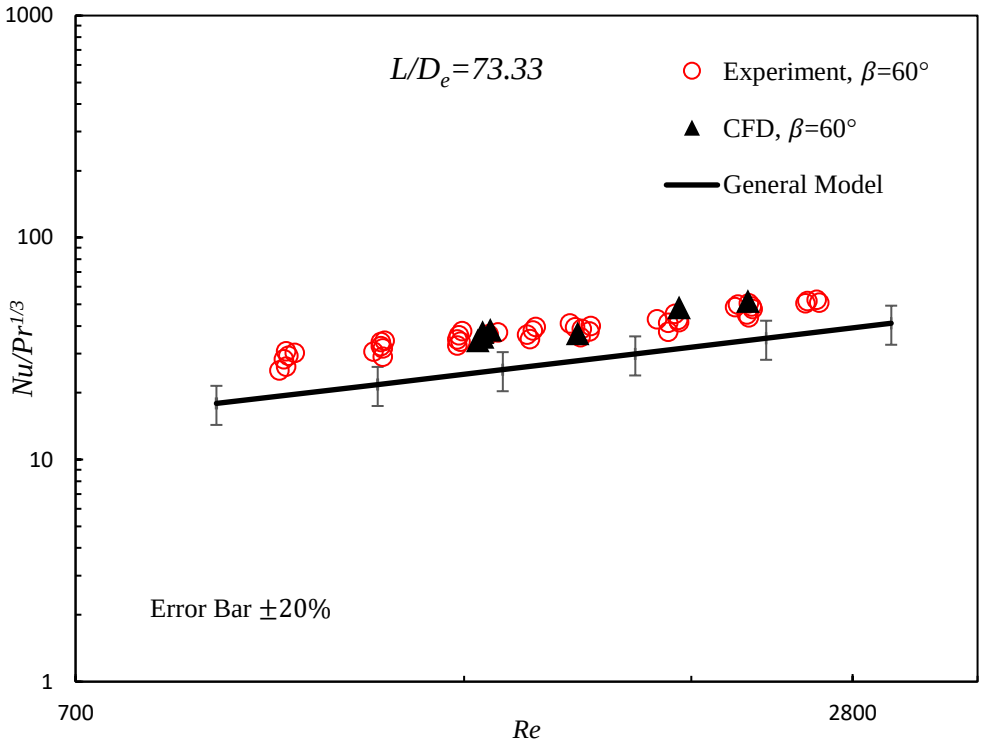

Fig. 6.17 Nusselt Number for chevron plates, data from Kanaris et al. (2006)

The experimental data of Muley and Manglik (1999), using water as the working fluid, are compared with the general model for three different chevron angles, $60°, 45°, 30°$ inFigs 6.18-6.20. It can be observed from Fig 6.18 that for $\beta = 60°$, there is excellent agreement between the model and all the data with an average RMS error $\pm 8.13\%$. Furthermore, Fig 6.19 shows good agreement between the model and data for $\beta = 60°/30° \approx 45°$ with an average RMS error $\pm 23.82\%$. As of $\beta = 30°$, see Fig. 6.20, the proposed model is in fair agreement with the data in the Reynolds number region $Re < 1600$, upper limit of the model, with an average RMS error $\pm 27.6\%$.

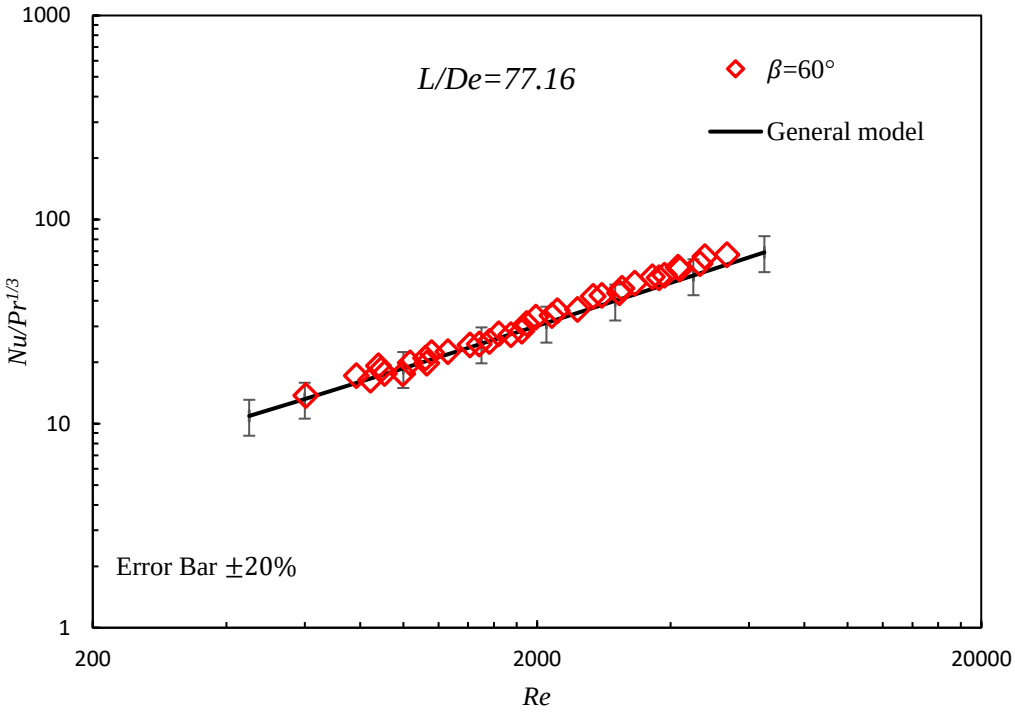

Fig. 6.18 Nusselt Number for chevron plates, data from Muley and Manglik (1999)

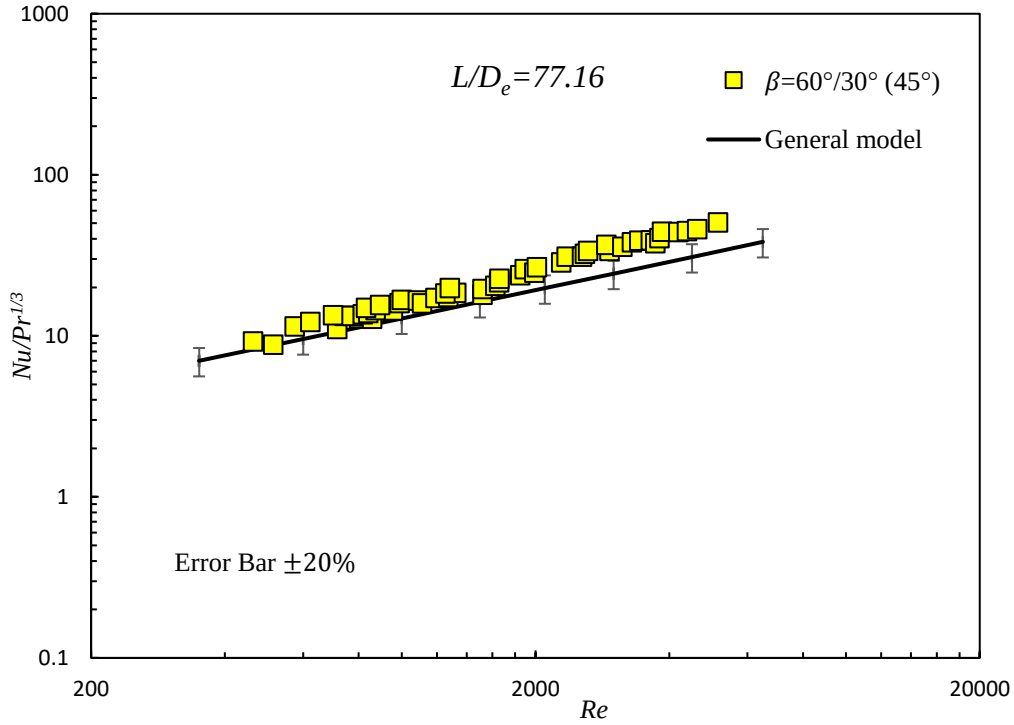

Fig. 6.19 Nusselt Number for chevron plates, data from Muley and Manglik (1999)

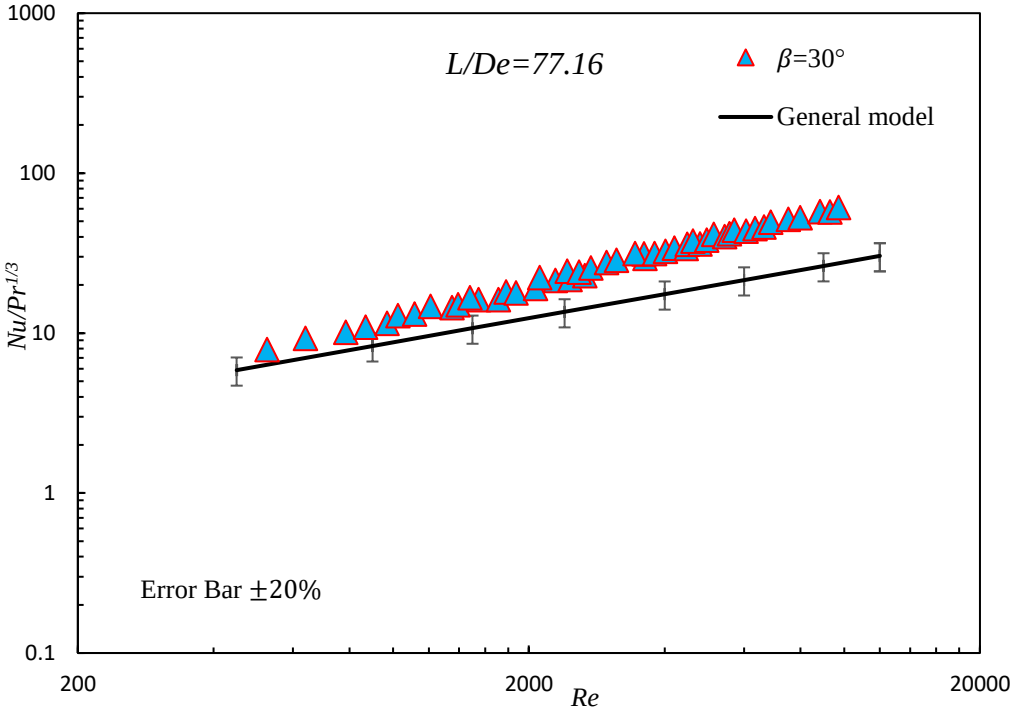

Fig. 6.20 Nusselt Number for chevron plates, data from Muley and Manglik (1999)

A comparison of the experimental work of Edwards et al. (1974) with the developed model is depicted in Fig. 6.21 for $\beta = 60°$. The model predicted the data with an average RMS error $\pm 38.07\%$. However, the general trend of the data is well captured by the model. Once again, the large deviation between the model and the data may be due to uncommon plate size. The working fluids were water, glucose solutions, lubricating oil, and various non-Newtonian liquids.

The general model prediction and the experimental data of Gherasim et al. (2011, a) are plotted in Fig. 6.22. The model underpredicted the data as their plates had trapezoidal shape corrugations and not sinusoidal. Moreover, the authors did not identify which heat transfer area has been used in the data reduction, A_{eff} or A_{proj}. Thus, if the A_{proj} is used,

the model predicted the reported data within an average RMS error $\pm$ 24.65%, otherwise, the average RMS error will be lower than that as all data need to be divided by ϕ, where $\phi > 1$. The working fluid was water and $\beta = 60°$.

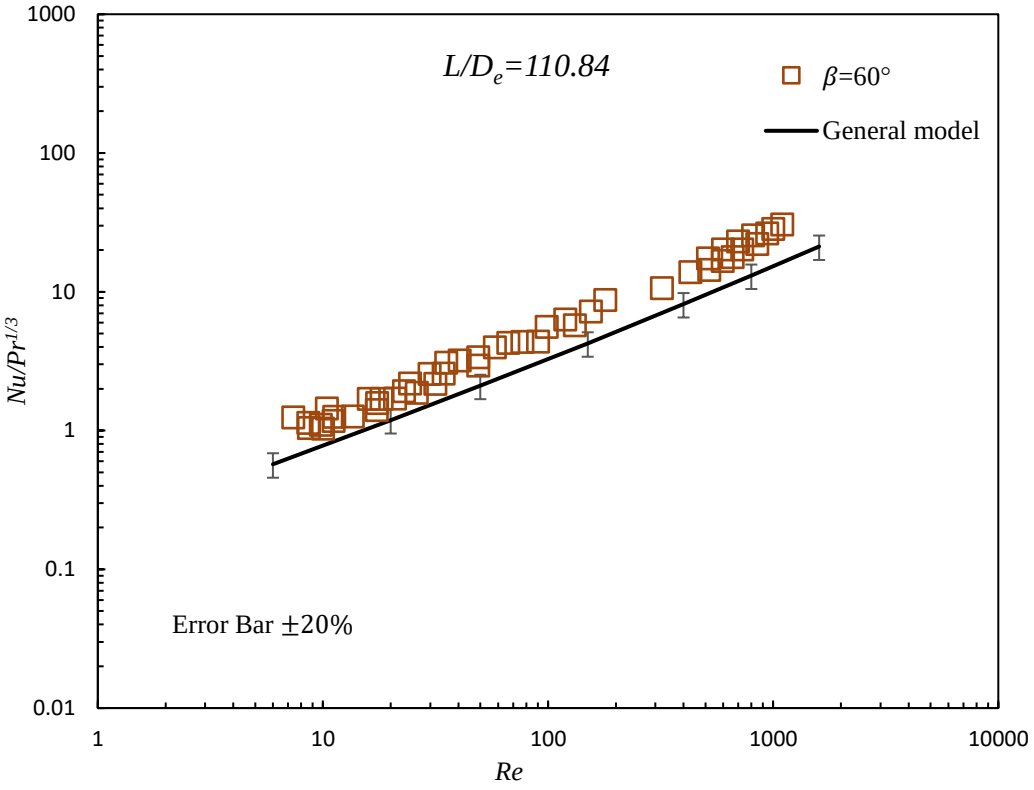

Fig. 6.21 Nusselt Number for chevron plates, data from Edwards et al. (1974)

The developed model predicted the experimental data of Kim and Park (2017) within an average RMS error $\pm$ 24.36%, which is plotted in Fig. 6. 23. The chevron angle was $\beta = 65°$ and the working fluid was water.

Predictions of the proposed model along with the experimental data of Roetzel et al. (1994) are plotted in Fig 6.24. The model and the data are in excellent agreement with an average RMS error $\pm$9.10%. The working fluid was water and $\beta = 70°$.

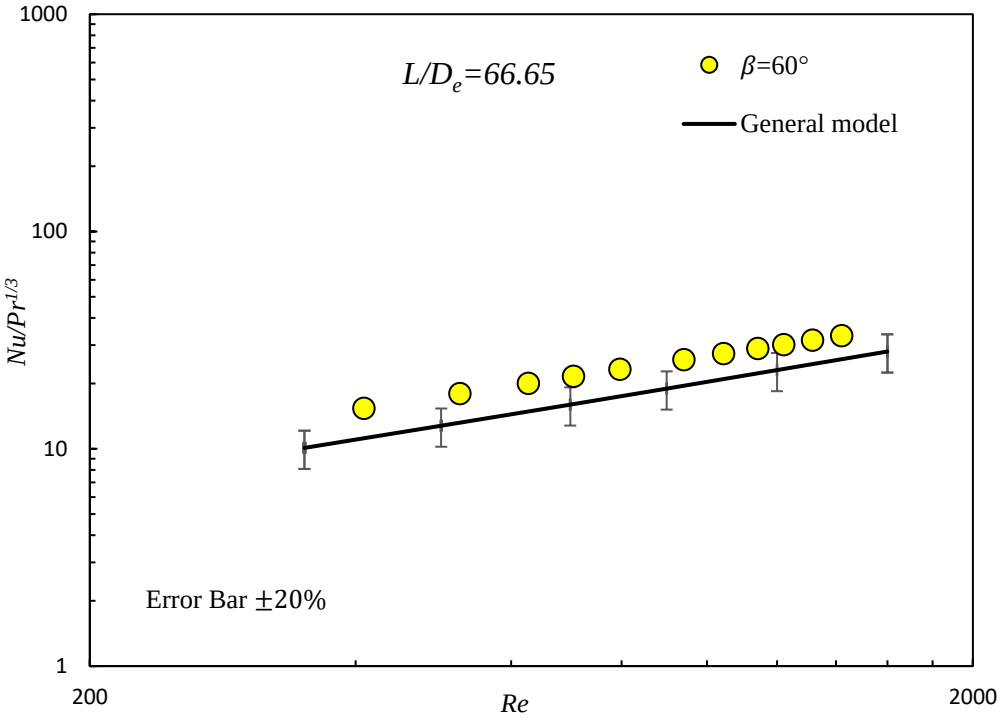

Fig. 6.22 Nusselt Number for chevron plates, data from Gherasim et al. (2011, a)

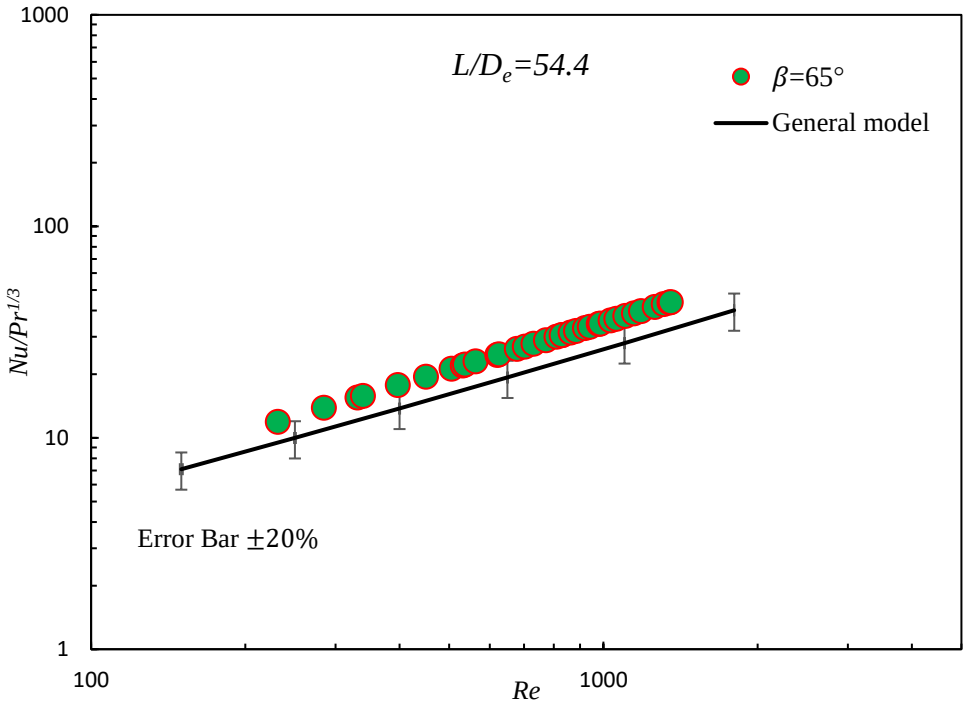

Fig. 6.23 Nusselt Number for chevron plates, data from Kim and Park (2017)

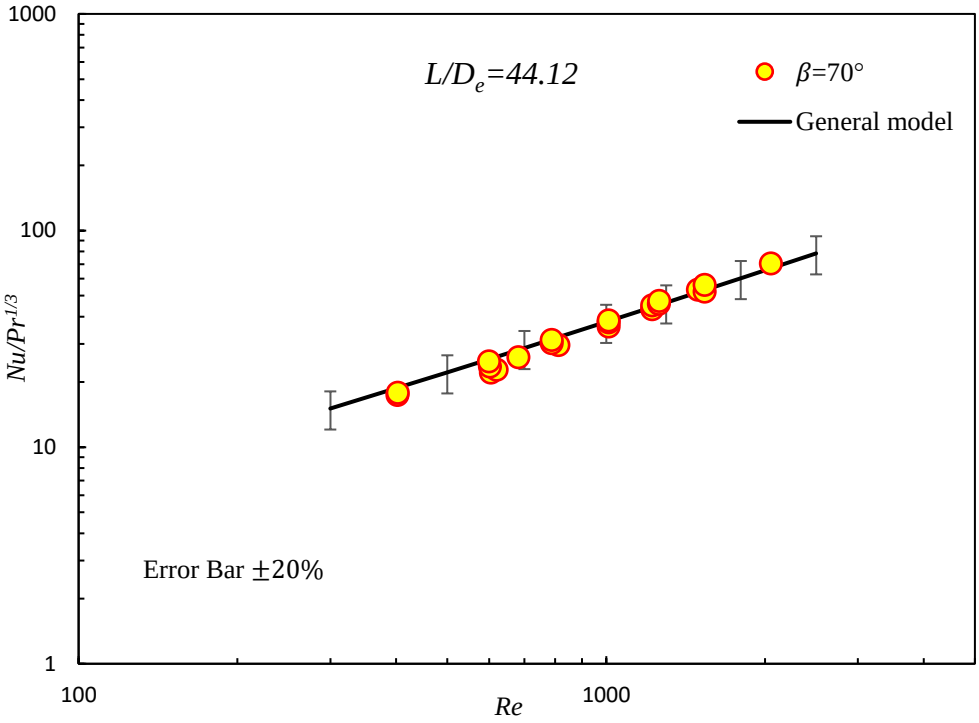

Fig. 6.24 Nusselt Number for chevron plates, data from Roetzel et al. (1994)

Experimental data of Gulenoglu et al. (2014) are compared with the proposed model and shown in Fig. 6.25. Authors did not identify which heat transfer area has been used A_{eff} or A_{proj} in the data reduction. Therefore, if the reported data are based upon A_{proj} the model predicted the data within an average RMS error $\pm$ 33.01%, otherwise, the average RMS error will be $\pm$ 13.83% as all data need to be divided by ϕ.

A comparison of the general model prediction with the experimental data of Muley et al. (1999) for $\beta = 30°, 30°/60°$ and $60°$, using vegetable oil as working fluid, are presented in Figs. 6.26-6.28. The general model predicted that data for $\beta = 30°, \sim 45°$, and $60°$, with an average RMS error $\pm$3.74%, $\pm$13.42% and $\pm$13.01%, respectively.

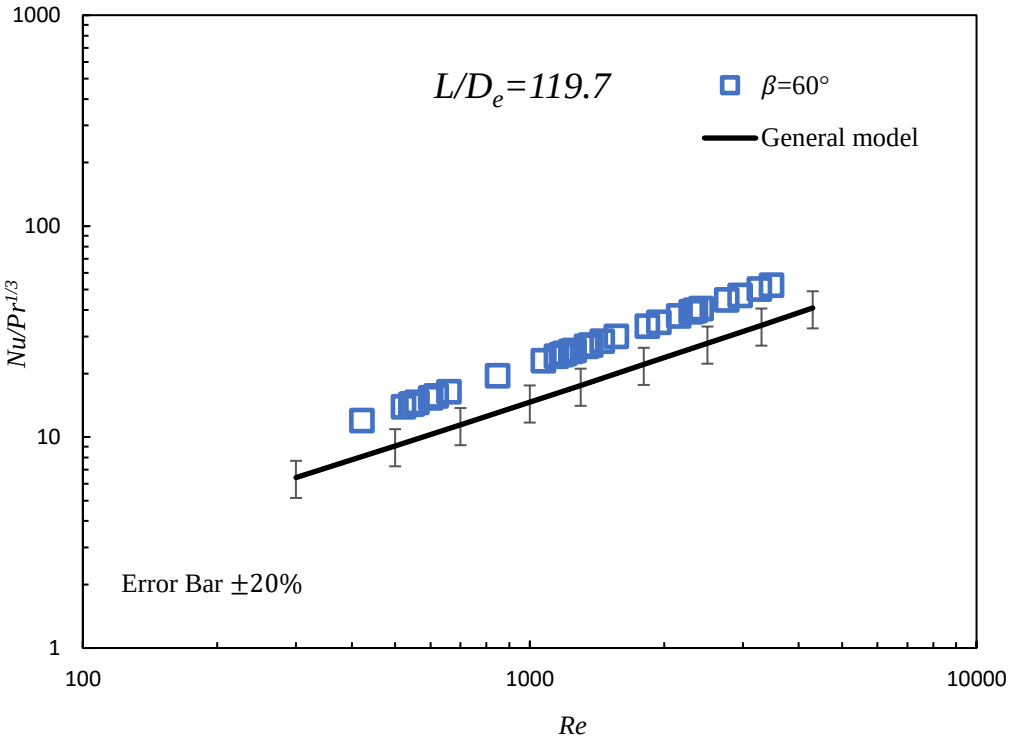

Fig. 6.25 Nusselt Number for chevron plates, data from Gulenoglu et al. (2014)

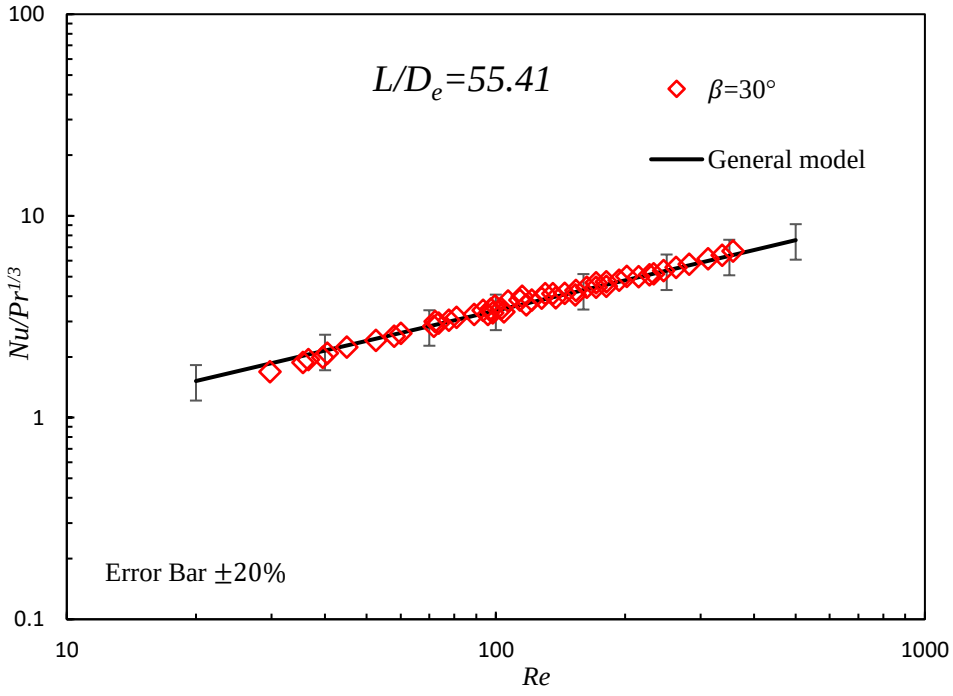

Fig. 6.26 Nusselt Number for chevron plates, data from Muley et al. (1999)

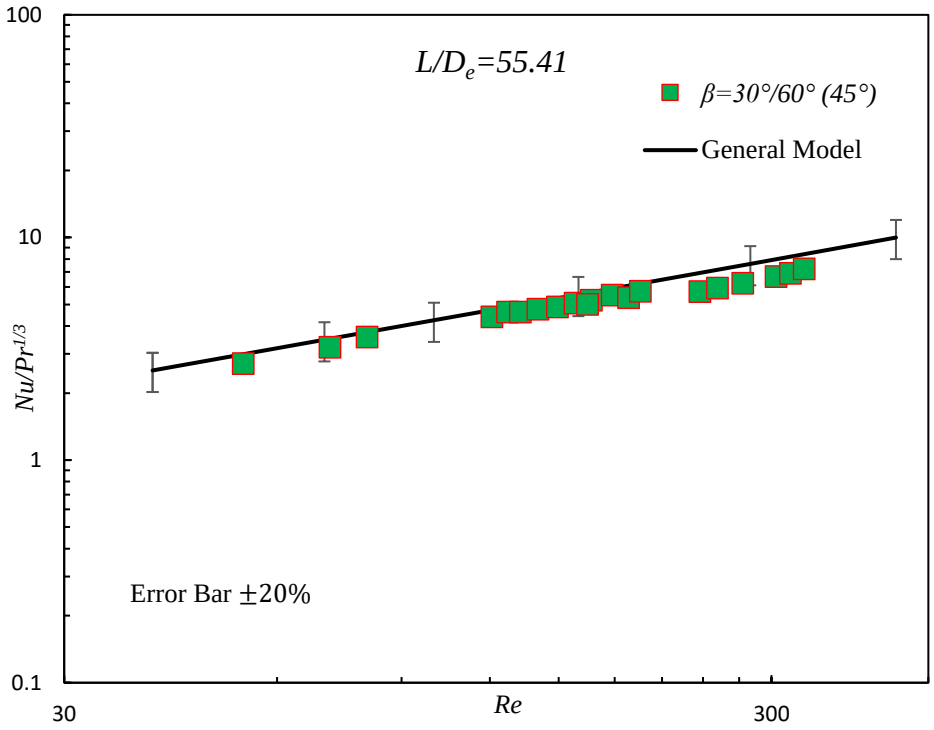

Fig. 6.27 Nusselt Number for chevron plates, data from Muley et al. (1999)

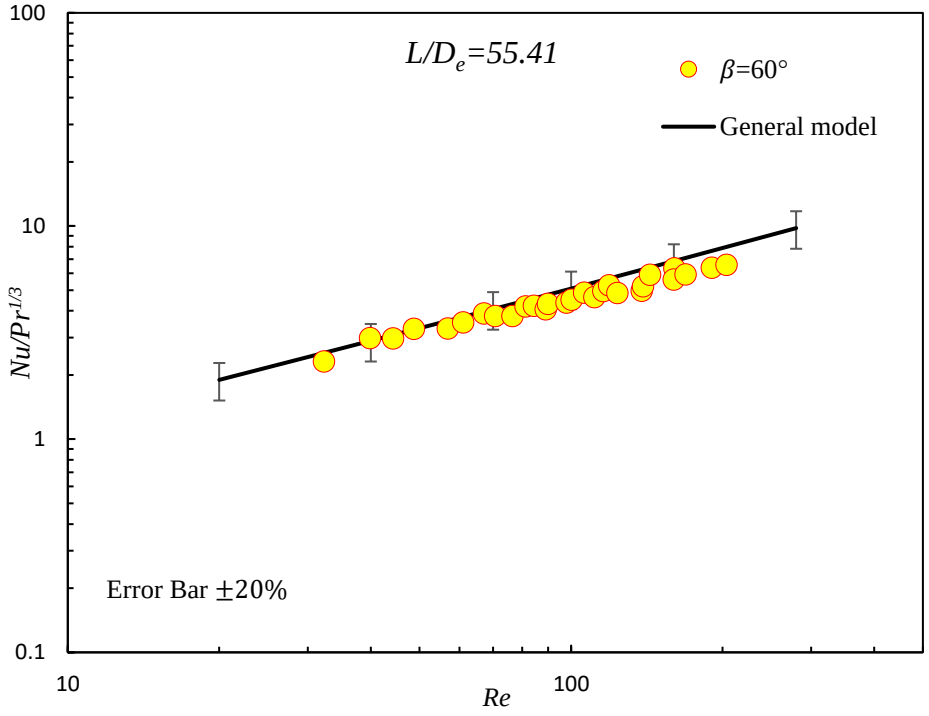

Fig. 6.28 Nusselt Number for chevron plates, data from Muley et al. (1999)

6.5 Conclusions

A general model to predict the Colburn factor in chevron plate heat exchangers with developing flow has been developed. The proposed model was developed using the asymptotic correlation method proposed by Churchill and Usagi (1972). This model covers the laminar, transition, and turbulent flow regions. For both the long and short channels, model predictions agreed well with experimental data with an average RMS error of $\pm 10\%$ or better. The agreement bewteen the model and existing numerical, CFD, and experimental data from the literaure was also very good in most of the selected studies within $\pm 20\%$ over entire the validation range.

Chapter 7

Conclusions and Recommendations

7.1 Conclusions

The thermal-hydraulic performance for flow in a chevron plate heat exchanger has been examined experimentally using water and mineral oil as working fluids. The effects of three different chevron angles $\beta = 30°, 45°,$ and $60°$ and two channel lengths, $L =$ 20.3 cm and 10.1 cm on the fluid friction and heat transfer characteristics of PHEs were investigated. The main goal of this thesis was to experimentally examine the effect of the channel length on f and Nu of PHE as well as to develop general models to predict the friction factor and colburn factor of PHE for single-phase flow applications, including the entrance region. The main objectives accomplished in this thesis are summarized as follows.

1. A comprehensive literature review on pressure drop and heat transfer in chevron plate heat exchangers for a single-phase flow has been presented. This included a collection of published general correlations / models to predict Nu and / or f. More than fifty correlations were summarized in Table 3.1.
2. A new experimental test apparatus was built in the Heat Transfer Lab to collect pressure drop and heat transfer measurements for single-phase flow in a PHE. The apparatus was benchmark tested to confirm its accuracy by comparing the pressure drop measurement for a pipe with laminar and turbulent flow theory in a pipe. The

results agreed within $\pm 10\%$. Next, heat transfer measurements for a smooth channel were verified against the Stephan correlation, and most of the results agreed with $\pm 10\%$. Two fluids with different orders of magnitudes of viscosity were used to allow laminar and turbulent flow regions to be examined.

3. The friction factor results were obtained for six sets of corrugated channels with $\beta = 30°, 45°,$ and $60°$ and two channel lengths using water and mineral. The results clearly showed that the chevron angle has a strong effect on the pressure drop, which increases by increasing β. Furthermore, at higher Reynolds numbers, the results clearly showed the friction factor for the short channel result was higher than those for the long channel, which can be attributed to the presence of entrance effects. On the other hand, at low Reynolds numbers, the results for long and short channels were nearly the same which means the fully developed flow condition is exist; hence, the hydrodynamic entrance effect can be neglected.
4. A comparison of the obtained experimental results with existing numerical, CFD, and experimental data from the open literature revealed good agreement; however, there was also some disagreement.
5. The experimental heat transfer results for the same sets of corrugated plates, $\beta = 30°, 45°,$ and $60°$ and two channel lengths, were acquired using water and mineral oil. The Nusselt number for the short plates was significantly greater than for the longer plates, indicating that thermal entrance effects were present. Moreover, heat transfer augmentation was clearly observed, which appears to increase by reducing the channel length and increasing the chevron angle and Reynolds numbers. The

current heat transfer results were compared to data from experimental and numerical, CFD, data from the literature, and very good agreement was obtained; however, some discrepancies were also observed.

6. According to the obtained experimental results for f, except at low Reynolds number, and Nu, the channel length is an important factor when it comes to developing general correlations or models to predict the thermal-hydraulic performance of PHEs, especially for PHE with short flow passages. If the channel length is not considered, it may lead to underestimating the pressure drop and heat transfer performance of the PHE.
7. General models for predicting the Colburn factor and Fanning friction factor were developed by combining the asymptote solutions using the Churchill and Usagi (1972) technique. The developed models are a function of the chevron angle, corrugation depth, and channel length, and Reynolds number. The model's predictions agreed with the experimental data within an average RMS error $\pm 20\%$ or less for both long and short channels. The models were also validated against data from the literature for numerical, CFD, and experimental studies and showed good agreement in most cases within the validation range. The RMS and (min/max) values of the percent differences between the Colburn factor model and Fanning friction factor model, and data from the present experiment and literature are summarized in Table 7.1 and 7.2, respectively.

Table 7.1 Summary of RMS and percent differences between j model and data

Author		Chevron angle (°)	j		Reynolds number range
			RMS	(min/max)	
Present experiment	Short channel	30	9.11	$-20.81/4.43$	All tested Re
		45	3.42	$-5.05/2.6$	
		60	3.6	$-7.6/8.16$	
	Long channel	30	1.43	$-2.08/-0.89$	
		45	7.27	$-11.73/4.88$	
		60	6.84	$-13.4/9.45$	
Kim and Park (2017)		65	24.36	$20.3/25.56$	All tested Re
Kanaris et al. (2006)		60	29.2	$17.1/36.27$	
Gherasim et al. (2011 a)		60	24.65	$22.2/27.4$	
Gulenoglu et al. (2014)		60	33.01	$32.4/33.29$	
Roetzel et al. (1994)		70	9.10	$-5.7/15.80$	
Muley and Manglik (1999)		60	8.13	$-0.4/15.74$	
Muley and Manglik (1999)		45	23.82	$0.84/36.12$	
Muley and Manglik (1999)		30	27.6	$19.7/34.35$	$Re < 1500$
Edwards et al. (1974)		60	38.07	$22.1/77.5$	All tested Re
Muley et al. (1999)		30	3.74	$-9.51/4.8$	
Muley et al. (1999)		45	13.01	$-20.8/-4.69$	
Muley et al. (1999)		60	13.42	$-25.08/3.31$	

Table 7.2 Summary of RMS and percent differences between f model and data

Author		Chevron angle (°)	f		Reynolds number range
			RMS	(min/max)	
Present Experiment	Short channel	30	10.04	$-14.98/17.9$	All tested Re
		45	6.28	$-4.49/14.13$	
		60	14.64	$-4.68/20.86$	
	Long channel	30	6.75	$-15.12/8.71$	
		45	19.43	$-34.78/18.29$	
		60	15.89	$-38.87/16.37$	
Junqi et al. (2018)		30	19.76	$3.4/30.36$	$Re < 1500$
Junqi et al. (2018)		45	29.77	$-3.1/-45.6$	All tested Re
Junqi et al. (2018)		60	12.62	$-5/24.7$	
Gherasim et al. (2011 a)		60	12.06	$7.54/20.15$	
Jain et al. (2007)		60	18.01	$15.04/22.50$	
Muley et al. (1999)		30	22.35	$-10.02/40.29$	
Muley et al. (1999)		45	10.45	$-25.09/7.32$	
Muley et al. (1999)		60	37.7	$-20.4/-66.3$	
Gherasim et al. (2011 b)		60	10.14	$-2.1/15.60$	
Edwards et al. (1974)		60	12.72	$-25.68/14.94$	$0.05 < Re < 20$

7.2 Recommendations for future work

The thermal-hydraulic performance of PHE has been investigated experimentally for three different chevron angles and two different lengths using two fluids with different Prandtl numbers. However, the effect of changing corrugation depth, corrugation wavelength, and plate width on the performance of PHE over awide range of Reynolds numbers needs further investigation. This may help to develop more general models or correlations with a larger predictions range. The following research areas are suggested to be considered and addressed in future work:

- There is a need for more experimental data on f and Nu for chevron plates with a broader range of geometrical parameters, such as corrugation angle and depth, plate length, width, and corrugation wavelength. This would allow for further validation and refinement of the developed models and extending their applicability range. This also should include fluids with different Prandtl numbers for a wide range of Reynolds numbers.
- A flow visualization study would be desirable to provide more information about the complexity of the flow pattern inside the PHE channel by testing different fluids, plates with different corrugation depths, wavelengths, plate sizes, and chevron angles for mixed and symmetric arrangements.
- Numerical simulations, for example, using CFD to predict the flow characteristics and the heat transfers in PHE for different plate geometrical parameters, need to be considered. This may also reveal more information about the flow mechanism

within the chevron plate heat exchanger channel, which might be challenging to obtain using experimental methods.

- Considering modifying or replacing the current PHE to study two-phase flows to develop models for predicting the thermal-hydraulic performance of PHE for two-phase flow applications.

References

Abu-Khader, M. M., 2012, ‘‘Plate Heat Exchangers: Recent Advances’’, *Renewable and Sustainable Energy Reviews,* Vol. 16, No. 4, pp. 1883-1891.

Abu-Khader, M. M., 2007, ‘‘Better Thermal Calculations Using Modified Generalized Leveque Equations for Chevron Plate Heat Exchangers’’, *International Journal of Green Energy,* Vol. 4, No. 4, pp. 351-366.

Akturk, F., Gulben, G., Aradag, S., Uzol, N.S., and Kakac, S., 2011, ‘‘Experimental Investigation of The Characteristics of a Chevron Type Gasketed Plate Heat Exchanger’’, *6th International Advanced Technologies Symposium (IATS’11)*. Elazığ, Turkey.

Alzahran, S., Islam, M., and Saha, S., 2019, ‘‘A Thermo-hydraulic Characteristics Investigation in Corrugated Plate Heat Exchanger’’, *Energy Procedia*. Vol. 160, pp. 597-605.

Arsenyeva, O.P. Tovazhnyanskyy, L.L. Kapustenko, P. O., and Khavin, G. L., 2011, ‘‘The Generalized Correlation for Friction Factor in Criss-cross Flow Channels of Plate Heat Exchangers’’, *Chem. Eng. Trans*., Vol. 25, pp. 399-404.

Arsenyeva, O.P., Tovazhnyanskyy, L.L., Kapustenko, P.O., and Demirskiy, O.V., 2014, ‘‘Generalised Semi-empirical Correlation for Heat Transfer in Channels of Plate Heat Exchanger’’, *Applied Thermal Engineering,* Vol. 70, No. 2, pp. 1208-1215.

Asif, M., Aftab, H., Syed, H.A., Ali, M.A., and Muizz, P.M., 2017, ‘‘Simulation of Corrugated Plate Heat Exchanger for Heat and Flow Analysis’’, *International Journal of*

Heat and Technology, Vol. 35, No. 1, pp. 205-210.

Awad, M. M., and Butt, S. D., 2009, ‘‘A Robust Asymptotically Based Modeling Approach for Two-Phase Flow in Porous Media’’, *Journal of Heat Transfer*, Vol. 131, No. 10.

Awad, M. M., and Muzychka, Y. S., 2010, ‘‘Two-Phase Flow Modeling in Microchannels and Minichannels’’, *Heat Transfer Engineering*, Vol. 31, No. 13, pp. 1023-1033.

Ayub, Z. H., 2003, ‘‘Plate Heat Exchanger Literature Survey and New Heat Transfer and Pressure Drop Correlations for Refrigerant Evaporators’’, *Heat Transfer Engineering*, Vol. 24, No. 5, pp. 3-16.

Bejan, A., and Kraus, A.D. eds., 2003, *Heat transfer handbook*, John Wiley & Sons.

Bergman, T.L., Incropera, F.P., DeWitt, D.P., and Lavine, A.S., 2011, *Fundamentals of Heat and Mass Transfer*. 7th ed. John Wiley & Sons.

Bond, M. P., 1981, ‘‘Plate Heat Exchangers for Effective Heat Transfer’’, *The Chemical Engineering*, Vol. 367, pp. 162-167.

Briggs, D. E., and Young, E. H., 1969, ‘‘Modified Wilson Plot Techniques for Obtaining Heat Transfer Correlations for Shell and Tube Heat Exchangers’’, *Chemical Engineering Progress Symposium Series*, Vol. 65, pp. 35-45.

Çengel, Y. A., and Cimbala, J. M., 2010, *Fluid Mechanics : Fundamentals and Applications*, 2nd Edition, McGraw-Hill Higher Education, Boston.

Charre, O., Jurkowski, R., Bailly, A., Meziani, S., and Altazin, M., 2002, ‘‘General Model

for Plate Heat Exchanger Performance Prediction'', *Journal of Enhanced Heat Transfer,* Vol. 9, pp. 181-186.

Chisholm, D., and Wanniarachchi, A. S., 1992, ''Maldistribution in Single-Pass Mixed-Channel Plate Heat Exchangers'', *Compact Heat Exchangers for Power and Process Industries,* Vol. 201, pp. 95-99.

Churchill, S. W., 1977, ''Friction Factor Equation Spans all Fluid-Flow Regimes'', *Chemical Engineering,* Vol. 84, No. 24, pp. 91-92.

Churchill, S. W., and Usagi, R., 1972, ''A General Expression for The Correlation of Rates of Transfer and Other Phenomena'', *AIChE Journal,* Vol. 18, No. 6, pp. 1121-1128.

Ciofalo, M., Di Piazza, I., and Stasiek, J. A., 2000, ''Investigation of Flow and Heat Transfer in Corrugated-undulated Plate Heat Exchangers'', *Heat and Mass Transfer,* Vol. 36, pp. 449-462.

Ciofalo, M., Stasiek, J., and Collins, M. W., 1996, ''Investigation of Flow and Heat Transfer in Corrugated Passages—II. Numerical Simulations'', *International Journal of Heat and Mass Transfer,* Vol. 39, No. 1, pp. 165-192.

Ding, J., and Manglik, R. M., 1996, ''Analytical Solutions for Laminar Fully Developed Flows in Double-sine Shaped Ducts'', *Heat and Mass Transfer,* Vol. 31, No. 4, pp. 269-277.

Dixon, J. C., 2007, *The Shock Absorber Handbook,* John Wiley, Chichester, England.

Dović, D., Palm, B., and Švaić, S., 2002, ''Basic Single-phase Flow Phenomena in

Chevron-type Plate Heat Exchangers'', *in Proc. IIR Conf, Zero Leakage, Minimum Charge*. Stockholm.

Dović, D., Palm, B., and Švaić, S., 2009, ''Generalized Correlations for Predicting Heat Transfer and Pressure Drop in Plate Heat Exchanger Channels of Arbitrary Geometry'', *International Journal of Heat and Mass Transfer,* Vol. 52, pp. 4553-4563.

Dović, D., and Švaić, S., 2007, ''Influence of Chevron Plates Geometry on Performances of Plate Heat Exchangers'', *Tehnički vjesnik,* Vol. 14, pp. 37-45.

Durmuş, A., Benli, H., Kurtbaş, İ., and Gül, H., 2009, ''Investigation of Heat Transfer and Pressure Drop in Plate Heat Exchangers Having Different Surface Profiles'', *International Journal of Heat and Mass Transfer,* Vol. 52, pp. 1451-1457.

Edwards, M. F., Changal Vaie, A. A., and Parrott, D. L., 1974, ''Heat Transfer and Pressure Drop Characteristics of a Plate Heat Exchanger Using Newtonian and Non-Newtonian liquids'', *Chemical Engineer,* No. 285, pp. 286-293.

Emerson, W. H., 1967c, ''The Thermal and Hydrodynamic Performance of a Plate Heat Exchanger: III. A Rosenblad Exchanger'', *National Engineering Laboratories,* No. 286.

Fernandes, C.S., Dias, R.P., Nóbrega, J.M., and Maia, J.M., 2007, ''Laminar Flow in Chevron-type Plate Heat Exchangers: CFD Analysis of Tortuosity, Shape Factor and Friction Factor'', *Chemical Engineering and Processing: Process Intensification,* Vol. 46, No. 9, pp. 825-833.

Fischer, L., and Martin, H., 1997, ''Friction Factors for Fully Developed Laminar Flow in

Ducts Confined by Corrugated Parallel Walls'', *Journal of Heat Mass Transfer*, Vol. 40, No. 3, pp. 635-639.

Focke, W. W., and Knibbe, P. G., 1986, ''Flow Visualization in Parallel Plate Ducts with Corrugated Walls'', *Journal of Fluid Mechanics*, Vol. 165, pp. 73-77.

Focke, W. W., Zachariades, J., and Olivier, I., 1985, ''The Effect of the Corrugation Inclination Angle on the Thermohydraulic Performance of Plate Heat Exchangers'', *International Journal of Heat and Mass Transfer*, Vol. 28, No. 8, pp. 1469-1479.

Gaiser, G., and Kottke, E. V., 1998, ''Effects of Wavelength and Inclination Angle on the Homogeneity of Local Heat Transfer Coefficients in Plate Heat Exchangers'', *in Proc. 11th Int. Heat Transfer Conf*, Kyongju, Korea, Vol. 6, pp. 203-208.

Gherasim, I., Taws, M., Galanis., N., and Nguyen, C. T., 2011a, ''Heat Transfer and Fluid Flow in a Plate Heat Exchanger Part I. Experimental Investigation'', *International Journal of Thermal Sciences*, Vol. 50, No. 8, pp. 1492-1498.

Gherasim, I., Galanis, N., and Nguyen, C.T., 2011b, ''Heat Transfer and Fluid Flow in a Plate Heat Exchanger Part II: Assessment of Laminar and Two-equation Turbulent Models'', *International Journal of Thermal Sciences*, Vol. 50, No. 8, pp. 1499-1511.

Gulenoglu, C., Akturk, F., Aradag, S., Uzol, N.S., and Kakac, S., 2014, ''Experimental Comparison of Performances of Three Different Plates for Gasketed Plate Heat Exchangers'', *International Journal of Thermal Sciences*, Vol. 75, pp. 249-256.

Gullapalli, V. S., and Sundén, B., 2014, ''CFD Simulation of Heat Transfer and Pressure

Drop in Compact Brazed Plate Heat Exchangers'', *Heat Transfer Engineering*, Vol. 35, No. 4, pp. 358-366.

Gut, J.A., Fernandes, R., Pinto, J.M., and Tadini, C.C., 2004, ''Thermal Model Validation of Plate Heat Exchangers with Generalized Configurations'', *Chemical Engineering Science*, Vol. 59, No. 21, pp. 4591-4600.

Heavner, R. L., Kumar, H., and Wanniarachchi, A. S., 1993, ''Performance of an Industrial Plate Heat Exchanger: Effect of Chevron Angle'', *in AIChE Symposium Series,* No. 295, AIChE, New York, pp. 262-267.

Hessami, M.A, 2003, ''An Experimental Investigation of the Performance of Cross-Corrugated Plate Heat Exchangers'', *Journal of Enhanced Heat Transfer*, Vol. 10, No. 4, pp. 379-393.

Holman, J. P., 2012, *Experimental Methods for Engineers*. 8th ed, McGraw-Hill, New York.

Ikegami, Y., Mutair, S., and Kawabata, Y., 2015, ''Experimental and Numerical Investigations on Plate-Type Heat Exchanger Performance'', *Open Journal of Fluid Dynamics*, Vol. 05, No. 01, pp. 92-98.

Islamoglu, Y., and Parmaksizoglu, C., 2003, ''The Effect of Channel Height on the Enhanced Heat Transfer Characteristics in a Corrugated Heat Exchanger Channel'', *Applied Thermal Engineering*, Vol. 23, No. 8, pp. 979-987.

Jain, S., Joshi, A., and Bansal, P. K., 2007, ''A New Approach to Numerical Simulation of

Small Sized Plate Heat Exchangers with Chevron Plates'', *Journal of Heat Transfer*, Vol. 129, No. 3, p. 291-297.

Junqi, D., Xianhui, Z., and Jianzhang, W., 2018, ''Experimental Study on Thermal Hydraulic Performance of Plate-Type Heat Exchanger Applied in Engine Waste Heat Recovery'', *Arabian Journal for Science and Engineering*, Vol. 43, No. 3, pp. 1153-1163.

Kakac, S., Liu, H., and Pramuanjaroenkij, A., 2012, *Heat Exchangers: Selection, Rating, and Thermal Design*, 3rd ed, CRC Press, Boca Raton, FL.

Kakac, S., Yener, Y., and Pramuanjaroenkij, A., 2014, *Convective Heat Transfer*, 3rd ed, CRC Press, Boca Raton, FL.

Kanaris, A. G., Mouza, A. A., and Paras, S. V., 2005, ''Flow and Heat Transfer in Narrow Channels with Corrugated Walls'', *Chemical Engineering Research and Design*, Vol. 83, No. 5, pp. 460-468.

Kanaris, A. G., Mouza, A. A., and Paras, S. V., 2006, ''Flow and Heat Transfer Prediction in a Corrugated Plate Heat Exchanger using a CFD Code'', *Chemical Engineering & Technology*, Vol. 29, No. 8, pp. 923-930.

Kapustenko, P., Arsenyeva, O., and Dolgonosova, O., 2011, ''The Heat and Momentum Transfers Relation in Channels of Plate Heat Exchangers'', *Chemical Engineering Transactions*, Vol. 25, pp. 357-362.

Khan, T.S., Khan, M.S., Chyu, M.C., and Ayub, Z.H., 2010, ''Experimental Investigation of Single Phase Convective Heat Transfer Coefficient in a Corrugated Plate Heat

Exchanger for Multiple Plate Configurations'', *Applied Thermal Engineering,* Vol. 30, pp. 1058-1065.

Khan, T. S., Khan, M. S., and Ayub, Z. H., 2017, ''Single-Phase Flow Pressure Drop Analysis in a Plate Heat Exchanger'', *Heat Transfer Engineering,* Vol. 38, No. 2, pp. 256-264.

Khartabil, H. F., and Christensen, R. N., 1992, ''An Improved Scheme for Determining Heat Transfer Correlations From Heat Exchanger Regression Models with Three Unknowns'', *Experimental Thermal and Fluid Science,* Vol. 5, pp. 808-819.

Kim, M. B., and Park, C. Y., 2017, ''An Experimental Study on Single Phase Convection Heat Transfer and Pressure Drop in Two Brazed Plate Heat Exchangers with Different Chevron Shapes and Hydraulic Diameters'', *Journal of Mechanical Science and Technology,* Vol. 31, No. 5, pp. 2559-2571.

Kline, S. J., and McClintock, F. A., 1953, ''Describing Uncertainties in Single-Sample Experiments'', *Mechanical Engineering,* Vol. 75, pp. 3-8.

Kumar, B., and Singh, S. N., 2017, ''Study of Pressure Drop in Single Pass U-Type Plate Heat Exchanger'', *Experimental Thermal and Fluid Science,* Vol. 87, pp. 40-49.

Kumar, H., 1984, ''The Plate Heat Exchanger: Construction and Design'', *In Institute of Chemical Engineering Symposium Series,* No. 86, pp. 1275-1288.

Lee, J., and Lee, K. S., 2014, ''Flow Characteristics and Thermal Performance in Chevron Type Plate Heat Exchangers'', *International Journal of Heat and Mass Transfer,* Vol. 78,

pp. 699-706.

Lee, J., and Lee, K. S., 2015, ‘‘Friction and Colburn Factor Correlations and Shape Optimization of Chevron-Type Plate Heat Exchangers’’, *Applied Thermal Engineering*, Vol. 89, pp. 62-69.

Lee, S.H., Cho, Y.I., Bai, C., and Cho, D.J., 2000, ‘‘The Effect of Aspect Ratio on Turbulent Flow Heat Transfer and Pressure Drop in a Plate Heat Exchanger’’, *International Journal of Heat Exchangers*, Vol. 1, No. 2, pp. 113-123.

Lozano, A., Barreras, F., Fueyo, N., and Santodomingo, S., 2008, ‘‘The Flow in an Oil/Water Plate Heat Exchanger for the Automotive Industry’’, *Applied Thermal Engineering*, Vol. 28, No. 10, pp. 1109-1117.

Martin, H., 1996 ‘‘A Theoretical Approach to Predict the Performance of Chevron-Type Plate Heat Exchangers’’, *Chemical Engineering and Processing*, Vol. 35, pp. 301-310.

Mehrabian, M. A., and Poulter, R., 2000, ‘‘Hydrodynamics and Thermal Characteristics of Corrugated Channels: Computational Approach’, *Applied Mathematical Modelling*, Vol. 24, pp. 343-364.

Metwally, H. M., and Manglik, R. M., 2004, ‘‘Enhanced Heat Transfer Due to Curvature-Induced Lateral Vortices in Laminar Flows in Sinusoidal Corrugated-Plate Channels’’, *International Journal of Heat and Mass Transfer*, Vol. 47, pp. 2283-2292.

Mohebbi, S., and Veysi, F., 2020, ‘‘An Experimental Investigation on the Heat Transfer and Friction Coefficients of a Small Plate Heat Exchanger with Chevron Angle’’, *Heat and*

Mass Transfer, Vol. 56, No. 3, pp. 849-858.

Muley, A., and Manglik, R. M., 1999, ‘‘Experimental Study of Turbulent Flow Heat Transfer and Pressure Drop in a Plate Heat Exchanger with Chevron Plates’’, *Journal of Heat Transfer,* Vol. 121, No. 1, pp. 110-117.

Muley, A., Manglik, R. M., and Metwally, H. M., 1999, ‘‘Enhanced Heat Transfer Characteristics of Viscous Liquid Flows in a Chevron Plate Heat Exchanger’’*, Journal of Heat Transfer,* Vol. 121, No. 4, pp. 1011-1017.

Muzychka, Y.S., 1999, ‘‘Analytical and Experimental Study of Fluid Friction and Heat Transfer in Low Reynolds Number Flow Heat Exchangers’’, Ph.D. Thesis, University of Waterloo, ON, Canada.

Muzychka, Y. S., Culham, J. R., and Yovanovich, M. M., 1999, ‘‘Experimental Measurement of Thermal-Hydraulic Characteristics of Corrugated Rib Channels’’,

Microelectronics Heat Transfer Laboratory, University of Waterloo, Waterloo, Ontario.

Muzychka, Y. S., and Yovanovich, M. M., 2004, ‘‘Laminar Forced Convection Heat Transfer in the Combined Entry Region of Non-Circular Ducts’, *Journal of Heat Transfer,* Vol. 126, No. 1, pp. 54-61.

Muzychka, Y. S., and Yovanovich, M. M., 1998, ‘‘Modeling Nusselt Numbers for Thermally Developing Laminar Flow in Non-Circular Ducts’’, *In 7th AIAA/ASME Joint Thermophysics and Heat Transfer Conference,* Albuquerque, NM.

O'Brien, J. E., and Sparrow, E. M., 1982, ''Corrugated-Duct Heat Transfer, Pressure Drop, and Flow Visualization'', *Journal of Heat Transfer,* Vol. 104, No. 3, pp. 410-416.

Okada, K., Ono, M., Tomimura, T., Okuma, T., Konno, H., and Ohtani, S., 1972, ''Design and Heat Transfer Characteristics of New Plate Heat Exchanger'', *Heat Transfer Japanese Research,* Vol. 1, pp. 90-95.

Palm, B., and Claesson, J., 2005, ''Plate Heat Exchangers: Calculation Methods for Single- and Two-Phase Flow (Keynote)'', *In ASME 3rd International Conference on Microchannels and Minichannels, Parts A and B,* Toronto, ON, pp. 103-113.

Pelletier, O., Strömer, F., and Carlson, A., 2005, ''CFD Simulation of Heat Transfer and Pressure Drop in Compact Brazed Plate Heat Exchangers'', *ASHRAE Transactions,* Vol. 111, No. 1, pp. 846-854.

Reppich, M., 1999, ''Use of High Performance Plate Heat Exchangers in Chemical and Process Industries'', *International Journal of Thermal Sciences,* Vol. 38, No. 11, pp. 999-1008.

Roetzel, W., Das, S. K., and Luo, X., 1994, ''Measurement of the Heat Transfer Coefficient in Plate Heat Exchangers Using a Temperature Oscillation Technique'', *International Journal of Heat and Mass Transfer,* Vol. 37, Suppl. 1, pp. 325-331.

Rohsenow, W.M., Hartnett, J.P., and Cho, Y.I., 1998, *Handbook of Heat Transfer,* 3rd ed, McGraw-Hill, New York.

Saha, S. K., and Khan, A. H., 2020, ‘‘Numerical Study on The Effect of Corrugation Angle on Thermal Performance of Cross Corrugated Plate Heat Exchangers’’, *Thermal Science and Engineering Progress,* Vol. 20, p. 100711.

Sarraf, K., Launay, S., and Tadrist, L., 2015, ‘‘Complex 3D-flow Analysis and Corrugation Angle Effect in Plate Heat Exchangers’’, *International Journal of Thermal Sciences,* Vol. 94, pp. 126-138.

Savostin, A.F., and Tikhonov, A.M., 1970, ‘‘Investigation of the Characteristics of Plate-Type Heating Surfaces’’, *Thermal Engineering*, Vol. 17, No. 9, pp. 113-117.

Shah, R. K., 1975, ‘‘Laminar Flow Friction and Forced Convection Heat Transfer in Ducts of Arbitrary Geometry’’, *International Journal of Heat and Mass Transfer*, Vol. 18, No. 7, pp. 849-862.

Shah, R. K., 1978, ‘‘A Correlation for Laminar Hydrodynamic Entry Length Solutions for Circular and Noncircular Ducts’’, *Journal of Fluids Engineering*, Vol. 100, pp. 177-179.

Shah, R. K., 1990, ‘‘Assessment of Modified Wilson Plot Techniques for Obtaining Heat Exchanger Design Data’’, *Proceedings of the 9th International Heat Transfer Conference,* Vol. 5, pp. 51-56

Shah, R. K., and London, A.L., 1978. *Advances in Heat Transfer, Supplement 1, Laminar Flow Forced Convection in Ducts,* Academic Press, NY.

Shah R.K., and Sekulic D.P., 2003, *Fundamentals of Heat Exchanger Design*, John Willey

& Sons.

Shaji, K., and Das, S. K., 2013, ‘‘Effect of Plate Characteristics on Axial Dispersion and Heat Transfer in Plate Heat Exchangers’’, *Journal of Heat Transfer*, Vol. 135, No. 4, pp. 041801-10.

Stasiek J., Collins M.W., Ciofalo M., and Chew P.E., 1996, ‘‘Investigation of Flow and Heat Transfer in Corrugated Passages, Part I: Experimental Results’’, *International Journal of Heat and Mass Transfer*, Vol. 39, No. 1, pp. 149-164.

Stephan, K., 1959, ‘‘Wärmeübergang und Druckabfall Bei Nicht Ausgebildeter Laminarströmung in Rohren und in ebenen Spalten’’, *Chemie Ingenieur Technik*, Vol. 31, No. 12, pp. 773-778.

Swamee, P.K., and Jain, A.K., 1976, ‘‘Explicit Equations for Pipe Flow Problems’, *Journal of the Hydraulics Division*, Vol. 102, No. 5, pp. 657-664.

Talik, A.C., Fletcher, L.S., Anand, N.K., and Swanson, L.W., 1995, ‘‘Heat Transfer and Pressure Drop Characteristics of a Plate Heat Exchanger Using a Propylene-Glycol/Water Mixture as the Working Fluid’’, *Proc. 1995 National Heat Transfer Conference*, Vol. 12, ASME, New York, pp. 83-88.

Teertstra, P.M., Michael Yovanovich, M., and Richard Culham, J., 2006, ‘‘Modeling of Natural Convection in Electronic Enclosures’’, *Journal of Electronic Packaging*, Vol. 128, No. 2, pp. 157-165.

Teertstra, P., Yovanovich, M. M., and Culham, J. R., 1997, ‘‘Pressure Loss Modeling for

Surface Mounted Cuboid-Shaped Packages in Channel Flow'', *IEEE Transactions on Components, Packaging, and Manufacturing Technology*: *Part A*, Vol. 20, No. 4, pp. 463-469.

Thonon, B., 2005, ''Plate Heat Exchangers: A Review of Correlations for Single Phase Flow Heat Transfer and Pressure Drop'', *International Journal of Heat Exchangers*, Vol. 6, pp. 1-34.

Thonon, B., Vidil, R., and Marvillet, C., 1995, ''Recent Research and Developments in Plate Heat Exchangers'', *Journal of Enhanced Heat Transfer*, Vol. 2, pp. 149-155.

Tovazhnyansky, L.L. Kapustenko, P. A., and Tsibulnic, V. A., 1980, ''Heat Transfer and Hydraulic Resistance in Channels of Plate Heat Exchangers'', *Energetika*, Vol. 9, pp. 123-125.

Troupe, R. A., Morgan, J. C., and Prifiti, J., 1960, ''The Plate Heater Versatile Chemical Engineering Tool'', *Chemical Engineering Progress*, Vol. 56, No. 1, pp. 124-128.

Tsai, Y.C., Liu, F.B., and Shen, P.T., 2009, ''Investigations of the Pressure Drop and Flow Distribution in a Chevron-Type Plate Heat Exchanger'', *International Communications in Heat and Mass Transfer*, Vol. 36, No. 6, pp. 574-578.

Vlasogiannis, P., Karagiannis, G., Argyropoulos, P., and Bontozoglou, V., 2002, ''Air-Water Two-Phase Flow and Heat Transfer in a Plate Heat Exchanger'', *International Journal of Multiphase Flow*, Vol. 28, pp. 757-772.

Wang, L., Sundén, B., and Manglik, R. M., 2007, *Plate Heat Exchangers Design: Applications and Performance*, WIT Press, Southampton.

Wang, Y.N., Lee, J.P., Park, M.H., Jin, B.J., Yun, T.J., Song, Y.H., and Kim, I.S., 2017, ‘‘A Study on 3D Numerical Model for Plate Heat Exchanger’’, *Procedia Engineering*, Vol. 174, pp. 188-194.

Wanniarachchi, A. S., Ratnam, U., Tilton, B. E., Dutta-Roy, K., 1995, ‘‘Approximate Correlations for Chevron-Type Plate Heat Exchangers’’, *Proc. 1995 National Heat Transfer Conference*, Vol. 12, ASME, New York, pp. 145 -151.

Wilson, E. E., 1915, ‘‘A Basis for Rational Design of Heat Transfer Apparatus’’, *ASME Transactions*, Vol. 37, pp. 47-70.

Yildiz, A., and Ersöz, M.A., 2015, ‘‘Theoretical and Experimental Thermodynamic Analyses of a Chevron Type Heat Exchanger’’, *Renewable and Sustainable Energy Reviews*, Vol. 42, pp. 240-253.

Yovanovich, M. M., 2003, ‘‘Asymptotes and Asymptotic Analysis for Development of Compact Models for Microelectronics Cooling’’, *in Proceedings of 19th Annual Semiconductor Thermal Measurement and Management Symposium and Exposition*. San Jose, CA.

Zhang, G.M., Tian, M.C., and Zhou, S.J., 2006, ‘‘Simulation and Analysis of Flow Pattern in Cross-Corrugated Plate Heat Exchangers’’, *Journal of Hydrodynamics*, Vol. 18, No. 5, pp. 547-551.

Zhang, L., and Che, D., 2011, ‘‘Turbulence Models for Fluid Flow and Heat Transfer between Cross-Corrugated Plates’’, *Numerical Heat Transfer; Part A: Applications*, Vol. 60, No. 5, pp. 410-440.

Appendix A

Uncertainty Analysis

A.1 Introduction

The approach proposed by Kline and McClintock (1953) has been employed to calculate the uncertainty in the experiment's measurements. This technique is often referred to as the root-sum squared (RSS) method. The uncertainty in the results can be estimated from the uncertainties in the primary measurements. Assume that experimental measurements of independent variables, $x_1, x_2, , x_3, \dots, x_n$ are taken and then these measurements are used to calculate some results R which may be expressed as

$$R = R(x_1, x_2, , x_3, \dots \dots, x_n) \tag{A.1}$$

Assume that $w_1, w_2, \dots w_n$ are the uncertainties in the independent variables $x_1, x_2, , x_3, \dots, x_n$ then the uncertainty in the results w_R can be determined from (Holman 2012)

$$w_R = \left[\left(\frac{\partial R}{\partial x_1} w_1\right)^2 + \left(\frac{\partial R}{\partial x_2} w_2\right)^2 + \dots + \left(\frac{\partial R}{\partial x_n} w_n\right)^2\right]^{1/2} \tag{A.2}$$

The uncertainty in the experimental measurements of temperature, pressure, and flow rate are summarized in Table A1. Furthermore, the uncertainties in the working fluids properties are $\pm 0.5\%$.

Table A1. Uncertainty in Measurements

Measurement	Uncertainty
Temperature [℃]	± 0.1 ℃
Flow Rate $[m^3/s]$	$\pm 0.05\%$
Pressure [Pa]	$\pm 0.08\%$

A.2 Uncertainty in Re and f

The uncertainty in the Reynolds number can be determined by employing Eq. (A.2) as follows

$$\frac{\delta Re}{Re} = \left\{ \left(\frac{\delta \dot{m}}{\dot{m}}\right)^2 + \left(\frac{\delta D_e}{D_e}\right)^2 + \left(\frac{\delta A_c}{A_c}\right)^2 + \left(\frac{\delta \mu}{\mu}\right)^2 \right\}^{1/2} \tag{A.3}$$

where

$$\frac{\delta \dot{m}}{\dot{m}} = \left\{ \left(\frac{\delta \rho}{\rho}\right)^2 + \left(\frac{\delta \dot{V}}{\dot{V}}\right)^2 \right\}^{1/2} \tag{A.4}$$

The uncertainty in the Fanning friction factor is determined from the following expression

$$\frac{\delta f}{f} = \left\{ \left(\frac{\delta \Delta P}{\Delta P}\right)^2 + \left(\frac{\delta D_e}{D_e}\right)^2 + \left(\frac{\delta L}{L}\right)^2 + \left(\frac{\delta \rho}{\rho}\right)^2 + \left(2\frac{\delta \overline{u}}{\overline{u}}\right)^2 \right\}^{1/2} \tag{A.5}$$

A.3 Uncertainty in Nu, Pr and j

The uncertainty in heat transfer measurements is calculated as follows

$$\frac{\delta Q}{Q} = \left\{ \left(\frac{\delta \dot{m}}{\dot{m}} \right)^2 + \left(\frac{\delta C_p}{C_p} \right)^2 + \left(\frac{\delta \Delta T}{\Delta T} \right)^2 \right\}^{1/2} \tag{A.6}$$

For the overall heat transfer coefficient, the uncertainty is calculated using the following expression

$$\frac{\delta UA}{UA} = \left\{ \left(\frac{\delta Q}{Q} \right)^2 + \left(\frac{\delta \Delta T_{LMTD}}{\Delta T_{LMTD}} \right)^2 \right\}^{1/2} \tag{A.7}$$

The uncertainty in the heat transfer coefficients for the cooling side, h_c, for long and short channels, refer to Eq. (4.40) and (4.41), may be calculated as

For long channel

$$\frac{\delta h_c}{h_c} = \left\{ \left(0.57 \frac{\delta Re}{Re} \right)^2 + \left(\frac{1}{3} \frac{\delta Pr}{Pr} \right)^2 + \left(\frac{\delta k}{k} \right)^2 + \left(\frac{\delta D_h}{D_h} \right)^2 \right\}^{1/2} \tag{A.8}$$

For short channel

$$\frac{\delta h_c}{h_c} = \left\{ \left(0.54 \frac{\delta Re}{Re} \right)^2 + \left(\frac{1}{3} \frac{\delta Pr}{Pr} \right)^2 + \left(\frac{\delta k}{k} \right)^2 + \left(\frac{\delta D_h}{D_h} \right)^2 \right\}^{1/2} \tag{A.9}$$

The uncertainty in the heat transfer coefficient on the hot side may be calculated from (Muzychka, 1999)

$$\frac{\delta h_h}{h_h} = \left\{ \left(\frac{\delta A}{A} \right)^2 + \left(\frac{\delta UA}{UA} \right)^2 + \left(\frac{\delta (h_c A)}{h_c A} \right)^2 \right\}^{1/2} \tag{A.10}$$

where

$$\frac{\delta (h_c A)}{h_c A} = \left\{ \left(\frac{\delta h_c}{h_c} \right)^2 + \left(\frac{\delta A}{A} \right)^2 \right\}^{1/2} \tag{A.11}$$

The uncertainty in the Nusselt number is then determined from

$$\frac{\delta Nu}{Nu} = \left\{ \left(\frac{\delta h_h}{h_h}\right)^2 + \left(\frac{\delta D_e}{D_e}\right)^2 + \left(\frac{\delta k}{k}\right)^2 \right\}^{1/2} \tag{A.12}$$

Finally the uncertainty in the working fluid Colburn factor is computed from

$$\frac{\delta j}{j} = \left\{ \left(\frac{\delta Nu}{Nu}\right)^2 + \left(\frac{\delta Re}{Re}\right)^2 + \left(\frac{1}{3}\frac{\delta Pr}{Pr}\right)^2 \right\}^{1/2} \tag{A.13}$$

where

$$\frac{\delta Pr}{Pr} = \left\{ \left(\frac{\delta \mu}{\mu}\right)^2 + \left(\frac{\delta C_p}{C_p}\right)^2 + \left(\frac{\delta k}{k}\right)^2 \right\}^{1/2} \tag{A.14}$$

Table A.2 summarizes the calculated uncertainties in the Fanning friction factor and the Colburn factor, as well as the Reynolds, Nusselt, and Prandtl numbers. The higher uncertainties in Nu and j were due to using the average value of the total heat transfer $\bar{Q}$ when reducing the data and not the more accurate process fluid side values, Q_h. The uncertainties in Nu and j were found to be $8.6/5.55$ percent and $8.85/5.94$ percent, respectively, when Q_h was used to reduce the data.

Table A 2 Uncertainty in f, Re, Nu, j and Pr

Parameter	**Uncertainty**
f	$4.54/3.65$ %
Re	$2.5/2.09$ %
Nu	$13.9/7.39$ %
j	$14.08/7.70$ %
Pr	0.87 %

Appendix B

Test Fixture Geometrical Information

The fixture consists of six sets of corrugated plates, two sets of coolant jackets, two test fluid inlet and exit manifolds, and four sets of coolant inlet and exit manifolds. In addition, one set of smooth channels were machined for heat transfer benchmark testing. Figures B.1 to B.21 illustrate the geometrical dimensions in millimeters for all the above-mentioned components.

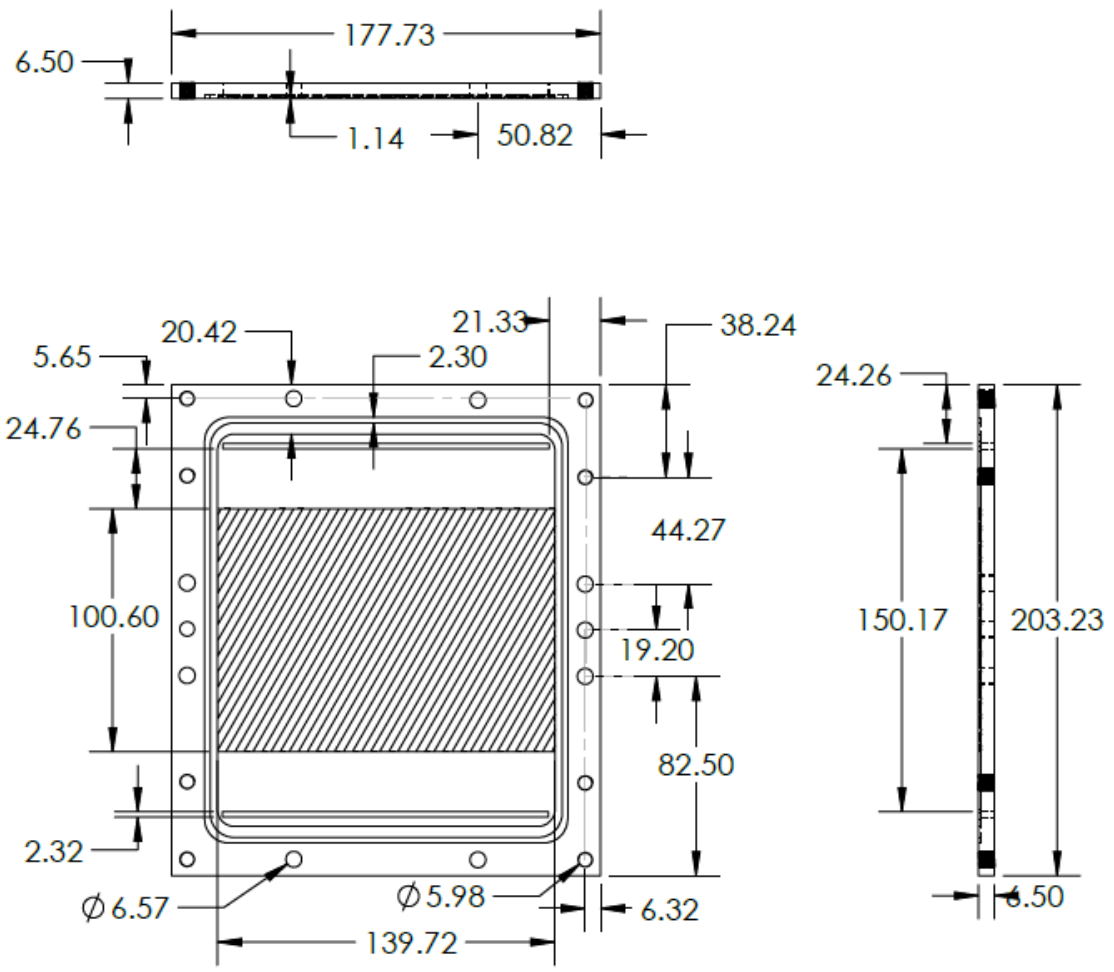

Fig. B. 1 Short test plate A for $\beta = 30°$

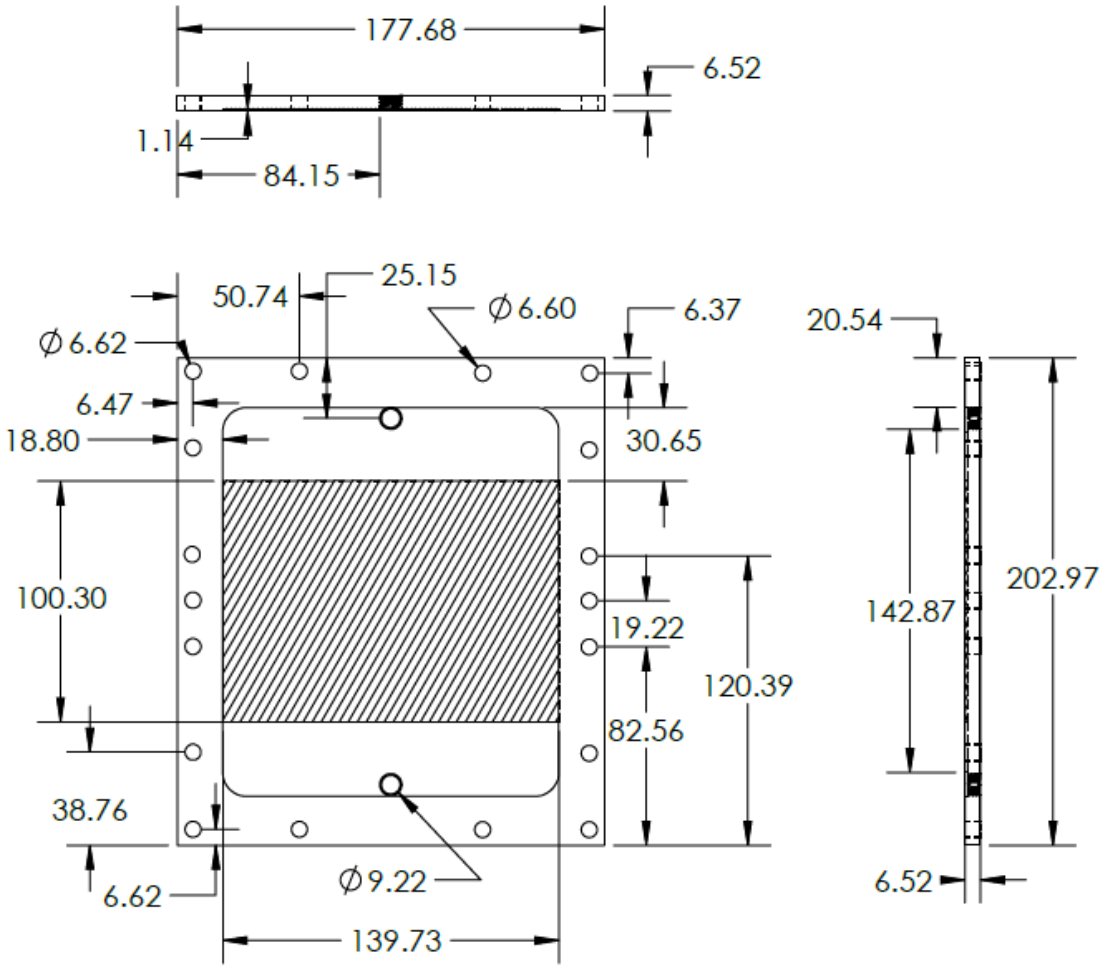

Fig. B. 2 Short test plate B for $\beta = 30°$

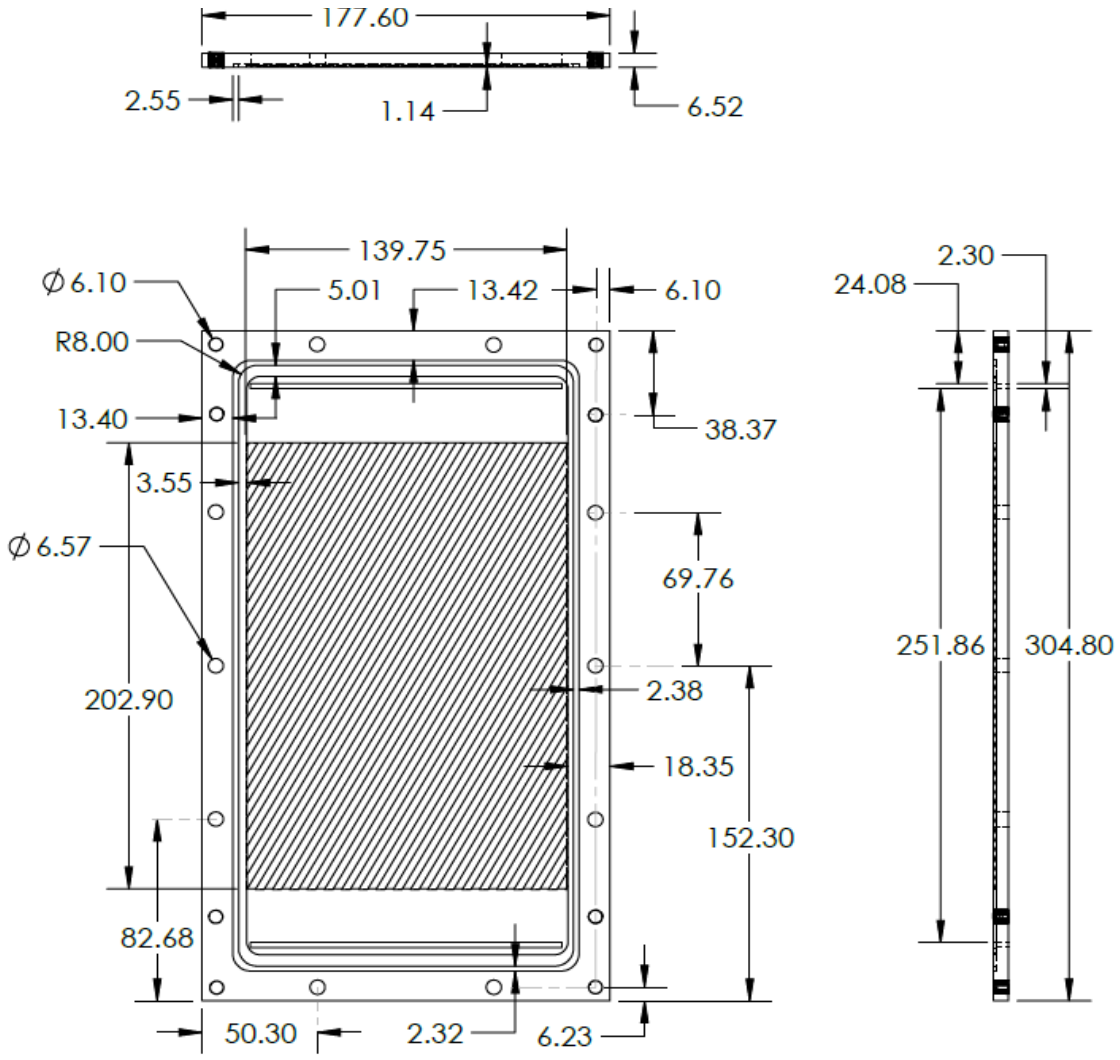

Fig. B. 3 Long test plate A for $\beta = 30°$

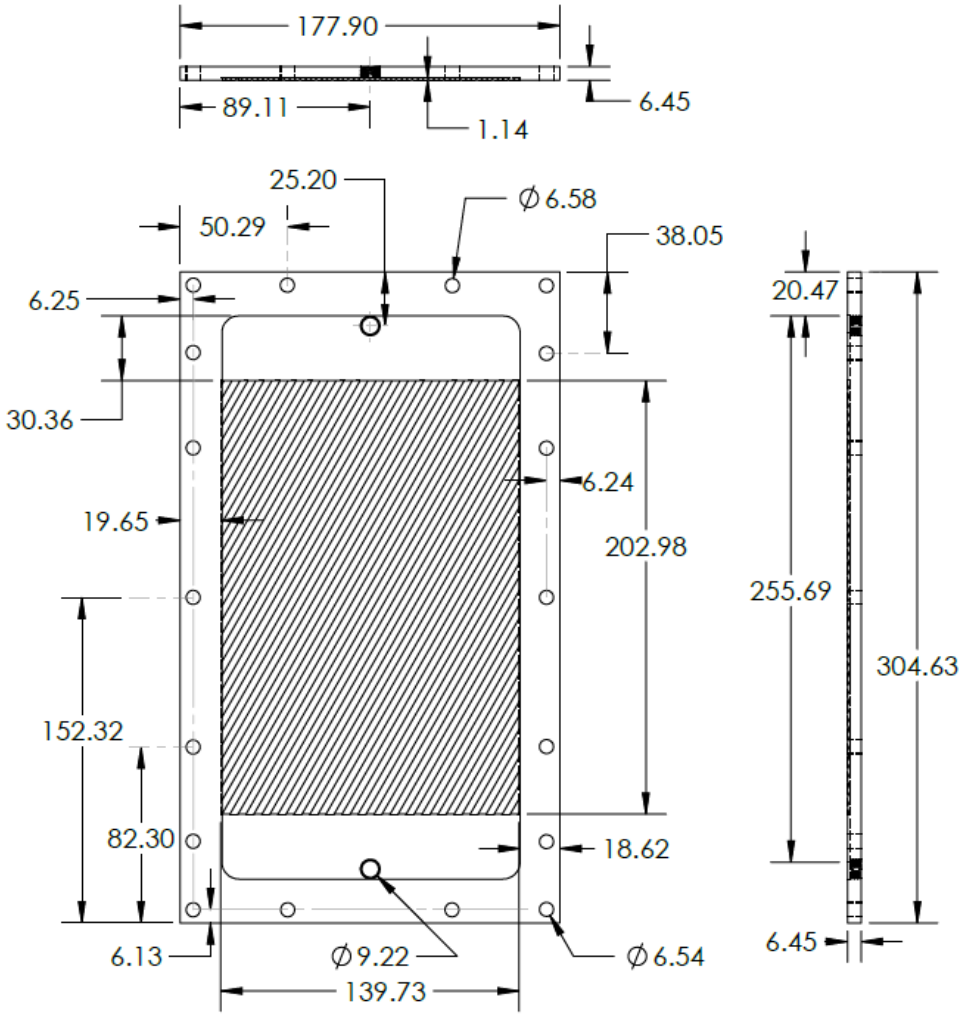

Fig. B. 4 Long test plate B for $\beta = 30°$

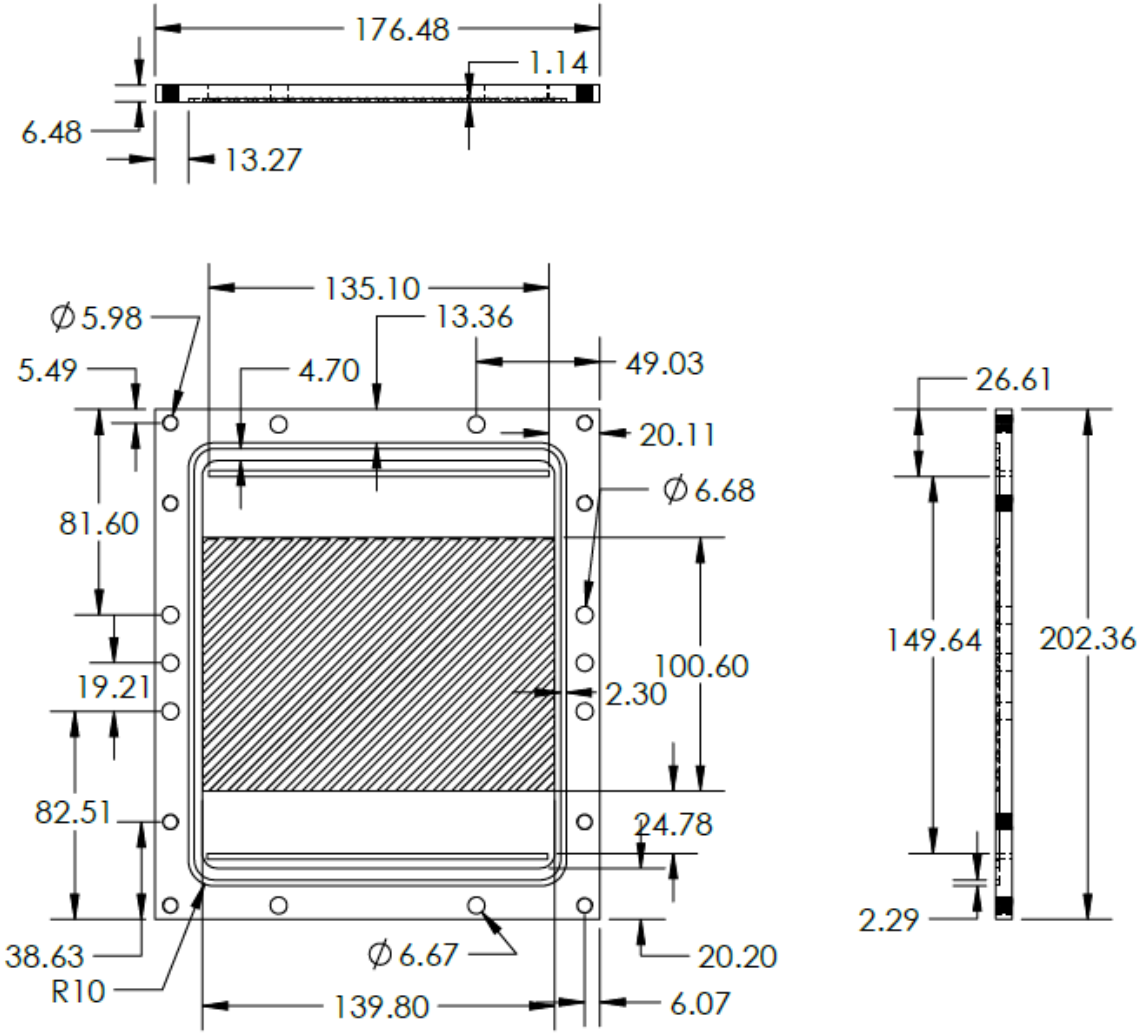

Fig. B. 5 Short test plate A for $\beta = 45°$

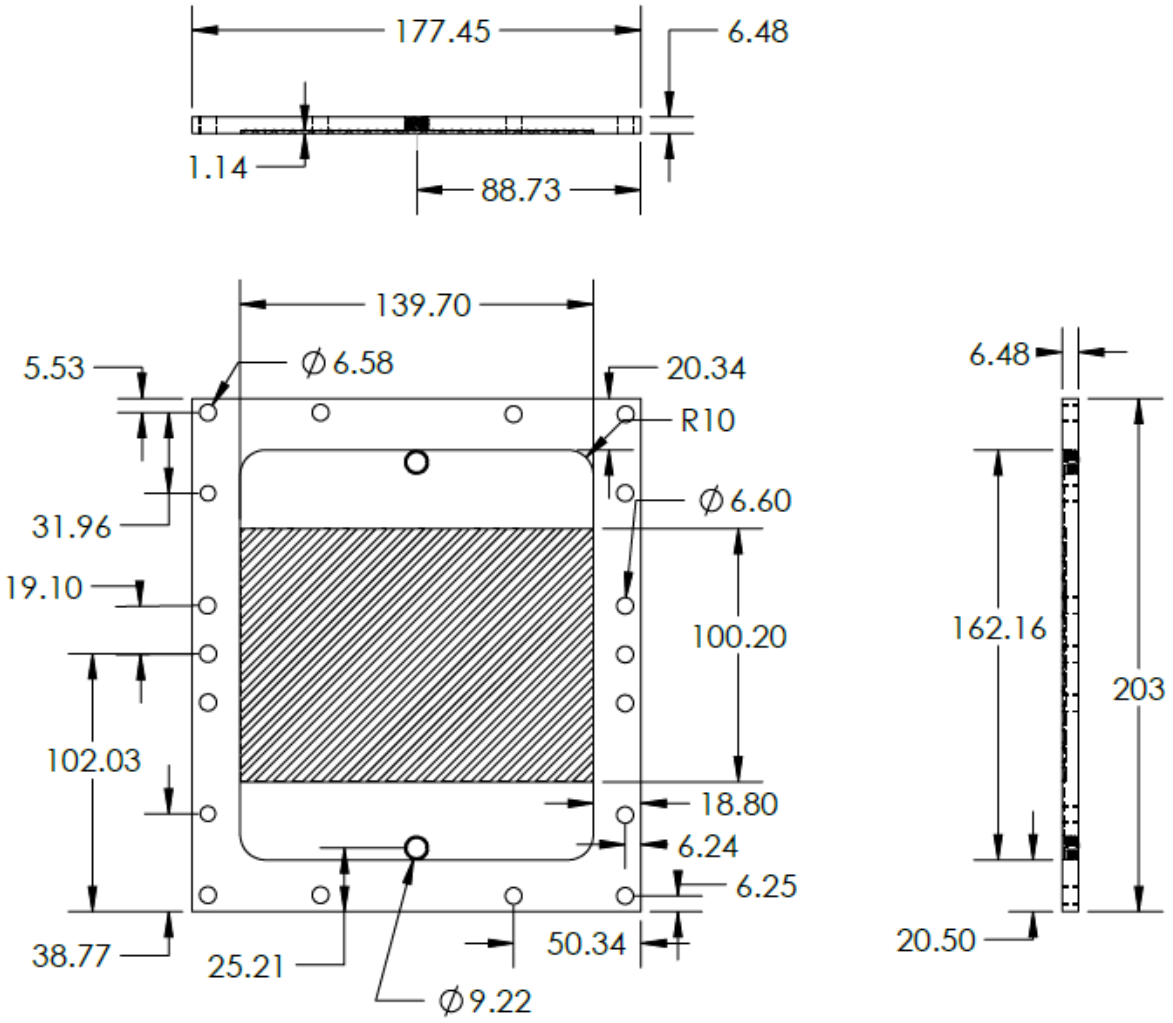

Fig. B. 6 Short test plate B for $\beta = 45°$

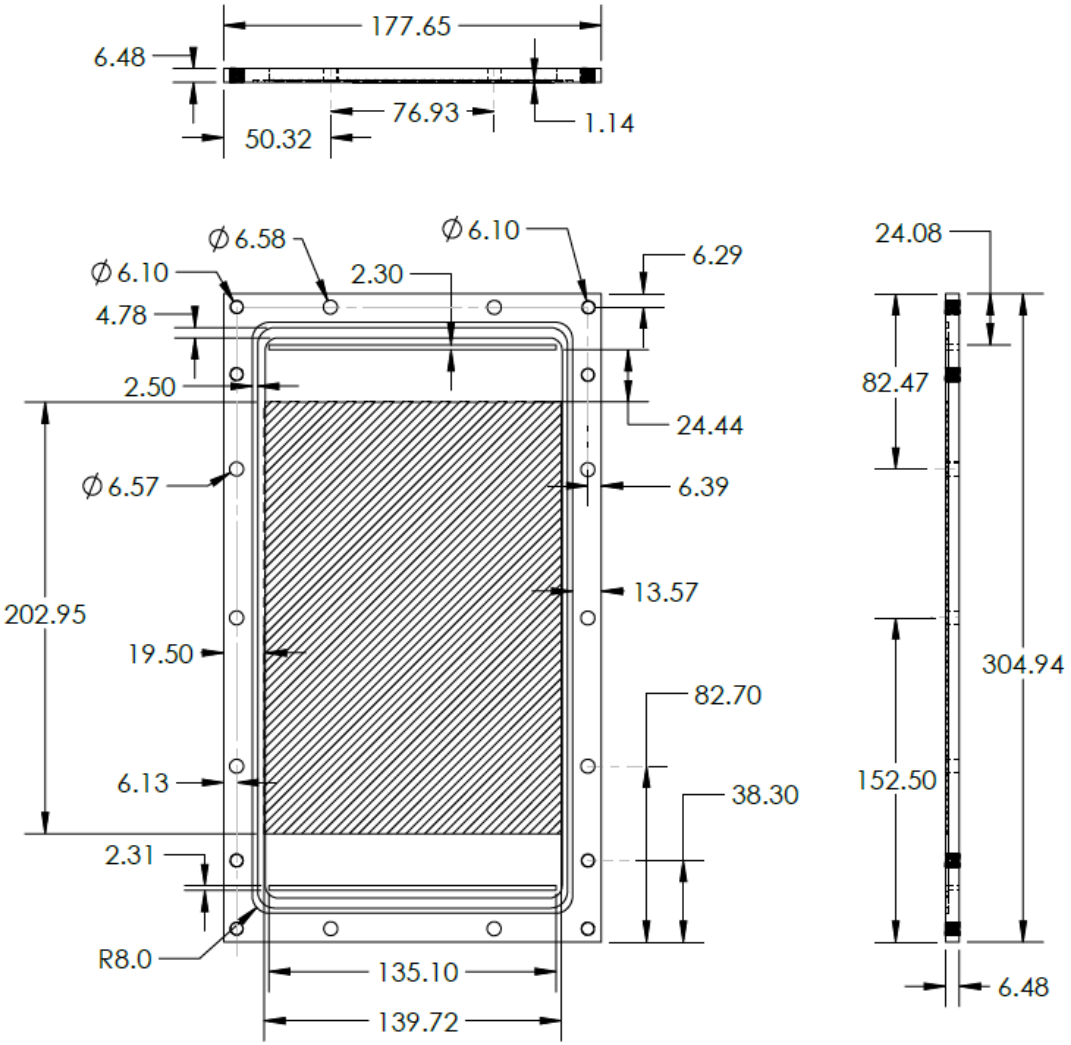

Fig. B. 7 Long test plate A for $\beta = 45°$

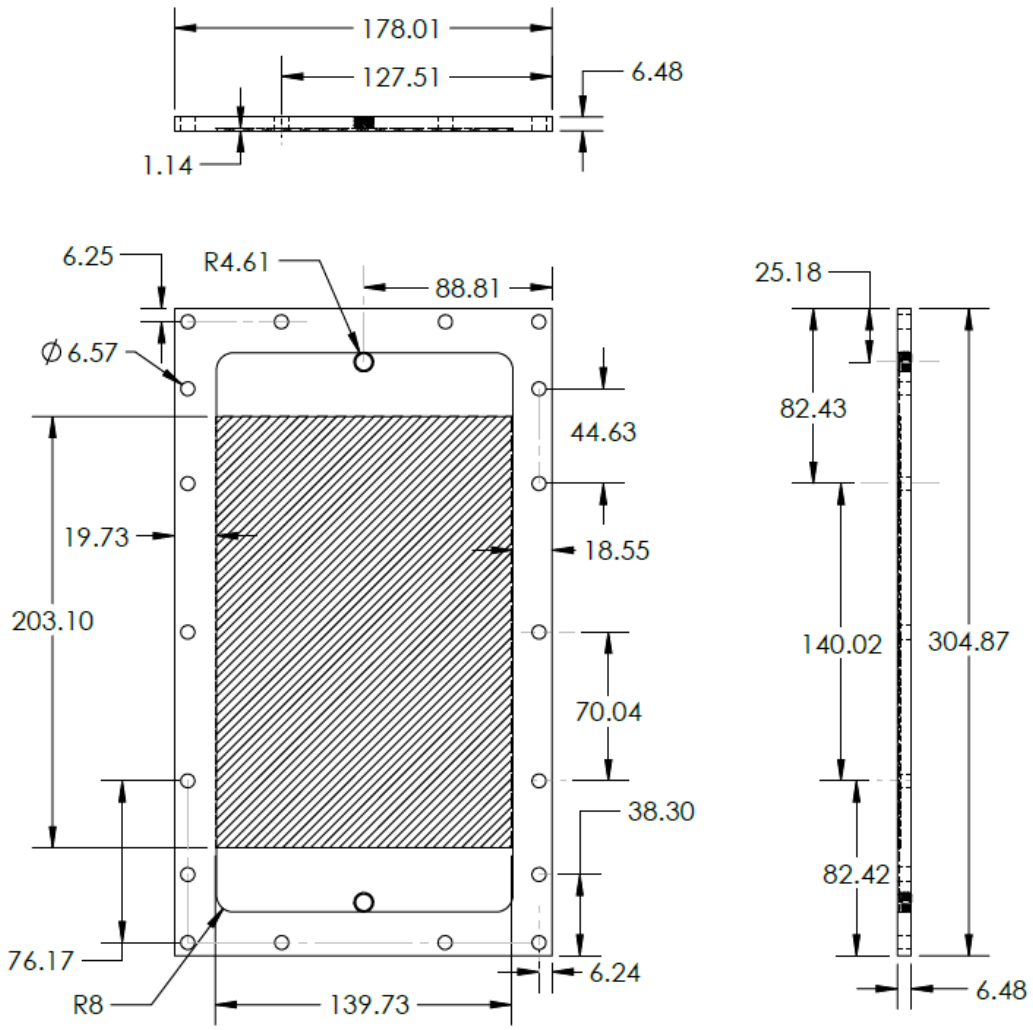

Fig. B. 8 Long test plate B for $\beta = 45°$

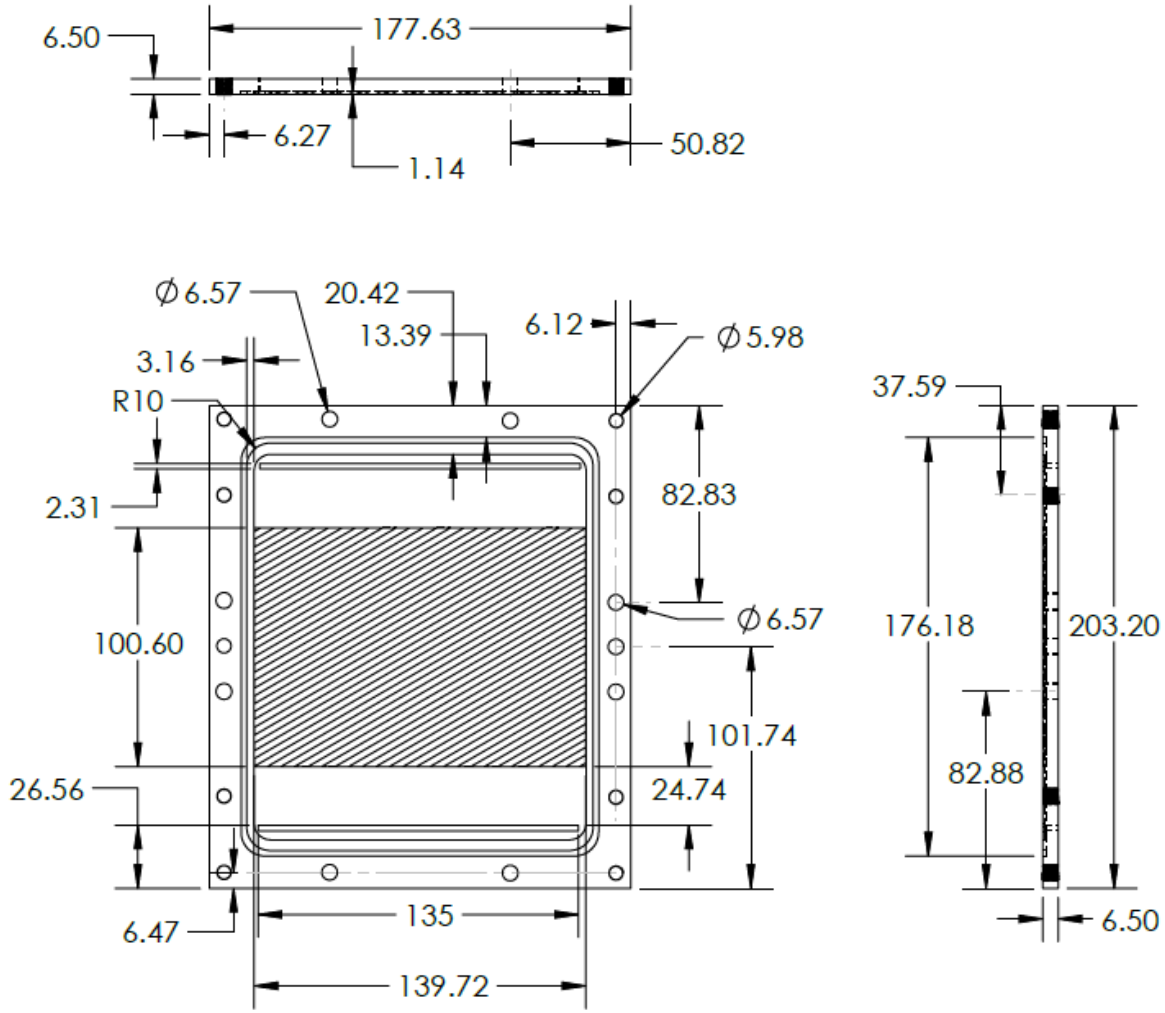

Fig. B. 9 Short test plate A for $\beta = 60°$

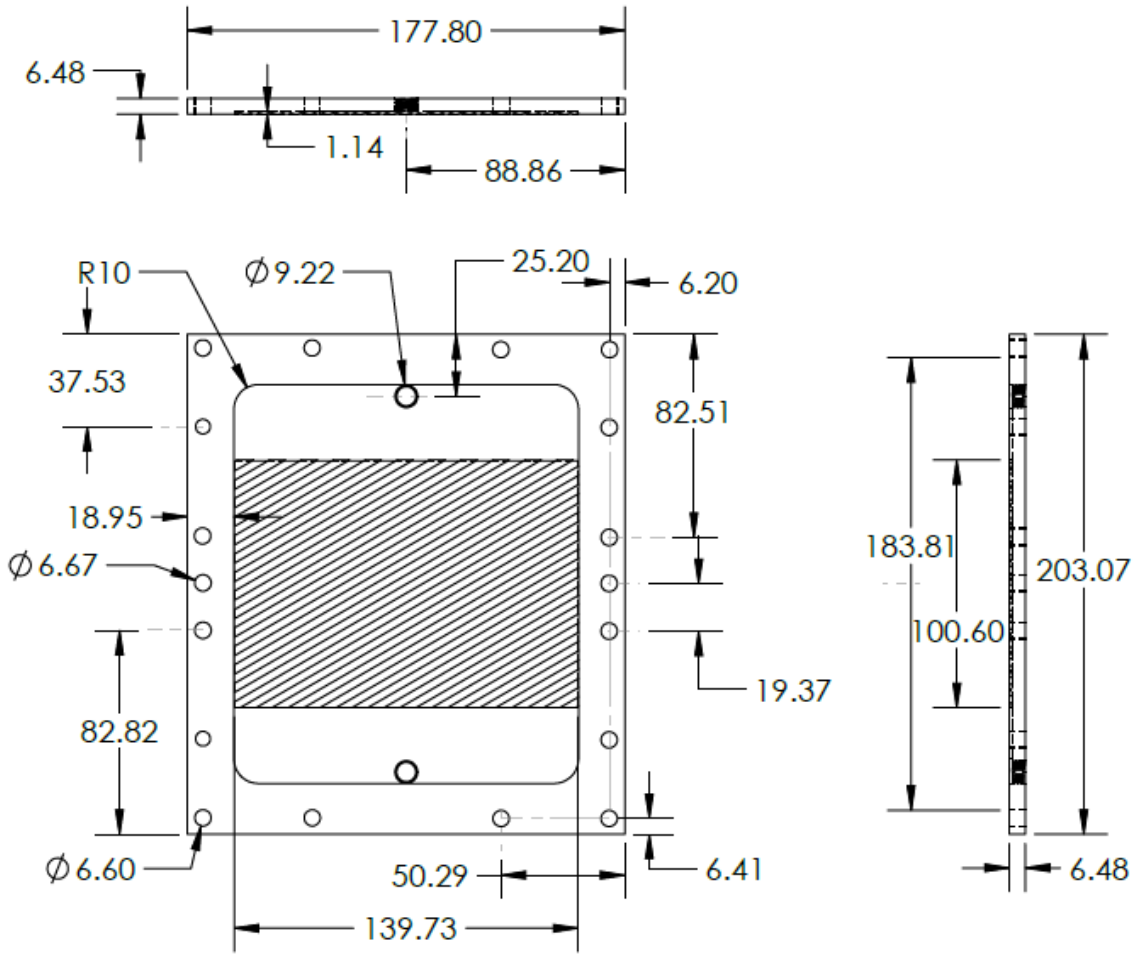

Fig. B. 10 Short test plate B for $\beta = 60°$

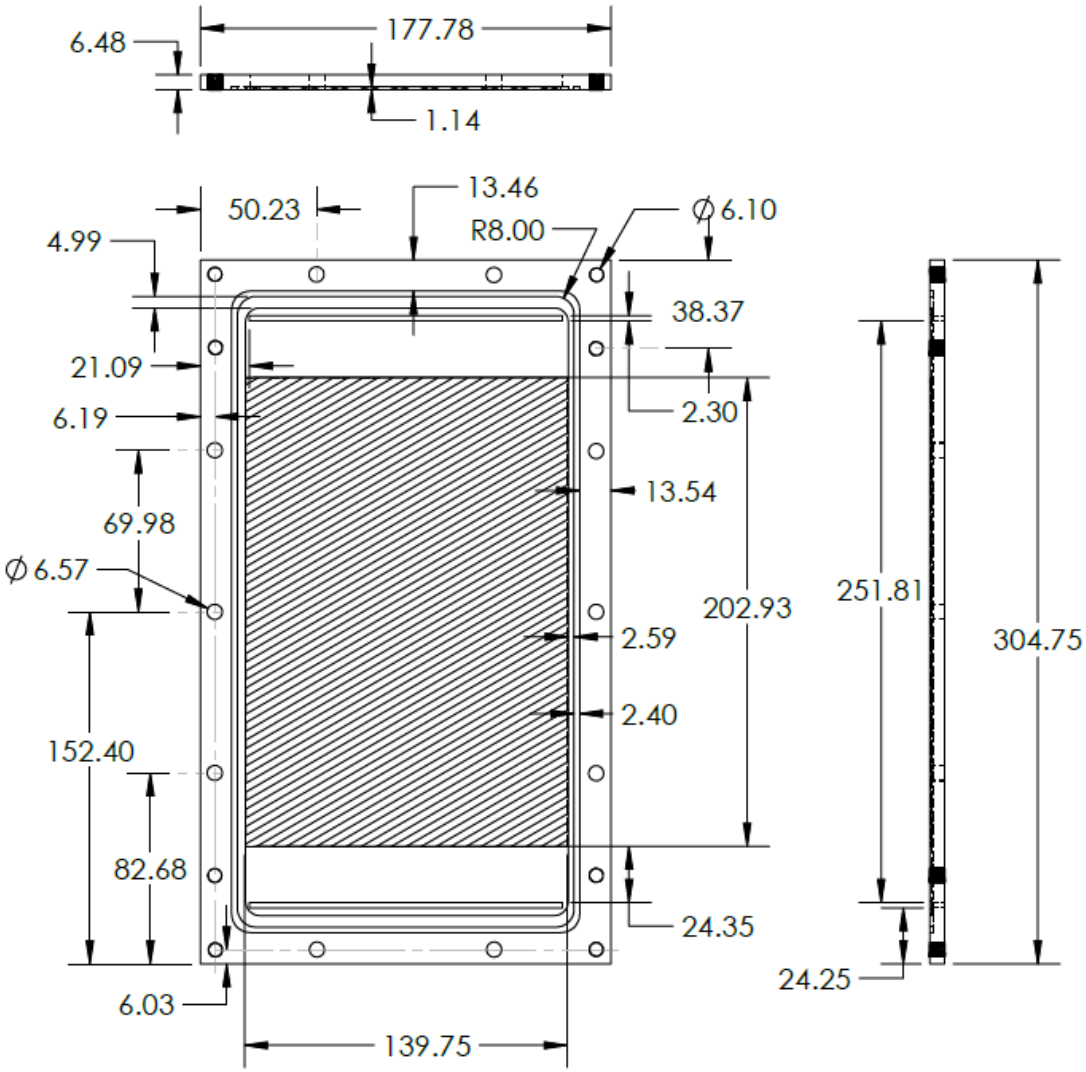

Fig. B. 11 Long test plate A for $\beta = 60°$

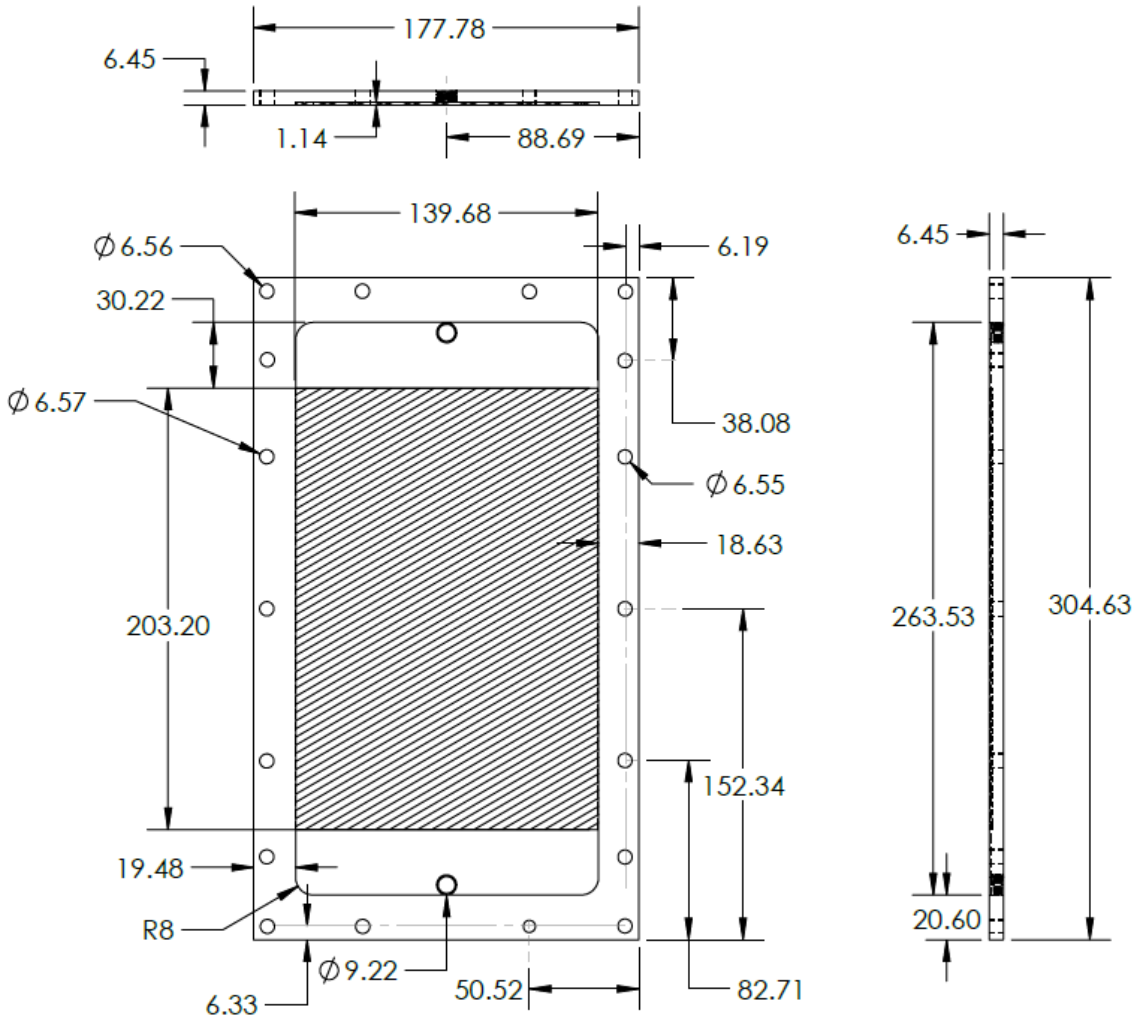

Fig. B. 12 Long test plate B for $\beta = 60°$

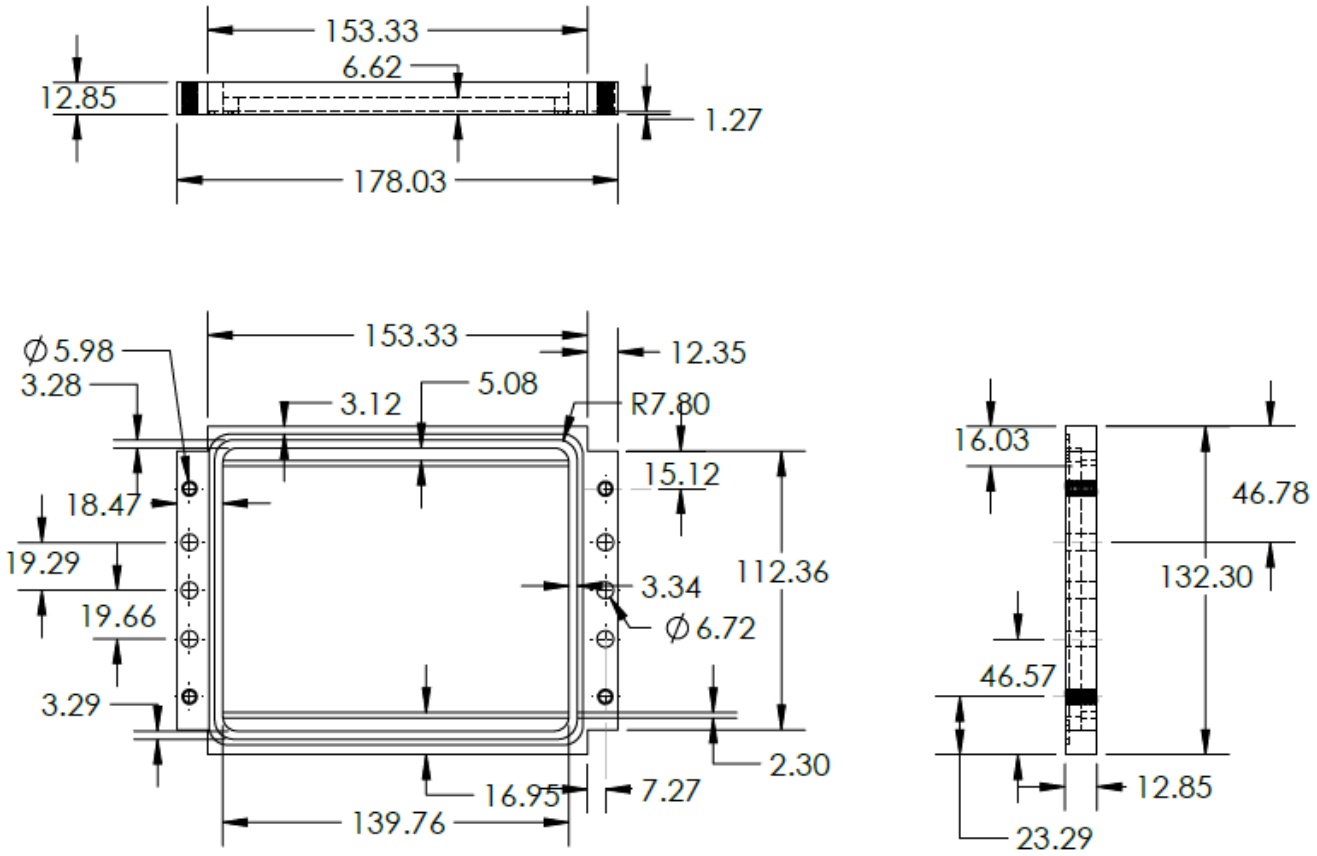

Fig. B. 13 Short coolant jacket plate A

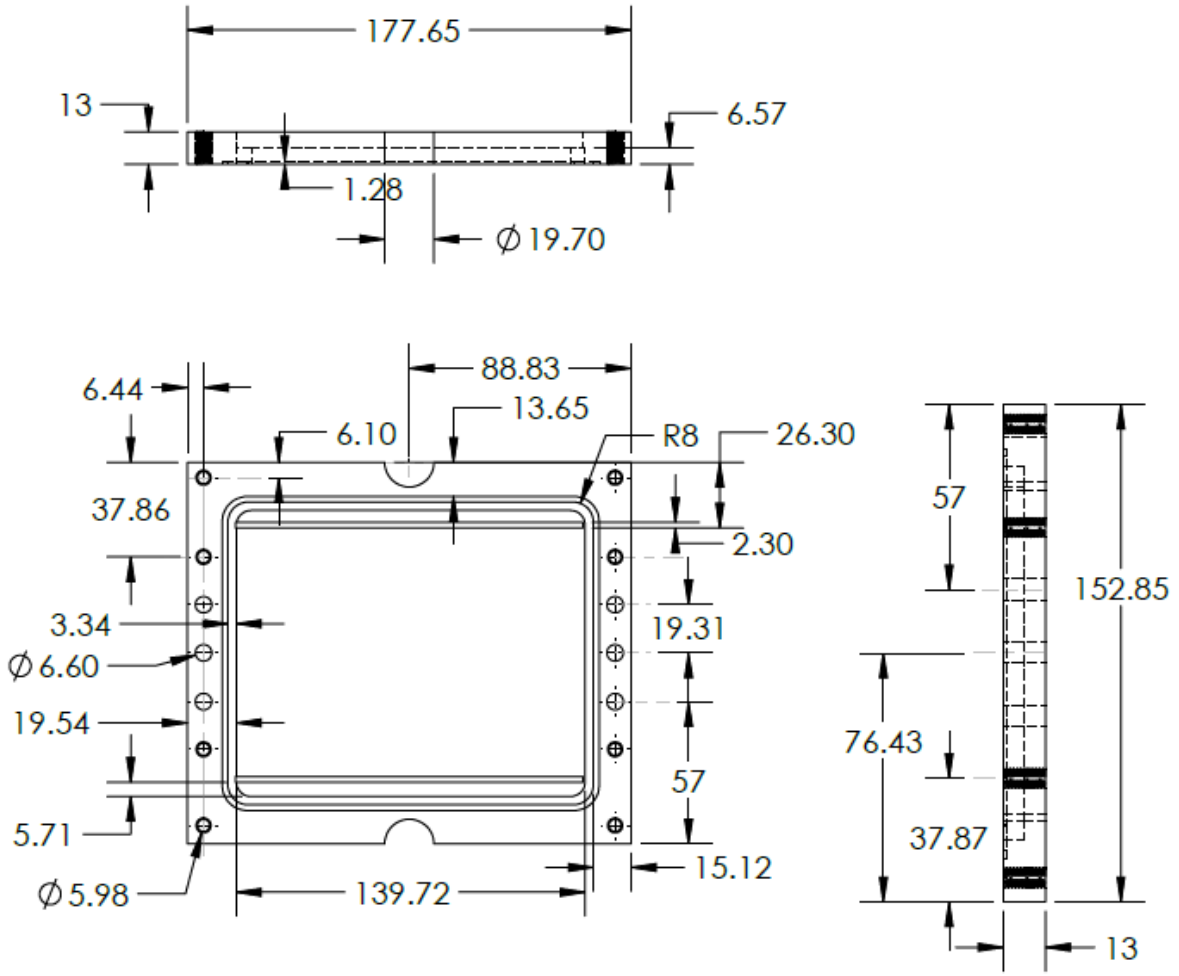

Fig. B. 14 Short coolant jacket plate B

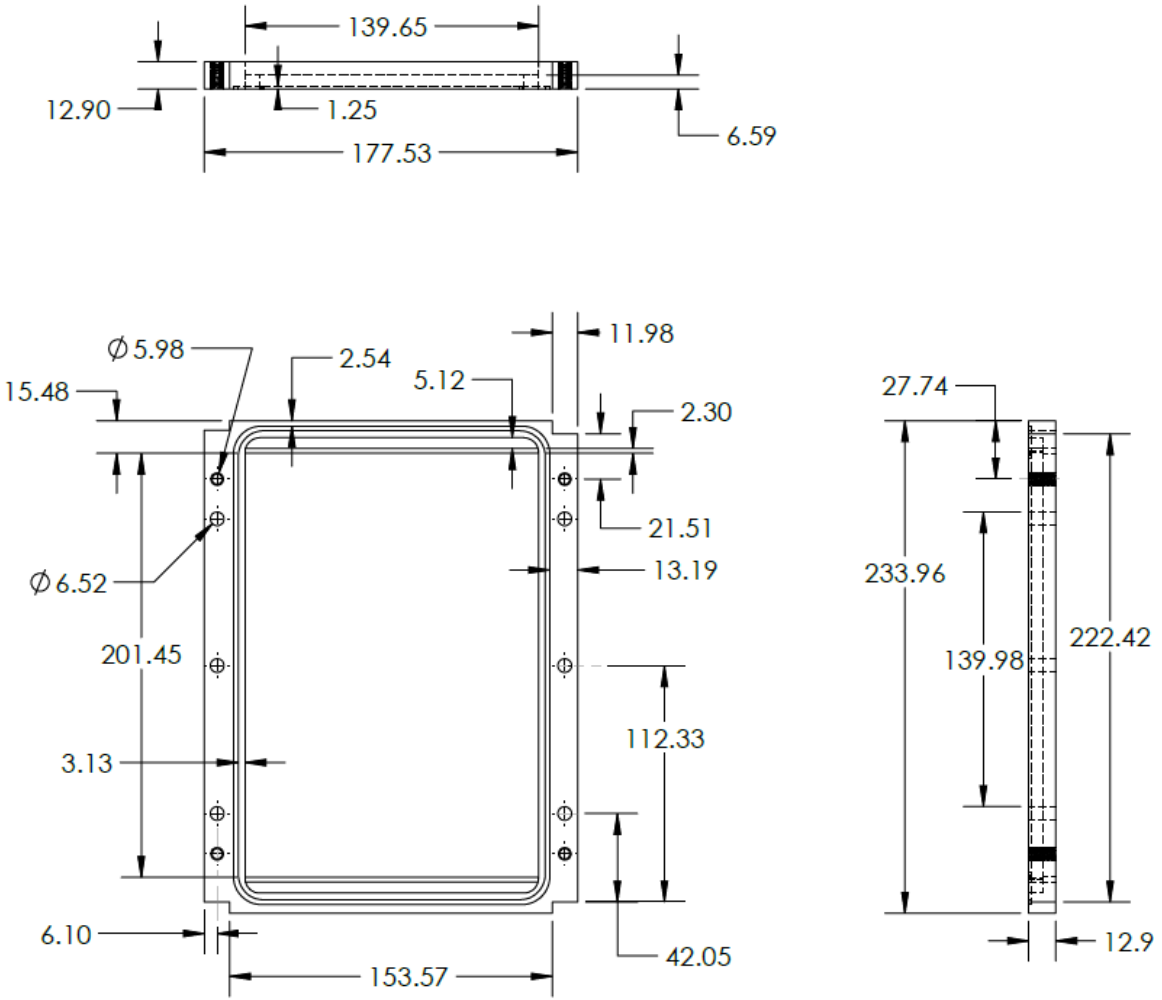

Fig. B. 15 Long coolant jacket plate A

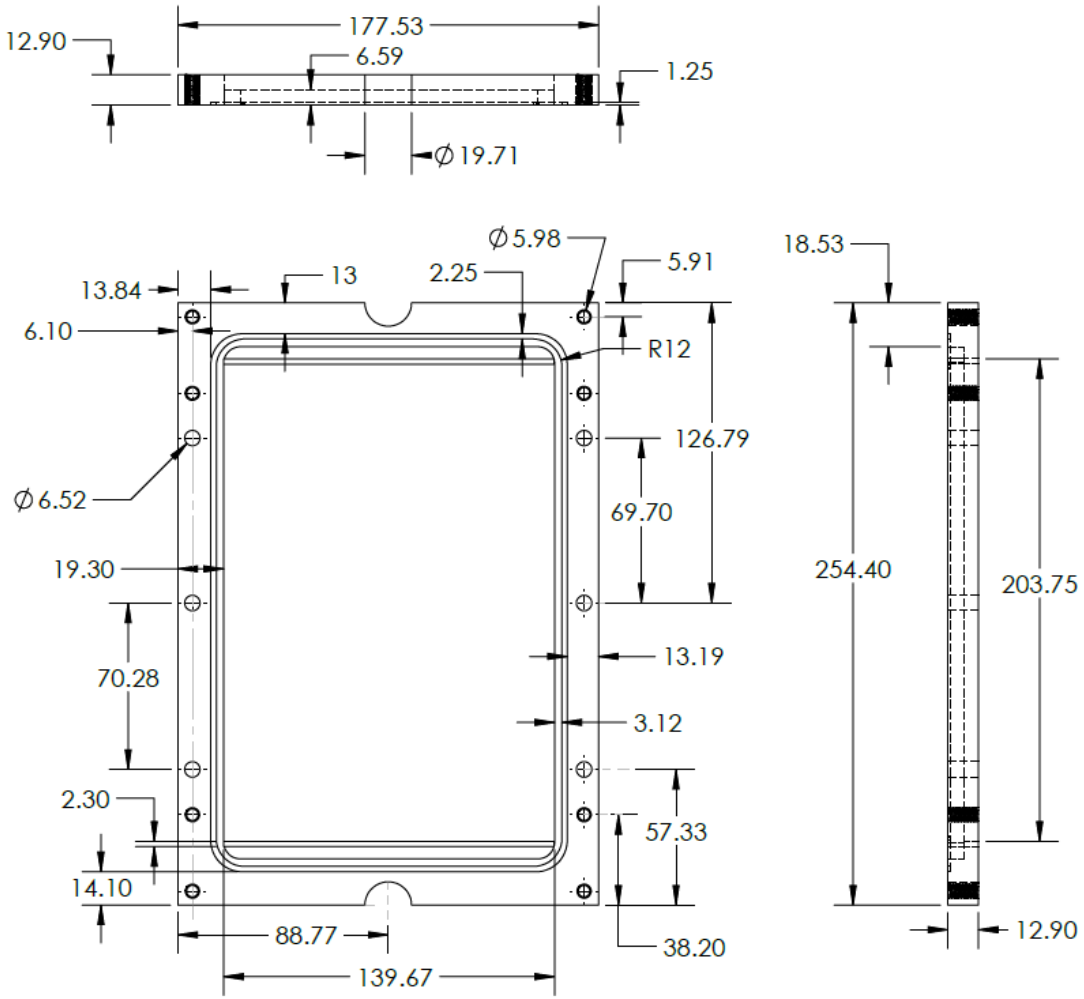

Fig. B. 16 Long coolant jacket plate B

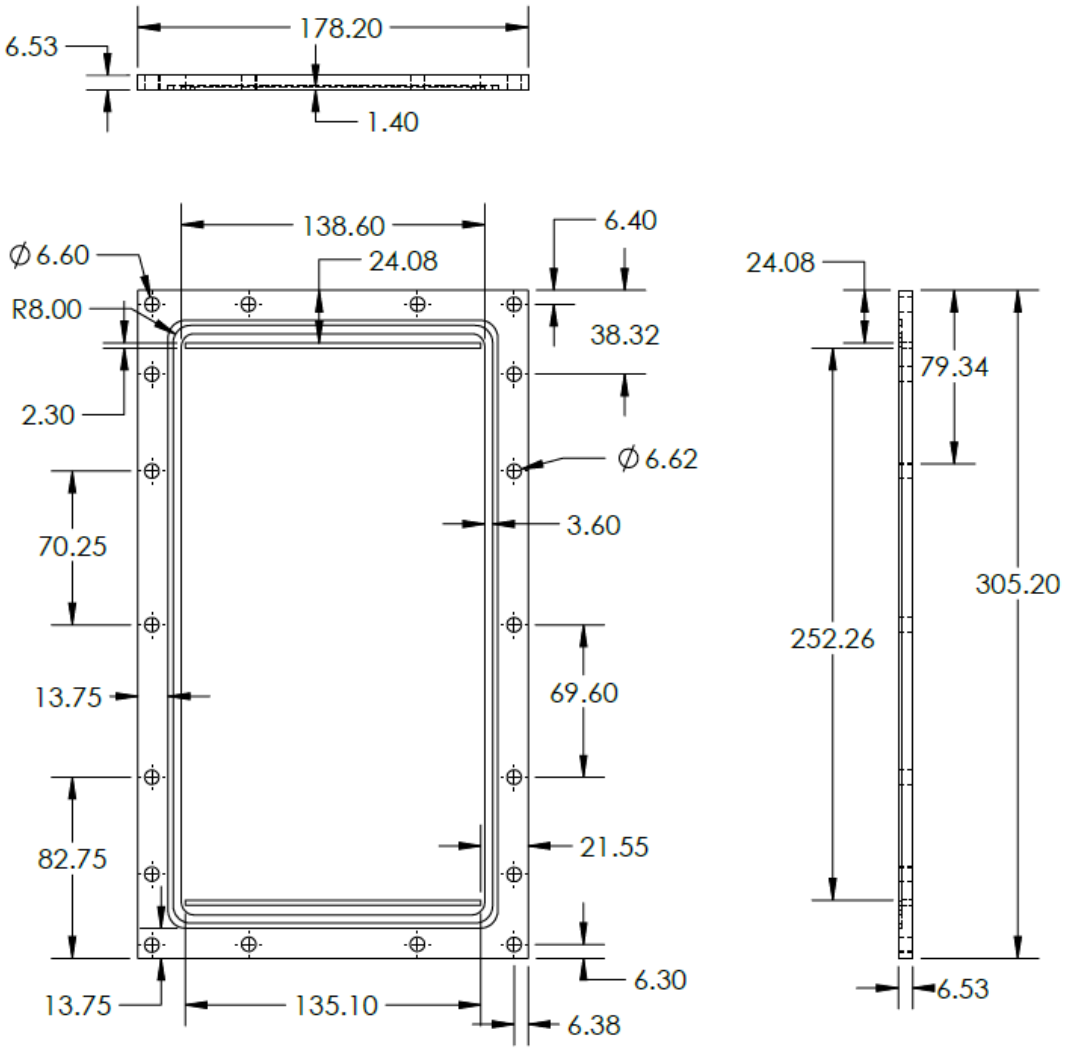

Fig. B. 17 Smooth channel plate A

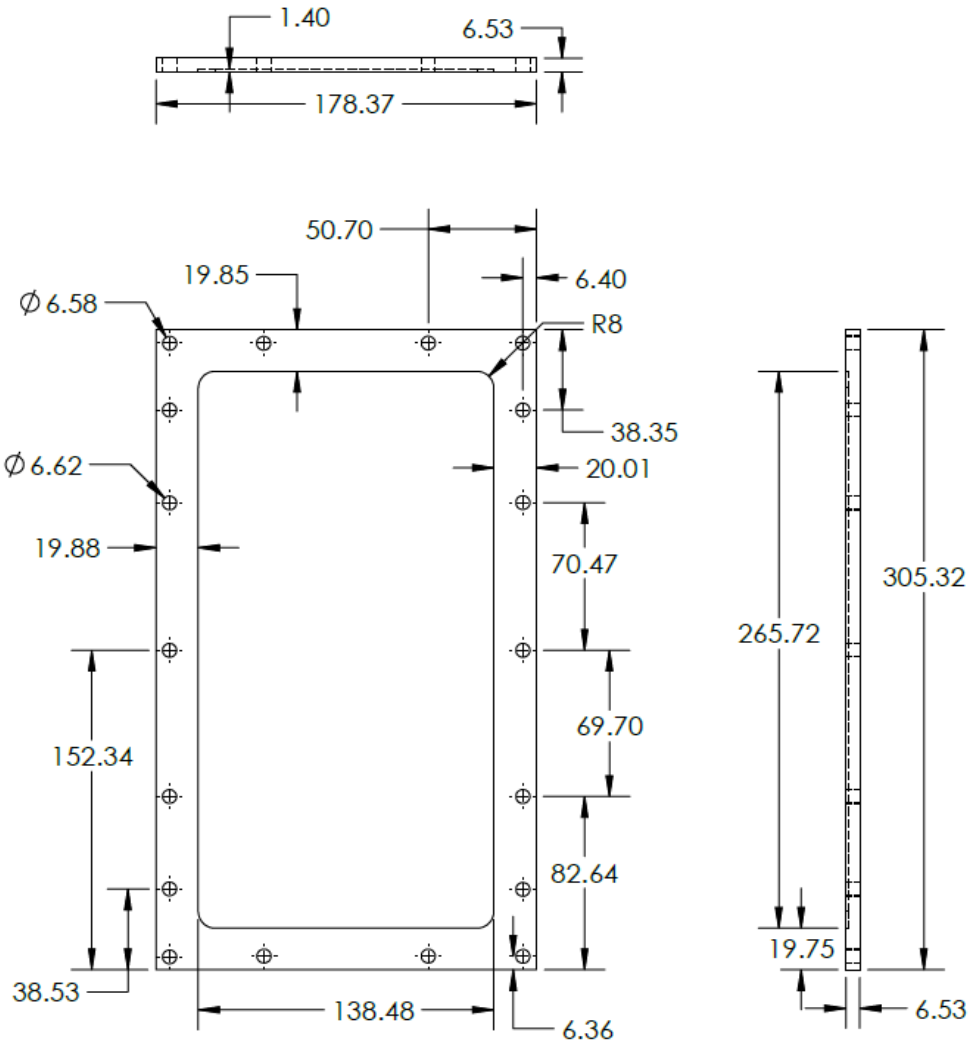

Fig. B. 18 Smooth channel plate B

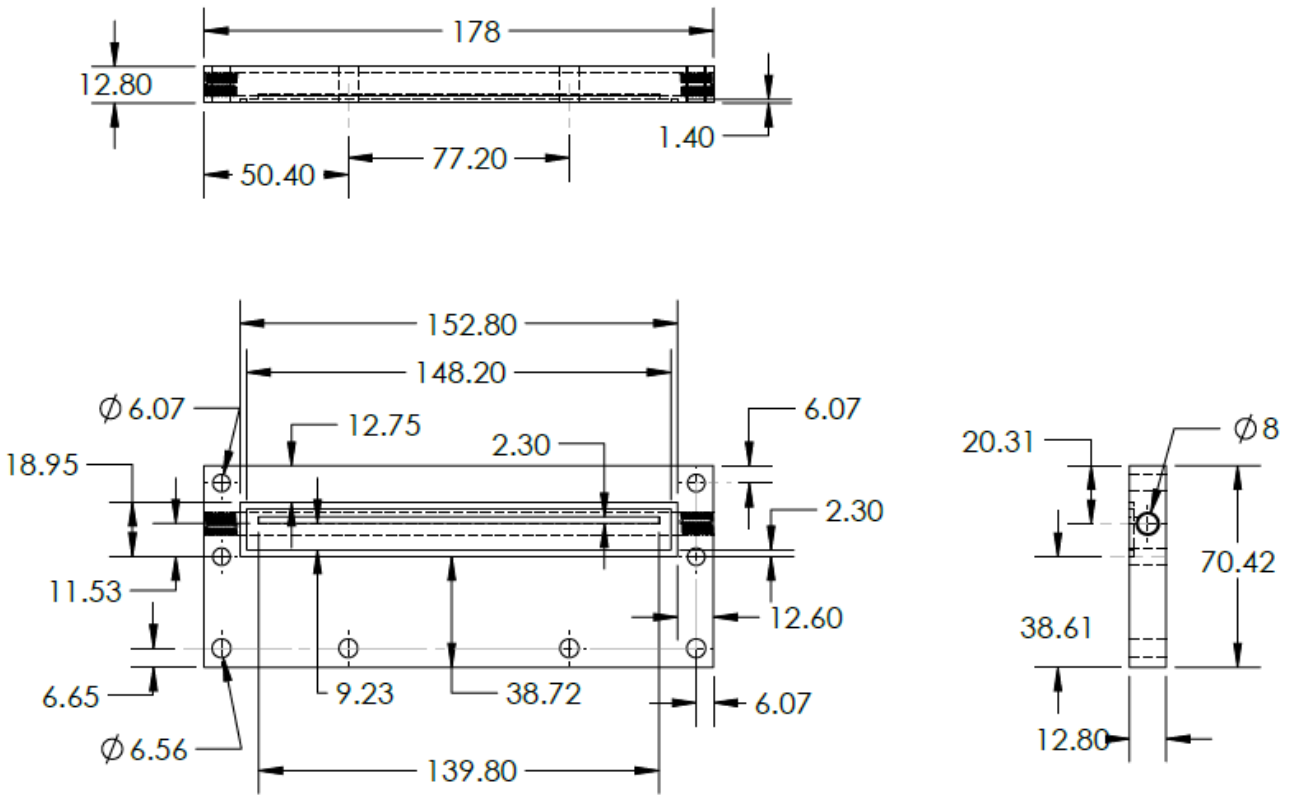

Fig. B. 19 Coolant side inlet/exit manifold

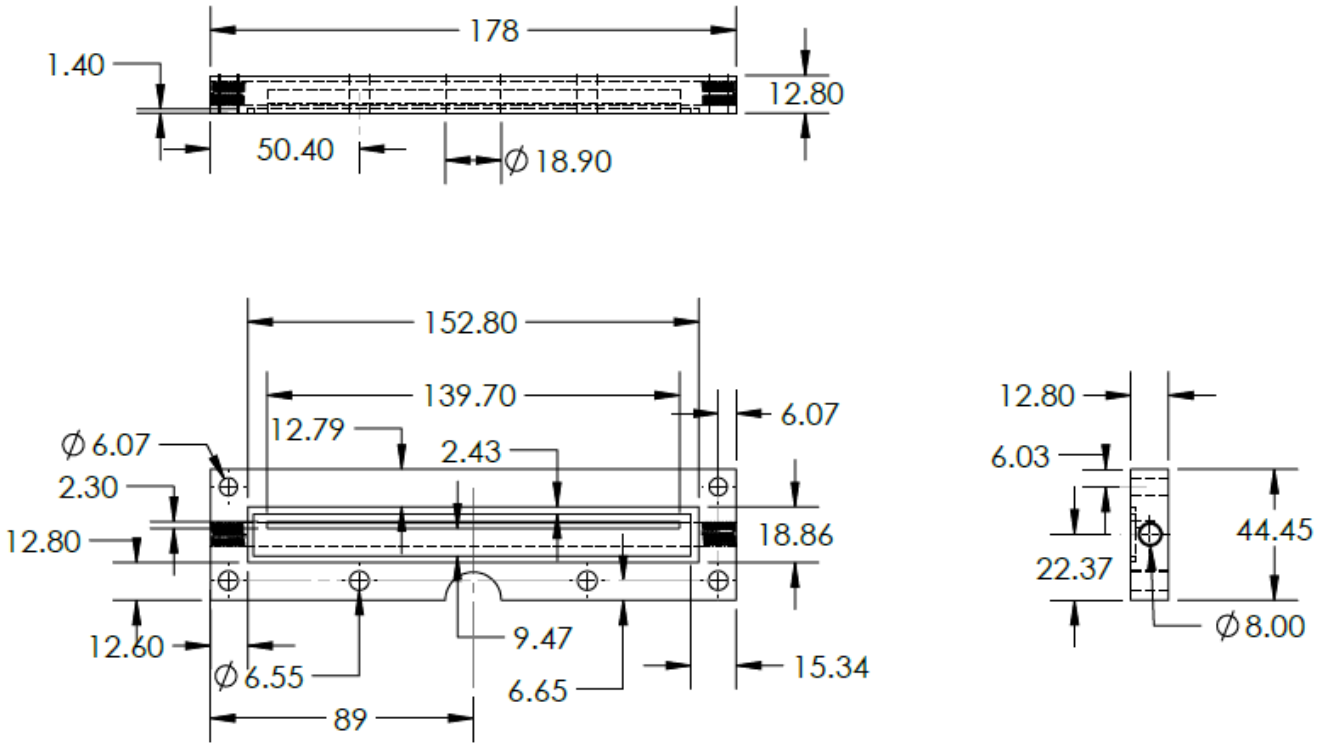

Fig. B. 20 Coolant side inlet/exit manifold

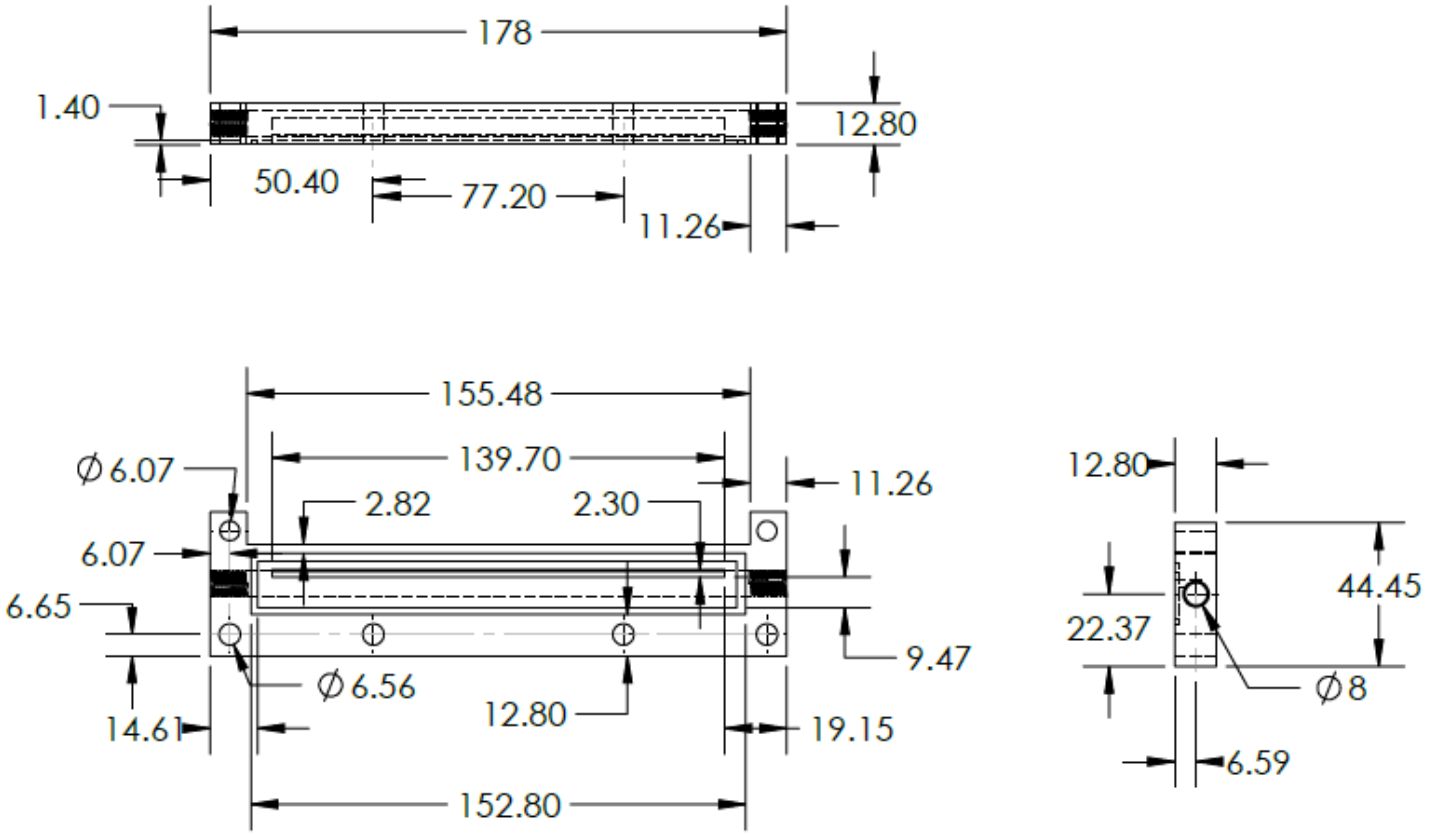

Fig. B. 21 Test side inlet/exit manifold